REC-ERC-84-16

CENTRIFUGAL MODEL TESTS FOR ULTIMATE BEARING CAPACITY OF FOOTINGS ON STEEP SLOPES IN COHESIONLESS SOIL

July 1984

Engineering and Research Center

U. S. Department of the Interior

Bureau of Reclamation

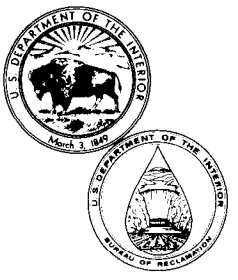

7-2090 (4-81)
Bureau of Reclamation

TECHNICAL REPORT STANDARD TITLE PAGE

1. REPORT NO.	2. GOVERNMENT ACCESSION NO.	3. RECIPIENT'S CATALOG NO.
REC-ERC-84-16		

4. TITLE AND SUBTITLE	5. REPORT DATE
Centrifugal Model Tests for Ultimate Bearing Capacity of Footings on Steep Slopes in Cohesionless Soil	June 1984
	6. PERFORMING ORGANIZATION CODE D-1542
7. AUTHOR(S) Mark C. Gemperline	8. PERFORMING ORGANIZATION REPORT NO. REC-ERC-84-16
9. PERFORMING ORGANIZATION NAME AND ADDRESS Bureau of Reclamation Engineering and Research Center Denver, Colorado 80225	10. WORK UNIT NO.
	11. CONTRACT OR GRANT NO.
12. SPONSORING AGENCY NAME AND ADDRESS Same	13. TYPE OF REPORT AND PERIOD COVERED
	14. SPONSORING AGENCY CODE DIBR

15. SUPPLEMENTARY NOTES

Microfiche and/or hard copy available at the Engineering and Research Center, Denver, CO

Ed: JTC

16. ABSTRACT

Analytical methods that are frequently used to predict the ultimate bearing capacities for shallow spread foundations on slopes yield widely varying solutions. As a result, the allowable foundation bearing pressures used for design are selected conservatively. This leads to the construction of shallow spread foundations that may be larger and more costly than necessary. To address this situation, the Bureau conducted a research program to evaluate the state of the art as it pertains to predicting the ultimate bearing capacity of shallow spread foundations located on or near slopes. This study consisted of developing and testing a technique for centrifugal modeling of shallow spread footings located on or near slopes; experimentally determining the maximum bearing pressure of four prototype shallow spread footings using scaled models; and comparing test results with state-of-the-art analytical solutions. Test equipment was fabricated to permit model footings to be loaded and their response to be measured at accelerations 100 times that of gravity. The model test results were compared with the results of theoretical solutions obtained using limit analysis, limit equilibrium analyses, a semiempirical method, and methods incorporating slip-line solutions.

17. KEY WORDS AND DOCUMENT ANALYSIS

a. *DESCRIPTORS--* centrifuges /bearing pressure /*bearing capacity /design strength /*foundations /foundation bearing tests /*footings /loading tests /*spread foundations /*cohesionless soils /*slopes /stress-strain relations/

b. *IDENTIFIERS--* foundation models /soil-structure interaction /limit analysis /centrifugal models

c. *COSATI Field/Group* 14B *COWRR:* 0813 *SRIM:*

18. DISTRIBUTION STATEMENT	19. SECURITY CLASS (THIS REPORT)	21. NO. OF PAGES
Available from the National Technical Information Service, Operations Division, 5285 Port Royal Road, Springfield, Virginia 22161. (Microfiche and/or hard copy available from NTIS)	UNCLASSIFIED	117
	20. SECURITY CLASS (THIS PAGE) UNCLASSIFIED	22. PRICE

REC-ERC-84-16

CENTRIFUGAL MODEL TESTS FOR ULTIMATE BEARING CAPACITY OF FOOTINGS ON STEEP SLOPES IN COHESIONLESS SOIL

by
Mark C. Gemperline

June 1984

Geotechnical Branch
Division of Research and Laboratory Services
Engineering and Research Center
Denver, Colorado

UNITED STATES DEPARTMENT OF THE INTERIOR ★ BUREAU OF RECLAMATION

ACKNOWLEDGMENTS

The author expresses thanks to Richard A. Young of the Bureau of Reclamation (Head – Soil Mechanics Section) and to Dr. Hon-Yim Ko of the University of Colorado for their valuable guidance, suggestions, and enthusiasm throughout the course of this study.

Michael B. Szygielski, Head – Project Studies Research and Computer Applications Unit; Paul C. Knodel, Chief, Geotechnical Branch; and Dr. Francis G. McLean, Chief, Division of Research and Laboratory Services, all encouraged me and provided valuable suggestions.

Also, I would like to thank Dr. Robert L. Schiffman and Dr. R. Jeffrey Dunn of the University of Colorado for their contributions. A special thanks is due Robert R. Carter for checking the analyses presented and assisting with the model testing; James M. Boernge for his assistance in writing data-plotting computer programs; Keith Bogus for assisting with the model testing; and to Mary Ann Trujillo for her editorial assistance.

The research covered by this report was funded under the Bureau of Reclamation Program-Related Engineering and Scientific Studies allocation, DR-437, *Bearing Capacity of Footings.*

CONTENTS

	Page
Introduction	1
State-of-the-art review	1
Common theoretical concepts	1
Slip-line method	1
Limit equilibrium method	2
Limit analysis method	2
General bearing capacity equation	2
Historical development of bearing capacity solutions for footings on slopes	3
Centrifugal model testing	4
Model tests	5
Scaling relations	5
Model testing program	6
Equipment	9
Centrifuge and accessories	9
Model container	12
Loading assembly	12
Recording equipment	12
Sand pouring device	12
Testing procedure	12
Test results	17
Modeling of models	19
Footing length-to-width ratio	26
Footing depth-to-width ratio	27
Footing width	27
Observations	27
Results of laboratory tests on sand	29
Introduction	29
Test program	29
Descriptive properties	29
CD triaxial shear test	29
Direct shear tests	30
Comparison of model test results with analytical methods	30
Introduction	30
Sand friction angle	30
Selected analysis conditions and results	31
Best-fit friction angle	31
Bowles' method	33
Myslivec and Kysela's method	34
Spencer's limit equilibrium method	35
Meyerhof's method	35
Hansen's method	36
Giroud's method	36
Kusakabe's method – upper-bound limit analysis	36
Discussion	37
Observed failure mechanism	37
Summary	38
Conclusions and recommendations	39
Bibliography	40

CONTENTS – Continued

Page

APPENDIXES

A Complete set of data for each of 59 footing tests 43
B Groups of bearing pressure versus relative displacement plots for tests representing conditions 1 through 17 75
C Bearing pressure versus relative displacement plots for groups of tests representing the same prototype footing width, depth, and length 87
D Photographs and sketches of observed shear surfaces for several tests 93
E Results of laboratory tests on sand 107

TABLES

Table

1 Scaling relationships for centrifugal modeling 6
2 Model test summary 7
3 Summary of test results 18
4 Best-fit friction angle and lowest average percent error 33
5 Comparison of computed values with values in Bowles' publication 34

FIGURES

Figure Page

1 Typical Bureau bridge 1
2 Graphic view of the prototype, represented by conditions 1 through 18 9
3 Model container 10
4 Model container with loading assembly attached 10
5 Model footings 11
6 Individual parts of the centrifuge 11
7 Schematic of the CCTV camera and test package in the "swung-up" position 11
8 Detailed drawing of the model container and loading assembly 13
9 Components of the loading assembly 14
10 Loading assembly 14
11 Hydraulic system flow chart 14
12 LVDT's mounted above a model footing 15
13 Schematic of the instrumentation system 15
14 Drawing of the sand pouring device 16
15 Sand pouring procedure 17
16 Illustration of the relative displacement correction 20
17a Scale versus maximum bearing pressure for test conditions 1 through 9 21
17b Scale versus maximum bearing pressure for test conditions 10 through 16 21
18 Footing length to width ratio versus maximum bearing pressure for test conditions 10 through 16 22
19a Footing depth to width ratio versus maximum bearing pressure for test conditions 4 through 9 23
19b Footing depth to width ratio versus maximum bearing pressure for test conditions 10, 11 and 18 23
20a Prototype footing width versus maximum bearing pressure for test conditions 1 through 6 24
20b Prototype footing width versus maximum bearing pressure for test conditions 10, 11, and 17 24

CONTENTS – Continued

FIGURES – Continued

Figure		Page
21a	Scale versus relative displacement at maximum bearing pressure for test conditions 1 through 9	25
21b	Footing length to width ratio versus maximum bearing pressure for test conditions 10 through 16	25
22	Footing length to width ratio versus relative displacement at maximum bearing pressure for test conditions 10 through 16	26
23a	Prototype footing width versus relative displacement at maximum bearing pressure for test conditions 1 through 6	28
23b	Prototype footing width versus relative displacement at maximum bearing pressure for test conditions 10, 11, and 17	28
24	Comparison of conditions 10 through 16 model test results with solutions by analytical methods	31
25	Comparison of condition 17 model test results with solutions by analytical methods	32
26	Comparison of condition 18 model test results with solutions by analytical methods	32
27	Average percentage error versus friction angle	32
28	Failure mechanism used in Bowles' analytical method	33
29	Failure mechanism used in Myslivec and Kysela's analytical method	34
30	Failure mechanism assumed when using the Spencer limit equilibrium approach	35
31	Failure mechanism used in Meyerhof's method of analysis	35
32	General failure mechanism used in both Hansen's and Giroud's methods of analysis	36
33	Upper-bound limit analysis failure mechanisms by Kusakabe	36

INTRODUCTION

The Bureau (Bureau of Reclamation) has found that using shallow spread footings for bridge foundations is often more cost effective than using drilled piers or piles. Bureau bridges commonly cross canals having side slopes as steep as 1.5H:1V (see fig. 1). The bridge footings are generally constructed in the slope or at the crest of the slope to minimize the bridge length, thereby minimizing costs. Analytical methods that are frequently used to predict the ultimate bearing capacity for design of shallow spread footings on slopes yield widely varying solutions. The ultimate bearing capacity calculated using one method may be 10 times greater than that calculated using another method. As a result, allowable foundation bearing capacities used to design the footings are selected conservatively. This leads to the construction of shallow spread footings that may be larger and more costly than necessary.

To address this situation, the Bureau initiated a research program to evaluate and improve the state of the art as it pertains to predicting the ultimate bearing capacity of shallow spread footings located on or near slopes.

The program involved: (a) reviewing state-of-the-art analytical solutions; (b) developing and testing a technique for modeling shallow spread foundations located on or near slopes; (c) experimentally determining the maximum bearing pressure[1] of prototype shallow spread footings using scaled models; and (d) comparing experimental results with state-of-the-art analytical solutions.

Figure 1. – Typical Bureau bridge. The canal shown has 1.5H:1V side slopes (both bridge and canal are under construction). Photo P801-D-80800

[1] Maximum bearing pressure is used to denote the largest footing pressure measured in a given model test. Ultimate bearing capacity is used to denote the largest footing pressure predicted by an analytical analysis technique.

The prototype footing and slope conditions selected for model testing reflect conditions similar to those the Bureau encounters at many bridge sites. The soil used in model testing was a medium-size sand. The slope was inclined at 33.7° (1.5H:1V), and the prototype footing widths were 4.17, 6.25, and 8.35 ft, with the footing located both on the surface and buried at the crest of the slope. Model footing widths ranged from 0.5 to 2.0 inches. Footings of both finite and infinite length were considered. The concept of "modeling of models" was applied to check the validity of the modeling procedure. This involved testing models of the same prototype at different scales and then comparing the results. Similar results indicate successful modeling.

The results of the research program are presented in this report. The state-of-the-art analytical methods are reviewed as are complete sets of model test results and laboratory test results on the model sand. The results of the model tests are compared with six readily available and frequently used bearing capacity analysis methods. These include analyses developed by Meyerhof [9][2], Hansen [10], Giroud [11], Bowles [17, 18], Kusakabe [19], and Myslivec and Kysela [15]. The results of a limit equilibrium method of analysis developed by Spencer [31] were also compared with the model test results. The model test results provide information necessary to evaluate these various methods of computing allowable bearing pressures for the design of footings on steep slopes in cohesionless soil.

STATE-OF-THE-ART REVIEW

Common Theoretical Concepts

The slip-line, limit equilibrium and limit analysis methods are the most common theoretical approaches to solving bearing capacity problems. These methods were first applied to the simple case of an infinitely long shallow footing on a horizontal ground surface and later adapted for use with footings of various shapes on ground surfaces having various geometries. An in-depth discussion of these three basic approaches and their origins are found in *Limit Analysis and Soil Plasticity* by Chen [1]. Portions of the following discussion were obtained from that publication.

Slip-line method. – Impending plastic flow of soil beneath a footing occurs when a sufficiently large region of the soil mass is stressed to its yield condition. The result of this condition is unrestricted

[2] Numbers in brackets refer to entries in the bibliography.

(plastic) flow of the soil beneath the footing. With the slip-line method, equilibrium and yield conditions in the soil mass near the footings are satisfied at the instant of impending plastic flow. A set of differential equations of plastic equilibrium may be derived by combining a yield criterion for soils (usually the Mohr-Coulomb criterion) with the equations of equilibrium. Combined with stress boundary conditions, this set of differential equations can be used to determine the stresses in the zone of the soil mass considered to be in plastic equilibrium beneath the footing. The equations are conveniently transformed into curvilinear coordinates defining a line in the yielded region, which coincides with the direction of failure or slip. These slip directions are known as slip lines, and the network is called the slip-line field.

Koetter [2] was the first to derive these slip-line equations for the case of plane deformations and Prandtl [3] was the first to obtain an analytical closed-form solution for a footing on a weightless soil mass. These methods have been applied to many footing bearing capacity problems.

The mathematical slip-line solution is complicated by the soil weight. Sokolovskii [4] adopted a numerical procedure based on finite difference approximation of slip-line equations. He solved problems dealing with the bearing capacity of footings for which closed-form solutions could not be found. A graphical procedure was developed by de Jong [5] to approximate the solution. Others, such as Spencer [6] and Dembicki [7], obtained approximate solutions by using perturbation and series expansion methods.

A weakness of the slip-line method is its neglect of the stress-strain relationship of the soil; only the equilibrium and yield conditions are used. Also, stresses in the soil mass are not defined beyond the zone considered to be in plastic equilibrium; therefore, equilibrium conditions might be satisfied everywhere in the soil mass.

Limit equilibrium method. – The limit equilibrium method has traditionally been used to obtain approximate solutions for stability problems in soil mechanics. This method entails assuming failure surfaces of various simple shapes (plane, circular, or log spiral) and satisfying the equations of equilibrium and yield conditions on these surfaces. Stability problems reduce to one of finding the least stable shape and position for the failure surface. In this method it is necessary to assume stress distributions along the failure surface. This approach makes it possible to solve bearing capacity problems by simple statics. The limit equilibrium method gives a satisfactory solution to bearing capacity problems, although it does not consider soil kinematics, and equilibrium conditions are satisfied only on an assumed failure surface, not necessarily throughout the entire soil mass.

Limit analysis method. – In the limit analysis method stress-strain relationships are used to determine whether given stress and displacement states agree and whether a unique solution exists. The stress-strain relationship of soil is considered in an idealized manner. This idealization, termed the "flow rule," establishes the limit theorem on which limit analysis is based.

This method, when applied to bearing capacity problems, yields an upper bound and a lower bound to the ultimate bearing capacity. When the upper and lower bound are the same, the exact limit analysis solution has been found.

The lower bound theorem of limit analysis may be stated as follows: If a statically admissible stress distribution can be found, uncontained plastic flow will not occur at a lower pressure. The lower bound considers only equilibrium and yield conditions; it gives no consideration to soil kinematics.

The upper bound theorem states that if a kinematically admissible velocity field can be found, uncontained plastic flow must be impending or has taken place. In other words, pressures determined by equating the externally applied energy to internal energy dissipation in an assumed deformation mode (satisfying velocity boundary conditions and strain and velocity compatibility conditions) are not less than the actual collapse pressure. The upper bound theorem considers only failure modes and energy dissipations. The stress distribution of the soil mass involved need not be in equilibrium.

By suitable choice of stress and velocity fields, the upper and lower bound theorems enable the ultimate bearing capacity pressure of the footing to be bracketed.

Limit analysis considers stress equilibrium within the soil mass, soil stress-strain relationships, and the compatibility between soil strain and displacement. This method assumes small strains, an idealized stress-strain soil behavior, coincidence of the direction of principal strain rate with the direction of principal stresses, and perfect elastic-plastic soil behavior. The method is easy to apply and has been found to yield satisfactory solutions.

General bearing capacity equation. – Many authors have derived theoretical and empirical solutions to problems pertaining to the bearing capacity of shallow foundations. Typically, these solutions take

the form of the general bearing capacity equation. The basic equation was developed around 1943 by Buisman, Cargaot, and Terzaghi. In Terzaghi's notation, it takes the following form:

$$Q/B = cN_c + \bar{q}N_q + 0.5\gamma BN_\gamma \quad (1)$$

This formula was developed for an infinitely long footing of width B, placed upon a horizontal soil surface. The soil has a unit weight, γ; and cohesion, c. The unit surcharge acting on the soil surface outside the foundation is $\bar{q}$, and Q/B is the ultimate bearing pressure per unit foundation length, provided that it is loaded centrally and vertically. N_c, N_q, and N_γ are dimensionless bearing capacity factors dependent on the soil friction angle, ϕ.

The literature contains many proposed values for the bearing capacity factors N_c, N_q, and N_γ. Differences in N_c and N_q values are relatively insignificant; however proposed N_γ values differ by as much as 150 percent.

Actual foundations deviate from the simple case considered above in several respects. Loads may be eccentric or inclined, or the footing may be placed below the surface. Of course, each foundation has a finite length and a shape that may be other than rectangular. Finally, the foundation base, ground surface, or both may be inclined. Additional factors are applied to the three terms in the bearing capacity equation to permit its use with various boundary conditions.

When these factors are applied the bearing capacity equation takes the form:

$$Q/B = cN_c s_c d_c i_c g_c b_c + \bar{q}N_q s_q d_q i_q g_q b_q + 0.5\gamma BN_\gamma s_\gamma d_\gamma i_\gamma g_\gamma b_\gamma \quad (2)$$

where:
- s = shape factors
- d = depth factors
- i = load inclination factors
- g = ground slope inclination factors
- b = footing base inclination factors

The factors have been derived from observations in engineering practice, from theory, and from model test results.

Another method used to account for changing boundary conditions is to simply derive the bearing capacity factors, N_c, N_q, and N_γ, to fit the conditions. The application of this method and the application of additional factors as they pertain to footings on slopes are demonstrated later in this report.

The actual load-carrying capacity of a footing depends on the permissible movement as well as the load it can safely carry without collapsing completely. The general bearing capacity equation, like all analytical methods discussed in this report, deals only with the state of complete collapse, giving no consideration to tolerable footing movements.

Historical Development of Bearing Capacity Solutions for Footings on Slopes

Many methods of footing bearing capacity analysis have been developed, and a large number of model tests have been conducted. This historical account is limited to the methods and model tests dealing specifically with shallow foundations of finite width adjacent to sloping ground surfaces.

Tests of model footings on slopes were conducted and reported by Peynircioglu [8] in 1948. These were the first recorded tests of this nature. Small footings of circular, square, and rectangular shapes were tested on a 20° (approximately 2.75H:1V) slope of cohesionless material. The purpose of the testing was to define the failure mechanism of footings on slopes. Actual loads were not reported. Peynircioglu concluded from his tests that: "The bearing capacity of a shallow foundation on the horizontal top surface of a sand fill can be determined by means of methods based upon the plastic equilibrium." No specific method of analysis was presented.

In 1956, slip-line theory was applied by Meyerhof to derive bearing capacity factors for the case of footings on slopes. Meyerhof combined the N_c and N_q factors and the N_γ and N_q factors of the general bearing capacity equation to form factors N_{cq} and $N_{\gamma q}$ used in the following equation:

$$Q/B = cN_{cq} + \frac{\gamma BN_{\gamma q}}{2} \quad (3)$$

Equation 3 gives the ultimate bearing capacity of the soil. This method, like all methods discussed in this report, does not take into consideration the friction along the vertical sides of the footing. In his 1957 paper, Meyerhof [9] writes: "While the theoretical mechanism of foundation failure is supported by previous observations of soil movements below model footings on sand slopes, no published information on the ultimate bearing capacity of foundations on slopes in practice appears available yet as a check."

The "previous observations" referred to by Meyerhof were those of Peynircioglu. Today, Meyerhof's method is probably the most widely used approach to solving problems pertaining to the ultimate bearing capacity of footings on slopes.

Around 1968, Hansen [10] developed correction factors for the three terms in the general bearing capacity equation to make it usable for footings located on sloping ground surfaces. Hansen, like Meyerhof, used the slip-line theory. However, Hansen treated the surcharge load differently than Meyerhof did. Also different from Meyerhof's was the method Hansen used to account for the soil self-weight. Hansen proposed correction factors g_c, g_q, and g_γ for use in equation 2.

In 1971, Giroud and Tran-Vo-Nhiem reported a slip-line solution, which was similar to that developed by Hansen in 1968. They conducted tests on small models using an analog soil (modeled using aluminum rods) as well as sand to verify the method. Their work is reported in a French publication [11]. An English translation was not found.

In 1974, Dembicki and Zadroga [12] presented the results of extensive model tests dealing specifically with footings on and near slopes. These model footings were tested on both real sand and soil modeled using aluminum rods. The tests considered the effects of load eccentricity and inclination, proximity of the footing with respect to the top of the slope, footing depth, and footing width. The slope angles ranged from 0° to 30° (horizontal to about 1.75H:1V). Dembicki and Zadroga compared their experimentally derived ultimate bearing capacity values with those computed using Meyerhof's, Hansen's, and Giroud's analytical methods. They found that the analytical methods yielded lower values than those found experimentally.

A limit analysis solution to the problem of a footing on a slope of weightless material was reported by Chen [1] in 1975.

In 1977, Shields et al. [13] reported the results of testing model footings on slopes of cohesionless soil. The tests were conducted on footings approximately 1 foot wide and on slopes inclined at 20° (about 2.75H:1V). The results were compared with solutions obtained using Meyerhof's and Giroud's analytical solutions. Shields et al. stressed the importance of friction angle selection on the computed bearing capacity. Their work showed that Meyerhof's and Giroud's methods overestimate or underestimate the actual bearing capacity, depending upon how ∅ is evaluated.

In 1978, an article entitled "Limiting Equilibrium Analysis of Strip Footings," by Craig and Parit [14], discussed the application of the Morgenstern and Price slope stability analysis to the problem of bearing capacity of footings on slopes.

In the same year, another limit equilibrium approach was presented in the book, *The Bearing Capacity of Building Foundations,* by Myslivec and Kysela [15]. A graphical solution was presented in the text. A numerical solution to this method was developed by Gemperline in 1980 and written into a computer program called BEARCAP [16]. It is currently used by the Bureau for the analysis of shallow spread footings for bridge foundations near slopes.

Bowles presented an empirical solution in the 1978 and 1981 editions of his book, *Foundation Analysis and Design* [17]. He proposed reduced values for the N_c and N_q terms in the general bearing capacity equation. These reduced values are obtained by multiplying the original values by the ratio of the simple geometric relationships of an assumed failure mechanism of a footing on a horizontal ground surface and an assumed failure mechanism of a footing on a sloping surface.

In 1981, Kusakabe et al. [19] derived the upper bound limit analysis solution to the problem of a footing on a slope of cohesionless or cohesive soil with soil self-weight included. They compared the analytical method with experimental model test results and found that it yielded conservative values.

Also in 1981, Bilz, Broedel, and Reinhardt [20] presented a method of calculating the stability of slopes subjected to three-dimensional surcharge loads of finite size, which incorporated a limiting equilibrium approach.

A 1982 publication by Mikhailov [21] discussed the development of a numerical computer solution for the slip-line method for soil having a finite density. This method dealt specifically with footings on the edge of an embankment.

In 1983, Azzouz and Baligh [22] compared three-dimensional stability analyses of undrained cohesive slopes subjected to square loaded areas with two-dimensional (plane strain) solutions.

The use of a general slope stability computer program to solve bearing capacity problems is briefly discussed in a 1981 Bureau publication [23]. The Spencer limit equilibrium method is incorporated in this program.

Centrifugal Model Testing

The idea of using small-scale models to study a physical phenomenon is common in many fields of engineering, including geotechnical engineering. However, geotechnical scaled models have a serious lack of similitude because stress levels in the soil model do not match those in the full-scale prototype. Modeling soil stress conditions is important because soil stress-strain and strength characteristics are functions of the stress state. This modeling may be

accomplished by artificially increasing the weight of the soil used in the models. The centrifuge is the best tool to produce an artificially high gravity, making model material seem heavier.

There are many difficulties involved in centrifugal modeling that are not encountered in standard modeling procedures. These include equipment vibration; scale, geometric, and boundary anomalies; effects of coriolis acceleration; and the accuracy of instrumentation under high acceleration. Despite these difficulties, use of the centrifuge in the past 2 decades has become an increasingly popular means of modeling geostructures.

Fillips [24], a French engineer, made the earliest suggestion (1869) for using a centrifuge to properly simulate the effects of self-weight in models of engineered structures. His suggestion was related to the self-weight stress in structural beams. Because this is of minor importance in construction, the modeling was not performed.

Bucky [24], an American, proposed the centrifugal modeling technique of simulating self-weight in models of mines in 1931. Two Soviet scientists, Pokrovsky and Davidenkov, performed similar research in 1932, independent of Bucky.

The technique did not achieve widespread acceptance in the United States, although Bucky, Panek, Clark, and others continued research using the technique. In contrast, the Soviet Union built over 50 centrifuges for geotechnical model testing of dams, foundations, earthfill embankments, etc., from 1932 to 1980 [24].

The Soviet use of centrifugal modeling was highly project oriented. Answers were sought for specific design questions on particular projects. After completion of the project many centrifuges were dismantled. As a consequence, Soviet scientists found it difficult to carry out research necessary to verify the effectiveness of centrifugal modeling with experimental evidence.

During the 1960's and 1970's, several centrifuges were built in England under the leadership of Roscoe, Rowe, and Schofield. Following their lead, the United States, Denmark, Sweden, Netherlands, France, and Japan developed centrifugal modeling facilities.

The centrifuge at the University of Colorado in Boulder, Colorado, was used in this study. It was built in 1978 and is one of approximately seven existing geotechnical centrifuge testing facilities constructed in the United States in the past 10 years.

Since 1975, three independent model footing studies have been conducted using centrifugal modeling techniques. These studies were performed by Ovesen [25], of the Danish Engineering Academy; Mikasa and Takada [26], of Osaka University, Japan; and Hardy and Townsend [27], at the University of Florida. All stress the importance and show the validity of centrifugal modeling. None of these centrifugal bearing capacity model studies attempted to investigate the effects of a sloping ground surface on model behavior.

MODEL TESTS

Scaling Relations

The basic approach to centrifugal modeling is explained as follows. If a model of a prototype structure is built with dimensions reduced by a factor $1/n$, then an acceleration field of n times g (where g is the acceleration due to gravity) is required for the self-weight stresses in the model to be similar to those of the prototype structure. If the same material is used in the model as in the prototype, the soil will develop the same state of deformation at homologous points of the structure. A set of scaling factors are developed for the various physical parameters that characterize the behavior so that model performance can be related to the prototype behavior.

These relationships were established using methods of dimensional analysis and analyzing differential equations governing soil, soil water, and soil structure behavior [24]. These scaling relationships are presented in table 1.

The concept of centrifugal model testing as it pertains to footings on sand slopes is to expose a model of a full-scale prototype, built to a length scale of $1/n$, to an artificial gravity field.

This artificial gravity field is generated by a centrifuge and has an acceleration of n times g. The same sand that forms the prototype slope is used in the model. The centrifugal model deviates from the prototype in two ways: first, the similarity requirement on sand grain size is not fulfilled because the prototype sand is used in the model; and second, the boundary conditions imposed by confinement in a model container are different from the boundary conditions of the prototype. The concept of "modeling of models" is applied to test the validity of the scaling relations and the significance of changing boundary conditions.

The application of the concept of "modeling of models" results in scale effects being studied by comparing the results of model tests conducted at different scales representing the same prototype. In this study, it involved testing footing and slope models of a specific prototype at different scales, then comparing the test results. If the model test

Table 1. – Scaling relationships for centrifugal modeling.

Quantity	Full scale (prototype)	Centrifuge model at n g's
Linear dimension	1	$1/n$
Area	1	$1/n^2$
Volume	1	$1/n^3$
Time		
Dynamic events	1	$1/n$
Hydrodynamic events	1	$1/n^2$
Viscous flow	1	1
Velocity (distance/time)	1	n
Acceleration (distance/time^2)	1	n
Mass	1	$1/n^3$
Force	1	$1/n^2$
Energy	1	$1/n^3$
Stress (force/area)	1	1
Strain (displacement/unit length)	1	1
Density	1	1
Frequency	1	n

Source: *Principles of Geotechnical Physical Modeling,* University Extension, University of California, Davis, California, 1982.

results from tests conducted in the centrifuge at different scales representing a specific prototype were identical, then it was concluded that the scaling relations were valid and that differing boundary conditions did not significantly influence the test results. The models used in this program were scaled at 1/50, 1/66.7, and 1/100 of the prototype size.

Model Testing Program

To execute the model testing program, a centrifuge owned by the University of Colorado Civil and Environmental Engineering Department was rented and operated by Bureau personnel. The results of 59 model tests representing 18 prototype footing and slope conditions and scales are discussed in this report. This slope geometry, footing sizes, and footing locations were selected to represent conditions common to Bureau bridge foundations near canal side slopes. The conditions were selected to accomplish four other tasks: (1) to provide a means of evaluating model scaling relationships; (2) to provide information needed to evaluate the performance of the test procedures and equipment; (3) to provide a means of evaluating the effects that changing footing length-to-width ratio, footing depth-to-width ratio, and footing width may have on maximum bearing pressure and relative footing displacement; and (4) to provide the data required to evaluate existing analytical bearing capacity methods.

Table 2 is a summary of the test conditions. A minimum of three tests were conducted for each test condition. Only two tests are reported for conditions 1 and 2 because one test representing each of these conditions was discarded for test irregularities. The test numbers correspond to the testing order. The ground surface slope used in all tests was 33.67° (1.5H:1V) above horizontal. The prototype slope height was a constant 25 feet. The model slope heights ranged from 3 to 6 inches. The footing was located on the surface at the crest of the slope or buried at a depth equal to its width at the crest of the slope. Prototype footing widths were 4.17, 6.25, and 8.33 feet. Model footings ranged from 0.5 to 2.0 inches. The conditions tested are shown on figure 2.

Table 2. – Model test summary.

Test condition	Test No.	Prototype characteristics			Scale	Model characteristics			Dimensionless parameters		
		Footing width (ft)	Footing depth (ft)	Footing length (ft)		Footing width (in)	Footing depth (in)	Footing length (in)	Footing depth to footing width ratio	Footing length to footing width ratio	Footing length to box width ratio
1	3	8.33	0.0	Infinite	1/50	2.00	0.0	5.90	0.0	3.0	0.98
	20	8.33	0.0	Infinite	1/50	2.00	0.0	5.90	0.0	3.0	0.98
2	21	8.33	0.00	Infinite	1/66.7	1.50	0.0	5.90	0.0	3.9	0.98
	25	8.33	0.00	Infinite	1/66.7	1.50	0.0	5.90	0.0	3.9	0.98
3	8	8.33	0.00	Infinite	1/100	1.00	0.0	5.90	0.0	5.9	0.98
	11	8.33	0.00	Infinite	1/100	1.00	0.0	5.90	0.0	5.9	0.98
	16	8.33	0.00	Infinite	1/100	1.00	0.0	5.90	0.0	5.9	0.98
4	1	4.17	0.00	Infinite	1/50	1.00	0.0	5.90	0.0	5.0	0.98
	2	4.17	0.00	Infinite	1/50	1.00	0.0	5.90	0.0	5.0	0.98
	5	4.17	0.00	Infinite	1/50	1.00	0.0	5.90	0.0	5.0	0.98
5	4	4.17	0.00	Infinite	1/66.7	0.75	0.0	5.90	0.0	7.9	0.98
	9	4.17	0.00	Infinite	1/66.7	0.75	0.0	5.90	0.0	7.9	0.98
	23	4.17	0.00	Infinite	1/66.7	0.75	0.0	5.90	0.0	7.9	0.98
	26	4.17	0.00	Infinite	1/66.7	0.75	0.0	5.90	0.0	7.9	0.98
6	7	4.17	0.00	Infinite	1/100	0.50	0.0	5.90	0.0	11.8	0.98
	18	4.17	0.00	Infinite	1/100	0.50	0.0	5.90	0.0	11.8	0.98
	24	4.17	0.00	Infinite	1/100	0.50	0.0	5.90	0.0	11.8	0.98
7	14	4.17	4.17	Infinite	1/50	1.00	1.0	5.90	1.0	5.9	0.98
	15	4.17	4.17	Infinite	1/50	1.00	1.0	5.0	1.0	5.9	0.98
	22	4.17	4.17	Infinite	1/50	1.00	1.0	5.0	1.0	5.9	0.98
8	13	4.17	4.17	Infinite	1/66.7	0.75	0.75	5.90	1.0	5.9	0.98
	19	4.17	4.17	Infinite	1/66.7	0.75	0.75	5.90	1.0	5.9	0.98
	12	4.17	4.17	Infinite	1/66.7	0.75	0.75	5.90	1.0	5.9	0.98
9	6	4.17	4.17	Infinite	1/100	0.50	0.50	5.90	1.0	5.9	0.98
	10	4.17	4.17	Infinite	1/100	0.50	0.50	5.90	1.0	5.9	0.98
	17	4.17	4.17	Infinite	1/100	0.50	0.50	5.90	1.0	5.9	0.98
10	31	4.17	0.0	21.7	1/66.7	0.75	0.0	3.90	0.0	5.2	0.65
	32	4.17	0.0	21.7	1/66.7	0.75	0.0	3.90	0.0	5.2	0.65
	33	4.17	0.0	21.7	1/66.7	0.75	0.0	3.90	0.0	5.2	0.65
	34	4.17	0.0	21.7	1/66.7	0.75	0.0	3.90	0.0	5.2	0.65
11	38	4.17	0.0	21.7	1/100	0.50	0.0	2.60	0.0	5.2	0.43
	39	4.17	0.0	21.7	1/100	0.50	0.0	2.60	0.0	5.2	0.43
	40	4.17	0.0	21.7	1/100	0.50	0.0	2.60	0.0	5.2	0.43
	45	4.17	0.0	21.7	1/100	0.50	0.0	2.60	0.0	5.2	0.43
12	57	4.17	0.0	10.4	1/50	1.00	0.0	2.50	0.0	2.5	0.42
	58	4.17	0.0	10.4	1/50	1.00	0.0	2.50	0.0	2.5	0.42
	59	4.17	0.0	10.4	1/50	1.00	0.0	2.50	0.0	2.5	0.42

Table 2. – Model test summary — Continued

Test condition	Test No.	Prototype characteristics			Scale	Model characteristics			Dimensionless parameters		
		Footing width (ft)	Footing depth (ft)	Footing length (ft)		Footing width (in)	Footing depth (in)	Footing length (in)	Footing depth to footing width ratio	Footing length to footing width ratio	Footing length to box width ratio
13	54	4.17	0.00	10.4	1/66.7	0.75	0.0	1.87	0.0	2.5	0.32
	55	4.17	0.00	10.4	1/66.7	0.75	0.0	1.87	0.0	2.5	0.32
	56	4.17	0.00	10.4	1/66.7	0.75	0.0	1.87	0.0	2.5	0.32
14	27	4.17	0.0	32.5	1/100	0.50	0.0	3.90	0.0	7.8	0.65
	28	4.17	0.0	32.5	1/100	0.50	0.0	3.90	0.0	7.8	0.65
	29	4.17	0.0	32.5	1/100	0.50	0.0	3.90	0.0	7.8	0.65
	30	4.17	0.0	32.5	1/100	0.50	0.0	3.90	0.0	7.8	0.65
15	41	4.17	0.0	38.3	1/100	0.50	0.0	4.60	0.0	9.2	0.77
	42	4.17	0.0	38.3	1/100	0.50	0.0	4.60	0.0	9.2	0.77
	43	4.17	0.0	38.3	1/100	0.50	0.0	4.60	0.0	9.2	0.77
	44	4.17	0.0	38.3	1/100	0.50	0.0	4.60	0.0	9.2	0.77
16	46	4.17	0.0	44.2	1/100	0.50	0.0	5.30	0.0	10.6	0.88
	47	4.17	0.0	44.2	1/100	0.50	0.0	5.30	0.0	10.6	0.88
	48	4.17	0.0	44.2	1/100	0.50	0.0	5.30	0.0	10.6	0.88
	49	4.17	0.0	44.2	1/100	0.50	0.0	5.30	0.0	10.6	0.88
17	50	6.25	0.0	32.5	1/100	0.75	0.0	3.90	0.0	5.2	0.65
	51	6.25	0.0	32.5	1/100	0.75	0.0	3.90	0.0	5.2	0.65
	52	6.25	0.0	32.5	1/100	0.75	0.0	3.90	0.0	5.2	0.65
	53	6.25	0.0	32.5	1/100	0.75	0.0	3.90	0.0	5.2	0.65
18	35	4.17	4.17	21.7	1/66.7	0.75	0.75	3.90	1.0	5.2	0.65
	36	4.17	4.17	21.7	1/66.7	0.75	0.75	3.90	1.0	5.2	0.65
	37	4.17	4.17	21.7	1/66.7	0.75	0.75	3.90	1.0	5.2	0.65

The prototype test conditions may be grouped as follows:

1. Conditions 1 through 9 consisted of plane strain tests; that is, the footing length was nearly equal to the model container width, thereby limiting soil displacement to a single phase (two dimensions). These conditions represent strip footings; i.e., footings with large length-to-width ratio. The model footing length in all tests was 5.9 in. A 0.05-in space existed between the model container walls and the ends of the model footing at the start of each test.

   a. Conditions 1, 2, and 3 were conducted with a prototype footing width *(B)* equal to 8.33 feet and a footing depth (*D*) equal to 0 feet at scales (1/*n*) equal to 1/50, 1/66.7, and 1/100, respectively.

   b. Conditions 4, 5, and 6 used B = 4.17 ft, D = 0 ft, and $1/n$ = 1/50, 1/66.7, and 1/100, respectively.

   c. Conditions 7, 8 and 9 used B = 4.17 ft, D = 4.17 ft, and $1/n$ = 1/50, 1/66.7, and 1/100, respectively.

2. Conditions 10 through 18 were termed three-dimensional tests because the footing lengths were significantly less than the model container width, thereby permitting soil displacement in three directions.

   a. Conditions 10 through 16 were conducted with B = 4.17 ft and D = 0 at various scales (1/*n*), with length-to-width (*L/B*) ratios between 2.5 and 11.8.

PROTOTYPE CONDITIONS (FEET)

Condition	D	B	L
1	0	8.33	infinite
2	0	8.33	infinite
3	0	8.33	infinite
4	0	4.17	infinite
5	0	4.17	infinite
6	0	4.17	infinite
7	4.17	4.17	infinite
8	4.17	4.17	infinite
9	4.17	4.17	infinite
10	0	4.17	21.7
11	0	4.17	21.7
12	0	4.17	10.4
13	0	4.17	10.4
14	0	4.17	32.5
15	0	4.17	38.3
16	0	4.17	44.2
17	0	6.25	32.5
18	4.17	4.17	21.7

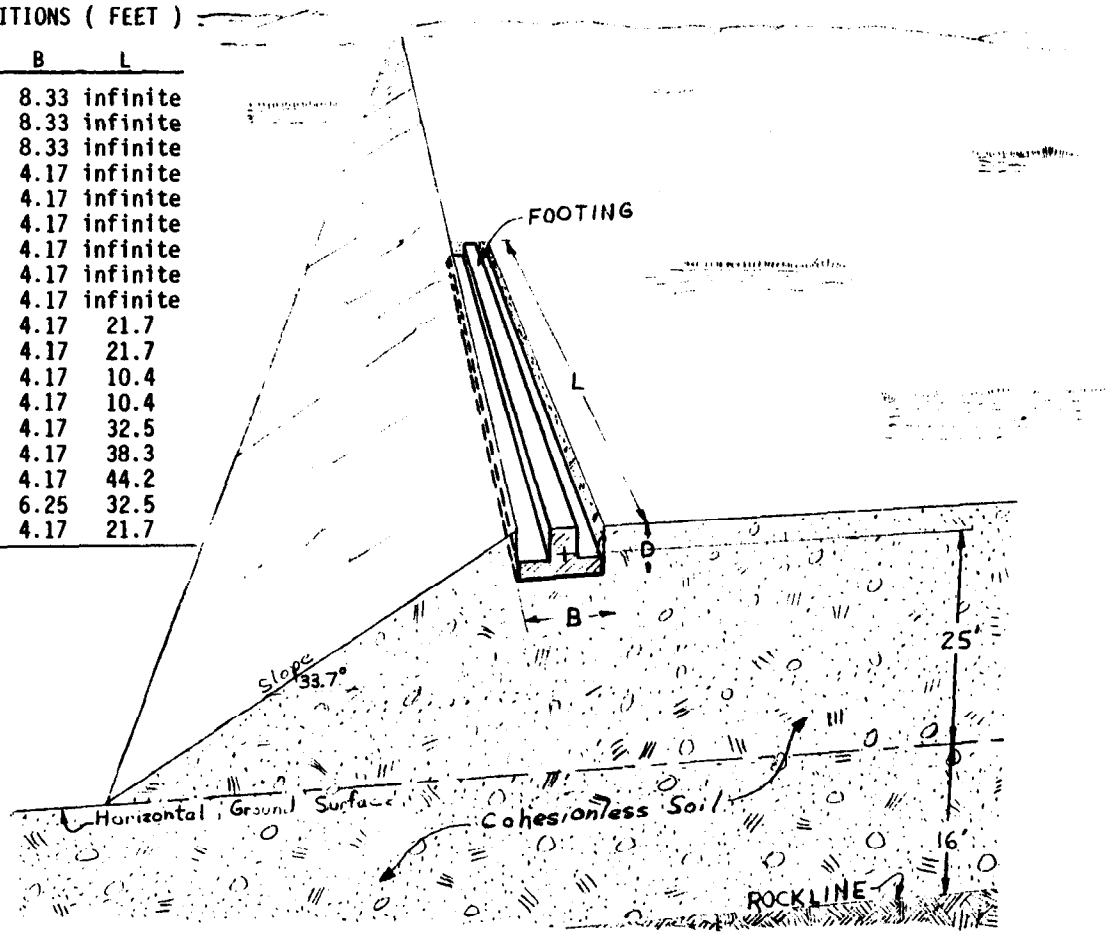

Figure 2. – Graphic view of the prototype, represented by conditions 1 through 18.

b. Condition 17 used B = 6.25 ft, D = 0 ft, L/B = 5.2, and $1/n$ = 1/100.

c. Condition 18 used B = 4.17 ft, D = 4.17 ft, L/B = 5.2, and $1/n$ = 1/66.7.

Equipment

The container in which the model slopes were constructed (see fig. 3) had inside dimensions of 11.5 in (deep), 5 in (wide), and 16 in (long). One side of the container was a Plexiglas plate through which the model was viewed. A hydraulic cylinder was attached to a load frame mounted on top of the model container (see fig. 4). The hydraulic cylinder was used to apply vertical loads to the model footings. A load cell located above the footing and attached to the hydraulic cylinder rod was used to register the force applied to the footing during the tests.

The load frame and hydraulic cylinder were easily removed for specimen placement. Rectangular-shaped model footings were constructed of aluminum (see fig. 5). The dimensions of the model footings were chosen so that the footings could be considered rigid. Throughout each test the footing was fixed so that it would rotate in the plane parallel to the Plexiglas. The vertical footing load, vertical footing displacement, and centrifuge speed were recorded. The tests were displacement controlled by regulating the flow of oil into the hydraulic cylinder. A flow control valve was used to regulate the oil flow rate. Because the flow rate varied with changes in the oil pressure in the hydraulic cylinder, a constant footing displacement rate was not achieved. This is discussed in more detail later in this report.

Centrifuge and Accessories. – The centrifuge used in the research program was a modified version of a Genesco Model 1230-5G accelerator. Figure 6 shows the centrifuge system with individual parts labeled. The radius of the centrifuge measured to the base of the swing basket was 53.5 in, and the weight capacity was 20 000 g-lb (10 g-ton).

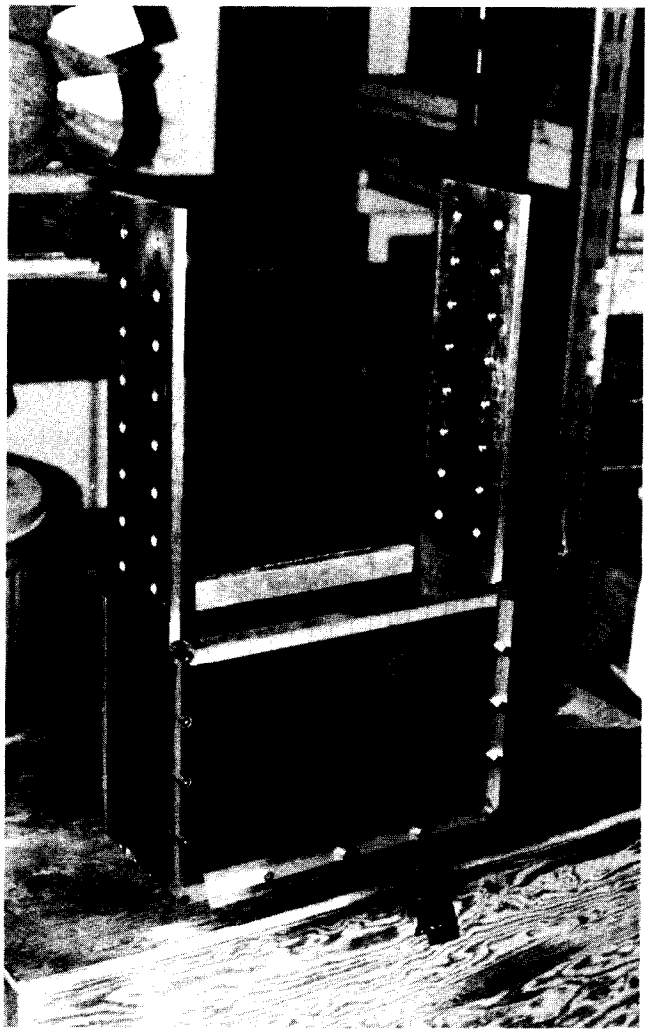

Figure 3. – Model container. Photo P801-D-80801

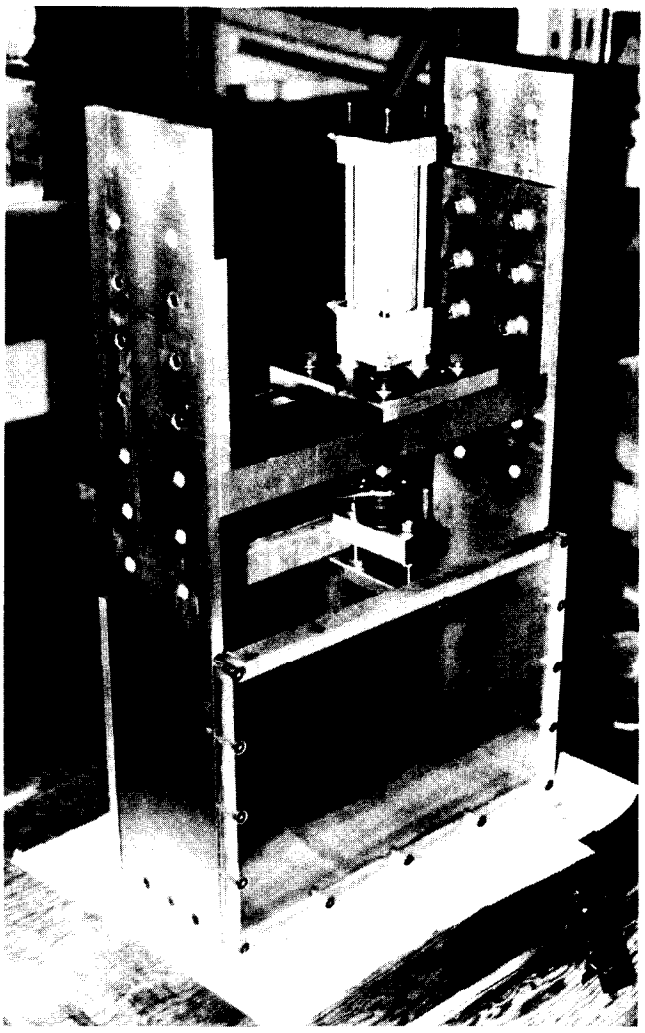

Figure 4. – Model container with loading assembly attached. Photo P801-D-80802

Four essential parts of the centrifuge were the electrical slip-ring assembly, hydraulic rotary joint assembly, swing baskets, and a CCTV (closed circuit television) camera.

The slip-ring assembly, consisting of 56 rings, was mounted on the lid of the enclosure over the main drive shaft. This assembly was used to transmit current both to the CCTV camera and to illuminate the test package. The slip-ring assembly was also used to transmit instrumentation signals back from the model.

The hydraulic rotary joint assembly was mounted on the axis of the centrifuge and above the electrical slip rings. During operation this provided a continuous flow of hydraulic oil from a pump outside the centrifuge to the hydraulic cylinder mounted on the model container inside the centrifuge. Two hydraulic transmission lines with pressure ratings of 3,000 lb/in^2 were used.

Two swing baskets were hinged to the ends of the rotating arm. One was used to mount a test package consisting of a model container and a mirror. The maximum allowable dimensions of the test package base on the basket were 18 by 18 inches. The other basket was used to carry the counterweights needed to balance the centrifuge.

The CCTV was mounted close to the axis of rotation and was focused on the test package. This permitted observing and recording the behavior of the model during the testing process. The CCTV monitor was connected to the slip-ring assembly and from there to a video recorder outside the centrifuge. A schematic drawing showing the CCTV camera and the test package in the "swung up" position are shown on figure 7.

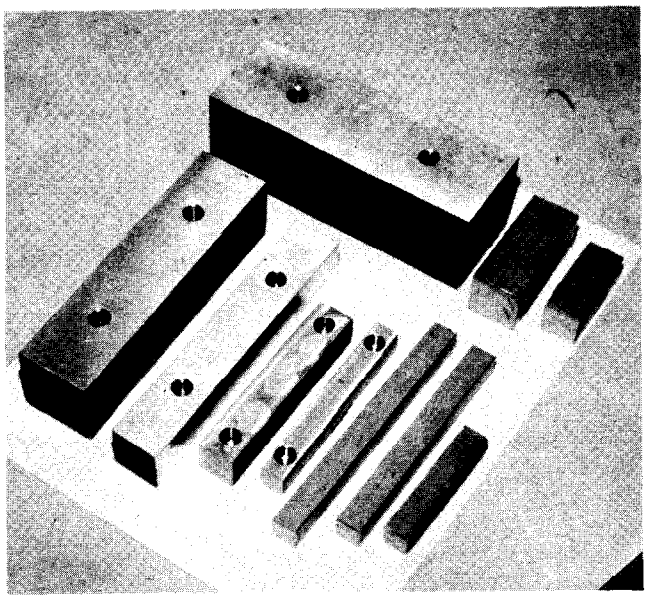

Figure 5. – Model footings. Photo P801-D-80803

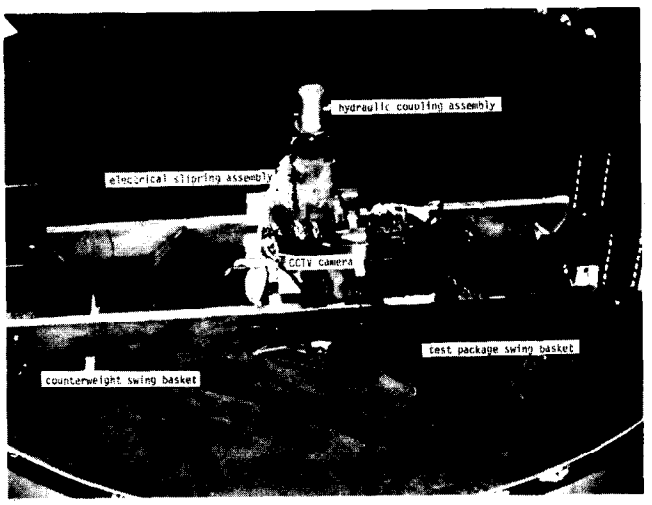

Figure 6. – Individual parts of the centrifuge. Photo P801-D-80804

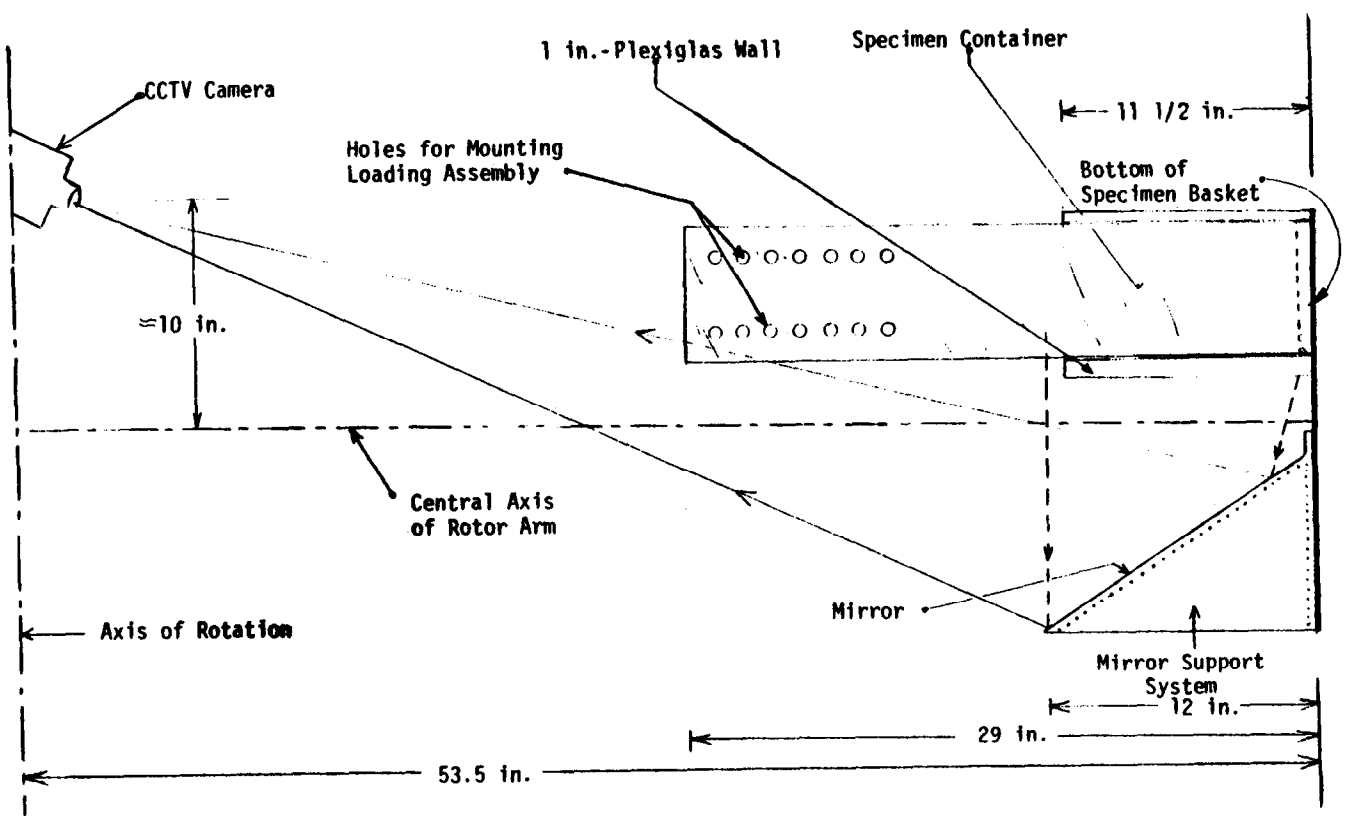

Figure 7. – Schematic of the CCTV camera and test package in the "swung-up" position.

Model Container. – A detailed drawing of the model container and loading assembly is provided on figure 8 and a photograph is shown on figure 4. The container had inside dimensions of 6 by 16 by 11½ in. Three sides and the bottom of the model container were constructed of ½-inch-thick 7075-T6 aluminum. The remaining side was made of 1-inch-thick Plexiglas.

Two ⅛-inch-thick sheets of Margard, a type of Plexiglas specially treated to increase scratch resistance, were placed against the 1-inch-thick Plexiglas side and against the opposite ½-inch-thick aluminum side. (Margard is a product of the General Electric Company, Plastics Division.) The treated surface was exposed to the inside of the model container. One-inch grids and model slope locations were drawn on the ⅛-inch Margard sheets, which were placed against the model container with the inked surfaces against the 1-inch Plexiglas side and the opposite ½-in aluminum container side. This was done so the ink would not be exposed to the abrasive action of the sand. The grids and slope lines were used during model construction and for determining the shear surface location after testing. Two sides of the model container were extended above the remaining two sides to support the loading assembly.

Loading Assembly. – The loading assembly consisted of a load frame, hydraulic cylinder, rod extension, load cell, loading head, and model footing. These are all shown in detail on figure 8. A photograph showing some of these components is included on figure 9.

Figure 9 also shows the LVDT (linear variable differential transformer), the LVDT mounting bracket, and the rod support plate. The photograph on figure 10 shows the assembly.

The hydraulic cylinder was a Milwaukee cylinder model LH10, NFPA style, MX1, with a 4-in stroke, 2-in piston diameter, ⅝ in rod diameter, and a 4,700-lb load limit. The hydraulic cylinder was operated remotely through the hydraulic rotary joints located on the axis of the centrifuge. An electrically powered hydraulic pump was used in conjunction with a flow control and pressure control valve to pressurize the hydraulic cylinder. The hydraulic system flow chart is shown on figure 11.

The model footings ranged in size from 2-in wide, 2-in high, and 6-in long, to 0.5-in wide, 0.5-in high, and 2.8-in long. All footings had square ends (see fig. 5).

Beowolf model 428, 1,000- and 5,000-lb-capacity load cells were used to measure the vertical load applied to the footing model by the hydraulic cylinder. These were statistically calibrated in the laboratory.

Two Shaevitz LVDT's, which measured vertical displacement of the model footing, were mounted to the load frame directly over the model footing, as shown on figure 12. The maximum displacement range of the LVDT's was ½ inch.

Voltage signals from the two LVDT's and the load cell were transmitted through three sets of slip rings to the recording equipment outside the centrifuge.

Recording Equipment. – The voltage signals from the LVDT's and load cell transmitted through the slip rings were conditioned, digitized, and recorded on paper automatically at equal time intervals (generally 3 or 4 s). An X-Y-Y analog recorder was used as a backup for the digital recorder. A schematic of the instrumentation is shown on figure 13.

The centrifuge was equipped with an optical speed measuring device. A constant centrifuge speed (measured in r/min) was maintained during each test. The speed was monitored and recorded in a logbook.

Sand Pouring Device. – Model slopes were constructed of air-dried, poorly graded sand, which was poured from a constant height into the model container in shallow lifts. This produced a uniform deposit at nearly 100-percent relative density. A drawing of the sand pouring device is provided on figure 14. The sand pouring device rolled on wooden tracks with the sand exiting through a ⅛- by 10-in slot at the bottom.

Testing Procedure

Approximately 500 lb of sand were prepared for use by dry sieving, to remove plus No. 30 and minus No. 40 sieve size material, and then washed over a No. 40 sieve. This resulted in a clean, poorly graded sand with particle sizes ranging from 0.016 to 0.023 inch. One pint of water-soluble black ink was mixed with approximately 90 lb of sand. This was used to make visible layers in the slope models.

The sand was air-dried and poured into the model container from a height of 7.25 ft in approximately $^1/_{10}$-inch-thick lifts. A photograph depicting the sand pouring procedure is shown on figure 15. The layering was accomplished by pouring alternate lifts of colored and uncolored sand. The model container held approximately 61 lb of sand, which was reused after each test. Before each test sand was added as needed and mixed with the previously used sand to replace the sand spilled during the previous pouring processes. In this manner, nearly all of the 500 lb of sand were used in testing.

For the tests conducted with a buried footing, the sand pouring process was suspended when the sand

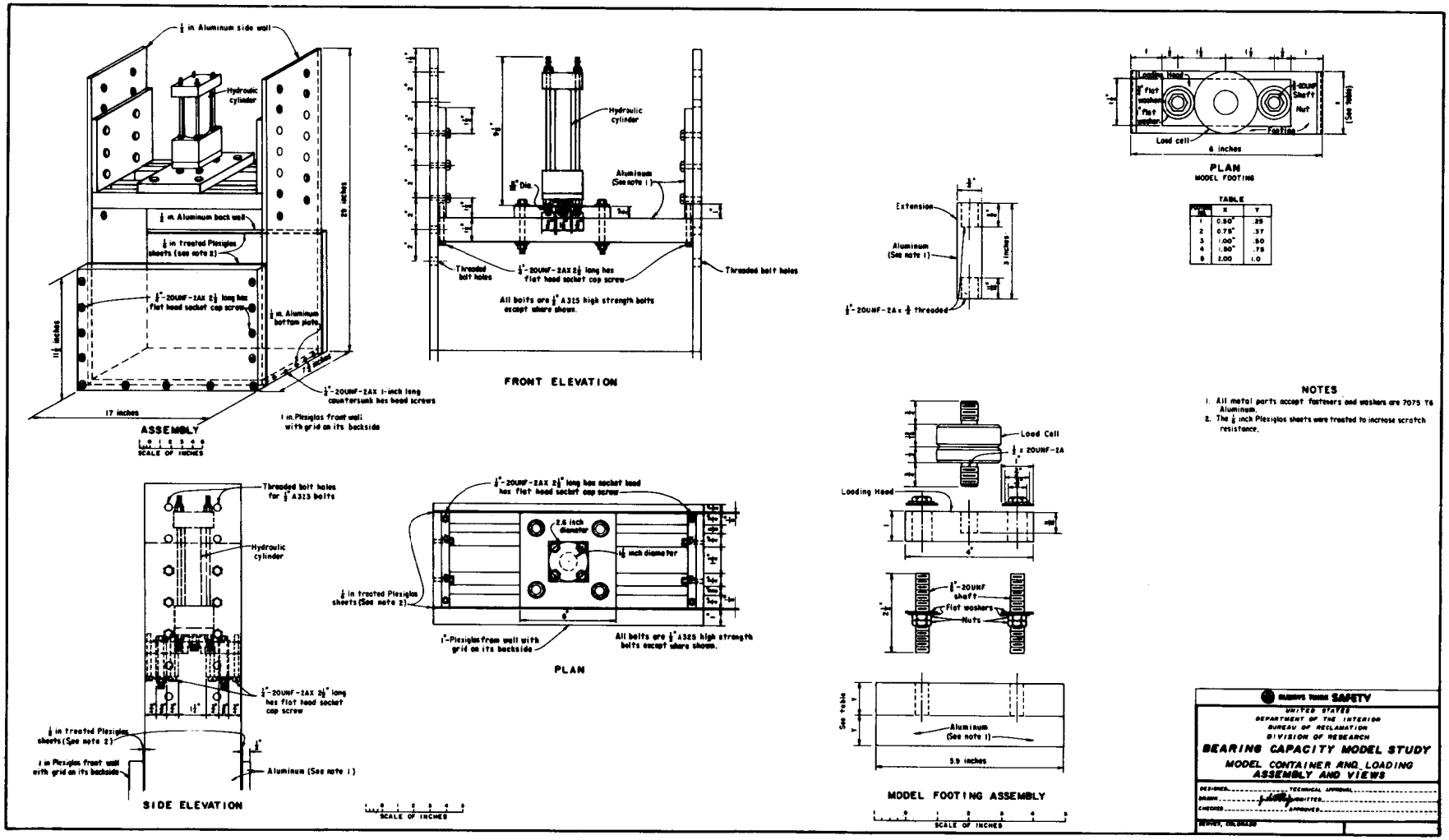

Figure 8. – Detailed drawing of the model container and loading assembly.

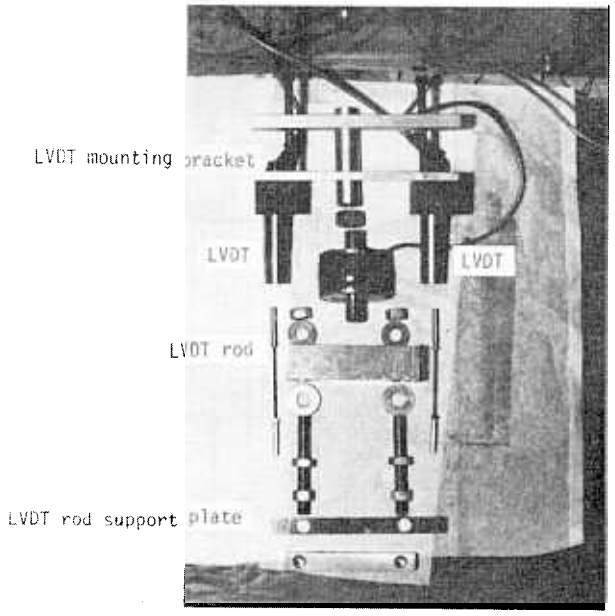

Figure 9. – Components of the loading assembly. Photo P801-D-80805

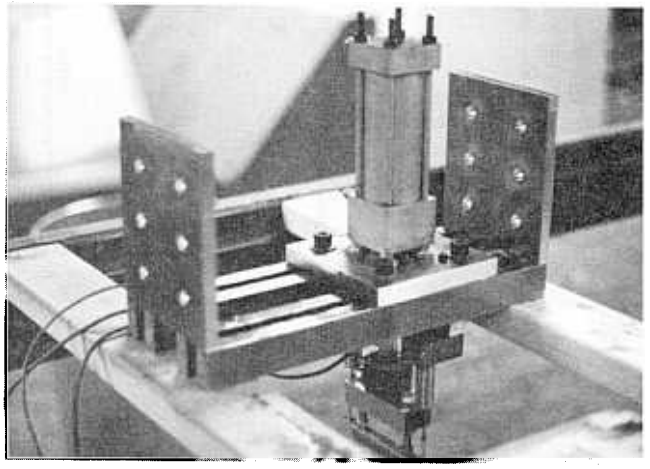

Figure 10. – Loading assembly. Photo P801-D-80806.

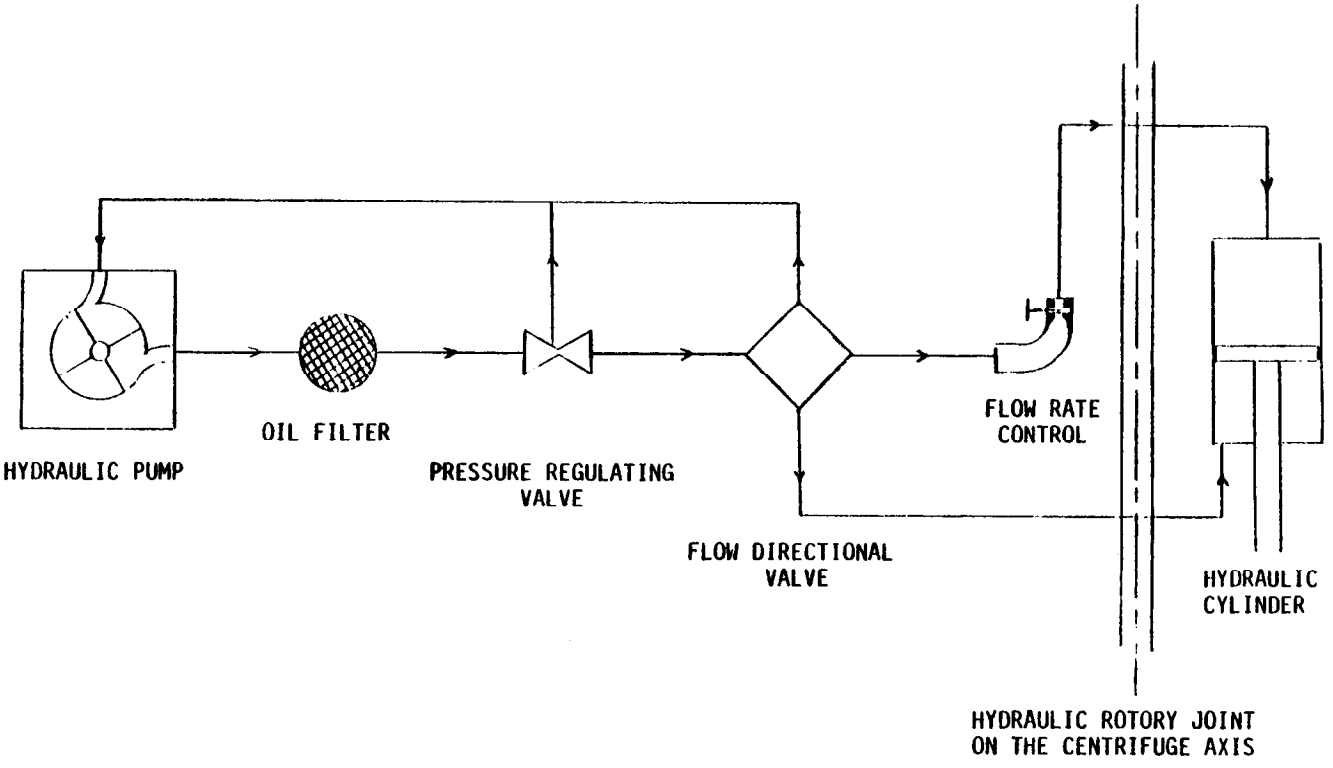

Figure 11. – Hydraulic system flow chart.

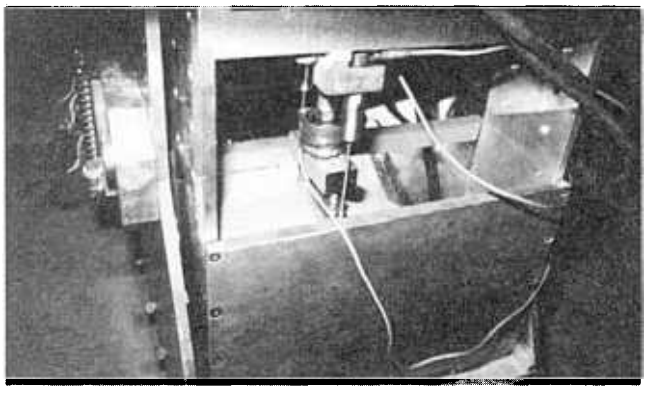

Figure 12. – LVDT's mounted above a model footing. Photo P801-D-80807

elevation was at the specified footing base elevation. The footing was placed on the surface in the proper location, and the pouring process was then continued. In these tests a thin sheet of spongy foam was placed between the ends of the footing and the sides of the model container to prevent sand from entering the 0.05-in gaps during the pouring process. These foam strips remained in place during the buried footing test. However, the foam strips were not used when surface footings were modeled.

After filling the model container the surface was carefully leveled flush with the top. The weight of the model container and sand was measured and recorded in the log. The scale used was accurate to ¼ lb.

The slopes were excavated to their rough shape by using a vacuum cleaner. Care was taken to avoid overexcavating. The excess soil was carefully removed by hand trimming.

The container, with the model slope and footing, was carefully placed in the centrifuge swing basket using overhead lifts. The loading assembly was mounted on the model container and the hydraulic cylinder was moved into position over the footing. The model footing was attached to the loading head. Care was taken so that the soil remained undisturbed and the footing base was flush with the ground surface at the crest of the slope at the appropriate footing depth. When the footing was buried, care was taken not to disturb it.

The following procedure was used for test conditions 10 through 17, in which the surface footings were

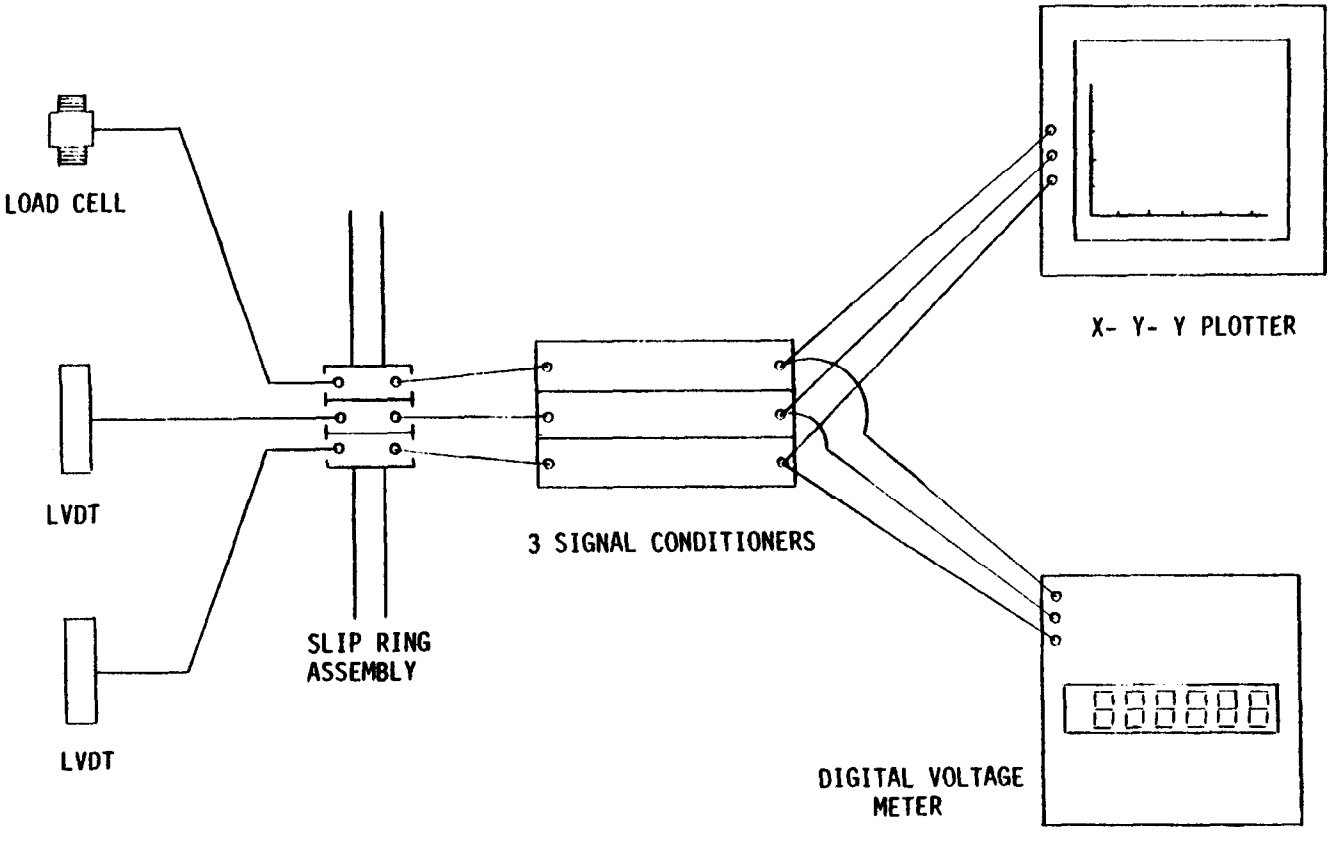

Figure 13. – Schematic of the instrumentation system.

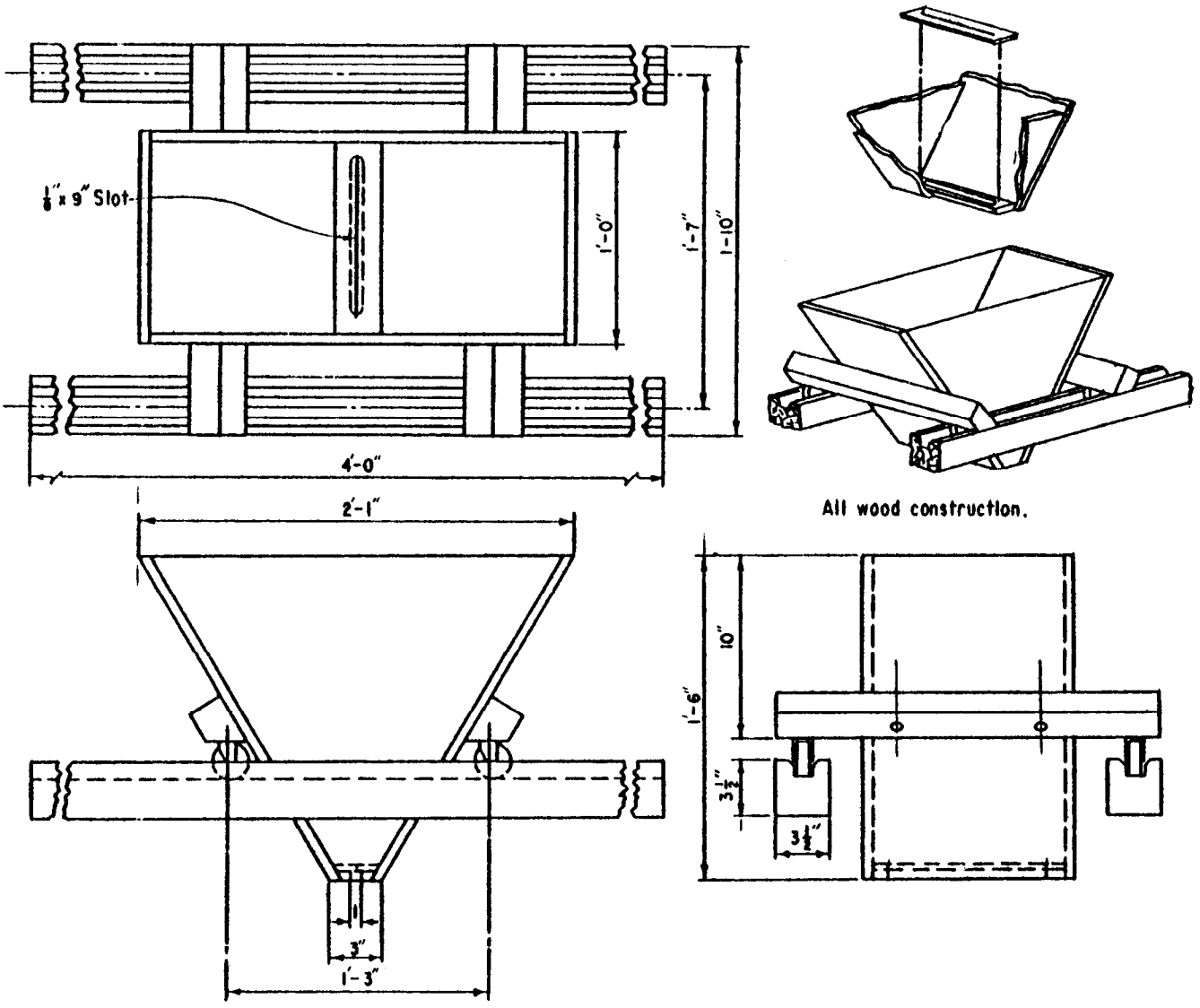

Figure 14. – Drawing of the sand pouring device.

tested. The footing was raised slightly from the slope before testing to prevent the loading of the soil slope by the footing during the application of the artificial gravity field. This procedure was not followed for test conditions 1 through 9 or 18, in which buried footings were tested. In some of those tests where this procedure was not followed, slight footing bearing pressures were observed when the required acceleration for testing was achieved.

After positioning the footing, the centrifuge was balanced and the acceleration process started. The acceleration was applied to the model at a rate no greater than 15 *g*'s per minute. The acceleration experienced by the model is a function of the distance from centrifuge axis. The acceleration is given by:

$$a = r\omega^2$$

where r = distance from centrifuge axis
ω = angular velocity

It was necessary to select the radius at which the acceleration required for modeling is achieved. This was arbitrarily selected as the distance from the centrifuge axis to the point at one-third the slope height below the slope crest.

Model behavior was monitored during the testing process using the CCTV camera. The hydraulic pump was turned on when the centrifuge speed reached the level appropriate for the test. The flow control valve, which regulated the oil flow rate from the hy-

Figure 15. – Sand pouring procedure. Photo P801-D-80808

draulic pump to the hydraulic cylinder, was opened. Valve characteristics prevented a constant oil discharge rate; therefore, the footing displacement rate was not constant. During the test the valve was adjusted to maintain a reasonable footing displacement area. Centrifuge speed, footing load, and footing displacement were monitored using a digital voltmeter and an X-Y-Y analog plotter.

A typical test was terminated after the maximum bearing pressure (peak load) was attained and the minimum postpeak load was reached. Occasionally, tests were stopped before reaching the postpeak load because LVDT displacement limits were exceeded. The model container was removed from the centrifuge after testing. Photographs of the slope were taken when the failure surface was observable. This was often the case when plane strain tests were performed and the slope was constructed of interbedded layers of colored sand.

Test Results

A complete set of data for each of the 59 footing tests is included in appendix A. These data consist of plots of the footing bearing pressure versus footing relative displacement and time versus footing relative displacement. Footing relative displacement (d/B) is the vertical displacement of the footing (d) divided by the footing width (B). On the figures in appendix A, the square points represent the relative displacement measured by the LVDT located nearest the Plexiglas side of the model container (LVDT 1). The triangular points represent the relative displacement measured by the LVDT located nearest the aluminum side of the model container (LVDT 2). The photograph on figure 9 shows the LVDT locations. LVDT's were not functioning during tests 35, 36 and 37; thus, relative displacement plots are not provided for test condition 18.

The footing bearing pressure was computed by dividing the load applied to the sand at the base of the footing by the cross-sectional area of the footing. The load applied at the footing base was computed as the difference between the load registered by the load cell when the footing was suspended above the slope and the load registered by the load cell during the loading process. The suspended load was obtained by raising the footing above the soil surface after test completion while maintaining the same centrifuge speed. Test results are in table 3.

Occasionally, footings were bearing on the soil at the start of the test. This was caused by the downward footing movement that occurred while the artificial gravity field was being applied. Test 29 (test condition 14) is an example of a test in which this happened. Figure A-29 shows the data for test No. 29. A 3,500-lb/ft^2 initial load was registered at the start of the test. For tests where this occurred, it was necessary to extrapolate the bearing pressure versus relative displacement curve through the origin so that the relative displacement during testing could be compared with those of other tests. This extrapolation involved computing the slope between adjacent data points on the bearing pressure versus relative displacement curve, computing the average slope, and then computing the relative displacement at the start of the test. The average slope was computed using the data points having bearing pressures less than 50 percent of the maximum bearing pressure. If there were less than three data points in this pressure range, the first three recorded data points were used.

The relative displacement at the start of the test was computed by dividing the initial bearing pressure by the computed average slope. Tests requiring relative displacement correction are easily recognized by observing that the first plotted data point is not at the origin of the bearing pressure versus relative displacement plot. Again, test No. 29 is a good example. Figure 16 illustrates the relative displacement correction.

Table 3. – Summary of test results.

Test condition	Test No.	Placement density lb/ft³	Bearing pressure at start of test kips/ft²	Maximum bearing pressure kips/ft²	Relative displacement at maximum bearing pressure
1	3	100	1.7	34.9	0.15
	20	100	0.2	37.8	0.19
2	21	101	0.1	42.5	0.18
	25	100	1.6	39.7	0.16
3	8	100	2.7	44.5	0.17
	11	101	0.7	44.8	0.20
	16	101	0.5	41.3	0.16
4	1	100	0.3	24.2	0.18
	2	100	0.0	22.4	0.17
	5	100	0.2	24.7	0.20
5	4	100	0.5	29.3	0.20
	9	101	1.3	35.3	0.19
	23	101	0.0	20.3	0.16
	26	100	1.1	24.0	0.21
6	7	101	3.9	32.7	0.21
	18	101	2.5	27.6	0.18
	24	100	7.7	30.5	0.18
7	14	100	0.0	40.4	0.30
	15	101	0.0	41.4	0.29
	22	101	0.0	38.9	0.27
8	13	100	2.7	42.8	0.23
	19	100	0.4	42.3	0.22
	12	101	0.6	43.3	0.21
9	6	100	4.9	50.0	0.23
	10	100	2.2	50.9	0.28
	17	101	0.5	41.8	0.20
10	31	100	0.0	23.8	0.20
	32	100	0.4	16.7	0.16
	33	100	0.0	22.4	0.17
	34	100	0.5	21.5	0.18
11	36	100	0.0	19.2	0.19
	39	101	0.0	21.4	0.18
	40	101	0.0	23.5	0.23
	45	100	0.0	20.5	0.18
12	57	100	0.4	21.7	0.21
	58	100	0.5	20.0	0.19
	59	101	0.2	21.9	0.18
13	54	101	0.6	21.4	0.20
	53	101	0.3	25.8	0.21
	56	100	0.0	21.4	0.19

Table 3. – Summary of test results – Continued

Test condition	Test No.	Placement density lb/ft³	Bearing pressure at start of test kips/ft²	Maximum bearing pressure kips/ft²	Relative displacement at maximum bearing pressure
14	27	100	6.3	19.6	0.12
	28	101	0.0	20.0	0.19
	29	100	3.5	20.9	0.15
	30	100	3.4	20.6	0.18
15	41	101	0.0	23.3	0.19
	42	101	0.1	22.6	0.19
	43	101	0.0	19.7	0.16
	44	101	0.2	21.4	0.18
16	46	101	0.0	17.4	0.17
	47	101	0.0	20.0	0.17
	48	100	0.0	23.6	0.19
	49	101	0.0	18.5	0.17
17	50	100	0.0	27.1	0.18
	51	100	0.0	32.2	0.20
	52	101	0.0	25.2	0.16
	53	101	0.0	31.3	0.17
18	35	100	1.9	45.5	*
	36	100	0.3	46.5	*
	37	100	0.0	47.2	*

* Displacement not recorded.

The tests were displacement controlled; the flow control valve governed the footing displacement rate. However, it did not provide a constant rate of displacement; the larger the applied load, the lower the displacement rate. The time versus bearing pressure plots in appendix A show this trend.

Although 61 tests were performed, results from only 59 tests are reported. Irregularities in the testing procedure were the cause for discarding two tests. A minimum of three tests were conducted for each test condition. The two discarded tests represented conditions 1 and 2; therefore, only two tests are reported for each of these conditions.

Groups of bearing pressure versus relative displacement plots for tests representing conditions 1 through 17 are provided in appendix B. Relative displacement was not recorded during tests 38, 39, and 40 (test condition 18). The plots of these data show that test results were reproducible.

Figures 17 through 20 are plots of maximum bearing pressure versus model scale, footing length-to-width ratio, footing depth-to-width ratio, and footing width, respectively. Figures 21 through 23 are plots of relative displacement at the maximum bearing pressure versus the model scale, footing length-to-width ratio, and footing width, respectively. The plotted data are divided into groups of tests representing similar conditions with only one variable changing. Solid and dashed lines on these plots connect average values.

Modeling of Models. – The results of the "modeling of models" process is exemplified on figures 17 and 21. Figure 17a indicates that the maximum bearing pressure measured in plane strain tests (conditions 1 through 9) has a pronounced scale effect. Figure 17b indicates that maximum bearing pressure measured in three-dimensional tests, i.e., the tests conducted with the model footing length considerably less than the specimen container width (conditions 10 through 16), modeled very well. Hence, there was

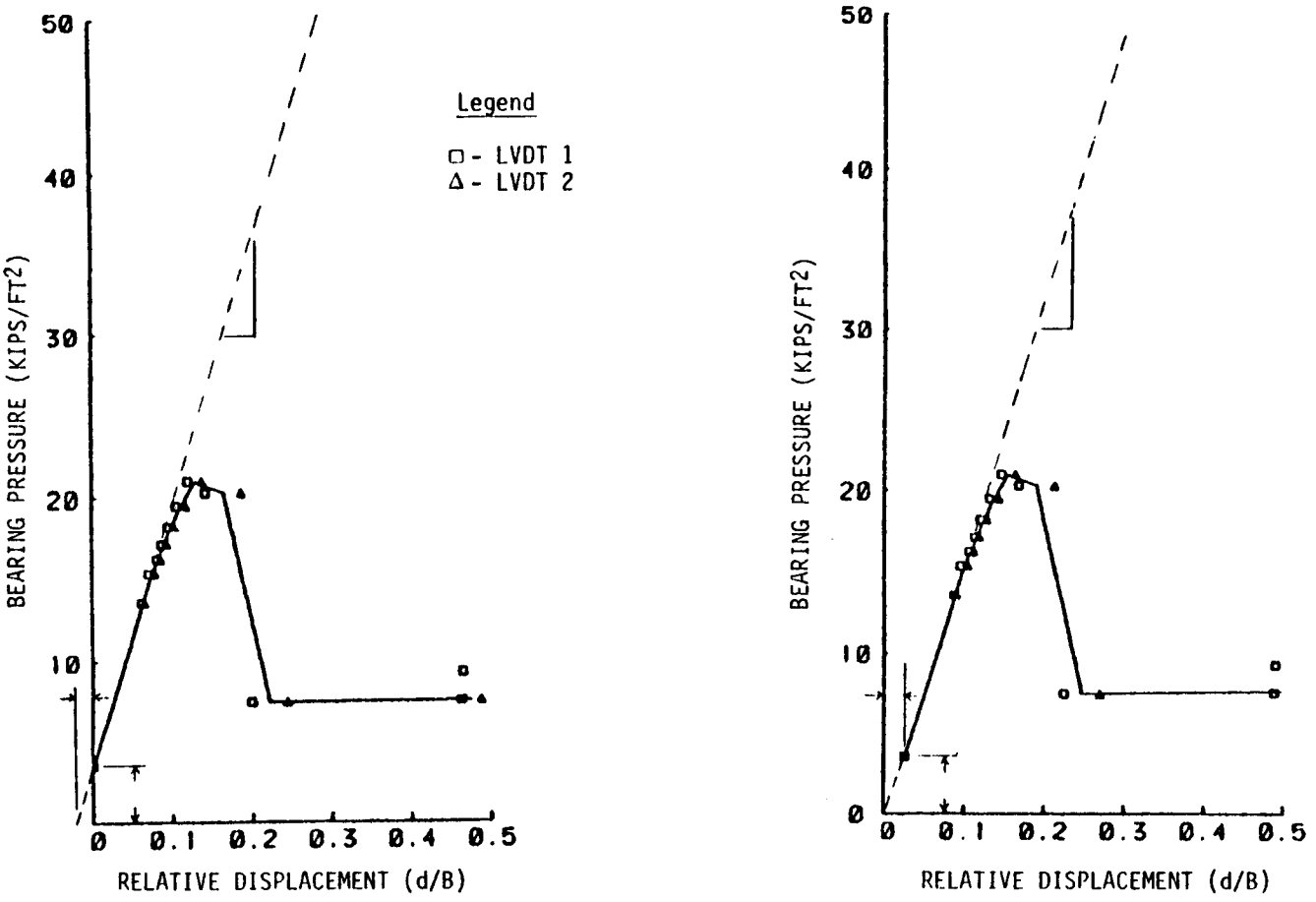

Figure 16. – Illustration of the relative displacement correction.

no scale effect. Figure 21 shows that the relative displacement at the maximum bearing pressure modeled well for the plane strain conditions representing surface footings (conditions 1 through 6) and poorly for the plane strain conditions representing buried footings (conditions 7 through 9). Figure 21 shows that the relative displacement at the maximum bearing pressure modeled very well for test conditions 10 through 16, which were three-dimensional surface footings. The relative displacement at the maximum bearing pressure for three-dimensional and plane strain models representing surface footings were both approximately 0.19. These results may be explained as follows.

During tests 1 through 24, considerable friction developed between the specially treated Plexiglas and the sand, and between the Plexiglas and the footing. Noticeable scratching of the Plexiglas sides occurred. When the footing was loaded, increased lateral soil pressure caused the model container sides to bulge slightly, and sand entered the small gap between the footing and the Plexiglas model container side. Stress relief occurred when the artificial gravity field or the footing bearing pressure was decreased. During the stress relief, the footing would bind against the walls. This expansion and the subsequent binding adversely influenced the plane strain models for test conditions 1 through 9. Neither expansion and binding nor Plexiglas scratching was observed during tests 25 through 59, the three-dimensional tests. In these tests the space between the side of the model container and the end of the footing was large and the footing loads were small.

The additional force required to overcome the friction between the wall and the footing combined with model container bulging, caused the maximum pressure recorded during tests 1 through 24 to be in error. It was expected that the relative displacement at the maximum pressure would also be affected. This is because the maximum pressure on the soil beneath the footing and the maximum recorded load on the load cell may not occur at the same relative

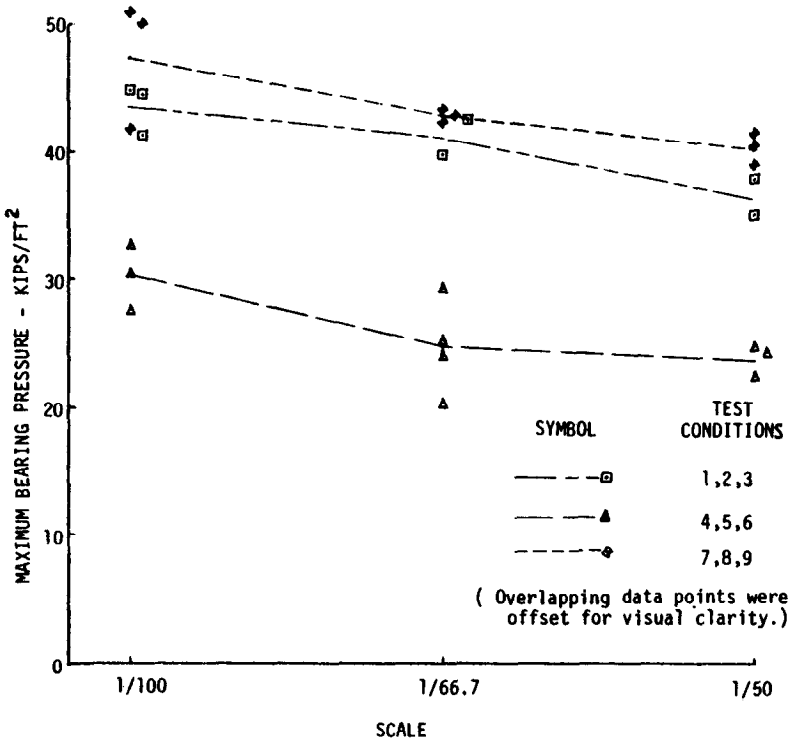

Figure 17a. – Scale versus maximum bearing pressure for test conditions 1 through 9.

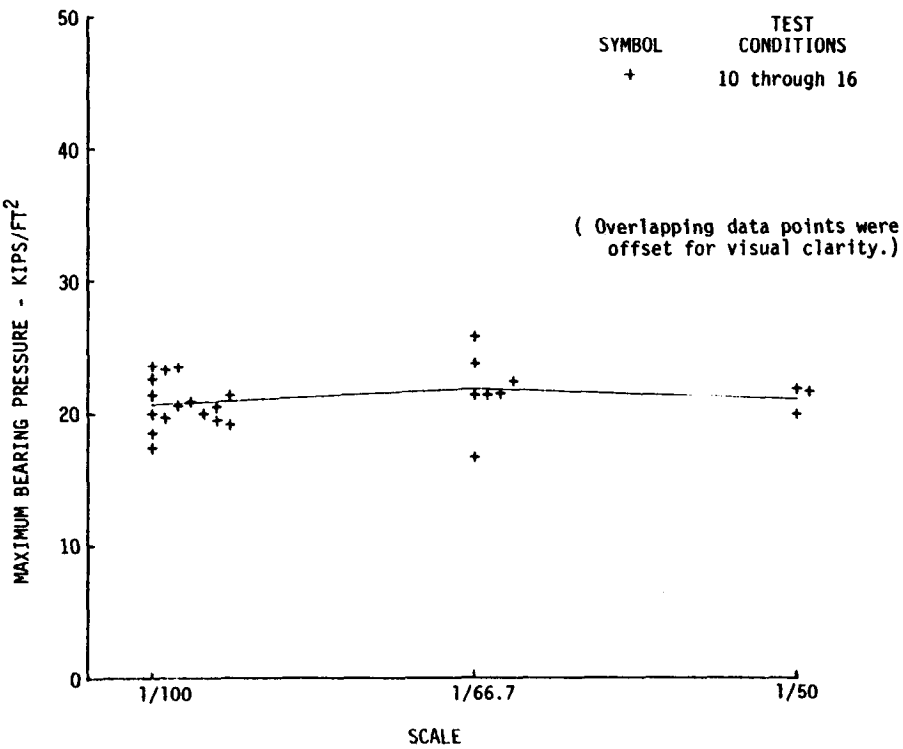

Figure 17b. – Scale versus maximum bearing pressure for test conditions 10 through 16.

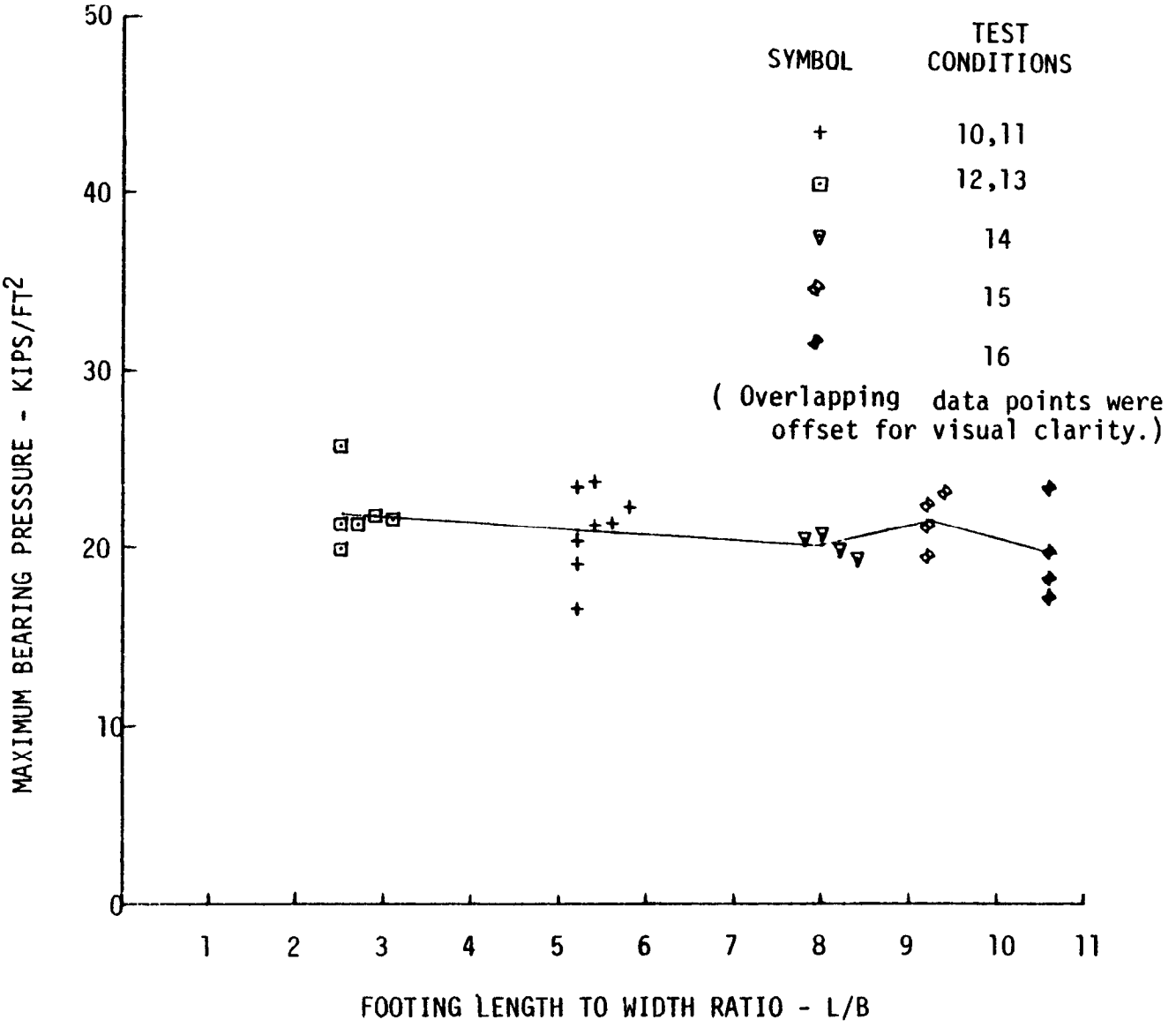

Figure 18. – Footing length to width ratio versus maximum bearing pressure for test conditions 10 through 16.

displacement. The friction between the sand composing the slope and the Plexiglas wall would add to this error. The data presented on figure 21a, previously discussed, indicate that the net error (with respect to the relative displacement at the maximum bearing pressure) may be very small for surface footings, but considerable for buried footings.

Bearing pressure versus relative displacement plots for groups of tests representing the same prototype footing width, depth, and length are provided in appendix C. The data in this appendix exemplify the process of modeling of models. The test results presented in appendix C also show the effect that model container expansion and side friction had on modeling. Figures C-1 and C-2 show the results from test conditions 1, 2, and 3, and conditions 4, 5, and 6, respectively. Conditions 1, 2, and 3 represent plane strain footings 8.33-ft wide, located on the surface at the crest of the slope. Conditions 4, 5, and 6 represent plane strain footings 4.17-ft wide, located on the surface at the crest of the slope. The relative displacement versus maximum bearing pressure curves are similar in shape, having approximately the same initial slope and reaching their peak at approximately the same relative displacement. However, it can be seen that the maximum bearing pressures were not the same for tests representing one condition compared with tests representing another. This indicates that deviating from complete similitude

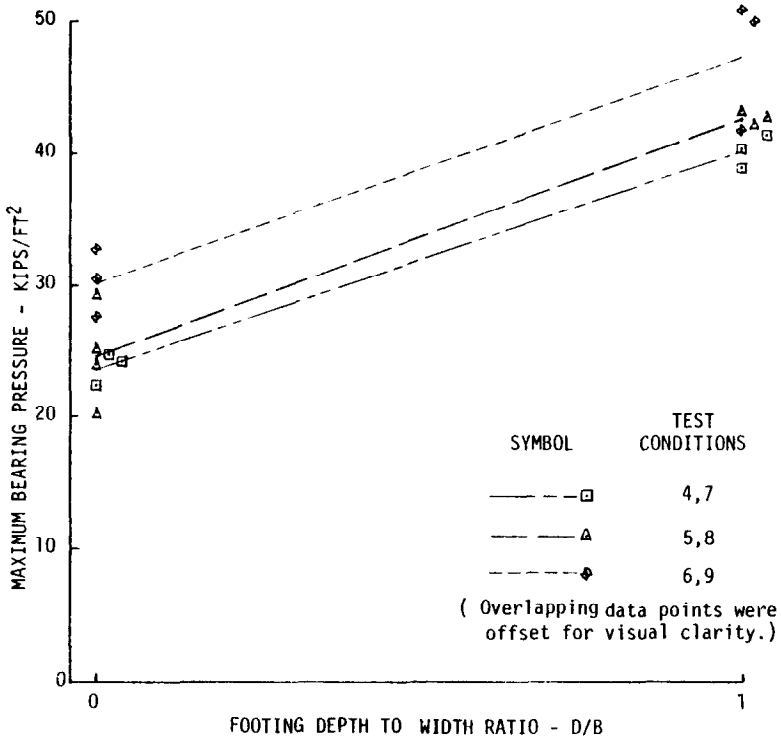

Figure 19a. – Footing depth to width ratio versus maximum bearing pressure for test conditions 4 through 9.

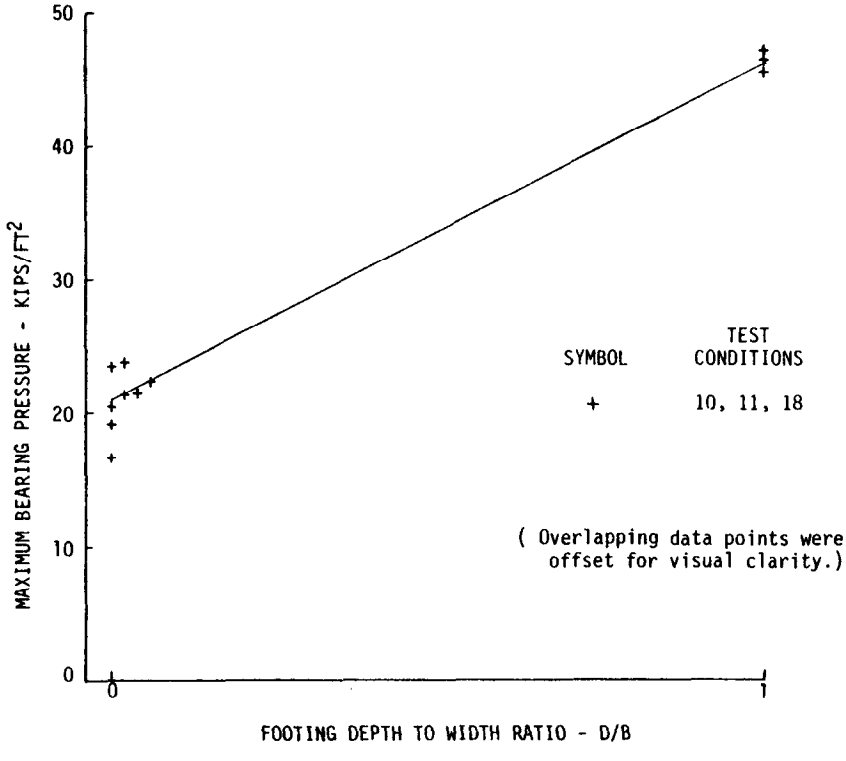

Figure 19b. – Footing depth to width ratio versus maximum bearing pressure for test conditions 10, 11 and 18.

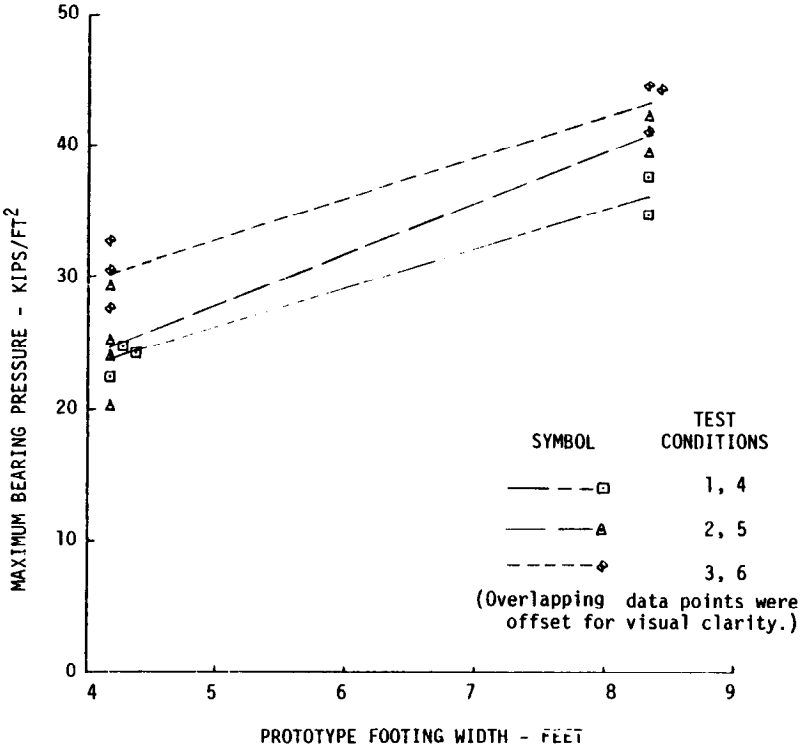

Figure 20a. – Prototype footing width versus maximum bearing pressure for test conditions 1 through 6.

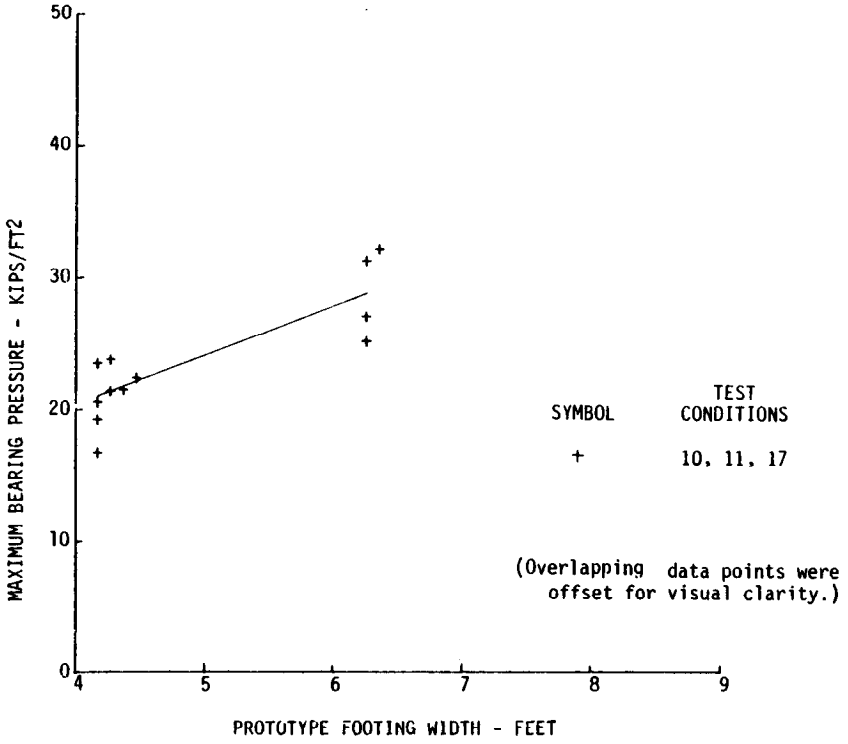

Figure 20b. – Prototype footing width versus maximum bearing pressure for test conditions 10, 11 and 17.

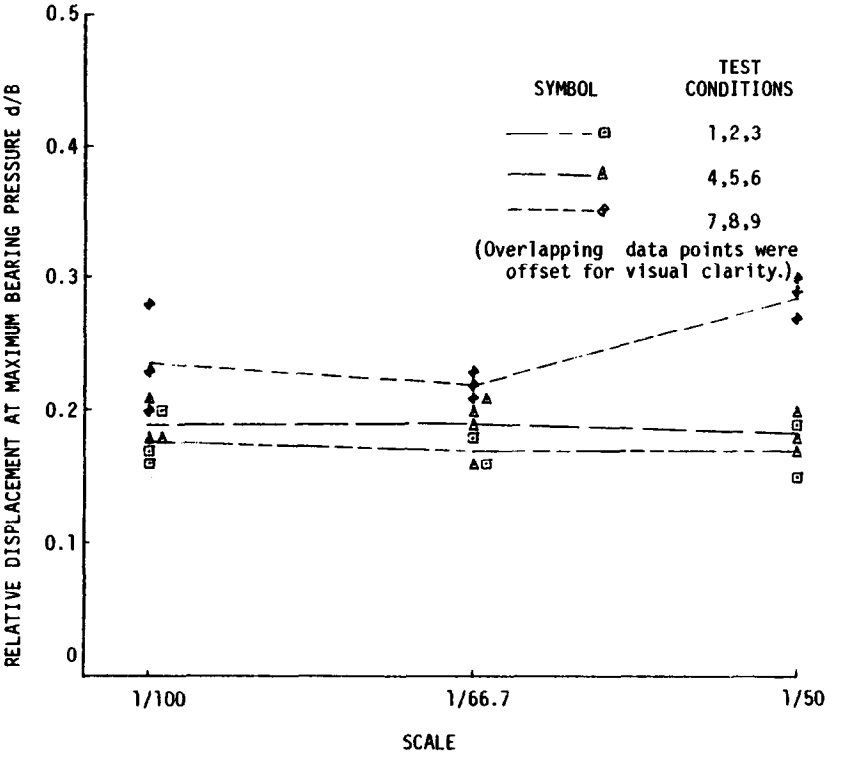

Figure 21a. – Scale versus relative displacement at maximum bearing pressure for test conditions 1 through 9.

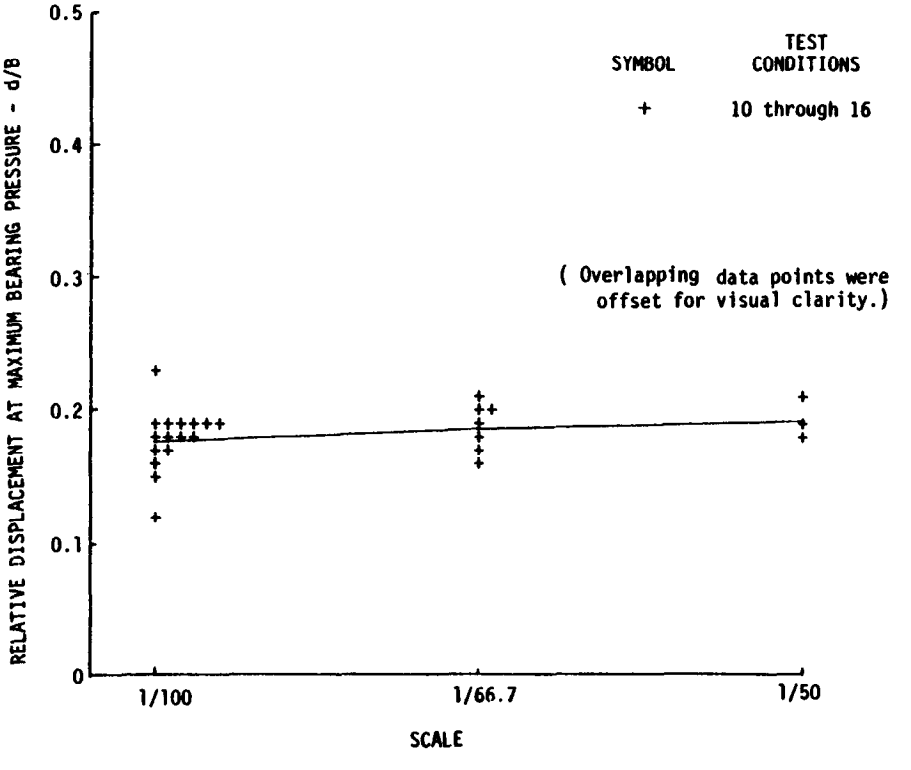

Figure 21b. – Footing length to width ratio versus maximum bearing pressure for test conditions 10 through 16.

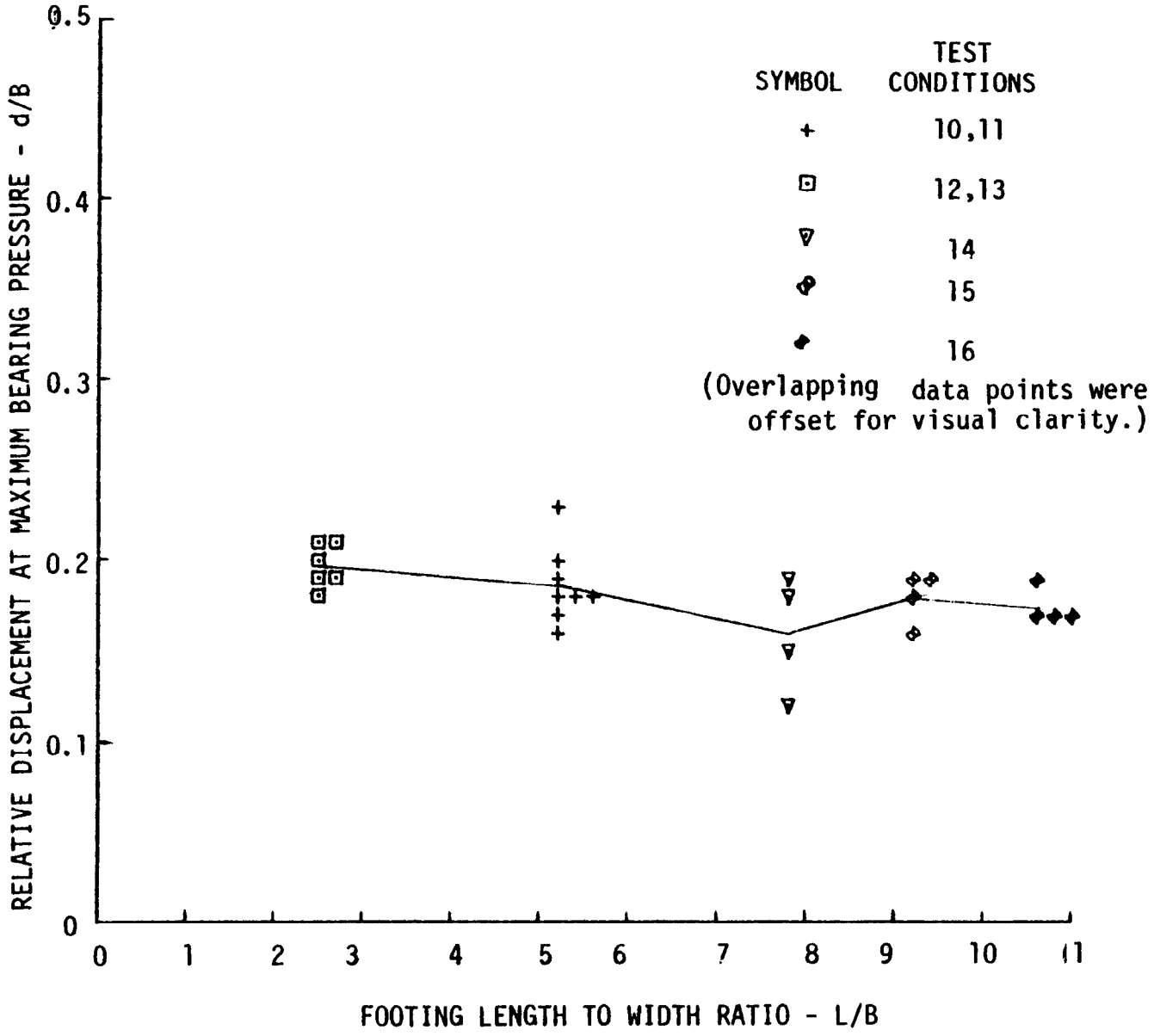

Figure 22. – Footing length to width ratio versus relative displacement at maximum bearing pressure for test conditions 10 through 16.

by changing boundary conditions did have an adverse effect on the modeling process during plane strain tests.

Figure C-3 shows that the plane strain tests on buried footings did not model with respect to maximum bearing pressure or relative displacement. The maximum bearing pressure and the relative displacement at maximum bearing pressure changed as the scale changed. Figures C-4 and C-5 show that models of the same prototype, which were tested at various scales allowing three-dimensional displacement, model very well. This indicates that deviations from complete similitude did not adversely affect the three-dimensional tests. That is, the effect of grain size and model container confinement did not influence the test results.

Footing Length-to-Width Ratio. – Changing the footing length-to-width ratio affected the maximum bearing pressure and relative displacement at the maximum bearing pressure, as shown on figures 18 and 22. It can be seen that changing the footing length-to-width ratio between 2.5 and 10.8 had no significant influence on the recorded maximum bearing pressure or on the recorded relative displacement at the maximum bearing pressure. The modeled prototype footing used for comparison was 4.17-ft wide and was located on the ground surface at the crest of the slope.

These results lead to the conclusion that the three-dimensional models failed in a plane strain manner. If footing end boundary effects had been significant to the modeling process and plane strain conditions had not predominated, then figures 18 and 22 would show the maximum bearing pressure or relative displacement at maximum bearing pressure deviating from a constant value as the length-to-width ratio changed.

Footing Depth-to-Width Ratio. – Changing the footing depth-to-width ratio from 0 to 1 increased the maximum bearing pressure approximately 67 percent comparing test conditions 4 through 9, and approximately 120 percent comparing test conditions 10, 11 and 18 (see figs. 19a and 19b). Test conditions 4 through 9 represent a 4.17-ft-wide footing with plane strain test conditions. Test conditions 10, 11, and and 18 represent a 4.17-ft-wide footing with a length-to-width ratio of 5.2. It has been shown that test conditions 4 through 9 did not model well, and that test conditions 10 and 11 did model well. Test condition 18, like 10 and 11, is a three-dimensional model; therefore, the emphasis should be on the data presented on figure 19b, which were obtained from test conditions 10, 11, and 18. The data from test conditions 4 through 9 are presented here only for completeness.

Because data were only collected at two depth-to-width ratios, the functional relationship between maximum bearing pressure and footing depth-to-width ratio cannot be determined. It is shown as a linear relationship on figures 19a and 19b for convenience. Relative displacement at the maximum bearing pressure versus depth-to-width ratio plots are not provided because relative footing displacements were not recorded during the three-dimensional tests on buried footings.

Footing Width. – The effects of prototype footing width on the maximum footing bearing pressure and the relative displacement at the maximum bearing pressure are shown on figures 20 and 23, respectively. Again, the value of the test data representing the plane strain test conditions shown on figures 20a and 23a are questionable and are presented only for completeness. Linear relationships are shown for convenience. In the plane strain conditions (test conditions 1 through 6), the maximum bearing pressure increased at the rate of approximately 3.5 kips/ft^2 per foot of width, and the relative displacement at the maximum bearing pressure decreased slightly as the footing width increased. The three-dimensional loading conditions are represented by tests 10, 11, and 17 – all having length-to-width ratios of 5.2. Under these conditions, the maximum bearing pressure increased at a rate of approximately 3.7 kips/ft^2 per foot of width, and the relative displacement at the maximum bearing pressure decreased slightly as the footing width increased.

Observations. – Photographs taken after completion of several plane strain tests show the observed failure surfaces. The failure surfaces for footings representing plane strain conditions were the only ones that could be observed through the Plexiglas. Because the three-dimensional models did not displace soil along the plane of the Plexiglas, direct observation of the failure surface for three-dimensional models was impossible.

Photographs and sketches of the observed shear surfaces for several tests are provided in appendix D. It was noted earlier in this discussion that the relative displacement at the maximum bearing pressure was probably influenced by the binding of the footing and friction between the sand slope and the Plexiglas wall. This influence was shown to be small for the surface footings but considerably larger for the buried footing. Therefore, the value of using the observed failure surfaces for defining failure mechanisms or comparison with theoretical failure mechanisms is questionable.

The horizontal movement of the footing toward the slope was observed in all tests. This movement is apparent on the photographs in appendix D. This horizontal movement was restricted by the rigidity of the hydraulic cylinder rod (⅝-in-diameter steel rod) and the ¾-in-diameter aluminum rod extensions, which were used to attach the model footing to the loading mechanism. The extent of the horizontal movement that occurred prior to reaching the maximum bearing pressure is uncertain. It is also not known how the horizontal footing movement influenced the magnitude of the maximum bearing pressure or relative displacement.

Observation indicates that vertical movement was the same from one end of the footing to the other end, although the maximum bearing pressure versus relative displacement plots shown in appendix A indicate otherwise. Graphs in appendix A show the plots from two sets of data for bearing pressure versus relative displacement. These plots reflect the differences in the vertical displacements recorded at the ends of the footings. The recorded displacements were not always identical at a given footing pressure. This may be explained as follows. Frequently, one side of the footing would move (more than the other side) horizontally toward the slope. When the footing moved horizontally, the LVDT rods (which were resting on the footing surfaces, one on each end of the footing) moved vertically and horizontally. When one side of the footing moved horizontally more than the other, the two LVDT's recorded different vertical displacements. Only minor discrepancies between the

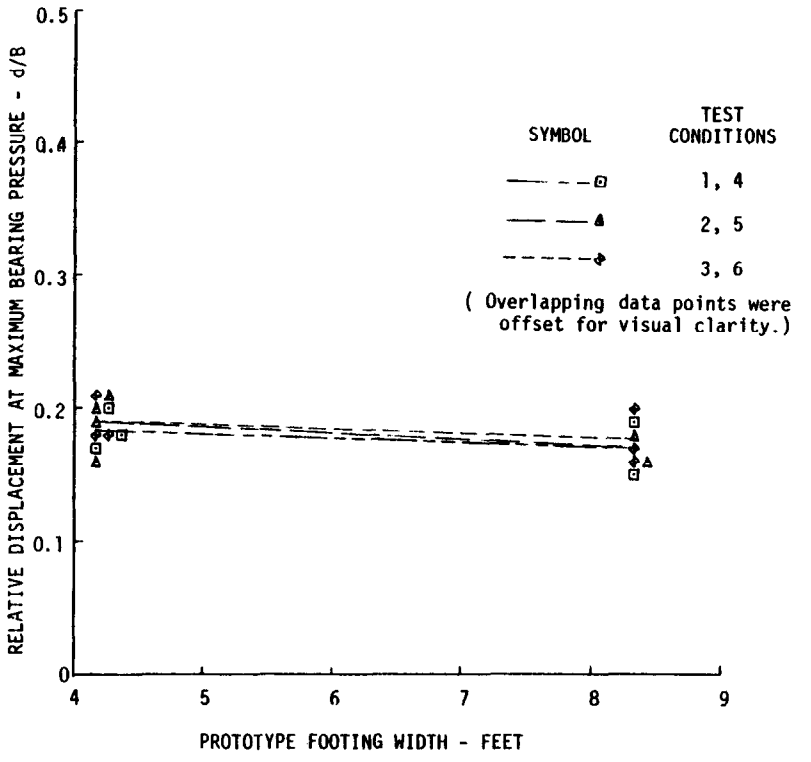

Figure 23a. – Prototype footing width versus relative displacement at maximum bearing pressure for test conditions 1 through 6.

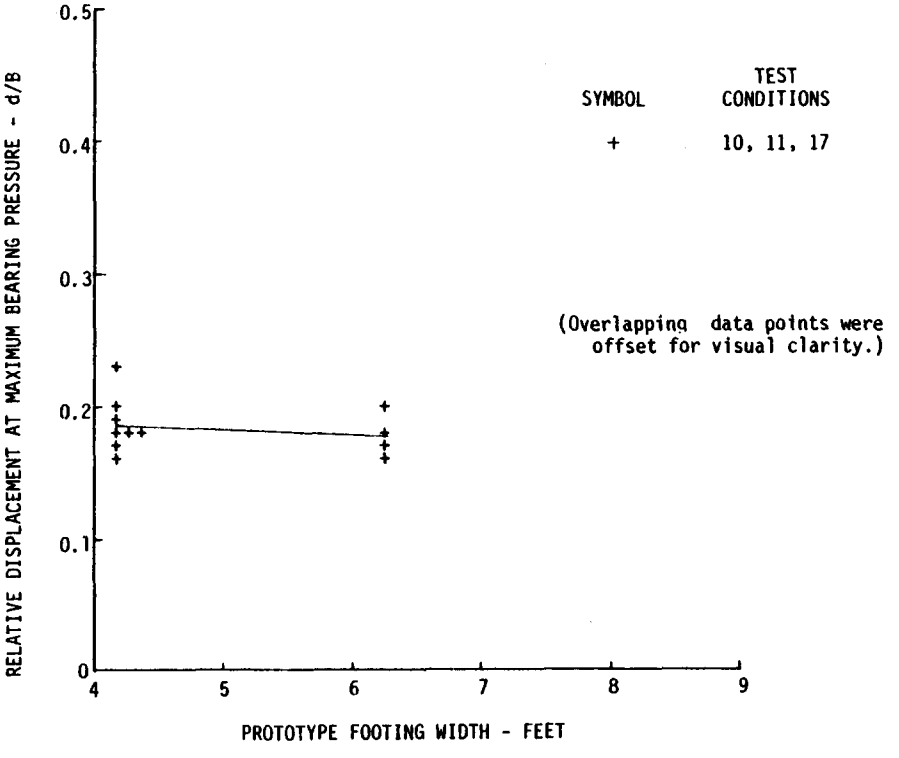

Figure 23b. – Prototype footing width versus relative displacement at maximum bearing pressure for test conditions 10, 11 and 17.

two vertical displacements recorded by the LVDT's occurred before reaching the maximum bearing pressure. Large differences occurred after the maximum pressure had been reached. This implies that very little differential horizontal footing movement occurred before the maximum bearing pressure was reached.

RESULTS OF LABORATORY TESTS ON SAND

Introduction

Laboratory tests were conducted on the sand used to construct the model slopes: (1) to define material properties used as input to analytical methods, and (2) to describe and classify the material.

Test Program

The sand was indexed as sample No. 44T-4 for Bureau identification. Gradation, specific gravity, relative density, direct shear, and CD (consolidated-drained) triaxial shear tests and petrographic analyses were performed on the model test sand. Laboratory tests were performed according to procedures described in the *Earth Manuel* [28], with the exceptions described in this section. The results of these tests are presented in appendix E.

Descriptive Properties

The sand used in the research program was prepared by dry sieving, to remove the plus No. 30 and minus No. 40 sieve size material, and then washing over a No. 40 sieve. This resulted in a clean, poorly graded sand with particle sizes ranging from 0.016 to 0.023 in. The specific gravity of the sand was 2.66. A relative density test showed the minimum and maximum dry densities to be 83 and 101 lb/ft^3, respectively.

The petrographic analysis consisted of an optical microscope review. It revealed that the sand was subangular to subrounded and was predominantly composed of granitic rock fragments, quartz, and feldspar, with significant amounts (approximately 3 percent of the sand grains) of mica.

CD Triaxial Shear Test

A CD triaxial shear test was performed on 2-inch-diameter by 5-inch-high specimens in accordance with current Bureau, Geotechnical Branch laboratory testing procedures.

The specimens were prepared by pouring sand into a specimen mold from a height of approximately 6 feet. This resulted in a density of approximately 101 lb/ft^3 (100 percent relative density). The specimens were consolidated at 25-, 50-, 100- and 200-lb/in^2 effective confining pressures. These were labeled as specimens 31, 32, 33, and 34, respectively. The sand remained dry during the tests. The displacement rate used was 0.02 in/min. The test results are presented in appendix E on figures E-1 through E-4 and summarized in table E-1. The failure condition was selected at the maximum deviator stress. The soil strength is expressed in terms of the Mohr-Coulomb failure criterion:

$$\tau_f = c = \sigma_f \tan \varnothing$$

where c is the cohesion, $\varnothing$ the friction angle, and τ_f and σ_f are the shear and normal stresses on the failure plane.

The friction angle ($\varnothing$) was found by computing the slope (tan ψ) of the best-fit line through the failure points plotted on the *P-Q* diagram and then computing $\varnothing$ by the relationship:

$$\varnothing = \sin^{-1}(\tan \psi)$$

The best-fit line was determined by linear regression analysis. The line was weighted through the origin. This was done by placing as many data points at the origin as necessary to obtain a cohesion of 0 lb/in^2 $\pm$ 0.01 lb/in^2.

Data from specimen 34 are included on the figures and tables, but were not used to compute $\varnothing$. This is because the stresses in the models were much lower than the pressures at which this specimen was tested; therefore, their inclusion in the data analyses is not essential and could be misleading.

The maximum pressure exerted on the soil by a model footing is the maximum principal stress in the slope at failure. The maximum pressure exerted on the soil by any model footing was approximately 350 lb/in^2. The average of the maximum pressures was approximately 200 lb/in^2. The maximum principal stress (axial stress at failure) in triaxial shear specimen 34, was 887 lb/in^2. This was considerably greater than those observed in the model tests. The maximum principal stresses in triaxial shear specimens 31, 32, and 33 were 147, 297, and 553 lb/in^2, respectively. Maximum principal stresses in specimens 32 and 33 bracketed the model test maximum value. Those in specimens 31 and 32 bracketed the model test average value.

The friction angle was computed in the manner described above by first using specimens 31, 32, and 33, and then using only specimens 31 and 32. The friction angles computed were 43.7° and 45.3°, respectively.

The difference in the friction angle indicates that a linear Mohr-Coulomb failure criterion may not fit the

experimentally defined failure conditions as well as nonlinear failure criterion.

Photographs of test specimens 31, 32, and 34, taken after test completion, are shown in appendix E on figure E-5. A 2-lb/in^2 vacuum was applied to the specimen through the end plates to support them for the photographs.

Direct Shear Tests

Two direct shear tests were performed. These were labeled test A and test B. The average specimen dry density in test A was 101 lb/ft^3; the average specimen dry density in test B was 100 lb/ft^3. The specimens were placed by pouring the sand into the direct shear specimen container from a height of approximately 4 ft to obtain a density of 100 lb/ft^3 and from 5 ft to obtain a density of 101 lb/ft^3. Four 2- by 2- by 1-inch-deep specimens were used for each test. The displacement rate was 0.02 in/min. Specimens 1, 2, 3, and 4 were tested with normal pressures of 20, 40, 80 and 160 lb/in^2, respectively. Appendix E, table E-2 and figures E-6 and E-7, summarize the direct shear test results.

The angle of the internal friction ($\varnothing$) was computed using the method of least squares applied to the peak strength of all four specimens and forcing the cohesion (c) to be zero. This resulted in $\varnothing$ equaling 42.8° for test A and 43.7° for test B. Figures E-6 and E-7 both show that the failure points at low normal stresses fall above the Mohr-Coulomb line as determined by direct shear tests; and at high normal stresses, the failure points fall below the Mohr-Coulomb line. A nonlinear failure criterion might describe the test results better than the linear Mohr-Coulomb criterion.

Some difficulty occurred in conducting tests at the lower confining pressures. The specimen dilation was uneven and caused the upper plate of the specimen container to rotate and eventually come in contact with the lower plate. The friction between these plates caused a sudden increase in the applied shearing force. The relative horizontal displacement versus normal shear stress plots on figures E-6 and E-7 show the effect of the increase in shearing force as a rapid increase in the normal shear stress shortly after the peak strength of the sand was reached.

COMPARISON OF MODEL TEST RESULTS WITH ANALYTICAL METHODS

Introduction

The maximum bearing pressures found by model testing were compared with the ultimate bearing capacities obtained from analytical solutions proposed by Meyerhof, Hansen, Giroud, Bowles, Kusakabe, and Myslivec and Kysela. An application of Spencer's limit equilibrium technique was also developed and compared with model test results. The stability of the slope was not investigated using general slope stability methods. Only the general bearing capacity failure mode was considered.

Analytical methods used in the comparison will be discussed and compared individually with the model test results. Conclusions will then be made regarding the usefulness of each analytical method for design purposes. The interrelationships of the analytical methods and their relationships with the model test results will then be discussed.

The maximum bearing pressures recorded for model tests 1 through 25, which represent test conditions 1 through 9, will not be considered for the comparison. This is because erroneous results were produced by the friction between the model footing and the sides of the model container, the expansion of the model container, and the friction between the soil composing the model slope and the sides of the model container.

Sand Friction Angle

All the analytical methods discussed use the Mohr-Coulomb failure criteria to describe soil shear strength. Therefore, the selection of the appropriate friction angle is critical. As discussed earlier, plane strain conditions predominated during the tests; therefore, the friction angle chosen should reflect plane strain conditions ($\varnothing_{pl}$). However, in practice, triaxial shear tests are typically performed to obtain the friction angle. Tests on a very dense sand have shown $\varnothing$ to be approximately 7° greater for plane strain shear than for triaxial shear [30]. Some authors (originally proposed by Hansen [10]) suggest using the following correction to the friction angle determined from the triaxial shear test ($\varnothing_{triax}$):

$$\varnothing_{pl} = 1.1\ \varnothing_{triax}$$

where $\varnothing_{pl}$ is an approximate plane strain shear friction angle.

Selection of friction angle is complicated by the apparent nonlinearity of the failure envelope observed in both triaxial shear and direct shear tests. The previously discussed tests show that the friction angle is dependent on the stress range considered. When selecting the friction angle to be used in the analysis, the maximum bearing pressure recorded (approximately 350 lb/in^2) reflected the upper bound to the major principal stress. Logically, the lower bound should be 0 lb/in^2 because the slope surface is not loaded. Results of the triaxial shear test indicate that

the soil friction angle ($\varnothing_{triax}$) may be rationally selected between 43.7° and 45.3°. If the previously mentioned correction for plane strain condition is applied to the triaxial shear friction angle, then $\varnothing_{pl}$ ranges approximately between 48° and 50°. Direct shear test results indicated a soil friction angle as low as 42.8°. It is, therefore, concluded that the friction angle selected might range anywhere between 42° and 50°. This is the range of the friction angle used in the analytical methods to determine the ultimate bearing capacities reported in this study.

Selected Analysis Conditions and Results

The ultimate bearing capacities representing solutions to the previously mentioned analytical methods were computed for the prototype test condition using soil friction angles between 42° and 50° in increments of 2°. As noted earlier, this range of friction angles for the sand used to make the model slopes incorporates friction angles determined by direct shear and triaxial shear testing as well as an approximated plane strain friction angle. A footing of infinite length was considered in all analyses. The computed ultimate bearing capacities are presented on figures 24, 25, and 26. The average, minimum, and maximum of the experimental maximum bearing pressures are also shown on these figures.

Figure 24 represents footings having a width (B) of 4.17 ft located on the surface at the crest of the slope. Data from model test conditions 10 through 16 are shown.

Figure 25 represents footings having a width (B) of 6.25 ft located on the surface at the crest of the slope. Data from test condition 17 are shown.

Figure 26 represents footings having a width (B) of 4.27 ft located at the crest of the slope at a depth (D) of 4.17 ft. Data from test condition 18 are shown.

Best-Fit Friction Angle

Emphasis is placed on the approximate friction angle that allows each analytical method to predict the model test results with the least error within the range of $\varnothing$ = 42° to $\varnothing$ = 50°. This is done because every method could be used to predict the maximum bearing pressure from the model tests by selecting an appropriate friction angle. The analytical method that predicts the observed maximum bearing pressure with the least error when using a friction angle in the plane strain range ($\varnothing$ = 48 to 50°) will undoubtedly be the best method for the conditions presented. The best-fit friction angle is defined for this purpose. The best-fit friction angle ($\varnothing_B$) is the friction angle which, when used with a given analytical

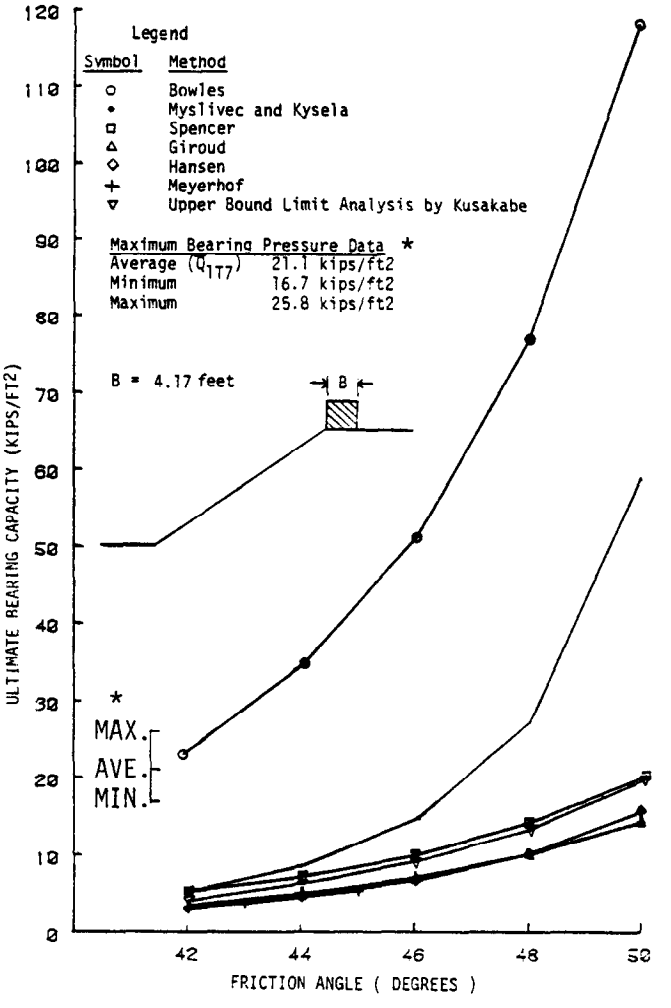

Figure 24. – Comparison of conditions 10 through 16 model test results with solutions by analytical methods.

method, yields the ultimate bearing capacity that predicts the average of the model test results with the lowest average percentage error.

The average percentage error (E) is defined by:

$$E = \frac{100}{3}\left(\left| Q_{10T16}(\varnothing) - \bar{Q}_{10T16} \right| / \bar{Q}_{10T16} + \left| Q_{17}(\varnothing) - \bar{Q}_{17}(\varnothing) \right| / \bar{Q}_{17} + \left| Q_{18}(\varnothing) - \bar{Q}_{18} \right| / \bar{Q}_{18} \right)$$

where:

$Q_{10T16}(\varnothing)$ is the ultimate bearing capacity computed for a given friction angle ($\varnothing$) using an analytical method. The prototype footing is represented by conditions 10 through 16.

$Q_{17}(\varnothing)$ is the ultimate bearing capacity computed for a given friction angle ($\varnothing$) using an analytical

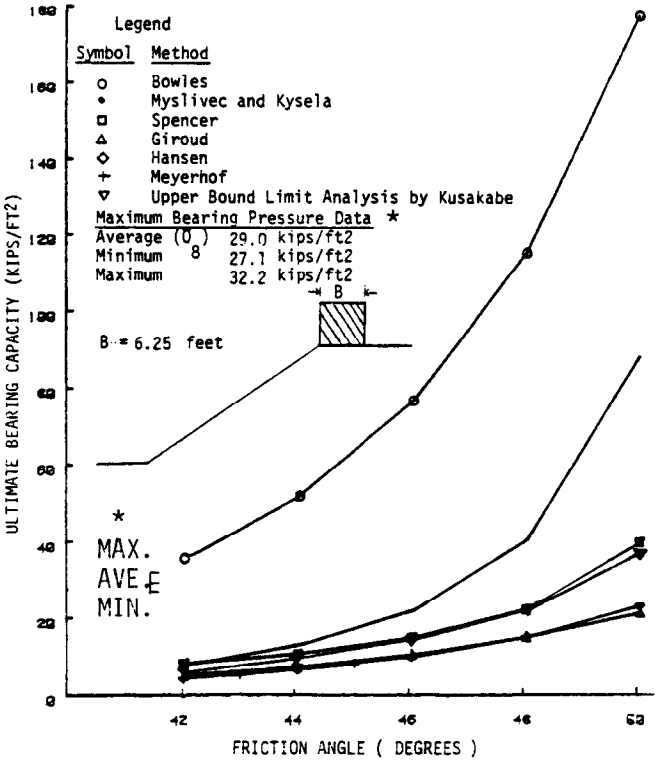

Figure 25. – Comparison of condition 17 model test results with solutions by analytical methods.

method. The prototype footing is represented by condition 17.

$Q_{18}(\varnothing)$ is the ultimate bearing capacity computed for a given friction angle ($\varnothing$) using an analytical method. The prototype footing is represented by condition 18.

$\bar{Q}_{10T16}$ is the average of the maximum bearing pressures recorded in the tests representing conditions 10 through 16. $\bar{Q}_{10T16}$ = 21.1 kips/ft².

$\bar{Q}17$ is the average of the maximum bearing pressures recorded in tests representing condition 17. $\bar{Q}_{17}$ = 29.0 kips/ft².

$\bar{Q}_{18}$ is the average of the maximum bearing pressures recorded in tests representing condition 18. $\bar{Q}_{18}$ = 46.4 kips/ft².

The values of E for values of $\varnothing$ between 42° and 50° are shown on figure 27. The values of $\varnothing_B$ for each method and the lowest average percentage error associated with that $\varnothing_B$ are given in table 4. The average experimentally recorded maximum bearing pressure and the computed ultimate bearing capacity using $\varnothing = \varnothing_B$ in each analysis are also given in table 4.

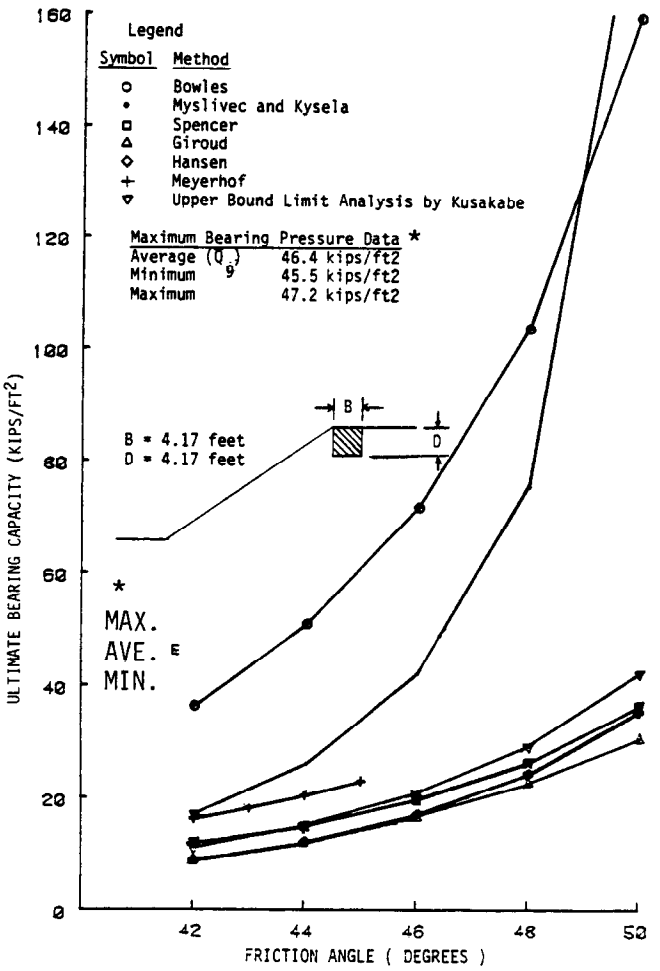

Figure 26. – Comparison of condition 18 model test results with solutions by analytical methods.

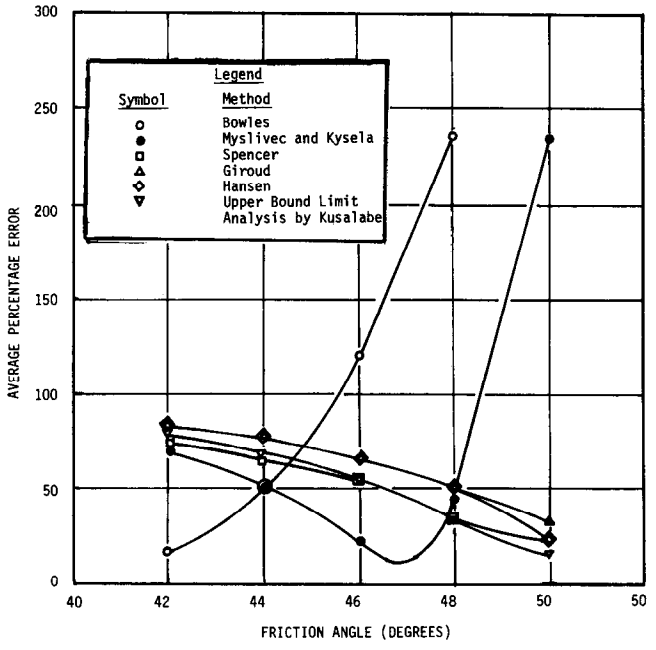

Figure 27. – Average percentage error versus friction angle.

Table 4. – Best-fit friction angle and lowest average percent error.

Analytical method	$\varnothing_B$ degrees	E lowest average percent error	Condition	$\bar{q}$ Average maximum bearing pressure from model test kips/ft²	Q_u Computed ultimate bearing capacity at $\varnothing = \varnothing_B$ kips/ft²
Bowles	42.0	19.0	10 through 16	21.1	23.8
			17	29.0	35.6
			18	46.4	36.4
Myslivec and Kysela	46.8	9.6	10 through 16	21.1	19.5
			17	29.0	29.3
			18	46.4	55.8
Spencer	50.0	21.4	10 through 16	21.1	20.0
			17	29.0	40.0
			18	46.4	36.6
Meyerhof	*	*	10 through 16	21.1	
			17	29.0	*
			18	46.4	
Hanson	50.0	22.8	10 through 16	21.1	15.6
			17	29.0	23.5
			18	46.4	35.5
Giroud	50.0	30.4	10 through 16	21.1	19.1
			17	29.0	21.6
			18	46.4	30.5
Limit analysis (by Kusakabe)	50.0	14.2	10 through 16	21.1	14.6
			17	29.0	37.0
			18	46.4	42.7

* Meyerhof's method does not permit the computation of all values required for $\varnothing_B$ calculation.

The best-fit friction angle may be interpreted visually using figures 24, 25, 26, and 27. For example, $\varnothing_B$ for Myslivec and Kysela's method is 46.8°. It can be observed on figures 24, 25, and 26 that, for this method, the bearing capacity computed using $\varnothing$ = 46.8° was in best agreement with the experimental results.

Bowles' Method

Bowles' semiempirical method yields values of ultimate bearing capacity near those observed in the model tests when a 42° friction angle is considered. The best-fit friction angle ($\varnothing_B$) for this method is 42°. The lowest average error was 19.1 percent. The method is very sensitive to the friction angle selection, as observed in figures 24, 25 and 26. Bowles' method for strip footings on cohesionless soils involves modifying the N_q value in the general bearing capacity equation to reflect slope influence. Bowles assumed a failure mechanism as shown on figure 28.

A reduced N_q called N_q' value is computed by multiplying the N_q factor for a footing on a horizontal ground surface by the ratio of A_1 to A_o where A_o = area gfae on figure 28a, and A_1 = area FAE on figure 28b.

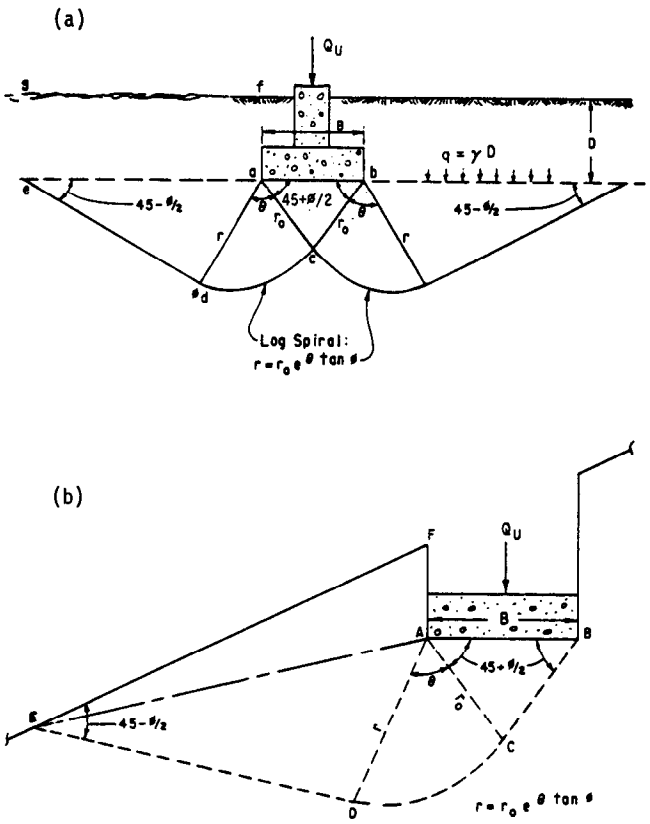

Figure 28. – Failure mechanism used in Bowles' analytical method: (a) horizontal ground surface, (b) sloping ground surface.

$$N_q' = N_q \frac{A_1}{A_o}$$

where:

$$N_q' = \exp(\pi \tan \varnothing) \times \tan^2(45° + \varnothing/2)$$

The ultimate bearing capacity is then computed using:

$$Q/B = \bar{q} N_q' + \frac{1}{2} \gamma B N_\gamma d_\gamma$$

where:

$N = 1.5 (N_q - 1) \tan \varnothing$, $q = \gamma D$, and d_γ = depth correction factor

$d_\gamma = 1$ for all $\varnothing$

It should be noted that some values of N_q' as provided in table 4-7 in Bowles' *Foundation Analysis and Design*, third edition [18] could not be computed using the method described. The values of N_q' computed using the area ratios are sometimes larger than those presented in the publication. Table 5

Table 5. – Comparison of computed values with values in Bowles' publication.

ø	N'_q Bowles (Table 4-7)*	N'_q (Computed)*
0	1.03	1.03
10	2.47	2.47
20	6.40	6.40
30	18.40	18.40
40	64.20	64.20

* The values of N'_q represent a surface footing at the crest of a slope. The slope is inclined 30° to the horizontal.

ø	N'_q Bowles (Table 4.7)**	N'_q (Computed)**
0	0.88	0.88
10	1.71	1.76
20	3.54	3.72
30	8.08	8.68
40	21.91	24.05

** The values of N'_q represent a buried footing at the crest of a slope. The depth to width ratio is 0.75. The slope is inclined 30° to the horizontal.

compares some computed values with the values in Bowles' table 4-7.

A problem occurs because the method makes no correction of the N_γ *factor in the general bearing capacity equation. Consider the case of a surface footing at the crest of a slope of cohesionless soil. The area ratio* $A_1/A_o = 1$; therefore, $N'_q = N_q$. In this condition the computed ultimate bearing capacity will be the same as that of a footing on a horizontal ground surface. This is not justified because, intuitively, the bearing pressure should decrease as the slope angle increases.

Bowles recommends using the friction angle determined from triaxial shear tests. In this case that friction angle is between 43.7° and 45.3°. As indicated earlier, this method yielded the best fit to the model footing test results when a friction angle of 42° was used. For all friction angles this method yielded ultimate bearing capacities greater than the measured model bearing pressures.

Myslivec and Kysela's Method

The method recommended by Myslivec and Kysela (which has been used in computer program BEARCAP by the Bureau) yields ultimate bearing capacities similar to those observed in the model tests when friction angles near 47° are considered. The best-fit friction angle ($ø_B$) is 46.8°, and the lowest average error is 8.7 percent (see fig. 27). Like Bowles' method, Myslivec and Kysela's method is very sensitive to the selected friction angle. The computed ultimate bearing capacity for a friction angle of 50° is considerably higher than the average of experimentally observed maximum bearing pressures. This method is a limit equilibrium solution. The assumed failure mechanism is shown on figure 29. Forces acting on the wedges are also shown on this figure. The wedges shown are treated as rigid masses and the forces acting on each wedge are determined for the condition of static equilibrium.

A graphical method of solution is provided in the publication *The Bearing Capacity of Building Foundations* [15]. The problem is solved numerically (in BEARCAP) by computing the forces needed for static equilibrium of each individual wedge, starting with the wedge nearest the slope, and working successively toward the wedge beneath the footing. Several failure surfaces, which intersect the slope and join the logarithmic spiral tangentially, are selected, and for each selection the ultimate bearing capacity is determined graphically or numerically. The failure surface that yields the lowest ultimate bearing capacity is selected as the solution.

The numerical approach is readily programmable and an existing Bureau computer program (BEARCAP)

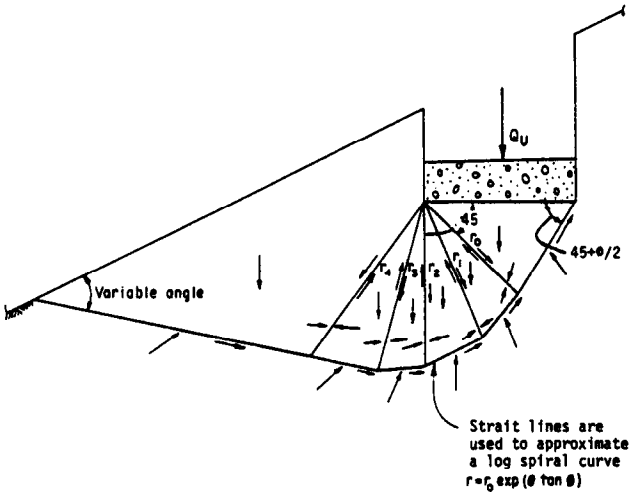

Figure 29. – Failure mechanism used in Myslivec and Kysela's analytical method.

was used to compute the values presented in table 4 and plotted on figures 24, 25, and 26.

Spencer's Limit Equilibrium Method

A general slope stability computer program, which uses the Spencer slope stability method of analysis, was used to determine ultimate bearing capacities. Spencer's method is based on the limit equilibrium approach. It permits the selection of a wide variety of failure surface shapes. The failure surface shape used in the analysis presented here is shown on figure 30a. The forces acting on a typical free body are shown on figure 30a. Detailed discussions of Spencer's limit equilibrium technique are available in [30, 31].

To calculate the ultimate bearing capacity using a slope stability method, safety factors are computed for many selected footing pressures. The footing pressure that produces a safety factor of 1 is selected as the ultimate bearing capacity.

The best-fit friction angle was computed to be 50° with an average error of 19.9 percent (see fig. 27). This approach did not always yield results equal to or lower than the average maximum bearing pressure at a friction angle of 50°. However, for friction angles less than 49° the results were all lower than the average maximum bearing pressure.

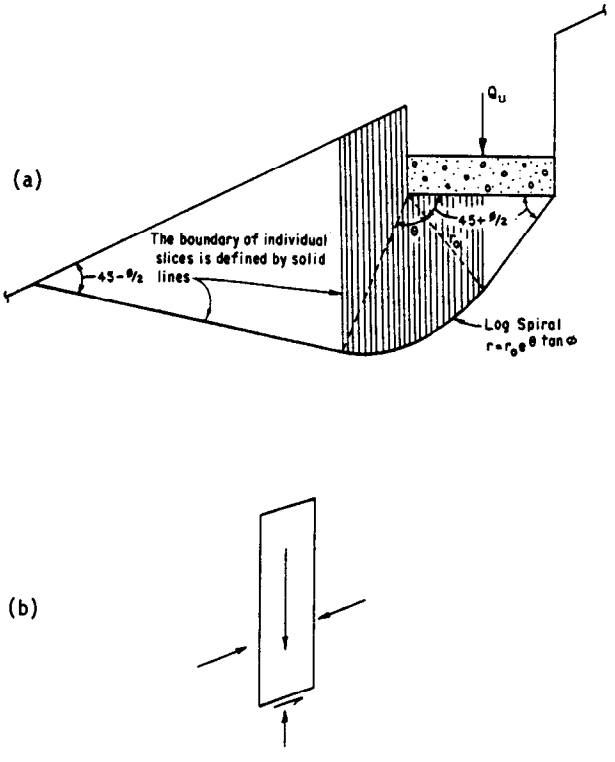

Figure 30. – Failure mechanism assumed when using the Spencer limit equilibrium approach: (a) failure surface shape, (b) forces acting on a typical free body.

Meyerhof's Method

Meyerhof assumed the region above the failure surface of a shallow rough strip footing to be divided into a rigid elastic zone *ABC*, a radial shear zone *ACD*, and a mixed shear zone *ADEF*, as shown on figure 31. He replaced the weight of soil wedge *AEF* by equivalent normal and tangential stresses, p_o and s_o, on plane *AE*, inclined from the horizontal at angle α. The slip-line method was used to solve for the stresses in the zone of plastic equilibrium. Meyerhof represents the ultimate bearing capacity by:

$$q = cN_{cq} + \frac{1}{2}\gamma BN_{\gamma q}$$

where N_q and N_{cq} are bearing capacity factors dependent on the depth-to-width ratio of the footing, the soil friction angle, and the slope angle.

Meyerhof [8] presented the bearing capacity factors N_{cq} and $N_{\gamma q}$ in chart form. The charts consider soil friction angles of 30°, 40°, and 45°. A linear-log interpolation was used to obtain factors between these values. Ultimate bearing capacities were not computed using friction angles greater than 45° because extrapolation would have been required. Therefore, the comparison shown on figures 24, 25, and 26 is restricted to friction angles between 42° and 45°.

It can be seen that Meyerhof's method results in ultimate bearing capacities less than the average maximum bearing pressures for friction angles less than 45°. It yields nearly identical ultimate bearing capacities as those computed using Giroud's or Hansen's methods for surface footings (figs. 24 and 25) and somewhat higher values for buried footings (fig. 26).

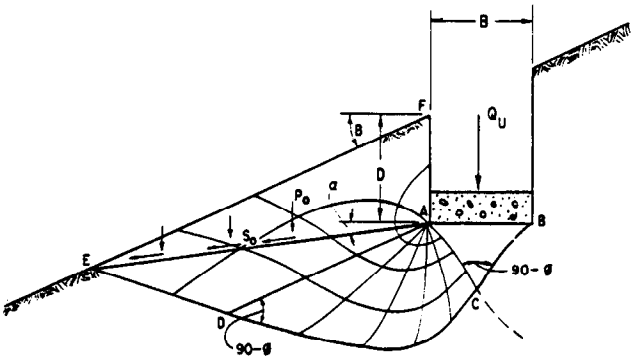

Figure 31. – Failure mechanism used in Meyerhof's method of analysis.

Hansen's Method

Hansen's method, like Meyerhof's, makes use of the slip-line method of solution. Hansen utilizes Prandtl's solution for N_q and N_c and derives an empirical formula for N_γ. The failure mechanism assumed by Hansen is shown on figure 32. The ultimate bearing capacity is given by the general bearing capacity equation. Semiempirical correction factors to the N_q, N_c, and N_γ terms are used to correct for the effect of the sloping ground surface. The correction factors were derived using the Coulomb earth pressure theory and exact slip-line solutions developed by various authors.

The best-fit friction angle using Hansen's method is 50°. The lowest average error is 19.7 percent (see fig. 27). It can be observed on figures 24, 25, and 26 that, at $\varnothing$ = 50°, Hansen's method consistently yields ultimate bearing capacities less than those experimentally observed. Hansen [10] recommends the use of the plane strain friction angle and the use of the equation $\varnothing_{pl} = 1.1\ \varnothing_{triax}$ to compute the plane strain friction angle from the triaxial shear test.

Giroud's Method

Giroud assumed a failure mechanism similar to Hansen's. He adjusted the N_c, N_q, and N_γ terms of the bearing capacity equation to account for the sloping ground surface. Giroud's work [11] is in French, and English translation is not available. The values of ultimate bearing capacities computed using Giroud's method were slightly lower than those computed using Hansen's method (see figs. 24, 25, and 26). A best-fit friction angle of 50° was computed for both methods (see fig. 27). The average error for Giroud's method was computed to be 30.4 percent, approximately 8 percentage points greater than Hansen's. Both methods predicted ultimate bearing capacities lower than experimental model test results when a friction angle $\varnothing$ = 50° is considered.

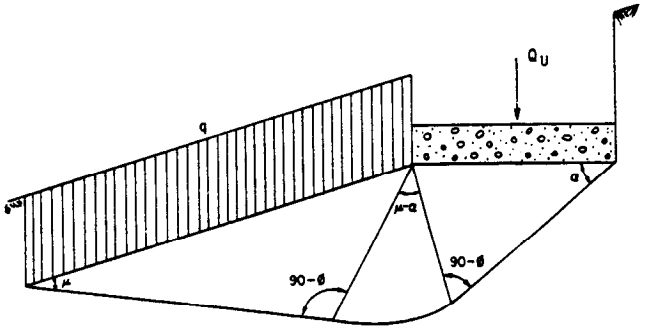

Figure 32. – General failure mechanism used in both Hansen's and Giroud's methods of analysis.

Kusakabe's Method – Upper-Bound Limit Analysis

Kusakabe et al. [19] used the upper-bound theorem of limit analysis to calculate N_c and N_γ values to be used in the equation:

$$q_{ult} = cN_c + \gamma \frac{B}{2} N_\gamma$$

to solve for the ultimate bearing capacity of surface footings at the top of a slope. The failure mechanism for this problem is shown on figure 33, in which triangular region ABC is an active wedge, CD is a logarithmic spiral, and DE is a straight line, which connects tangentially with the log spiral and intersects the slope. Solutions were presented for only surface footings. This author extended the analyses to provide for use with a buried footing. The assumed failure mechanism is shown on figure 33a. The extension of Kusakabe's original solution simply involved computing the area of wedge ADEF, shown on figure 33b, and substituting it in the analysis wherever the area of wedge ADE was previously used. This agrees with the upper bound approach. The friction between the side of the footing and the soil was not considered.

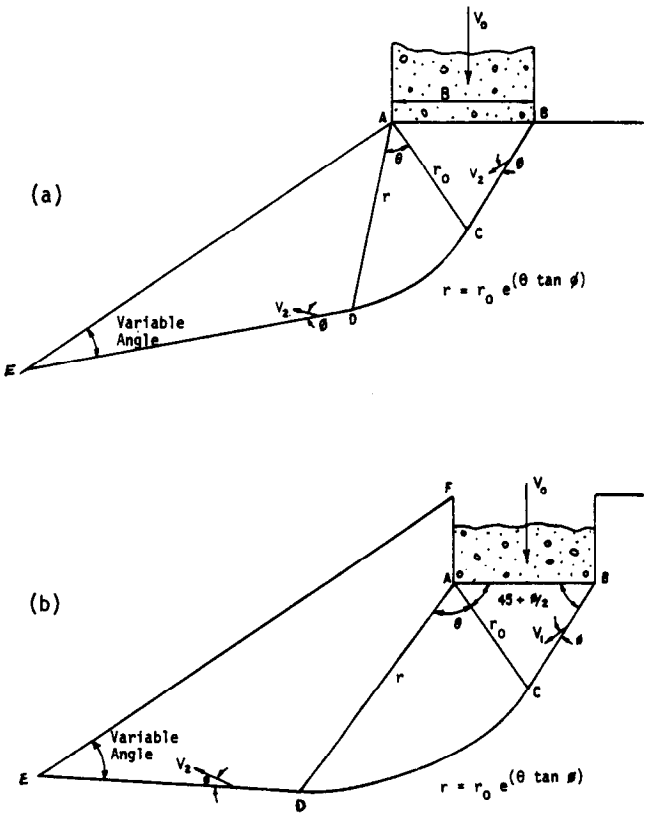

Figure 33. – Upper-bound limit analysis failure mechanism: (a) by Kusakabe, (b) Kusakabe's mechanism modified to account for footing burial.

The upper bound ultimate bearing capacity is found by moving the intersection of the failure surface with the slope, computing the ultimate bearing capacity for each selected failure surface, then selecting the lowest of these values.

The computed ultimate bearing capacities are compared with the model test results on figures 24, 25, and 26. The best-fit friction angle was computed to be 50° with the lowest average error equal to 14.2 percent (see fig. 27). At $\varnothing$ = 50°, the computed values of ultimate bearing capacity are reasonably close to observed test results.

Discussion

A plane strain failure mechanism prevailed during model testing for conditions 10 through 16, as discussed earlier. It is assumed that plane strain failure also represents the failure mechanism experienced during model testing for conditions 17 and 18. Therefore, the plane strain friction angle should be used in calculating the ultimate bearing capacity using the different theories. This friction angle is approximated to be 48° to 50° using the equation $\varnothing_{pl} = 1.1\ \varnothing_{triax}$. The best agreement with model test results in this range of friction angles was achieved by the limit analysis solution by Kusakabe and by the application of a limit equilibrium technique, which involved Spencer's slope stability method. Hansen's and Giroud's methods also predicted the experimentally observed maximum bearing pressure within reason at $\varnothing$ = 50°. The lowest average errors for these methods were 14.2 (Kusakabe), 21.4 (Spencer), 22.8 (Hansen), and 30.4 (Giroud) percent. Neither the Spencer limit equilibrium approach nor Kusakabe's limit analysis approach always yielded conservative results. Using these methods, the ultimate bearing capacities predicted for the case of 6.25-foot-wide surface footing (condition 17) with $\varnothing$ = 50° were approximately 38 (Spencer) and 27 (Kusakabe) percent greater than the experimentally observed maximum bearing pressure. Analyses by Hansen's and Giroud's methods were conservative in all cases.

Figures 24 and 25 show that Meyerhof's analysis method results in ultimate bearing capacities similar to Hansen's and Giroud's for the case of a surface footing. The curve on figure 26, which represents the analyses results using Meyerhof's method for the buried footing (condition 18), appears to be parallel and higher than the curves representing Hansen's and Giroud's methods.

Because Meyerhof's analysis did not provide bearing capacity factors for friction angles greater than 45°, ultimate bearing capacities were not calculated for $\varnothing$ greater than 45°. Therefore, it is impossible to make a complete comparison of his method with the model test results.

Meyerhof, like Hansen and Giroud, used a slip-line method of solution. Therefore, Meyerhof's method is expected to give similar results for surface footings. Meyerhof's method yields a higher value for a buried footing because he assumed a different failure mechanism for this condition than Giroud and Hansen assumed.

The limiting equilibrium method proposed by Myslivec and Kysela predicted the experimentally observed maximum bearing pressures with the lowest average error (9.6 percent) for $\varnothing_B$ = 46.8°. The lowest average error using this method was smaller than any other method. However, at the plane strain friction angle of approximately 50°, the computed ultimate bearing capacity increases considerably. This emphasizes the method's sensitivity to the selected friction angle. Myslivec and Kysela's method cannot be dismissed as inaccurate because the plane strain friction angle is approximated and may be off by several degrees. Obviously, care should be taken when using this method.

On figures 24 and 25, it appears that the extreme of the computed ultimate bearing capacities was obtained using Bowles' method. This method consistently predicted ultimate bearing capacities greater than those experimentally observed.

This method is not recommended for calculating the ultimate bearing capacity of spread footings on steep slopes of cohesionless soils because it has been shown that other methods predict model test results much more accurately.

Observed Failure Mechanisms

The model slopes in several tests were constructed with alternating horizontal layers of colored sand. Displacement of these layers was observed and photographed through the Plexiglas model container wall.

The photographs taken after the completion of tests 3, 5, 8, 9, 21, 23, and 25 are provided in appendix D on figures D-1 through D-7. Tests 5, 9, and 23 represent a 4.17-foot-wide surface footing at the crest of a slope. Tests 3, 8, 21, and 25 represent an 8.33-foot-wide surface footing at the crest of a slope.

Interpreted failure mechanisms for tests 3, 5, 8, 9, 21, 23, and 25 are provided on figures D-8 through D-14. The prototype footing and ground surface locations after test completion are designated by the dashed lines. These lines are also used to define

zones 1, 2, and 3, which were selected to represent the observed failure mechanism. The lower limits of these zones could not be defined for test 3.

Zone 1 is in the form of a triangular wedge beneath the footing. One side is defined by the footing base, and the other two by observed shear surfaces. Zone 3 is roughly triangular in shape, with one side defined by the slope surface; another side is defined by an observable shear surface, which intersects the slope; and the last side was arbitrarily selected to represent the boundary between observed small vertical shear strains and negligible vertical shear strains. Zone 2, between zones 1 and 3, represents a transition zone between observed large vertical shear strains and small vertical shear strains.

The use of three zones to represent the failure mechanism is analogous to the use of three zones common in theoretical analyses. However, the shape of the zones on figures D-8 through D-14 are considerably different from those generally assumed by theory. This may be the result of modeling problems, which were discussed earlier, or it may be due to the large strains experienced by the soil after the failure condition had been achieved. The modeling problems include bulging of the model container and friction between the sand and the container sides. Intuitively, the shapes of the observed failure surfaces and the zones are influenced by the magnitude of the footing displacement. The relative footing displacements, shown in the photographs (figs. D-1 through D-5) are very large, generally in excess of 0.5. Failure mechanisms used in analytical methods are typically developed at zero vertical displacement. For these reasons, discretion must be used when comparing the shape of the observed failure surfaces with those assumed in analytical solutions.

From the photographs in appendix D, zone 1 appears to move as a rigid wedge. This corresponds with the assumption used in most theoretical analyses.

Zone 2 is analogous to the radial shear zone assumed in the slip-line and limit analysis methods, but its shape is different from most theoretical assumptions. This difference is expected considering the large strains the sand has undergone in this zone during the test. When the footing was at the relative displacement corresponding to the maximum bearing pressure, zone 2 may have appeared more triangular in shape.

Zone 3 experiences only a small amount of shear strain; therefore, it may be considered to have behaved predominantly as a rigid mass. This is the assumption used in most theoretical analyses.

More research is needed to define the failure mechanisms and its development. The failure mechanism observed in this study is conceptually the same as that proposed by most theories; however, a well-defined failure mechanism cannot be established.

SUMMARY

The Bureau initiated a study to evaluate and improve the state of the art of predicting the ultimate bearing capacity of shallow spread footings located on or near slopes. The study involved: (1) reviewing the state-of-the-art analytical solutions; (2) developing and testing a technique for modeling shallow spread footings located on or near slopes; (3) experimentally determining the maximum bearing pressure of prototype shallow spread footings using scaled models; and (4) comparing experimental results with state-of-the-art analytical solutions.

The results of the research program are presented in this report. A state-of-the-art review of analytical methods is included as is a complete set of model test results and laboratory test results on the sand used in the models. Model test results are compared with six readily available and frequently used analytical bearing capacity analyses. These include analyses developed by Meyerhof, Hansen, Giroud, Bowles, Kusakabe, and Myslivec and Kysela. A limit equilibrium analysis using a technique developed by Spencer is also compared with model test results.

Slip-line, limit equilibrium, and limit analysis are the most common theoretical approaches to solving bearing capacity problems. Many authors have derived theoretical and empirical solutions to problems pertaining to the bearing capacity of shallow footings. These solutions often take the form of the general bearing capacity equation.

The first recorded model test pertaining to footings on slopes was conducted and reported by Peynircioglu in 1948. Since then, the problem has been considered by many investigators.

Despite difficulties involved in centrifugal modeling, the use of a centrifuge has become an increasingly effective means for modeling geostructures. These difficulties include equipment vibration; scale, geometric, and boundary anomalies; the effect of coriolis acceleration; and instrumentation problems. The centrifugal testing method was used in this study. The concept of modeling of models was applied to test the validity of the scaling relations and the significance of altered boundary conditions.

Sixty-one models representing 18 prototype footings, slope conditions, and scales were tested. The results of 59 of these tests were reported. The slope geometry, footing sizes, and footing locations were selected to represent conditions common to Bureau

bridge foundations on or near canal slopes. Plane strain and three-dimensional conditions were tested. Models were constructed in a model container having dimensions 6 by 11.5 by 16 inches. The model slopes were constructed of dense, poorly graded, air-dried sand, and the model footings were constructed of aluminum. Model tests were conducted under artificial gravity equal to 50, 66.7, and 100 *g*, where *g* is the earth's gravitational acceleration.

Considerable friction developed between the container walls and the sand, and between the container walls and the footing, during tests representing plane strain conditions. This prevented accurate modeling of the maximum bearing pressures recorded in plane strain tests. This was discovered by the process of modeling of models. For plane strain conditions, the relative displacement at maximum bearing pressure modeled for surface footings but not for buried footings.

Both the maximum bearing pressure and the relative displacement at the maximum bearing pressure modeled satisfactorily for three-dimensional model tests. A minimum of three tests were conducted for each test condition. A comparison of tests representing the same condition showed that test results were readily reproducible.

Changing footing length-to-width ratios from 2.5 to 10.8 had no significant influence on the recorded maximum bearing pressure or the relative displacement at the maximum bearing pressure, when footings having the same widths were considered. This led to the conclusion that the three-dimensional models failed predominantly in a plane strain manner.

Vertical footing displacement was observed to be uniform from one end of the footing to the other. However, horizontal movement of the footing toward the slope was observed in all tests. Frequently, one end of the footing moved toward the slope more than the other end did.

The sand composing the model slopes was compacted to approximately 100 percent relative density. The friction angle determined by triaxial shear tests was stress dependent and, for the stresses encountered in the experiments, ranged from 43.7° to 45.3°. Two direct shear tests series resulted in a friction angle of 42.8° and 43.7°. The plane strain friction angle most suitably represents the soil shear strength for the conditions modeled. The plane strain friction angle ranged from approximately 48° to 50°. This is 10 percent greater than the triaxial shear test friction angle.

The upper bound limit analysis method of Kusakabe and the limit equilibrium method of Spencer predicted the maximum bearing pressure in best agreement with model test results using an approximated plane strain friction angle of $\varnothing = 50°$.

Hansen's and Giroud's methods also predicted the experimentally observed maximum bearing pressure within reason, with $\varnothing = 50°$.

The upper bound limit analysis and the Spencer slope stability approach did not always yield results lower than measured pressures, whereas both Hansen's and Giroud's methods did.

The use of Meyerhof's method was limited to friction angles less than 45°, making its comparison with test results using the plane strain friction angle impossible. Meyerhof, like Hansen and Giroud, used a slipline method of solution. Meyerhof's method gave similar results for surface footings and higher maximum bearing pressures than Giroud's or Hansen's methods for the case of a buried footing. This is caused by a difference in the assumed failure mechanism.

The limit equilibrium approach proposed by Myslivec and Kysela predicted the experimentally observed maximum bearing pressure with the least error for $\varnothing = 46°$. However, the method is very sensitive to small changes in $\varnothing$. At $\varnothing = 50°$, this method yielded an ultimate bearing capacity pressure considerably greater than the experimentally observed maximum bearing pressure.

Bowles' method consistently predicted bearing pressures greater than those experimentally observed.

CONCLUSIONS AND RECOMMENDATIONS

Footings on steep slopes of cohesionless soil were successfully modeled using centrifugal modeling techniques. This was proven by applying the concept of modeling of models. Modeling of models showed that the combined effects of model container expansion and friction between the soil and model container walls adversely affected model behavior during tests of plane strain footings. On the other hand, it proved that three-dimensional footing models were not significantly affected by the boundary conditions imposed by confinement in the model container.

The maximum bearing pressures from 59 model tests were compared with numerical solutions by using seven analytical methods. These included methods suggested by Meyerhof, Hansen, Giroud, Bowles, Kusakabe, Myslivec and Kysela, and an analysis using an adaptation of Spencer's limit equilibrium method. These methods represent solutions by slipline, limit equilibrium, and limit analysis methods.

Any of the methods and friction angles considered on figure 24 could be used by an engineer to analyze the prototype footing and slope condition represented by model conditions 10 through 16. There is a factor of 38 between the highest and lowest ultimate bearing capacity shown on this figure. This evidence established the need for care in selecting the analysis method and the appropriate friction angle.

Plane strain conditions were shown to predominate during the model tests; therefore, the plane strain friction angle is most appropriate for use in the analytical methods.

Meyerhof's method could not be compared directly with model test results when a plane strain friction angle was selected. This is because Meyerhof did not report bearing capacity factors for friction angles greater than 45°, and the plane strain friction angle was selected at approximately 50°. However, comparison of Meyerhof's method with Giroud's and Hansen's methods indicates that the approach is similar. Therefore, it is concluded that Meyerhof's method would agree closely with test results if a comparison were possible.

Model test results indicate that the limit analysis method of Kusakabe, the Spencer limit equilibrium approach (described in this report), and the methods of Meyerhof, Hansen, and Giroud all may be used with the plane strain friction angle and standard bearing capacity safety factors (2.5 to 4) to predict safe allowable bearing pressures. However, the method proposed by Myslivec and Kysela is not recommended for use in design because of its extreme sensitivity to small changes in the selected soil friction angle. Research is needed to evaluate the effect that the changing soil friction angle has on the maximum bearing pressure.

Bowles' method consistently predicted maximum bearing pressures greater than those experimentally determined; therefore, its use is not recommended for design.

Future related research should include investigating, in detail, the influence of the following factors with regard to the ultimate bearing capacity, failure mechanism, and displacement characteristics of footings on slopes of cohesionless soil:

1. Soil friction angle
2. Slope inclination angle
3. Footing location
4. Footing depth
5. Footing width
6. Footing length
7. Loading mechanism

Although there are many other factors that influence the ultimate bearing capacity, these seven were selected because they are relatively easy to control and test. Testing the effects of these factors will provide data needed to better understand the bearing capacity problem as it pertains to slopes of cohesionless soil. It will also permit more complete comparison of the existing analytical methods and thereby improve the state of the art.

BIBLIOGRAPHY

[1] Chen, Wai-Fah, *Limit Analysis and Soil Plasticity,* Elsevier Scientific Publishing Company, New York, N.Y., 1975.

[2] Koetter, F., "Die Bestimmung des Druckes an gekrummten Gleitflachen, eine Aufgabe aus der Lehre vom Erddruck," *Monatsber, Akad. Wiss. Berlin,* pp. 229-203, 1903.

[3] Prandtl, L., "Uber die Harte plastischer Korper," *Nachr, K. Ges. Wiss. Gott., Math-Phys. Kl.,* pp. 74-85, 1920.

[4] Sokolovskii, V. V., *Statics of Grandular Media,* Pergamon Press, New York, N.Y., 1965.

[5] de Jong, D.J.G., "Graphical Method for the Determination of Slip-Line Fields in Soil Mechanics," (in Dutch) *Ingenieru,* vol. 69 (29), pp. 61-65, 1957.

[6] Spencer, A.J.M., "Perturbation Methods in Plasticity. III, Plane Strain of Ideal Soils and Plastic Solids with Body Forces," *Journal of the Mechanics and Physics of Solids,* vol. 10, pp. 165-177, 1962.

[7] Dembicki, E., J. Dravtchenko, and E. Sibille, "Sur les Solutions Analytiques Approchees des Problemes D'Eeuilibre Limite Plan Pour Milieux Coherents et Pesants," *Journal de Mechanique,* vol. 3, pp. 277-312, 1964.

[8] Peynircioglu, H., "Test on Bearing Capacity of Shallow Foundations on Horizontal Top Surfaces of Sand Fills," *Proceedings,* Second International Conference on Soil Mechanics and Foundation Engineering, vol. 3, p. 194, 1948.

[9] Meyerhof, G. G., "The Ultimate Bearing Capacity of Foundations on Slopes," *Proceedings,* Fourth International Conference on Soil Mechanics and Foundation Engineering, London, 1957.

[10] Hansen, J. Brinch, "A Revised and Extended Formula for Bearing Capacity," Reprint of Lecture in Japan, October 1968.

[11] Giroud, J. P., and Tran-Vo-Nhiem, "Force Portante d'une Fondation sur une Pente," *Theories et Methodes de Calcul,* pp. 131-140, July-August 1971.

[12] Dembicki, Eugeniusz, and Bohdan Zadroga, "Model Tests on Bearing Capacity of Foundations on Slope," *Proceedings* 4th Danube-European Conference on Soil Mechanics and Foundation Engineering, Bled, Slovenia, 1974.

[13] Shield, D. H., J. D. Scott, G. E. Bauer, J. H. Deschenes, and A. K. Barsvary, "Bearing Capacity of Foundations Near Slopes," *Proceedings,* Ninth International Conference on Soil Mechanics and Foundation Engineering, vol. 1, Tokyo, Japan, 1977.

[14] Craig, Robert F., and Lakshmi N. M. Pariti, "Limiting Equilibrium Analysis of Strip Footings," *Journal of the Geotechnical Engineering Division,* American Society of Civil Engineers, vol. 104, No. GT3, March, 1978.

[15] Myslivec, Alois, and Zdenek Kysela, *The Bearing Capacity of Building Foundations,* Elsevier Scientific Publishing Company, New York, N.Y., 1978.

[16] Gemperline, Mark C., "Ultimate Bearing Capacity Program, BEARCAP," Program for the Tektronic Computer, Bureau of Reclamation, Denver, Colo., January, 1981.

[17] Bowles, Joseph E., *Foundation Analysis and Design,* 2nd edition, McGraw-Hill Book Company, New York, N.Y., 1977.

[18] _____ , *Foundation Analysis and Design,* 3rd edition, McGraw-Hill Book Company, New York, N.Y., 1982.

[19] Kusakabe, Osamu, Tsutomu Kimura, and Hakuju Yamaguchi, "Bearing Capacity of Slopes Under Strip Loads on the Top Surface," *Soils and Foundations,* Japanese Society of Soil Mechanics and Foundation Engineering, vol. 21, No. 4, December 1981.

[20] Blitz, P., Ch. Brodel, and K. Reinhardt, "Spatial Calculation of Slope Stability Under Definite Surcharges," *Proceedings,* Tenth International Conference on Soil Mechanics and Foundation Engineering, vol. 3, Stockholm, Sweden, June 1981.

[21] Mikhailov, Yu B., "Computing the Stability of a Foundation Located Near the Edge of an Embankment," *Soil Mechanics and Foundation Engineering,* vol. 19, No. 3, (Translated from Russian by Consultants Bureau, New York, N.Y.), pp. 96-106, May-June 1982.

[22] Assouz, Amr S., and Mohsen M. Baligh, "Loaded Areas on Cohesive Slopes," *Journal of Geotechnical Engineering,* American Society of Civil Engineers, vol. 109, No. 5, May 1983.

[23] Chugh, Ashok K., *User Information Manual – Slope Stability Analysis Program "SSTAB2" (A Modified Version of "SSTAB1" by Stephen G. Wright),* Bureau of Reclamation, Denver, Colo., February 1981.

[24] *Principles of Geotechnical Physical Modeling,* University Extension, University of California, Davis, Calif., 1982.

[25] Ovesen, N. Krebs, "Centrifugal Testing Applied to Bearing Capacity Problems of Footings on Sand," *Geotechnique,* vol. 25, No. 2, June 1975.

[26] Mikasa, M., and N. Takada, "Significance of Centrifugal Model Test in Soil Mechanics," *Proceedings,* Eighth International Conference of Soil Mechanics and Foundation Engineering, vol. 1.2, 1973, Moscow, U.S.S.R.

[27] Herdy, A. C., and F. C. Townsend, *Preliminary Investigation of the Bearing Capacity of Layered Soils by Centrifugal Modeling,* Paper presented to the Transportation Research Board, January 18, 1982.

[28] *Earth Manual,* 2nd Edition, U.S. Department of the Interior, Bureau of Reclamation. U.S. Government Printing Office, Washington, D.C., reprint 1974.

[29] Marachi, N. D., C. K. Chan, H. B. Seed, and J. M. Duncan, *Strength and Deformation Characteristics of Rockfill Materials,* Report No. TE-69-5 to State of California Department of Water Resources, University of California, Department of Civil Engineering, Institute of Transportation and Traffic Engineering, 1969.

[30] Winterkorn, Hans F., and Hsai-Yang Fang, *Foundation Engineering Handbook,* VanNostrand Reinhold Company, New York, N.Y., 1975.

[31] Spencer, E., "A Method of Analysis of the Stability of Embankments Assuming Parallel Inter-Slice Forces," *Geotechnique,* XVII, No. 1, pp. 11-16, 1967.

APPENDIX A

COMPLETE SET OF DATA FOR EACH OF 59 FOOTING TESTS

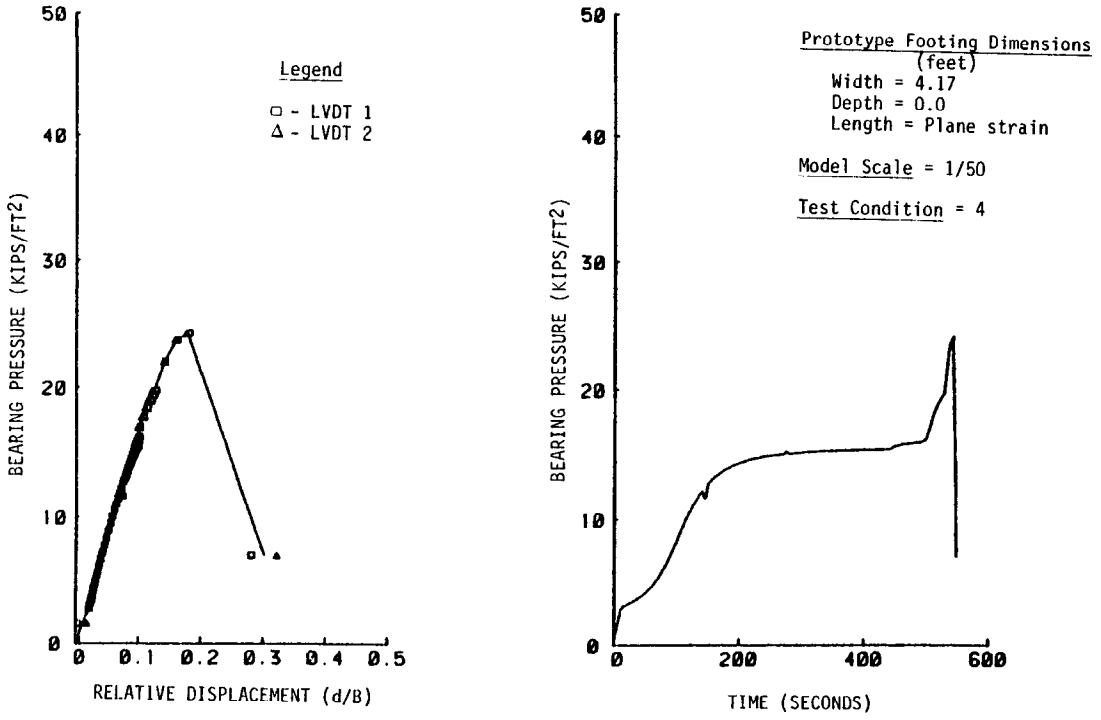

Figure A-1. – Results of test No. 1.

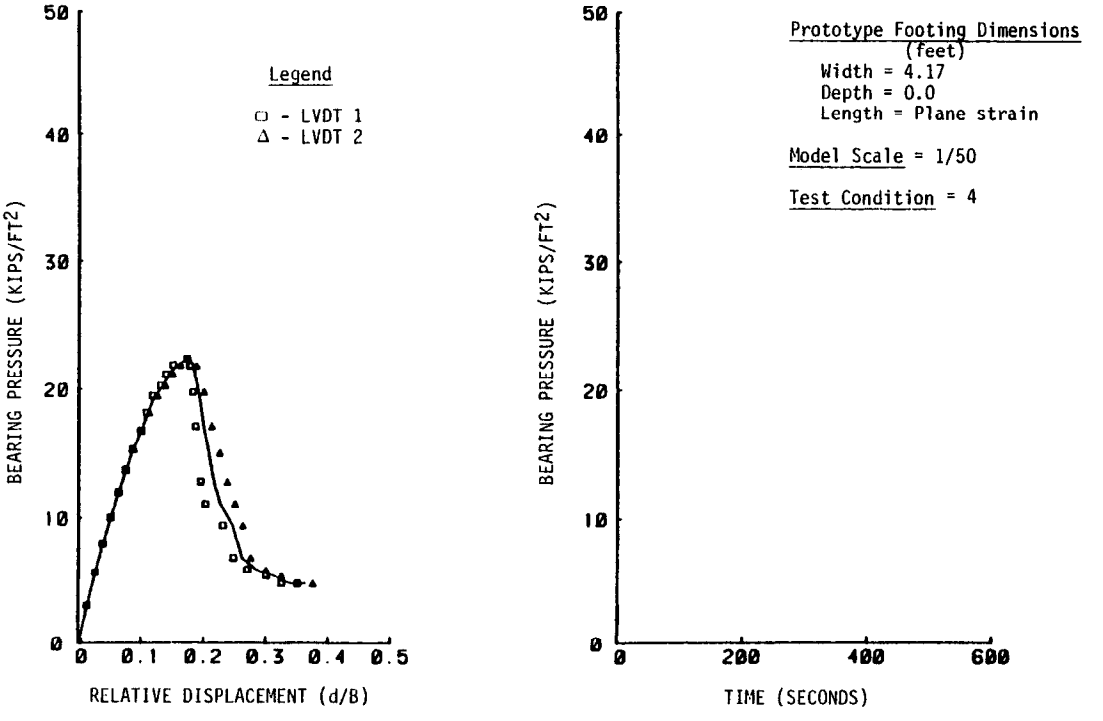

Figure A-2. – Results of test No. 2.

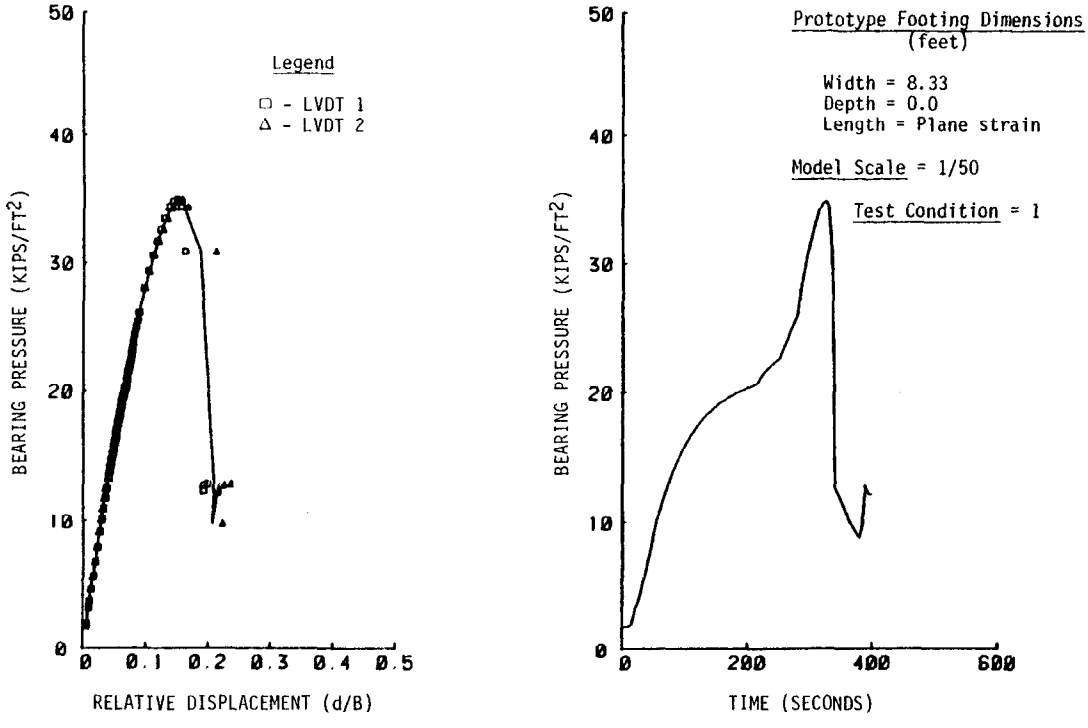

Figure A-3. – Results of test No. 3.

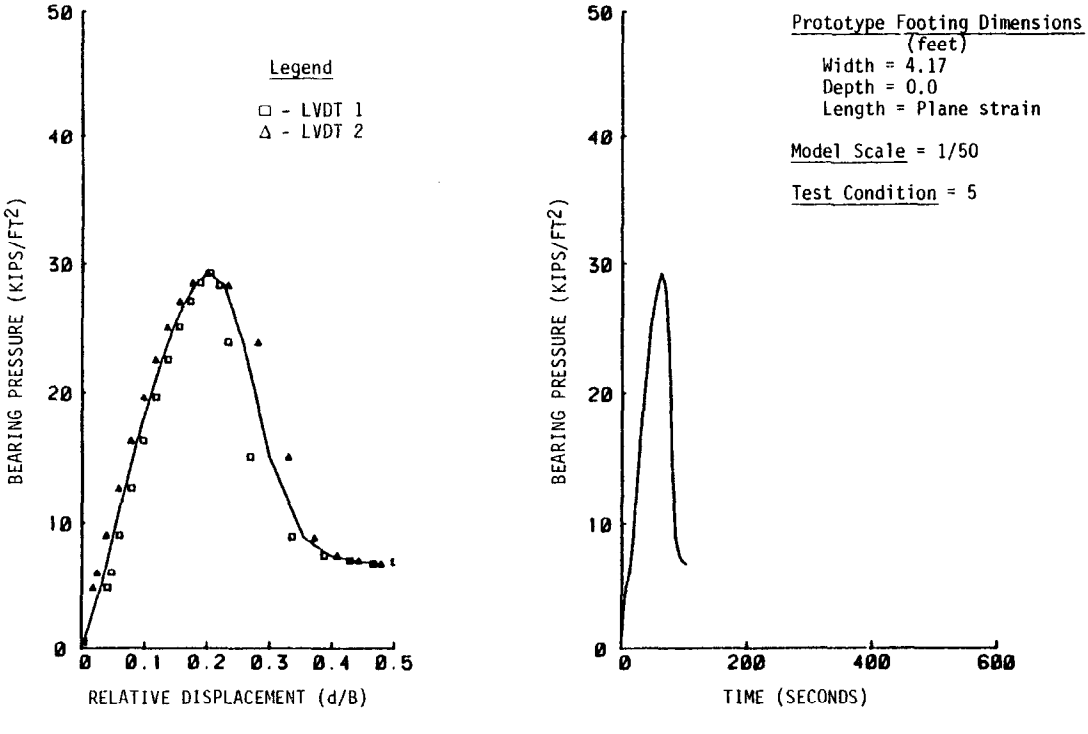

Figure A-4. – Results of test No. 4.

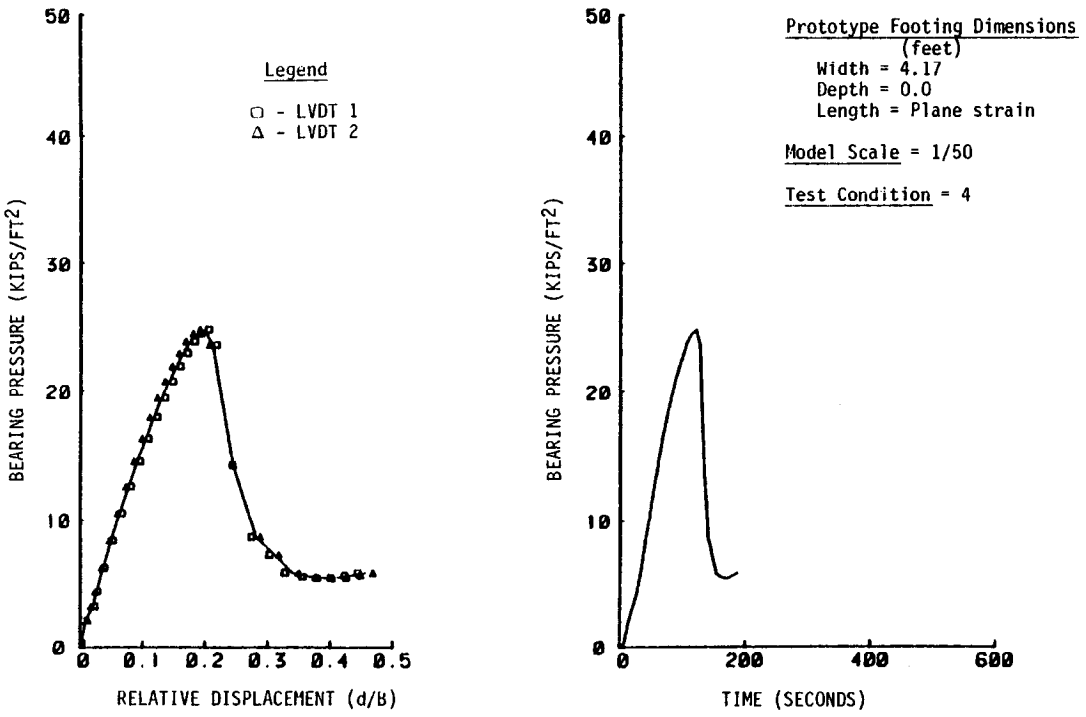

Figure A-5. – Results of test No. 5.

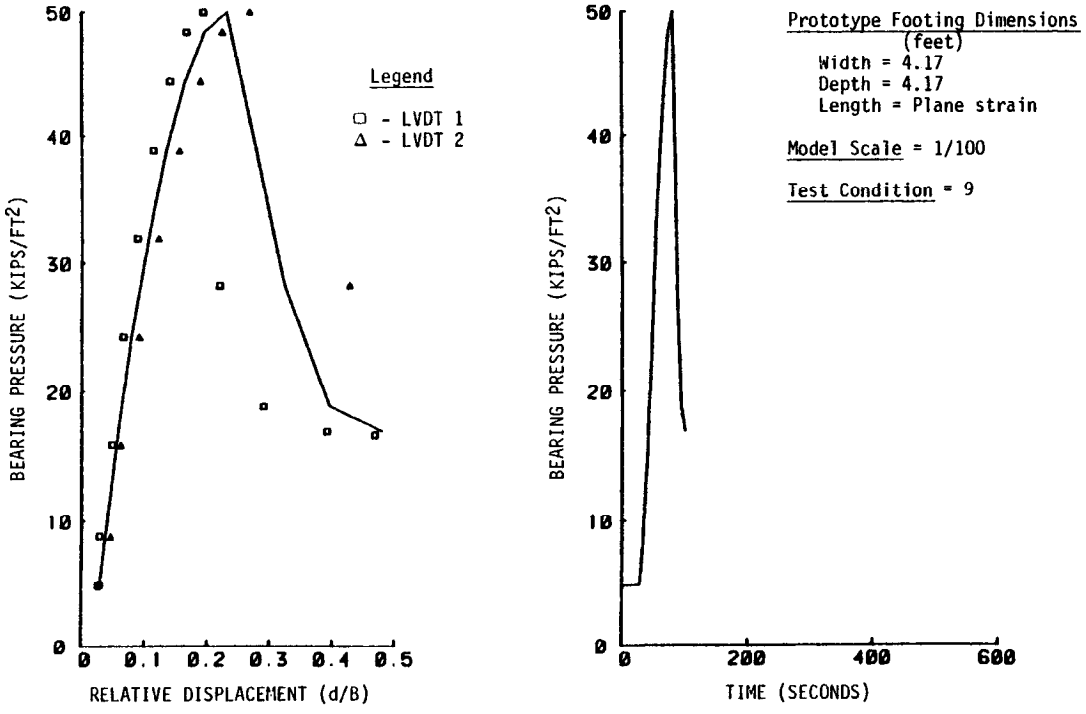

Figure A-6. – Results of test No. 6.

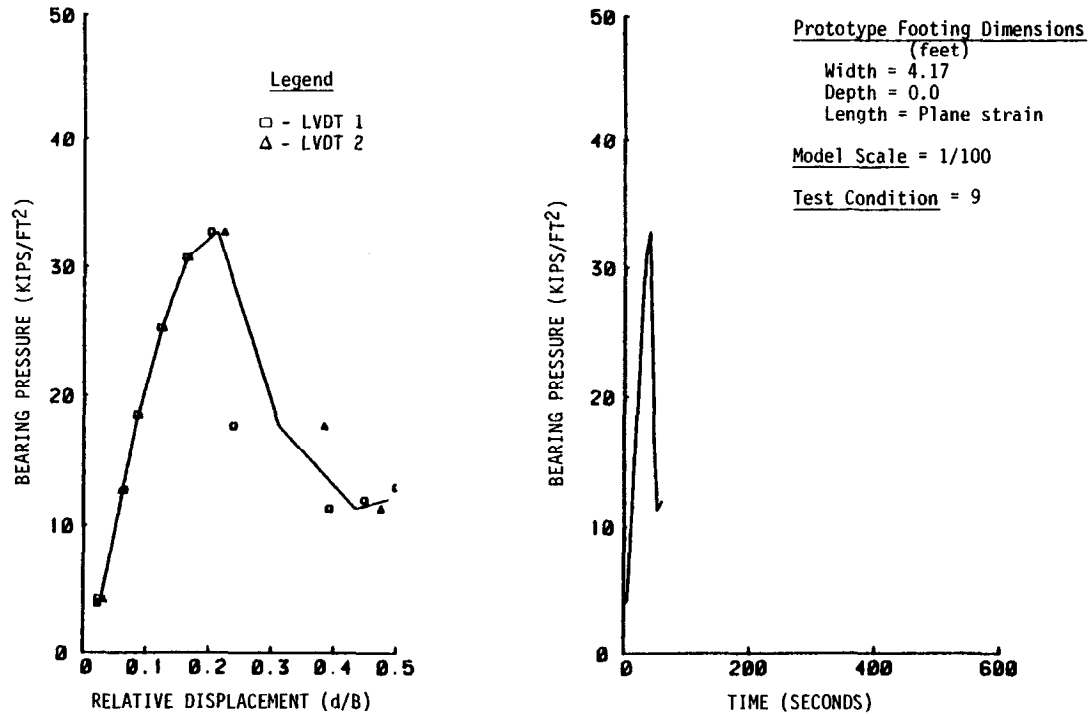

Figure A-7. – Results of test No. 7.

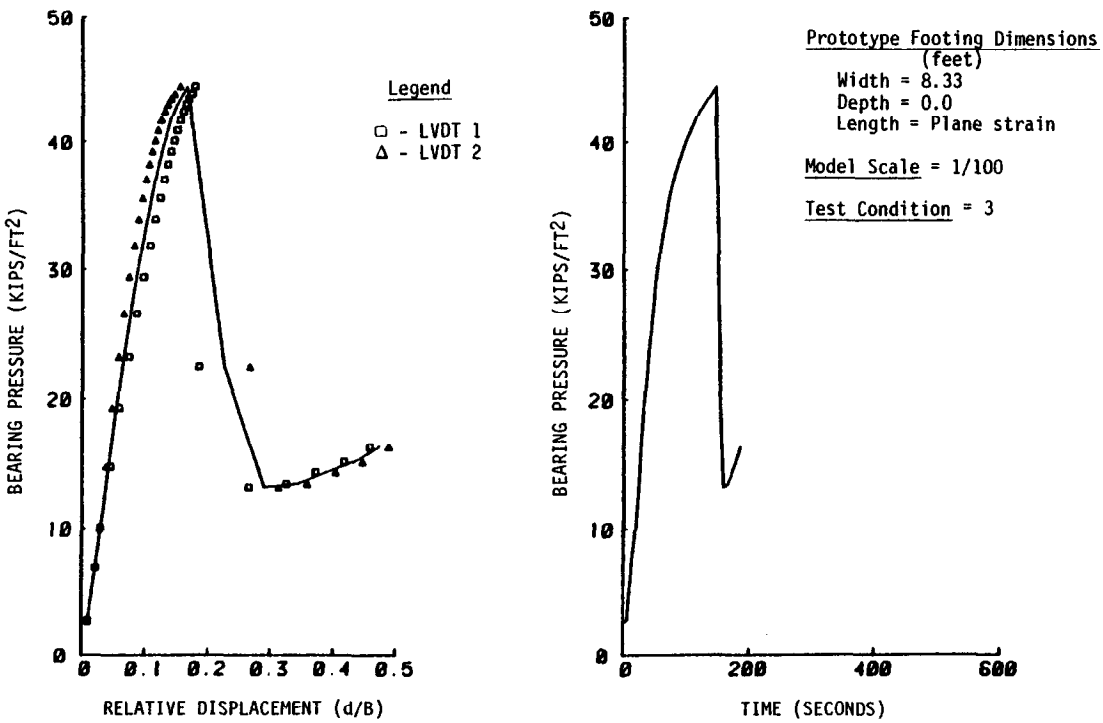

Figure A-8. – Results of test No. 8.

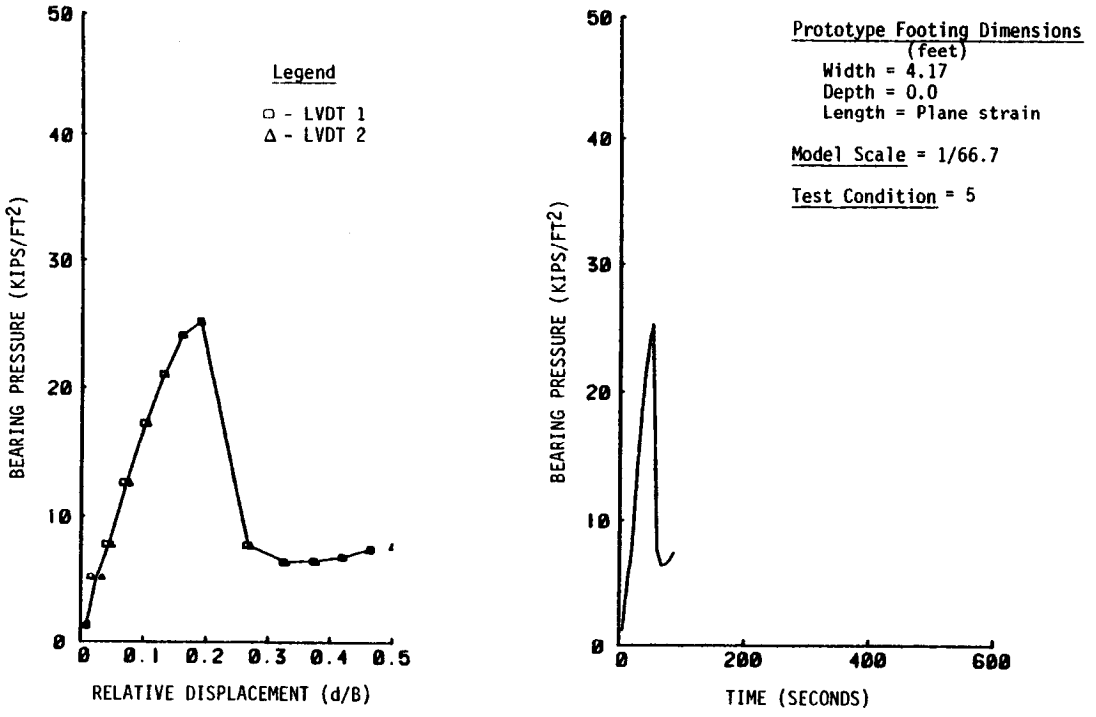

Figure A-9. – Results of test No. 9.

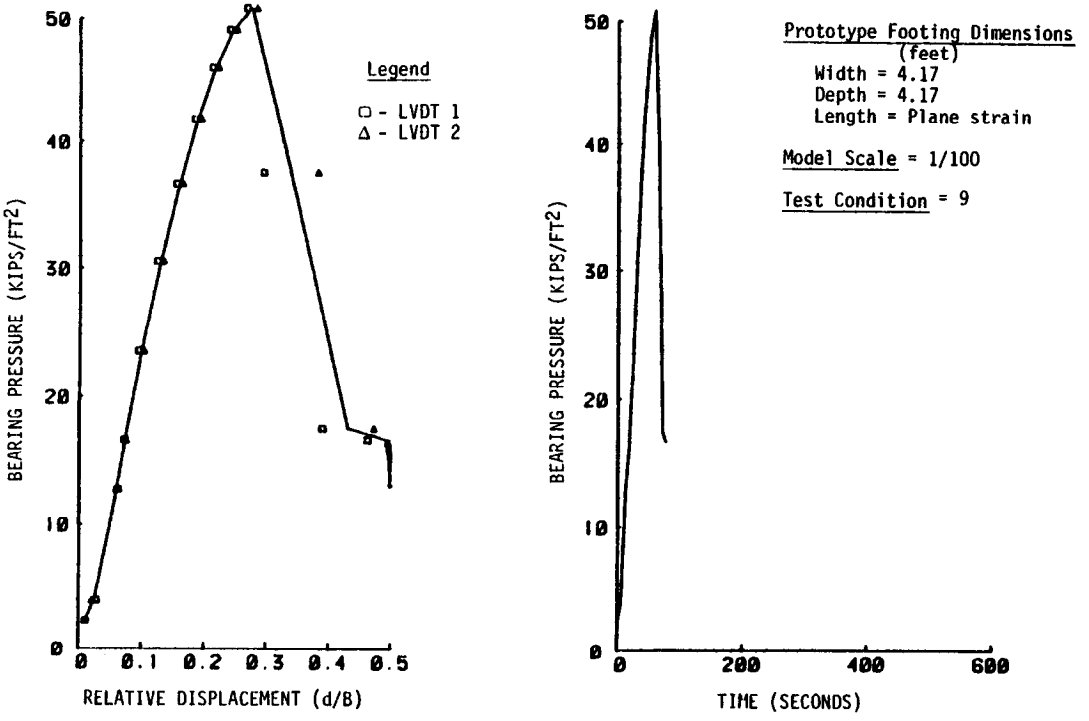

Figure A-10. – Results of test No. 10.

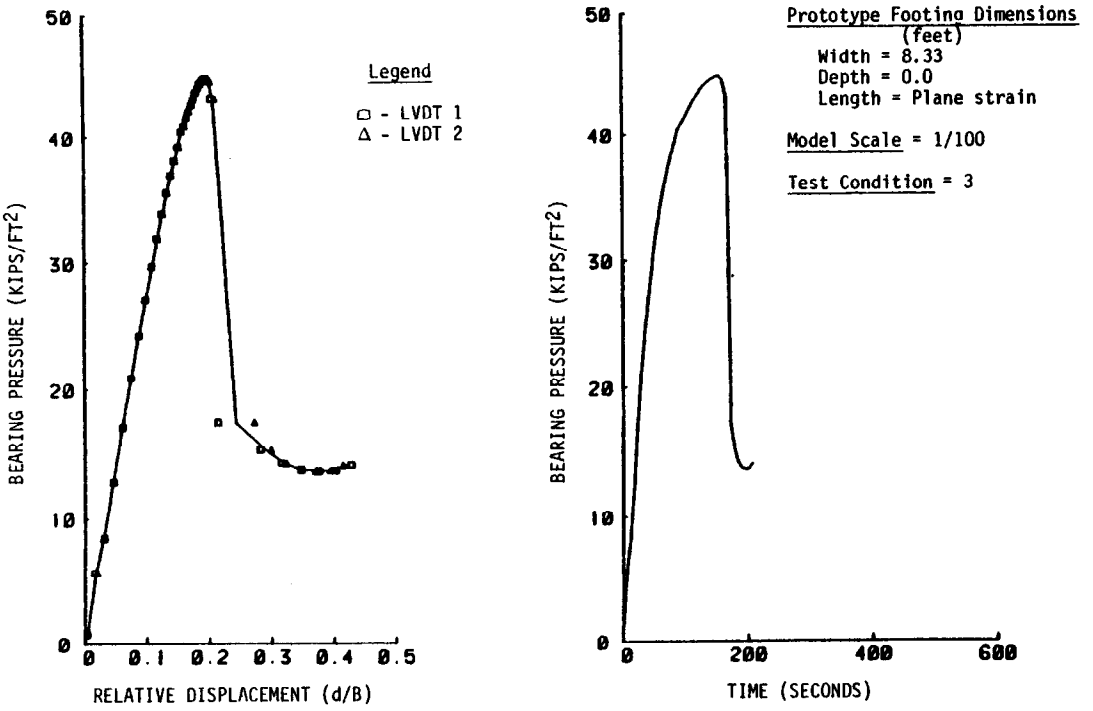

Figure A-11. – Results of test No. 11.

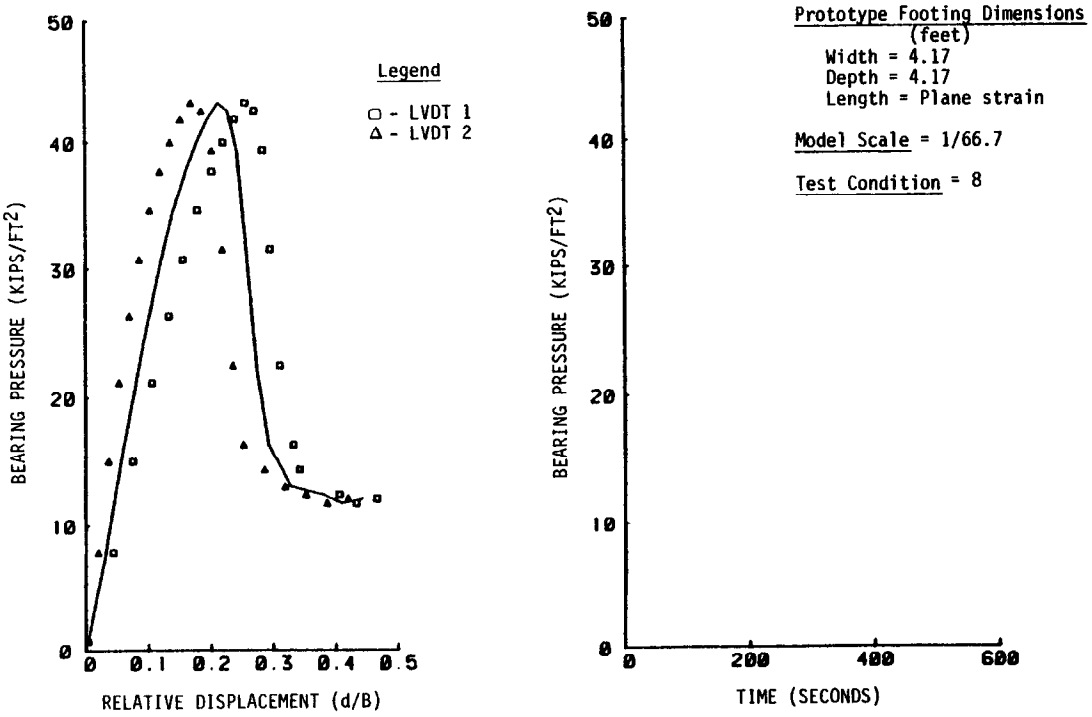

Figure A-12. – Results of test No. 12.

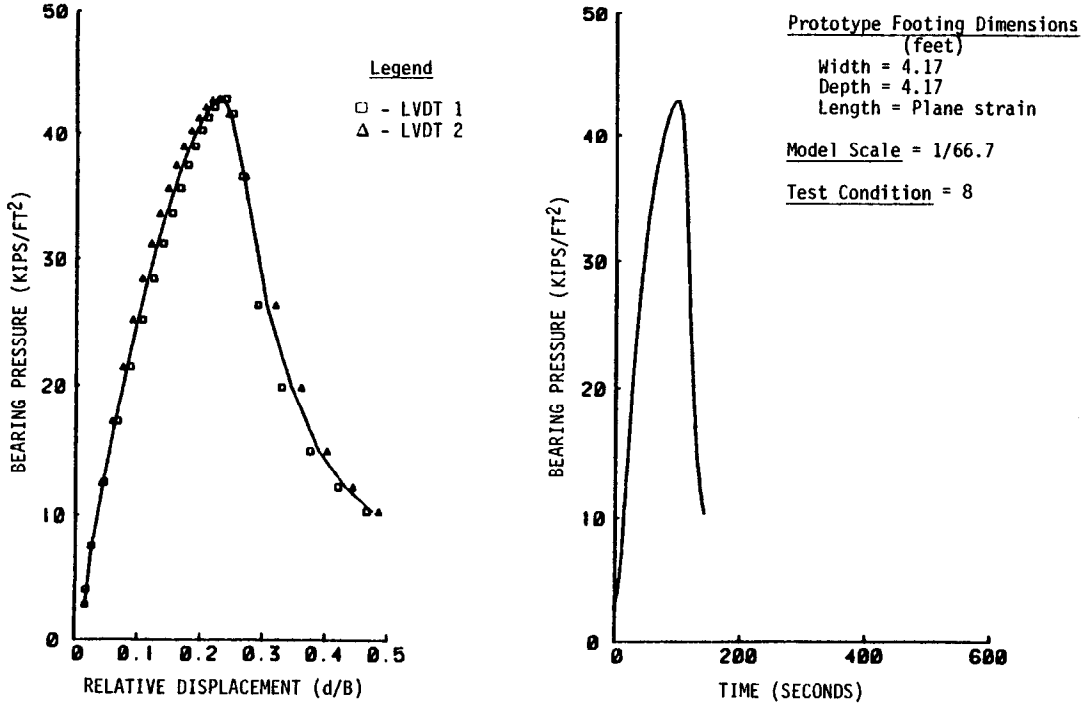

Figure A-13. – Results of test No. 13.

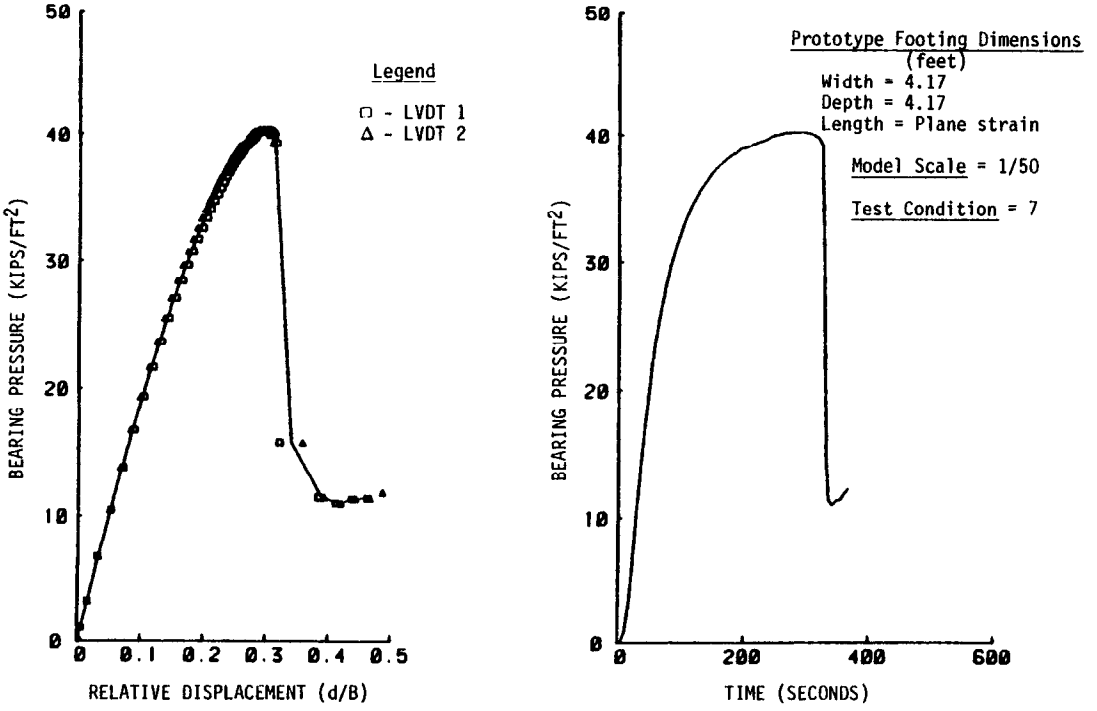

Figure A-14. – Results of test No. 14.

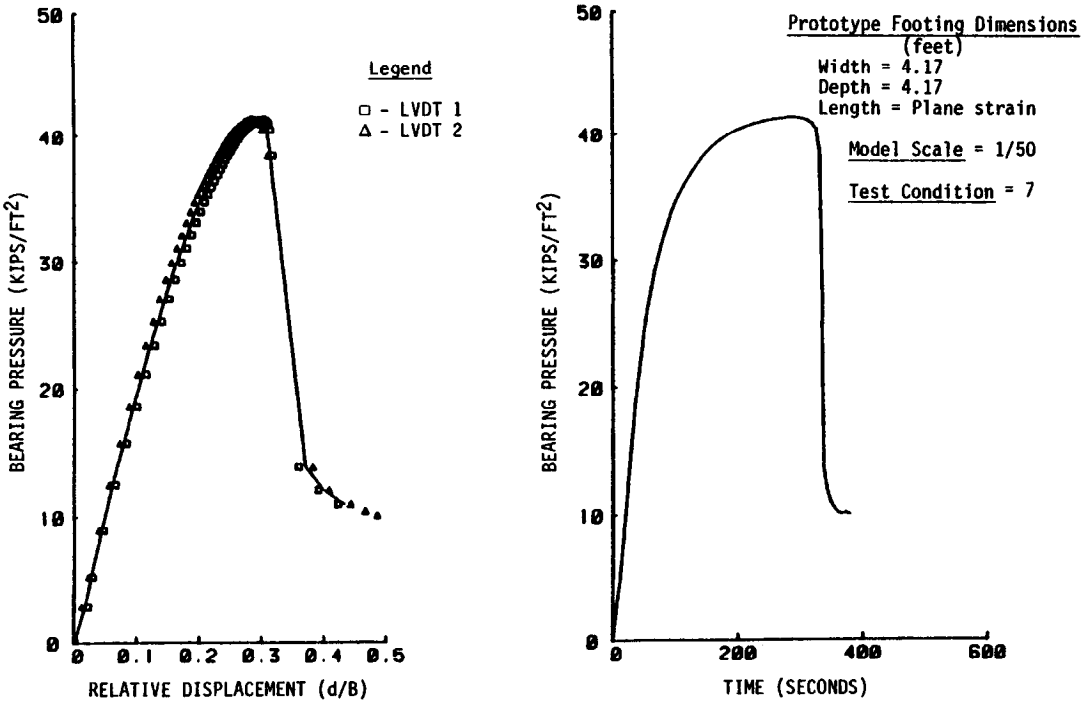

Figure A-15. – Results of test No. 15.

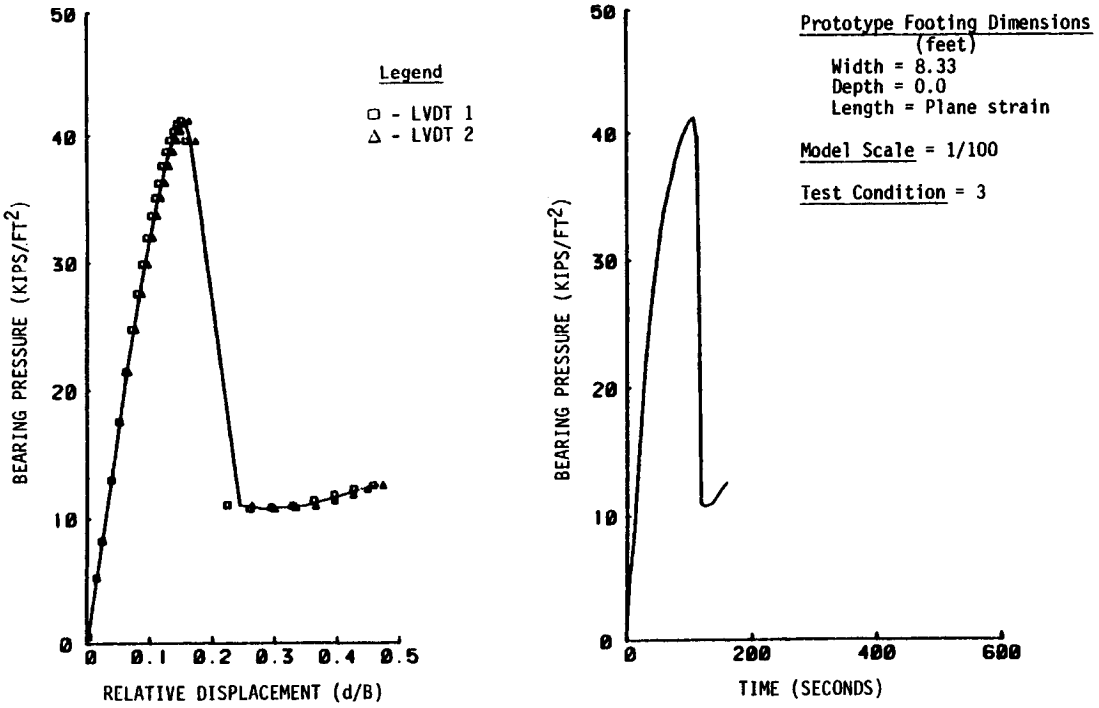

Figure A-16. – Results of test No. 16.

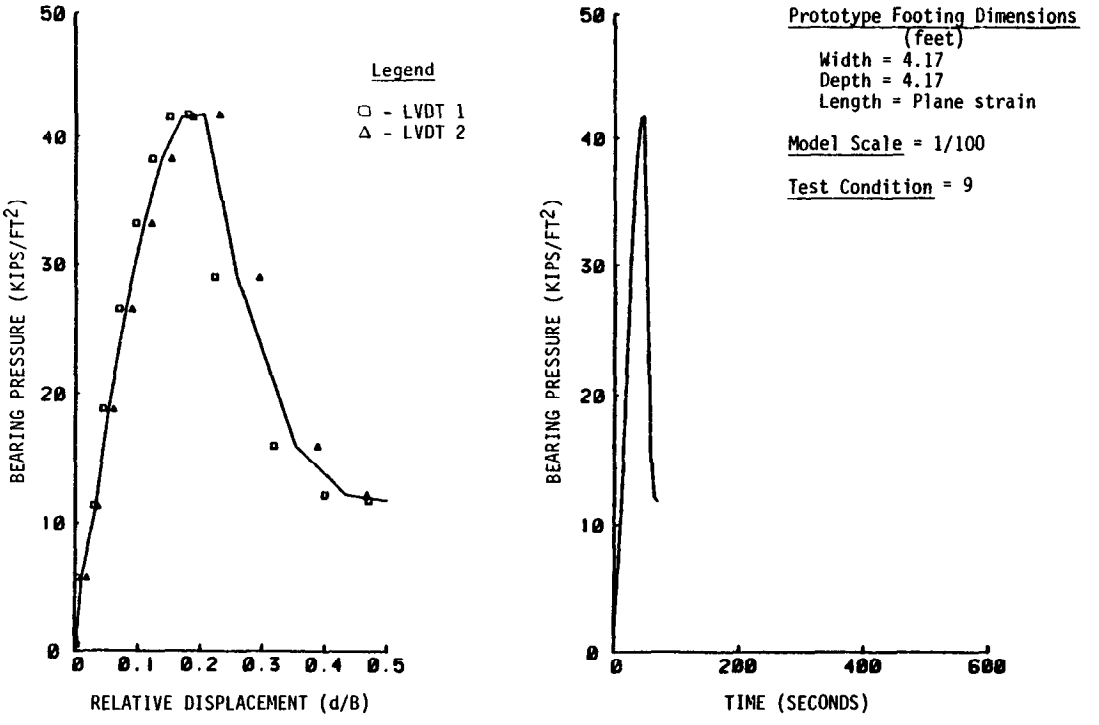

Figure A-17. – Results of test No. 17.

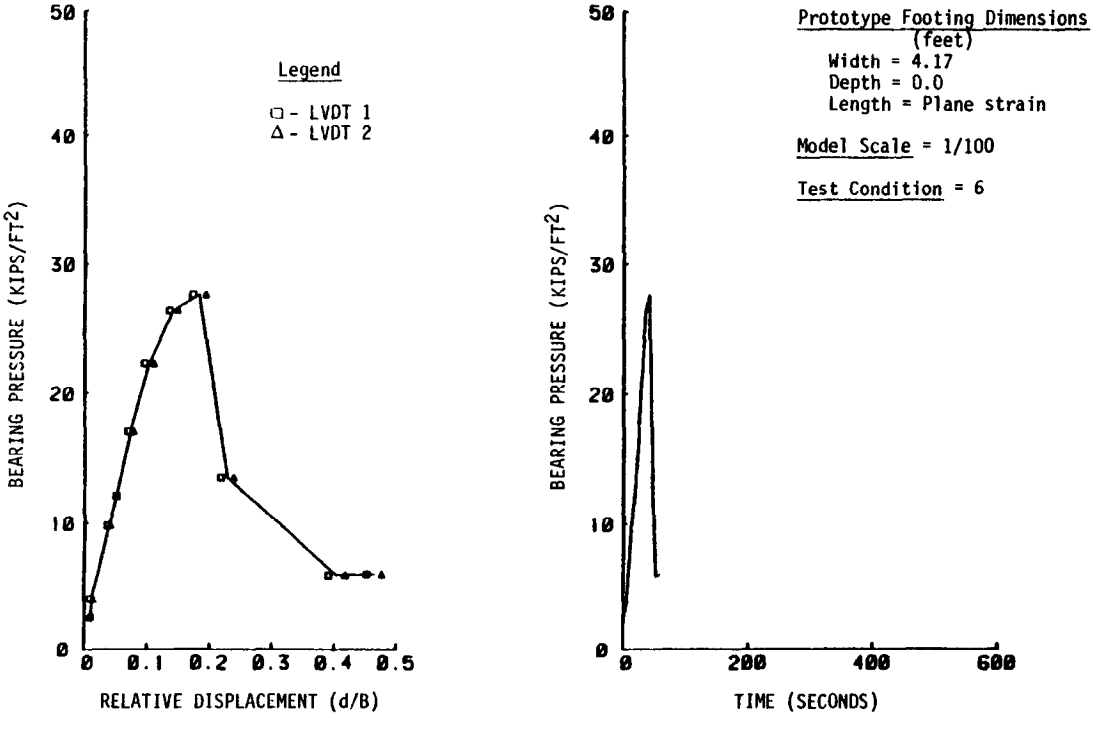

Figure A-18. – Results of test No. 18.

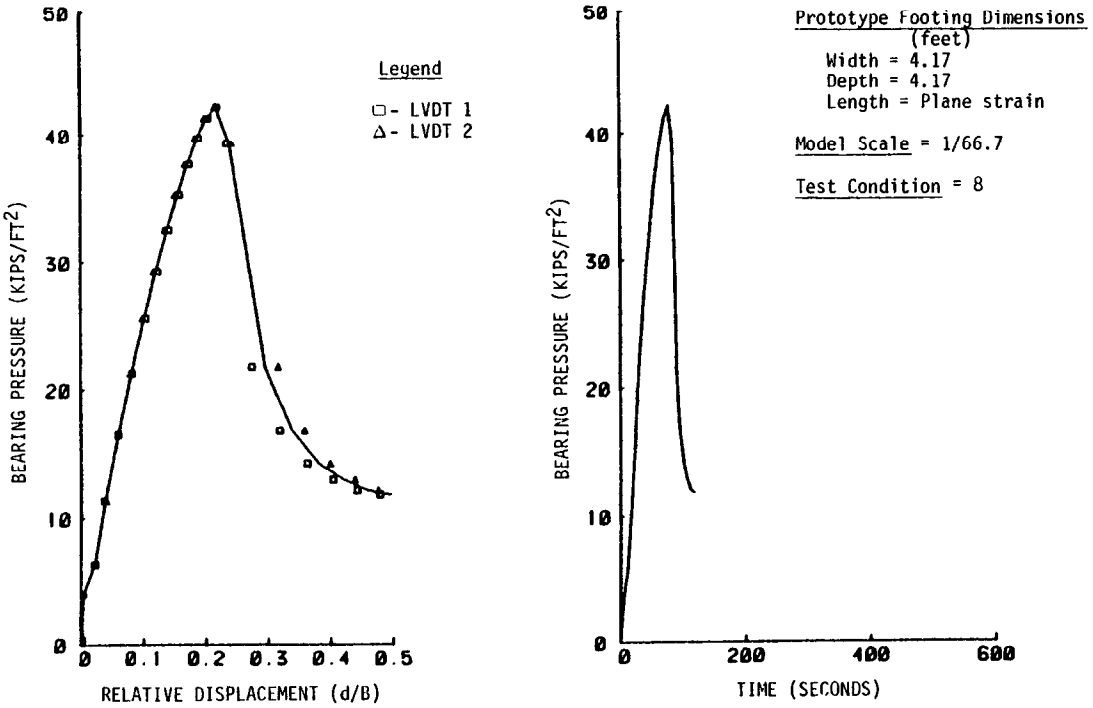

Figure A-19. – Results of test No. 19.

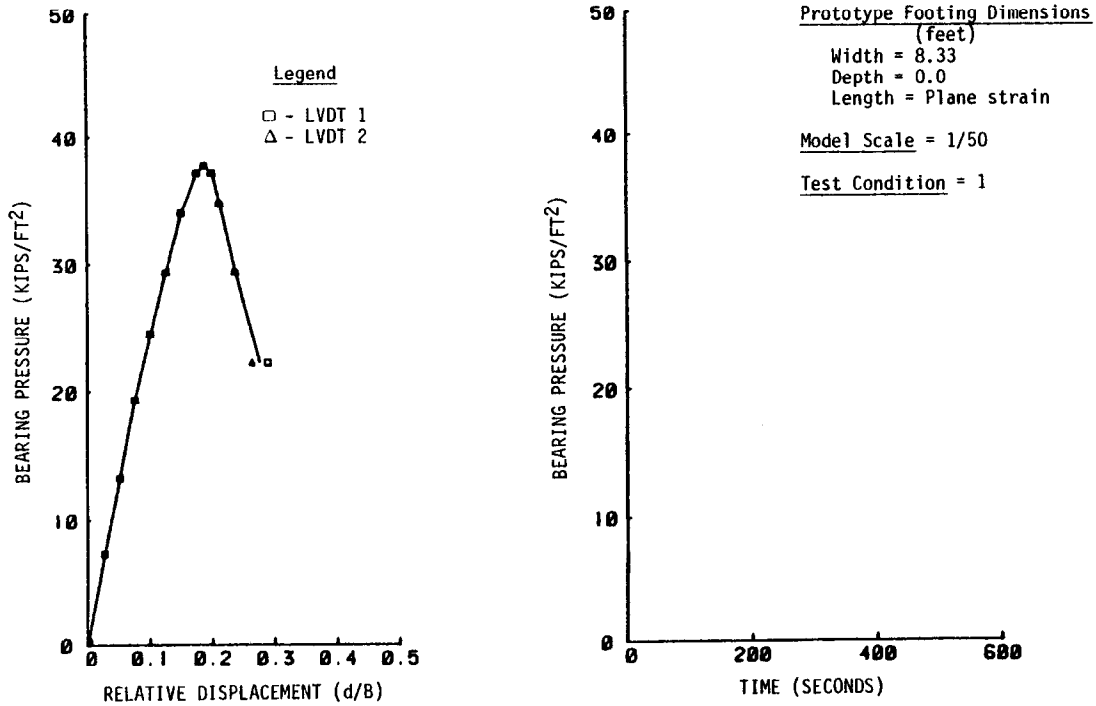

Figure A-20. – Results of test No. 20.

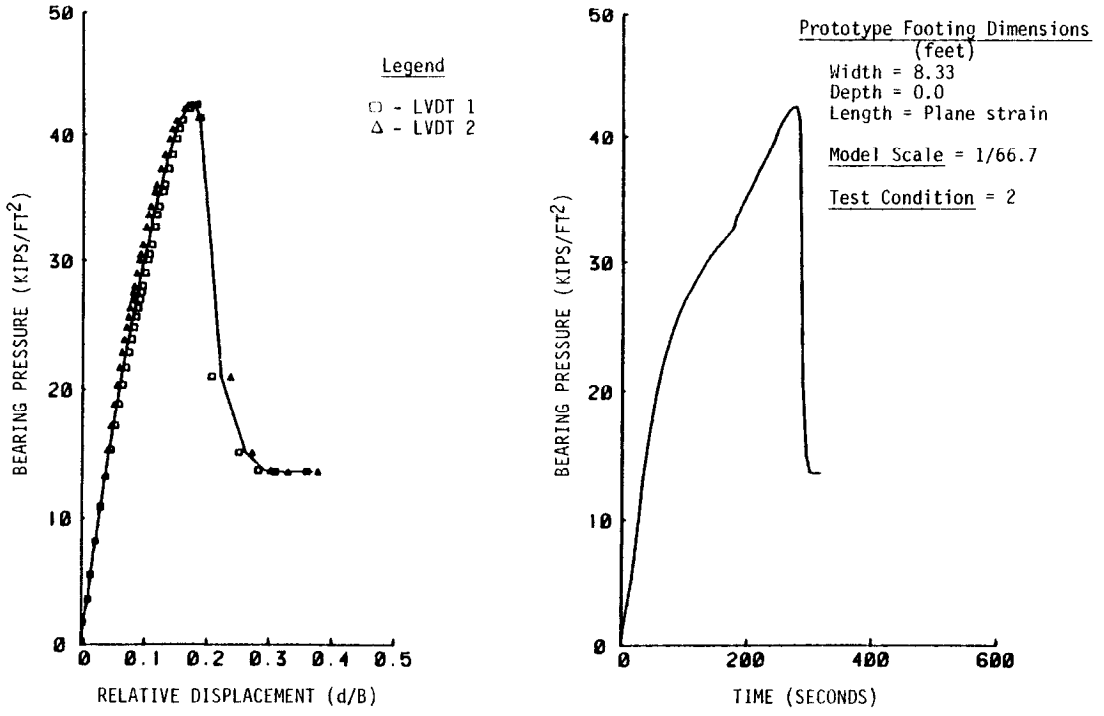

Figure A-21. – Results of test No. 21.

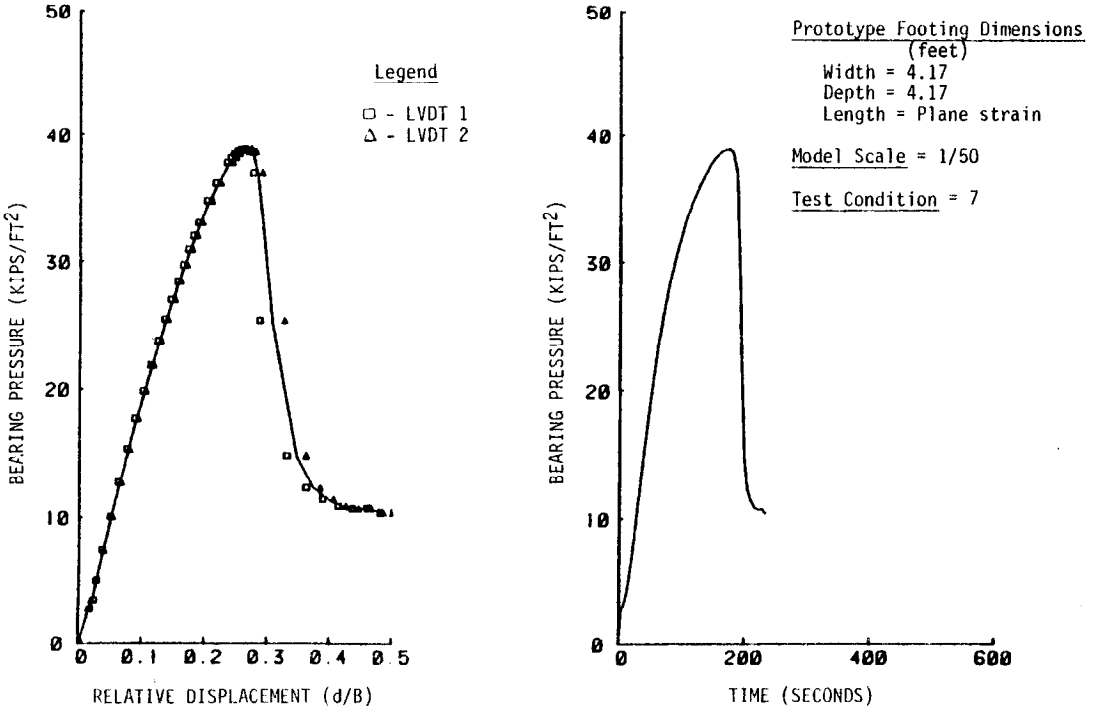

Figure A-22. – Results of test No. 22.

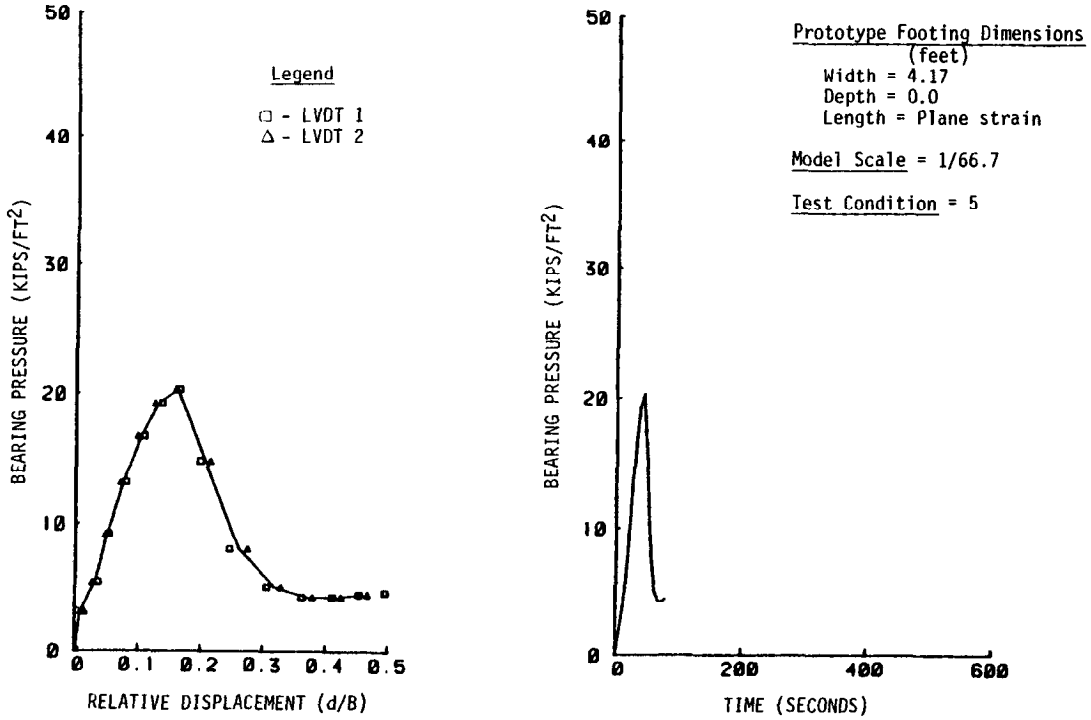

Figure A-23. – Results of test No. 23.

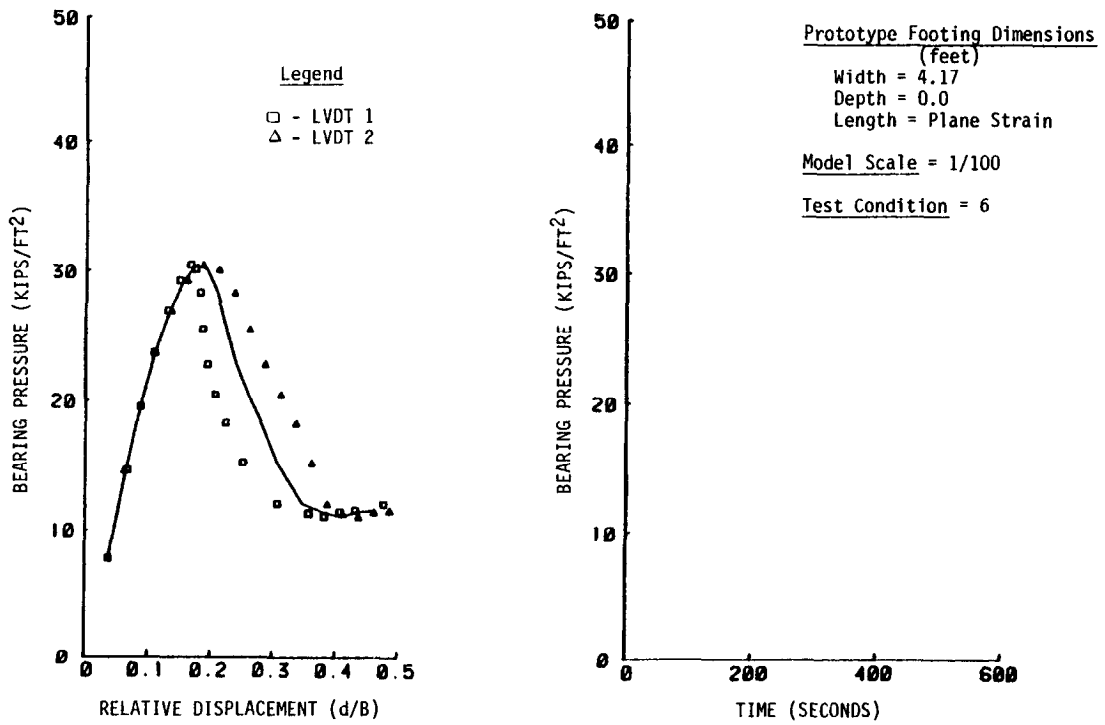

Figure A-24. – Results of test No. 24.

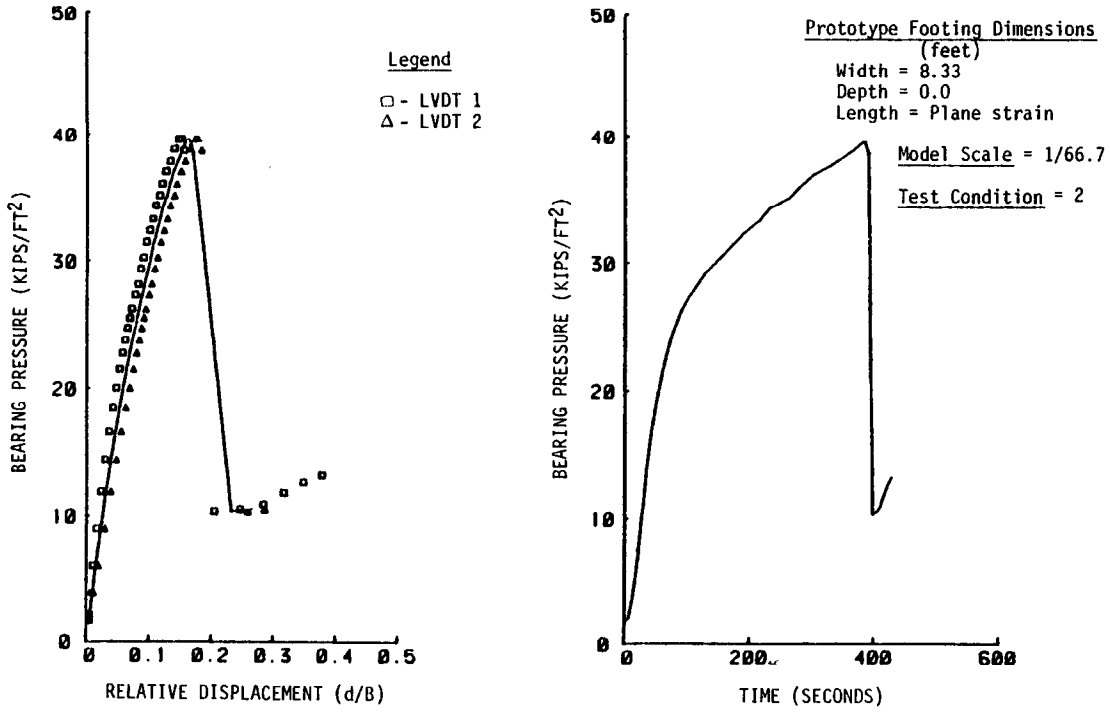

Figure A-25. – Results of test No. 25.

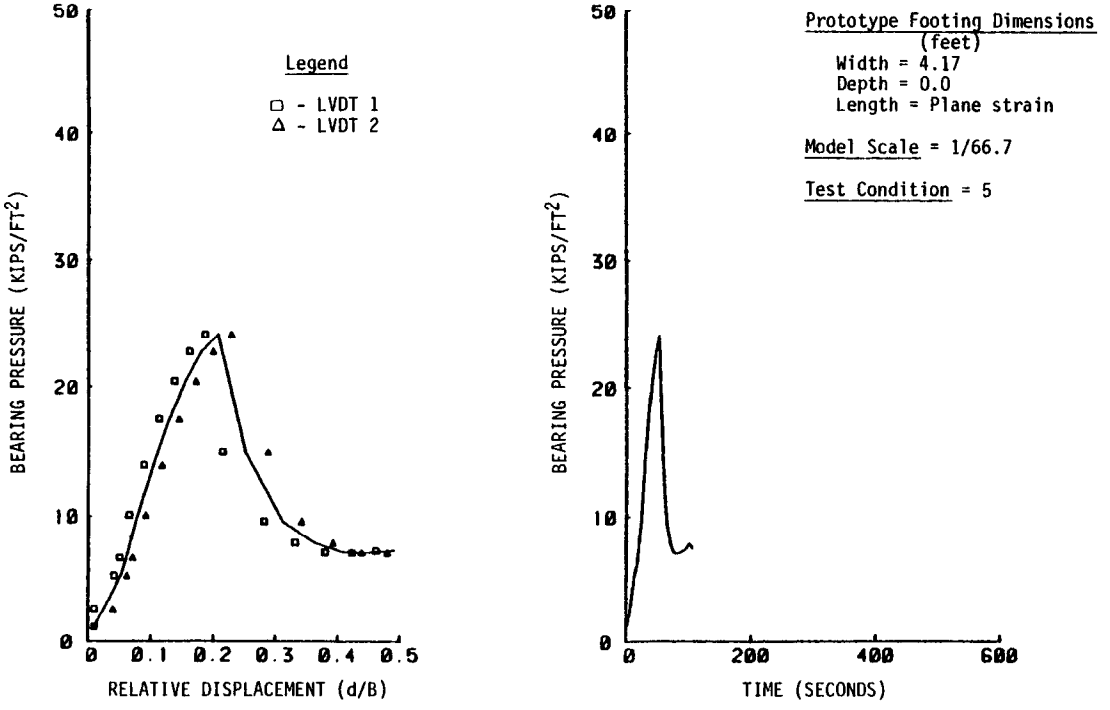

Figure A-26. – Results of test No. 26.

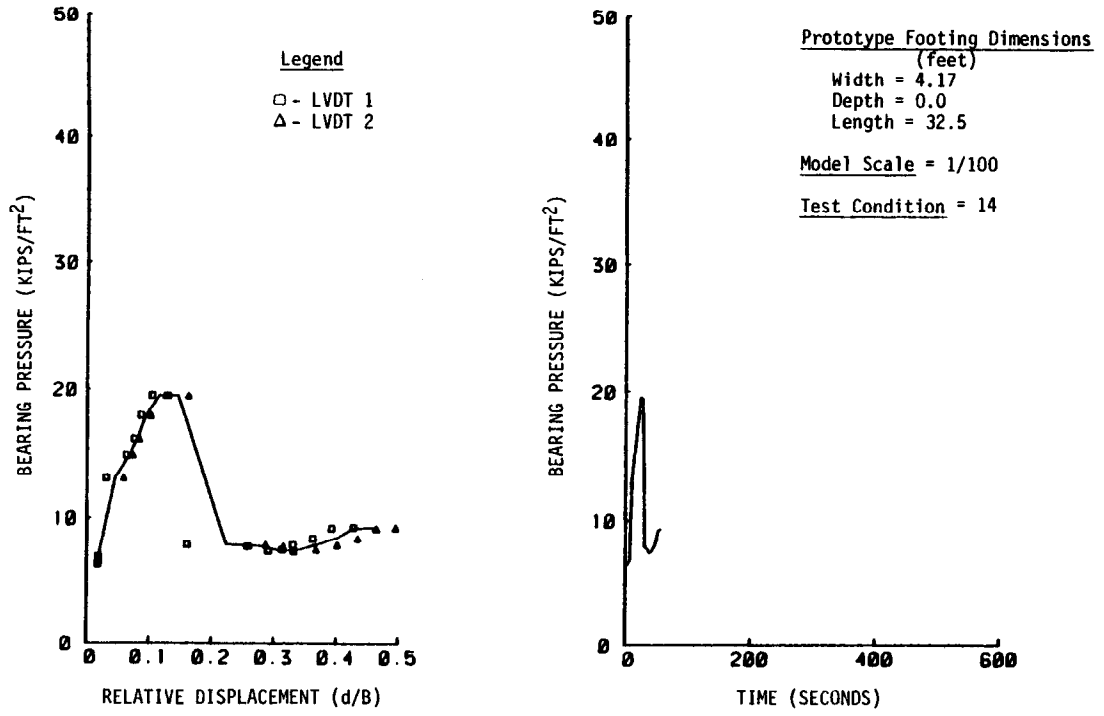

Figure A-27. – Results of test No. 27.

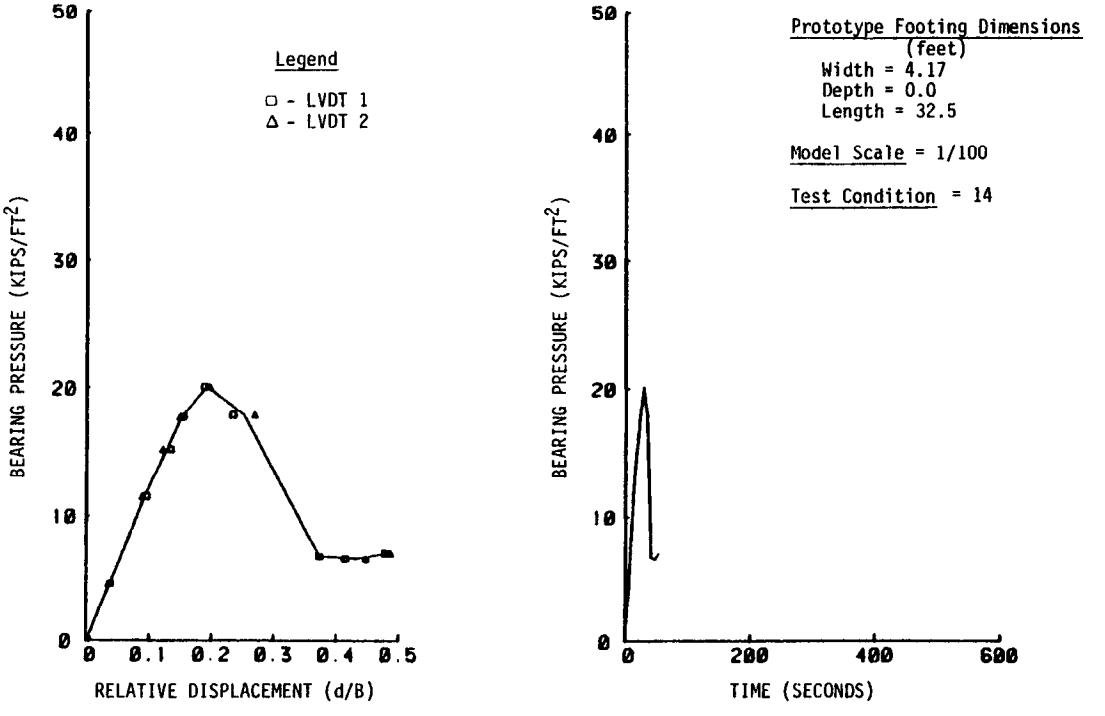

Figure A-28. – Results of test No. 28.

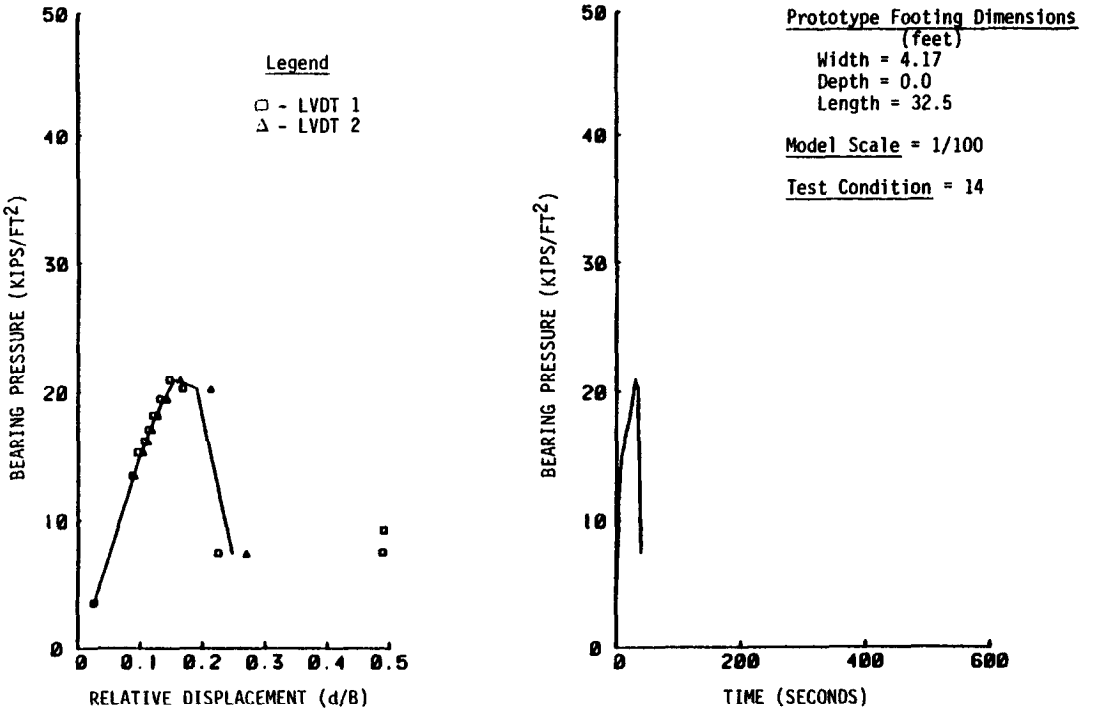

Figure A-29. – Results of test No. 29.

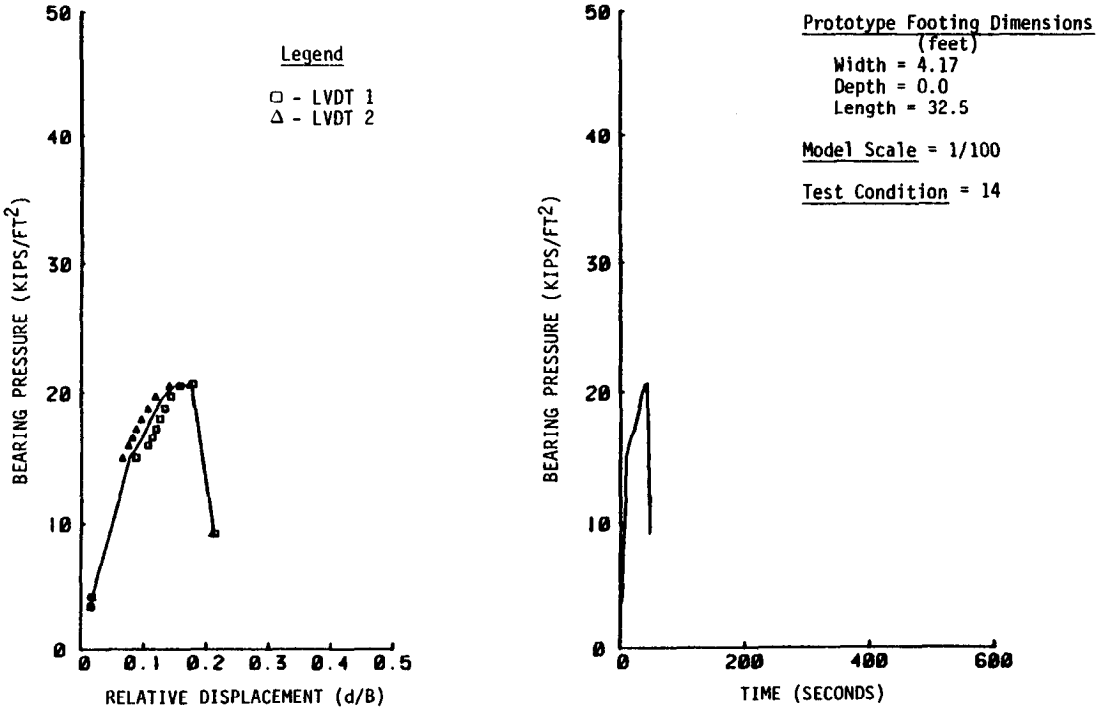

Figure A-30. – Results of test No. 30.

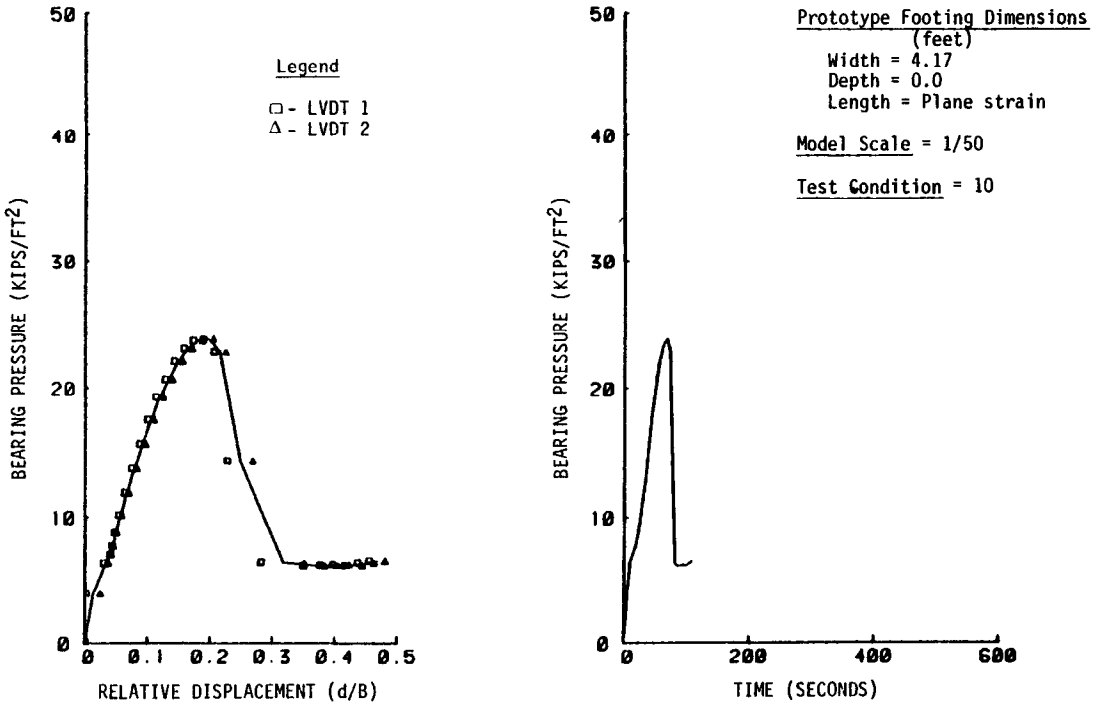

Figure A-31. – Results of test No. 31.

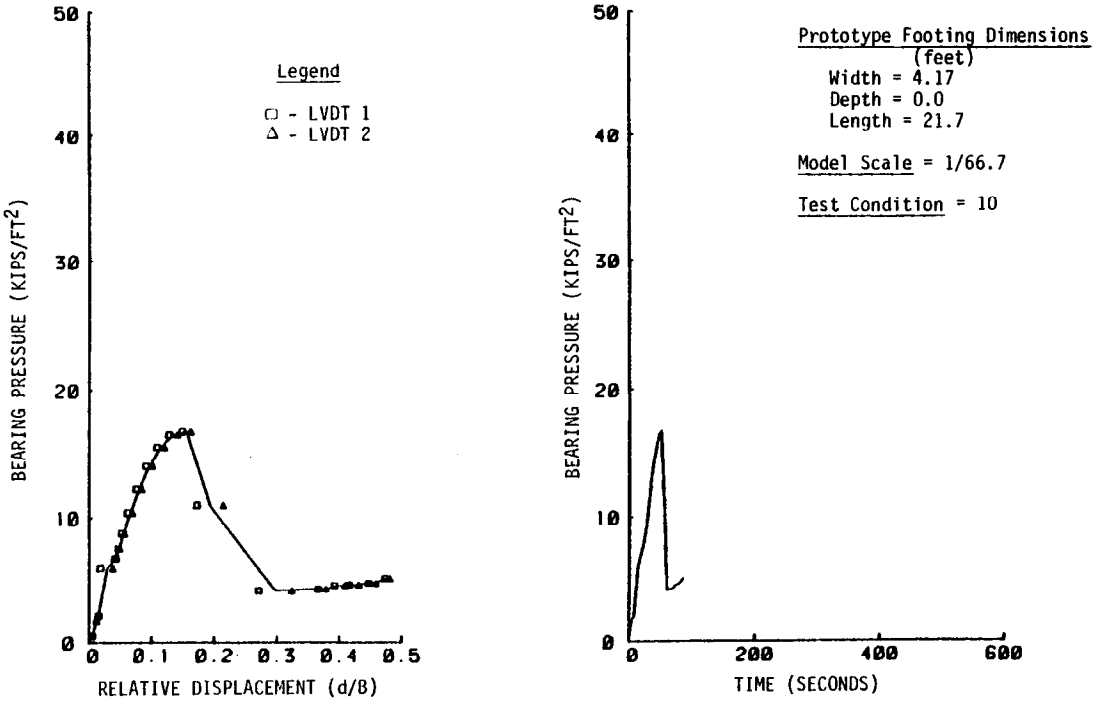

Figure A-32. – Results of test No. 32.

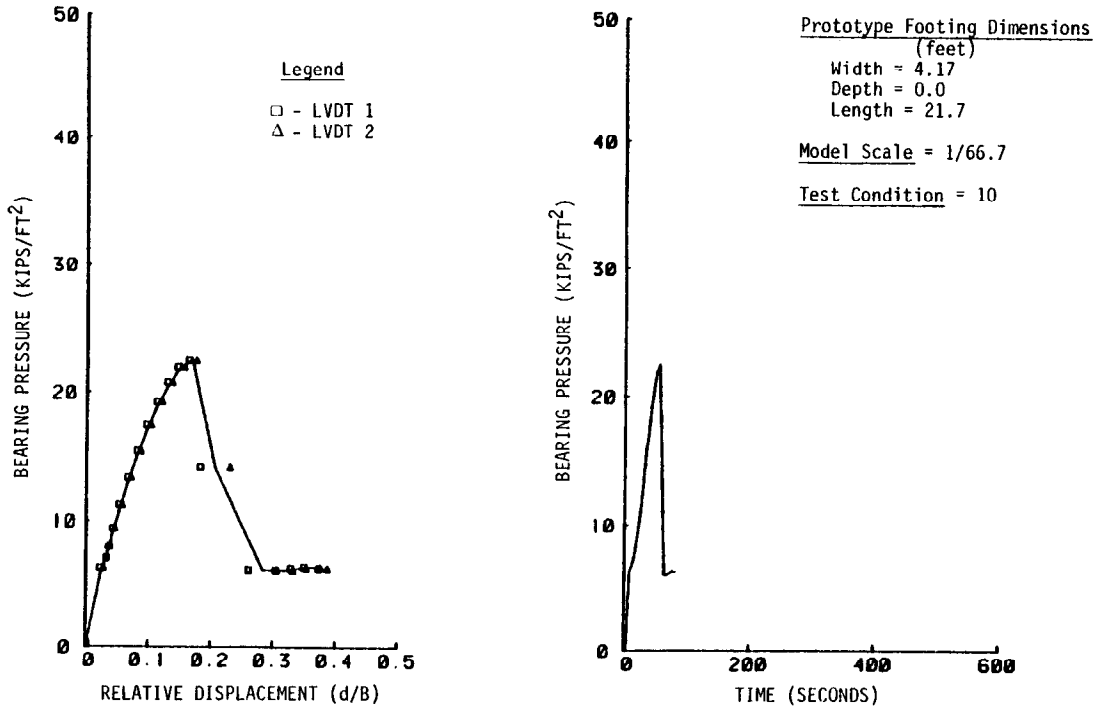

Figure A-33. – Results of test No. 33.

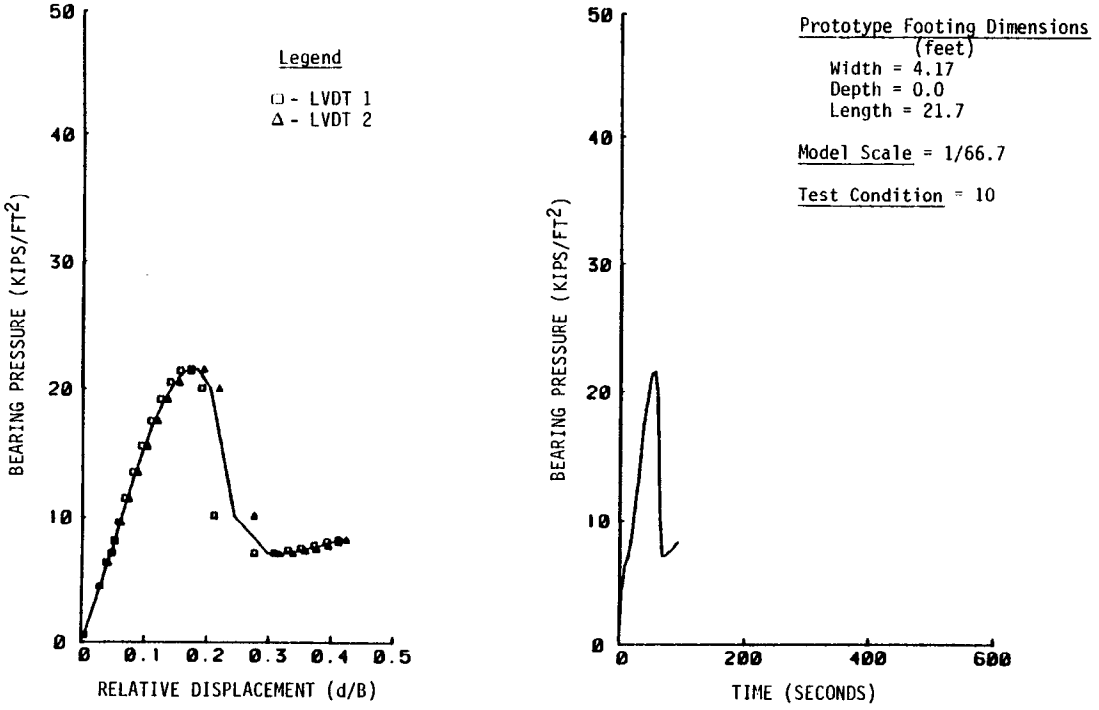

Figure A-34. – Results of test No. 34.

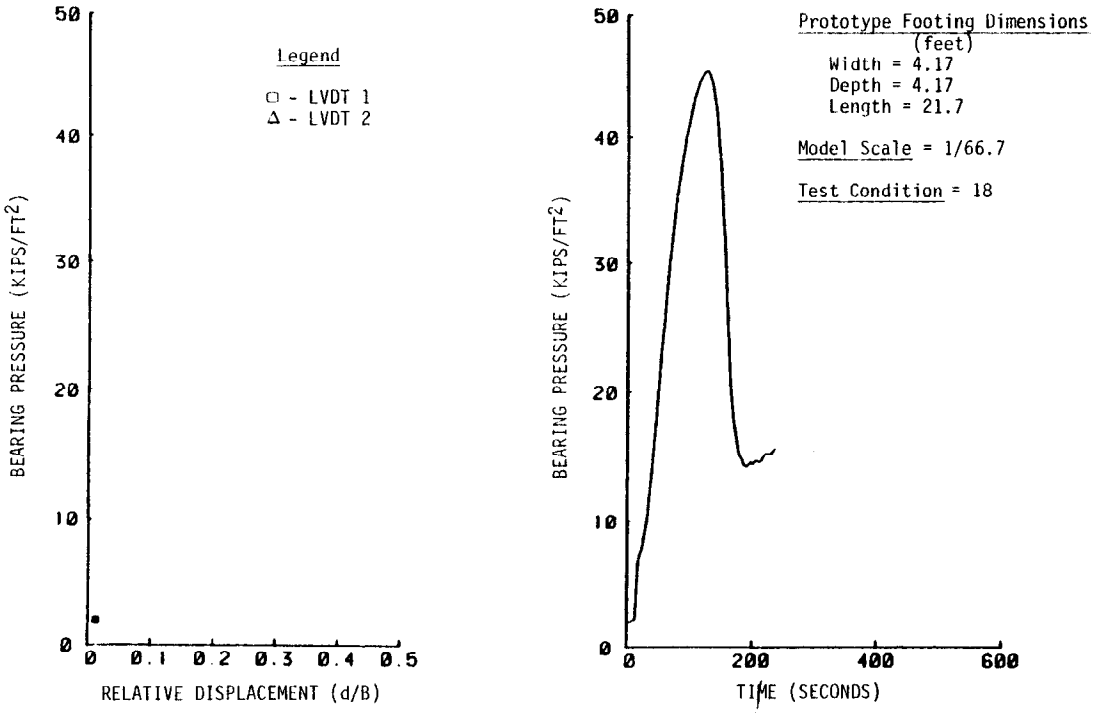

Figure A-35. – Results of test No. 35.

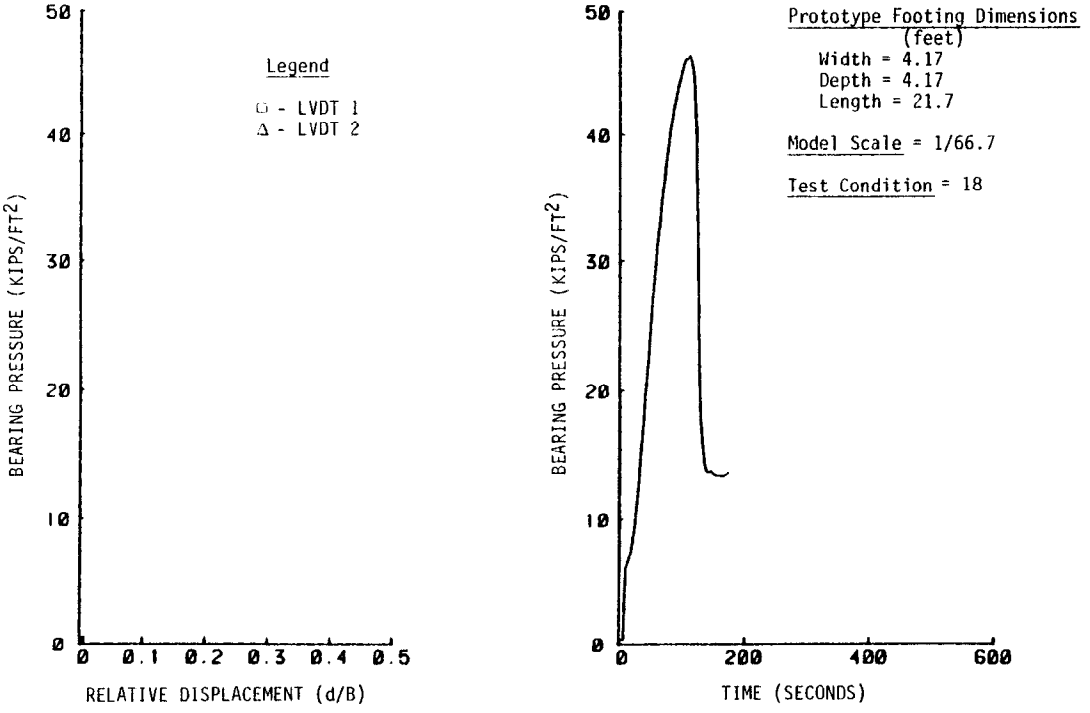

Figure A-36. – Results of test No. 36.

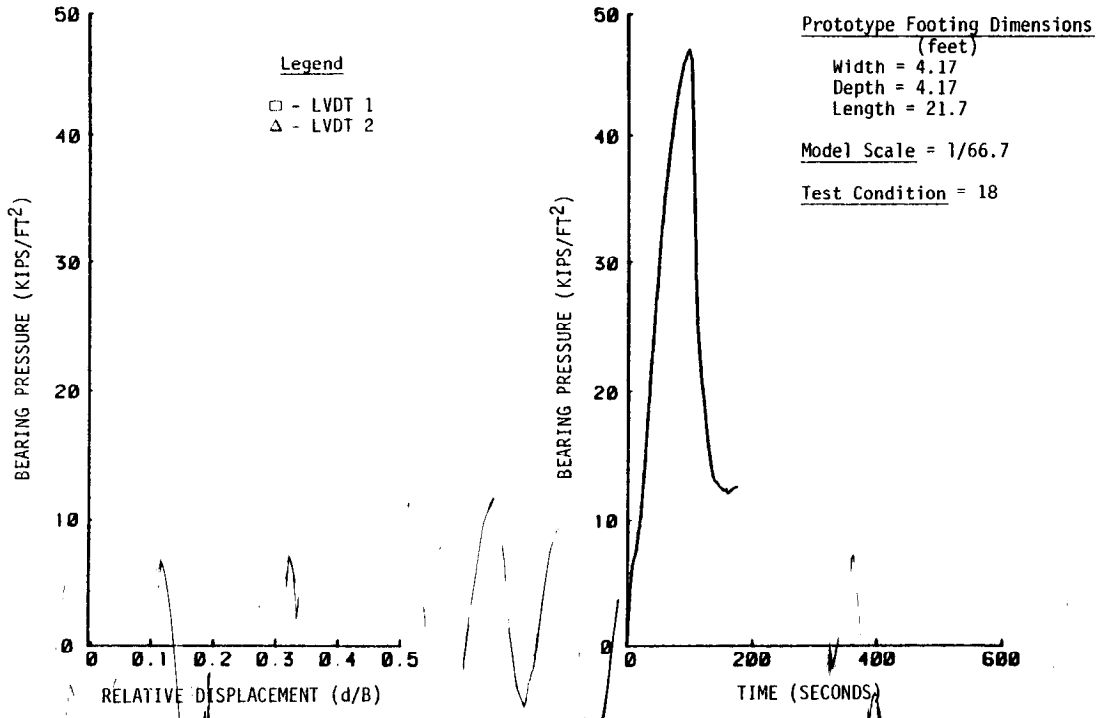

Figure A-37. – Results of test No. 37.

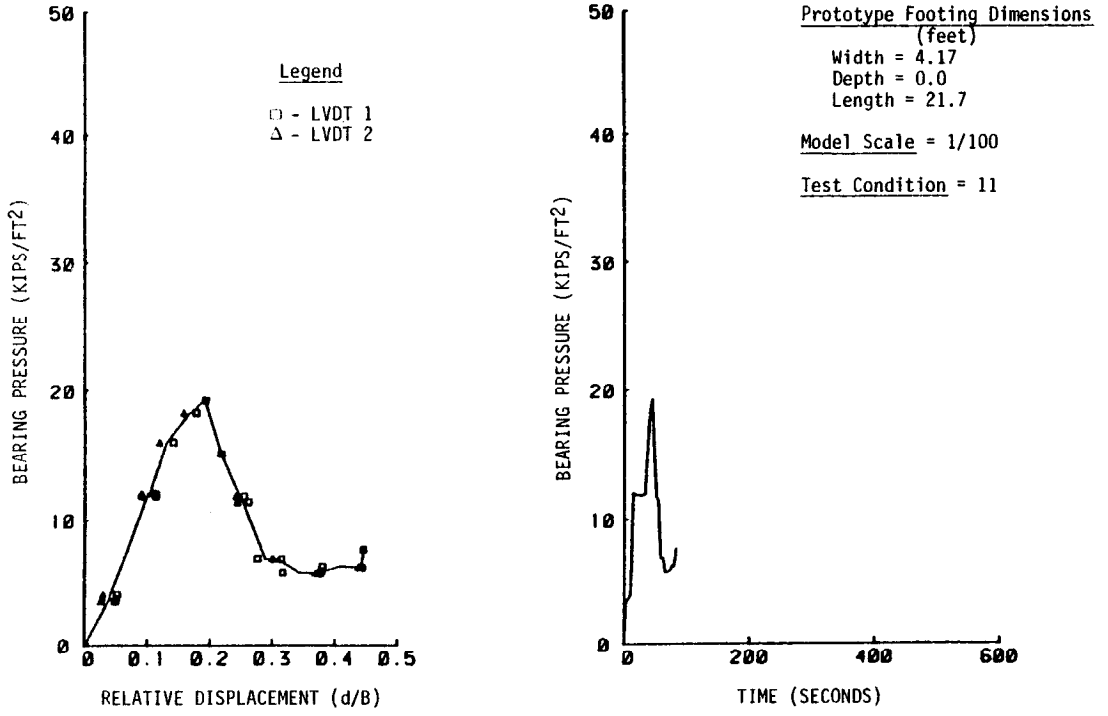

Figure A-38. – Results of test No. 38.

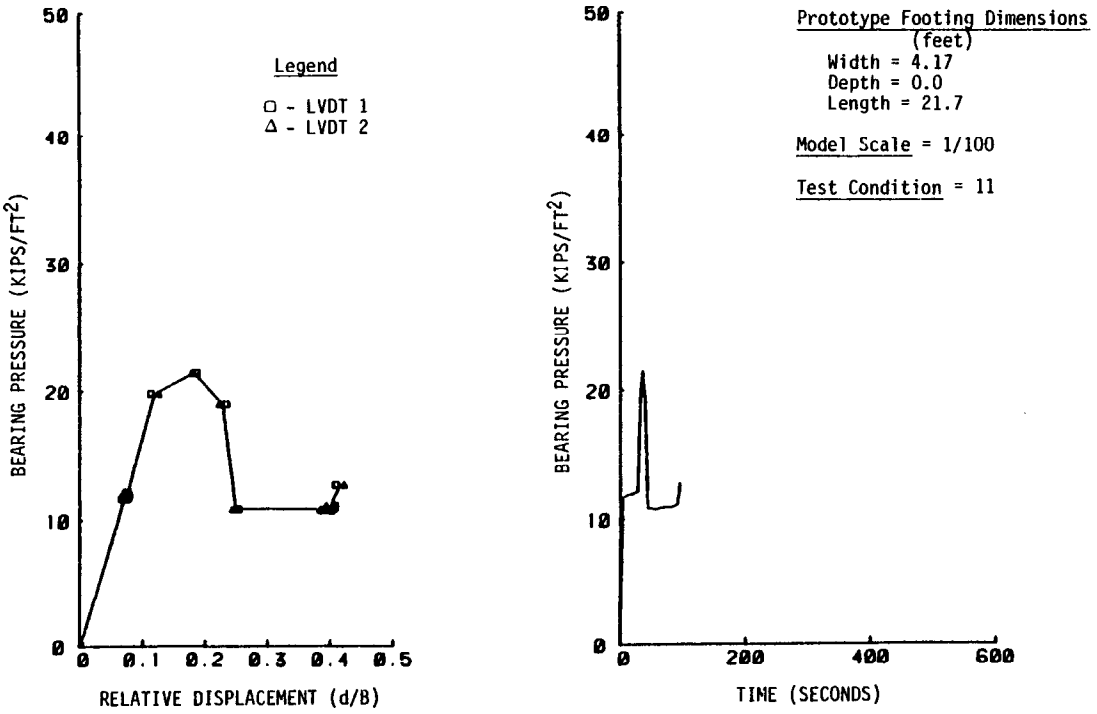

Figure A-39. – Results of test No. 39.

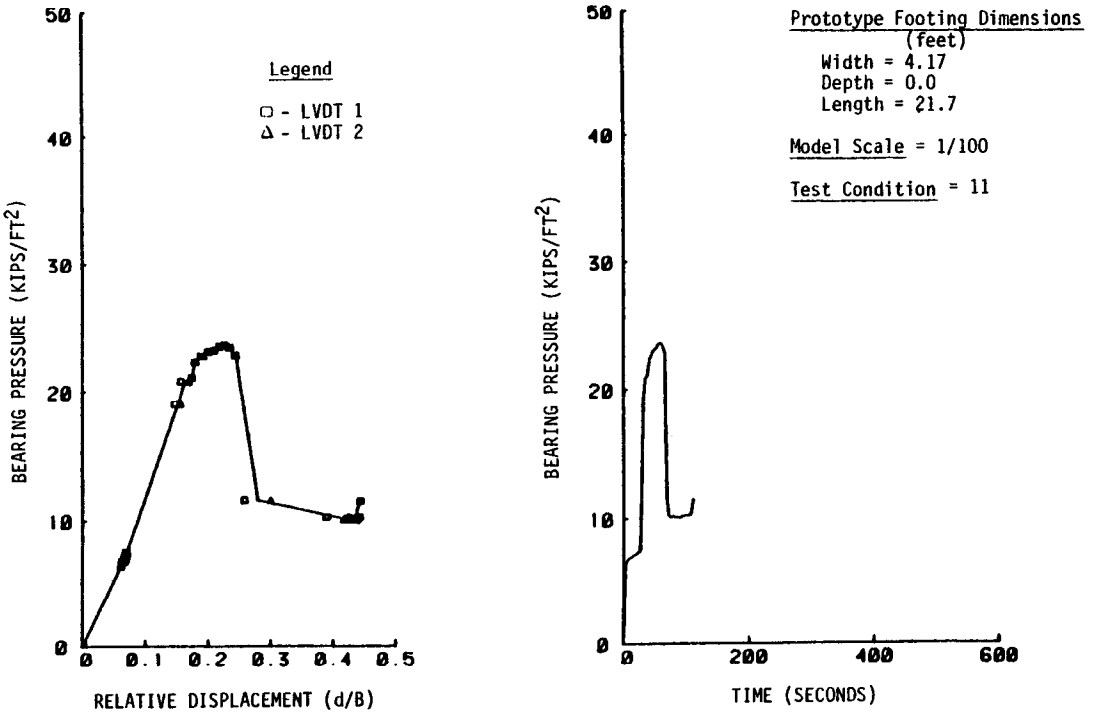

Figure A-40. – Results of test No. 40.

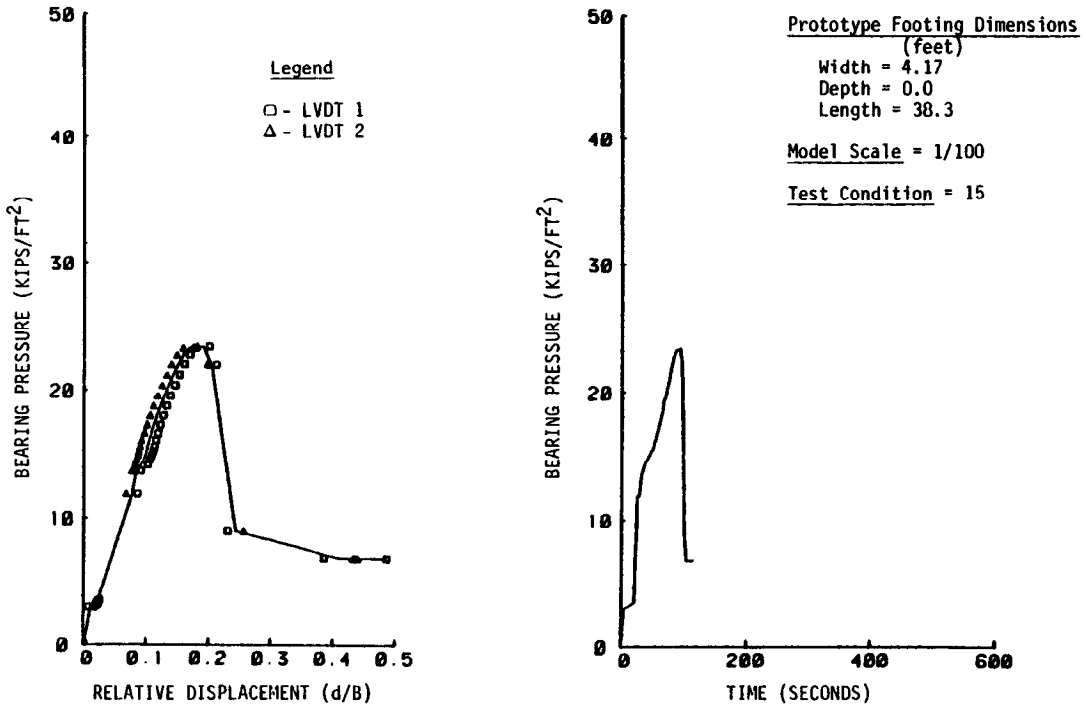

Figure A-41. – Results of test No. 41.

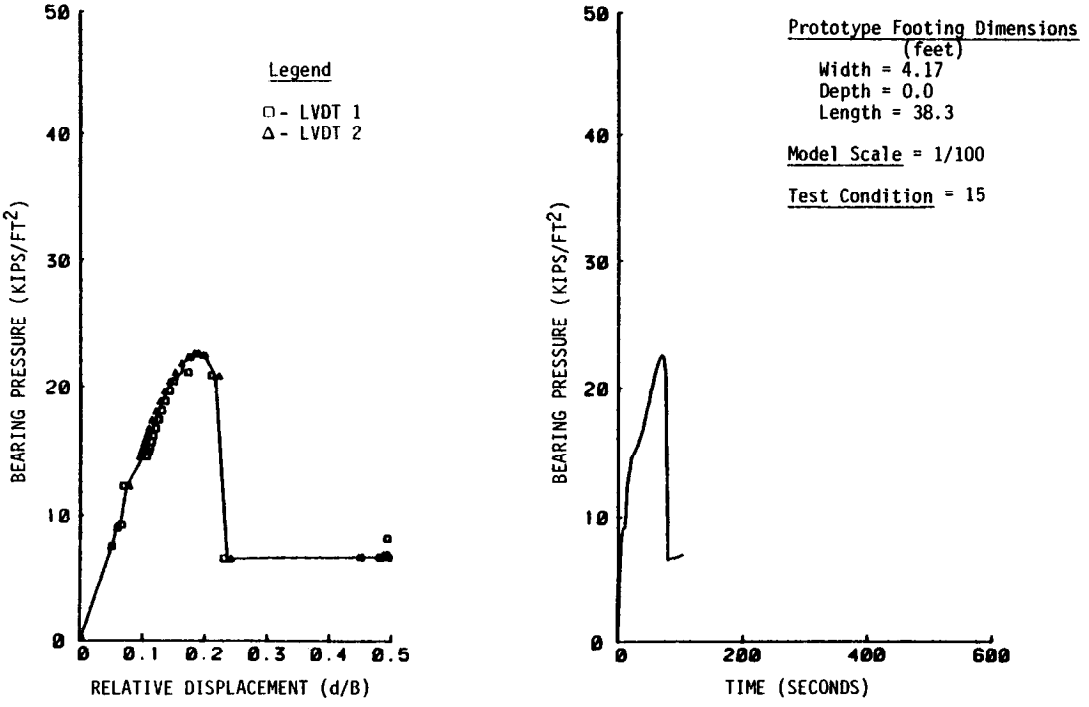

Figure A-42. – Results of test No. 42.

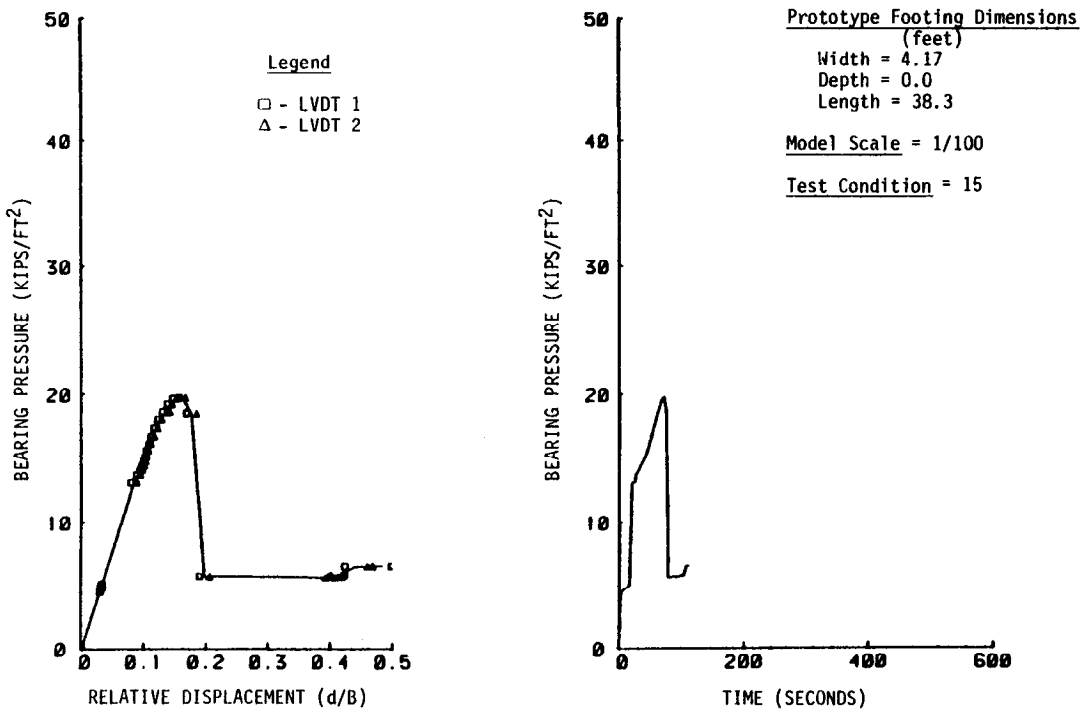

Figure A-43. – Results of test No. 43.

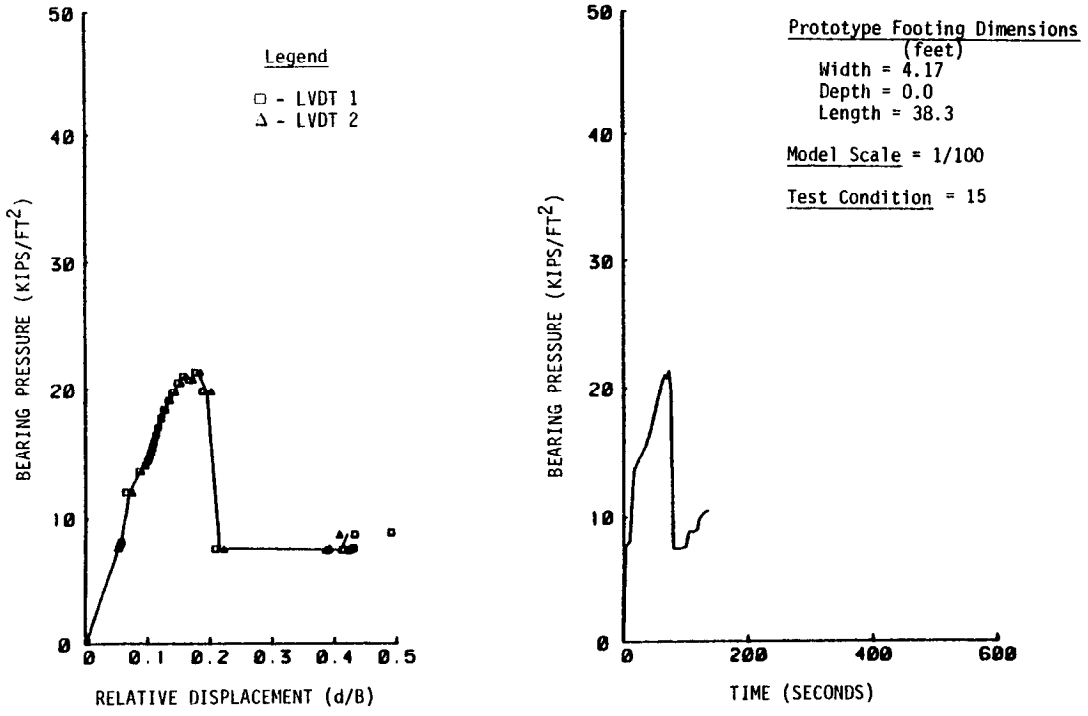

Figure A-44. – Results of test No. 44.

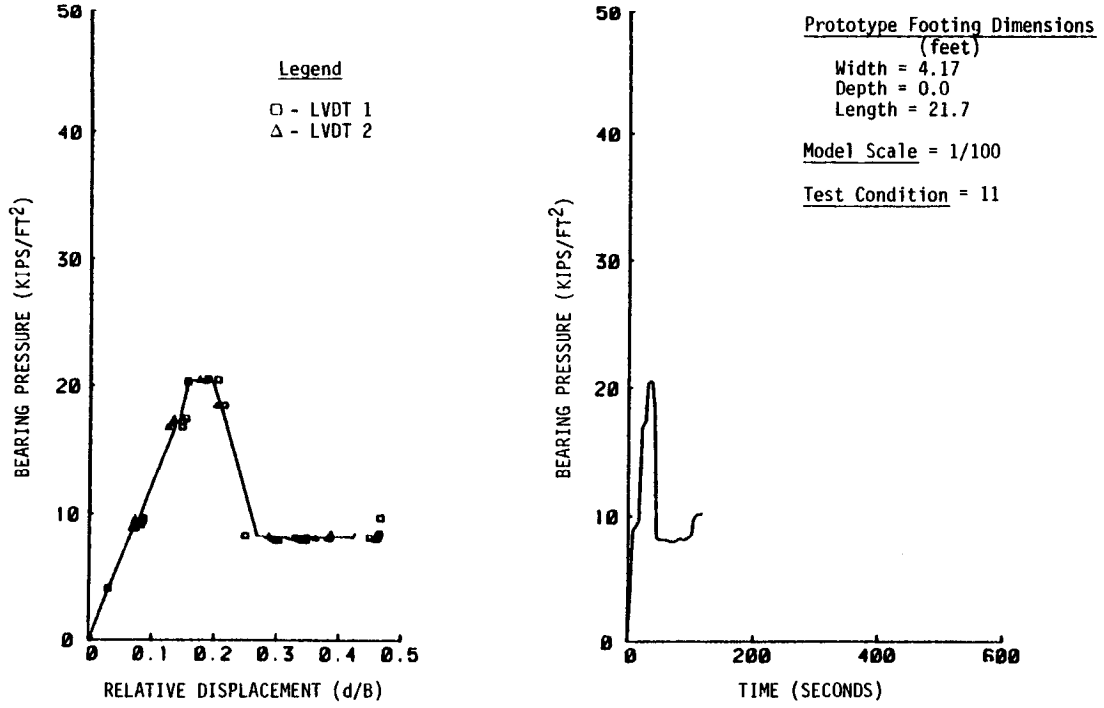

Figure A-45. – Results of test No. 45.

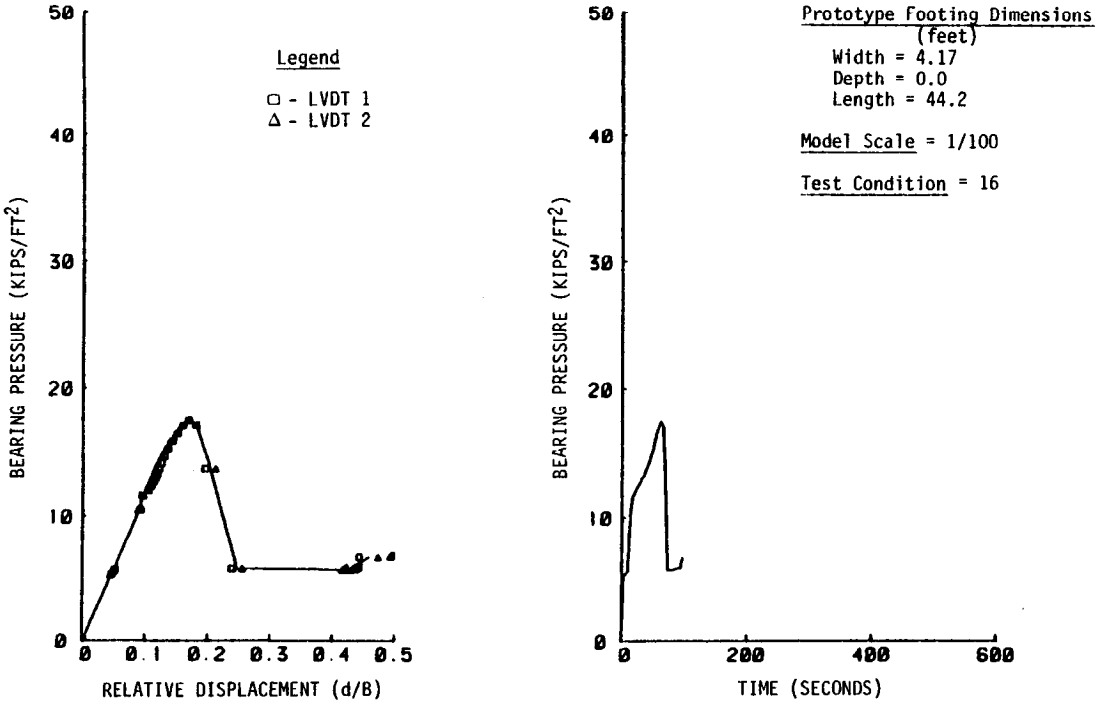

Figure A-46. – Results of test No. 46.

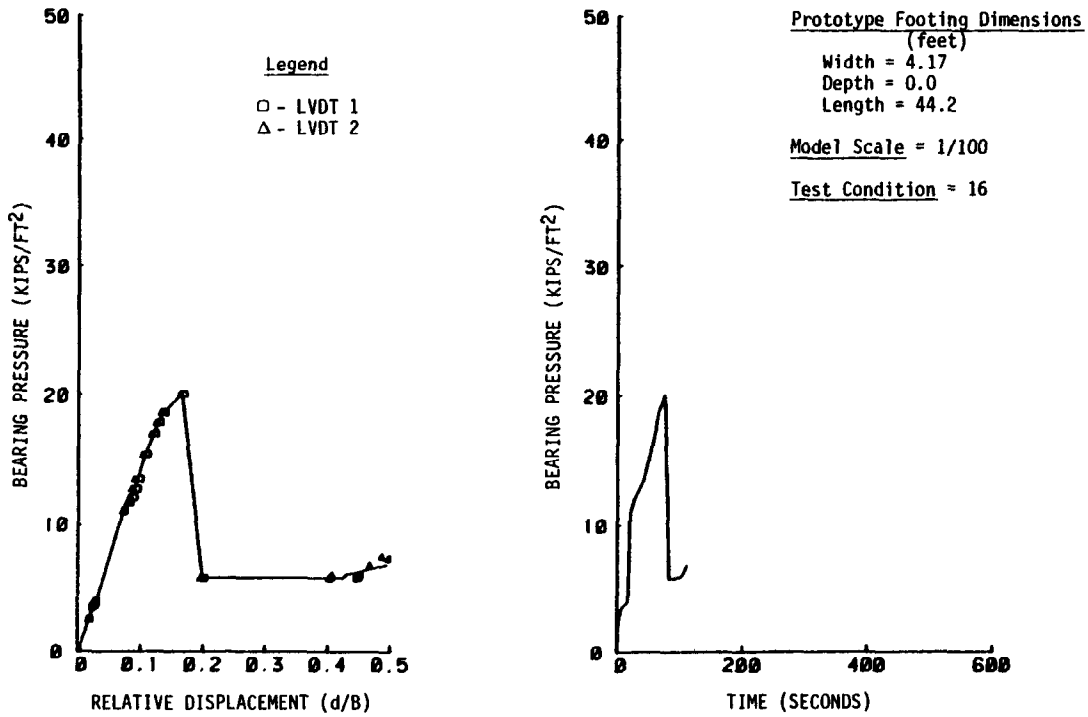

Figure A-47. – Results of test No. 47.

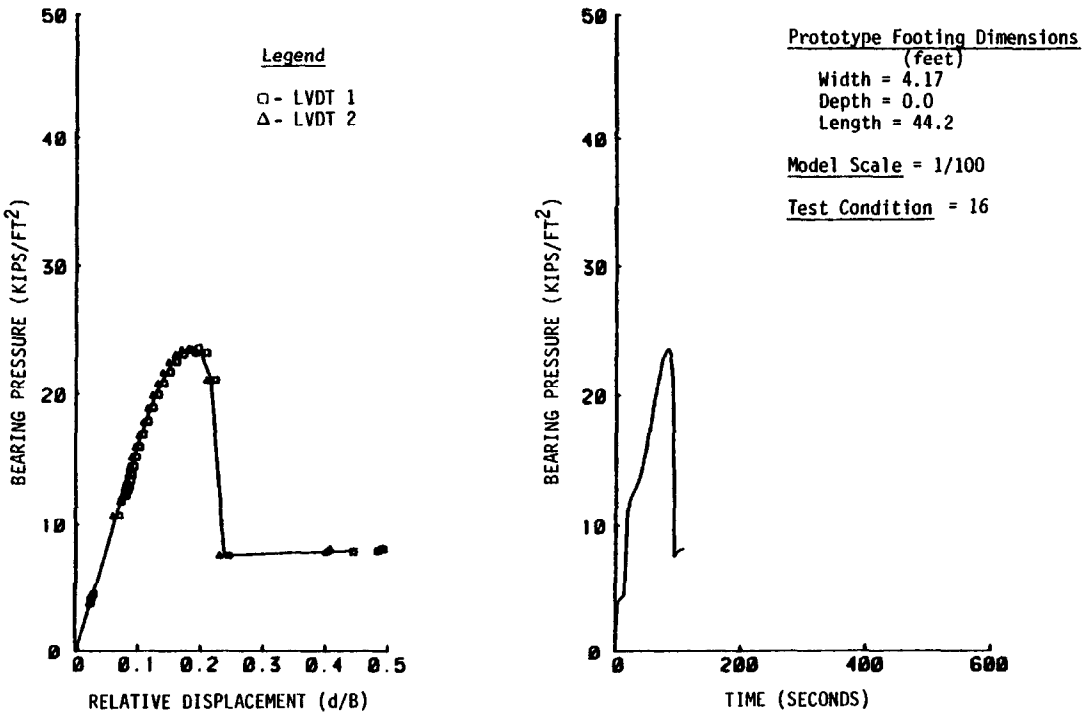

Figure A-48. – Results of test No. 48.

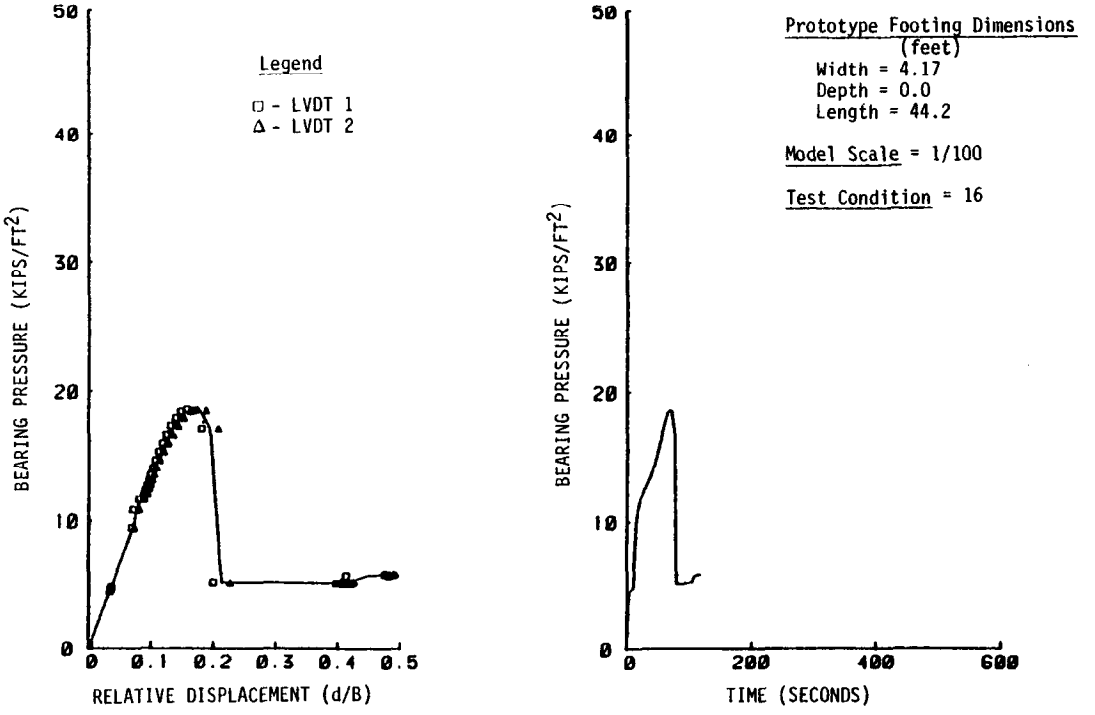

Figure A-49. – Results of test No. 49.

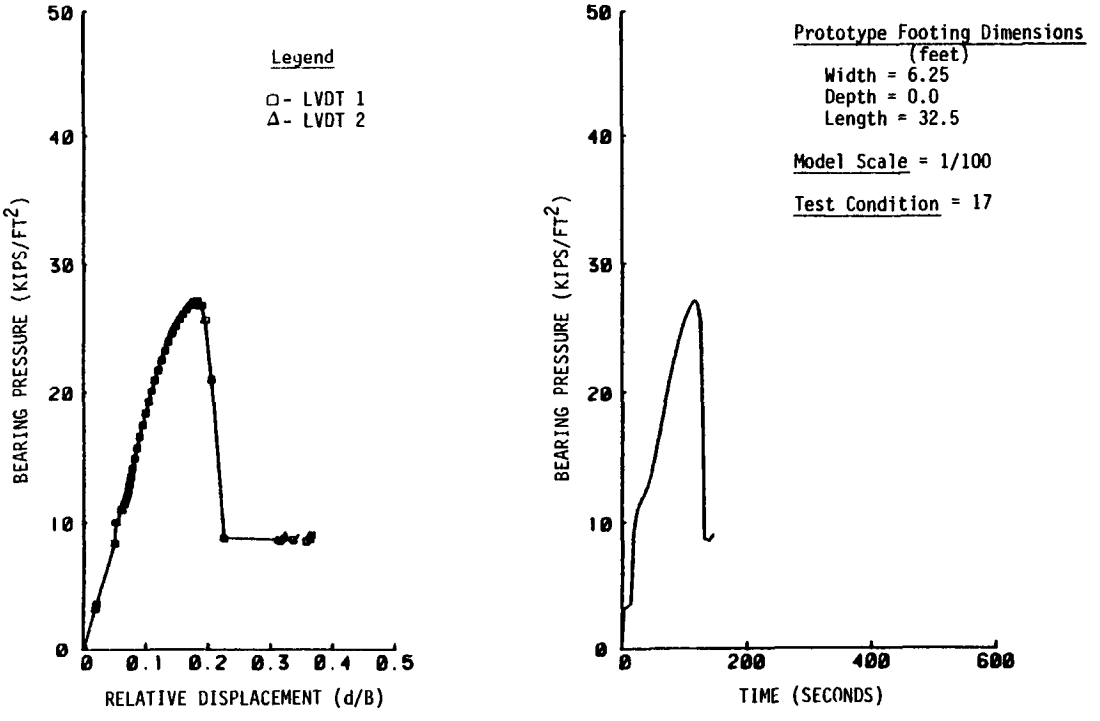

Figure A-50. – Results of test No. 50.

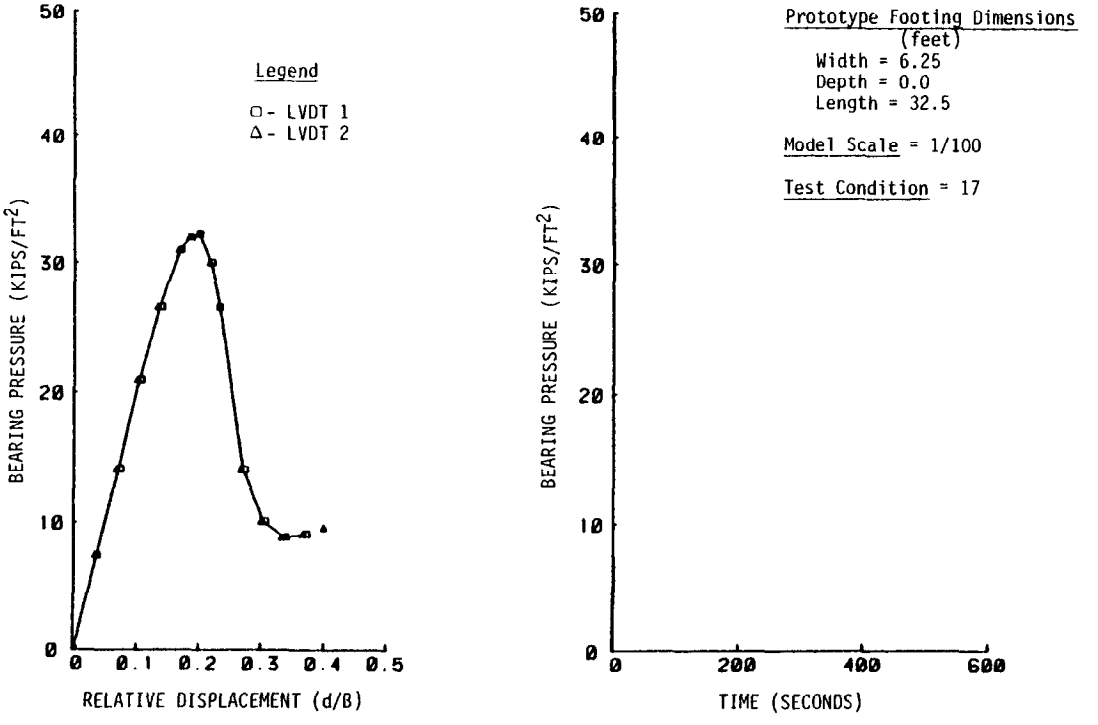

Figure A-51. – Results of test No. 51.

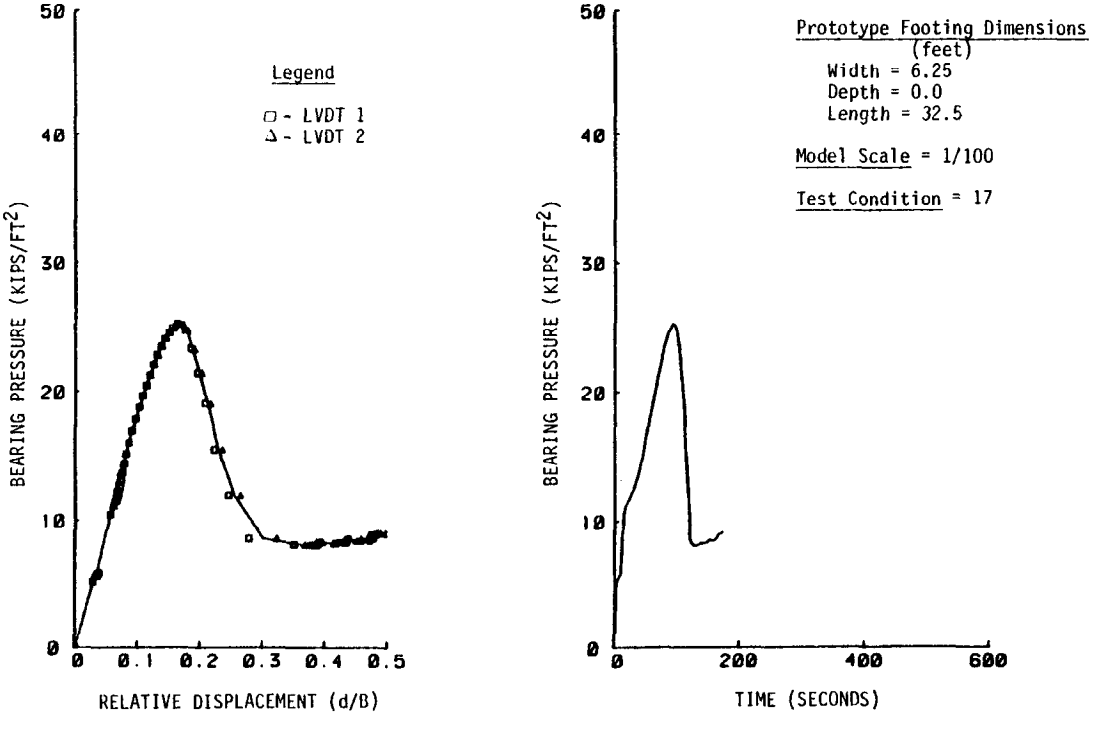

Figure A-52. – Results of test No. 52.

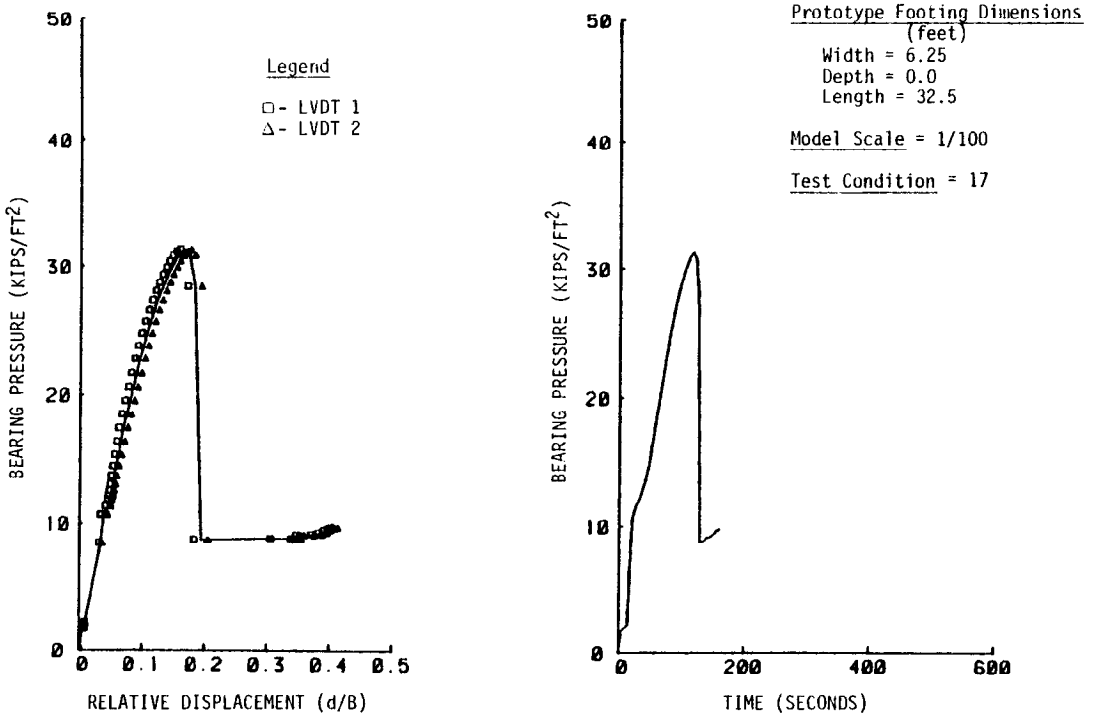

Figure A-53. – Results of test No. 53.

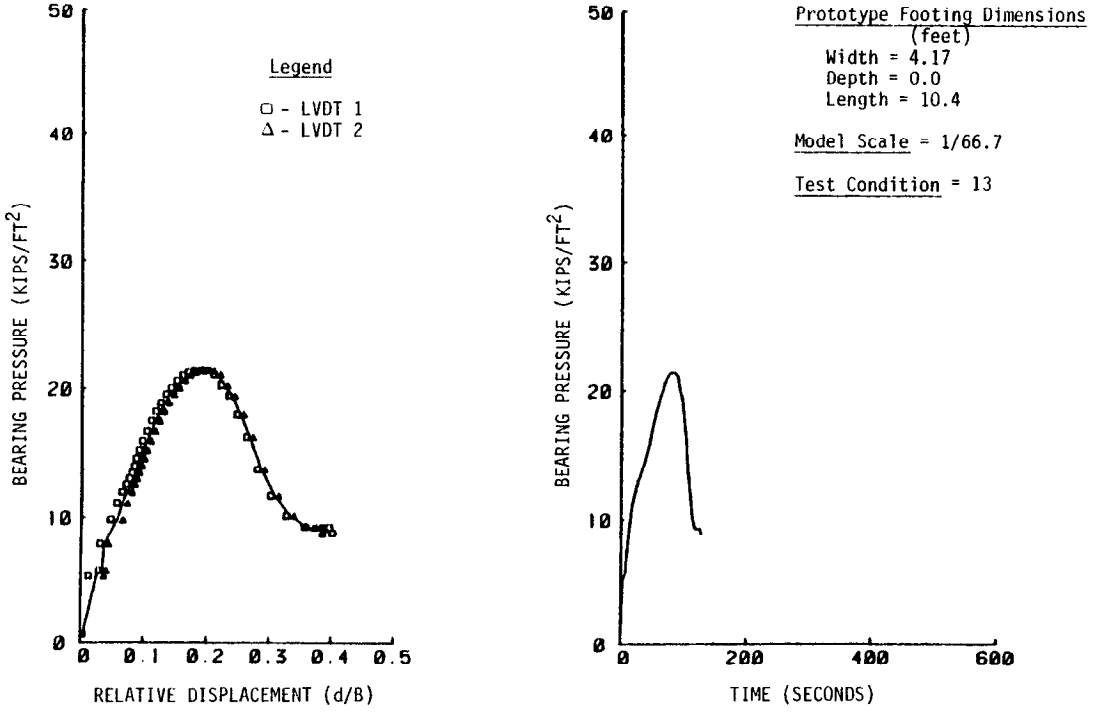

Figure A-54. – Results of test No. 54.

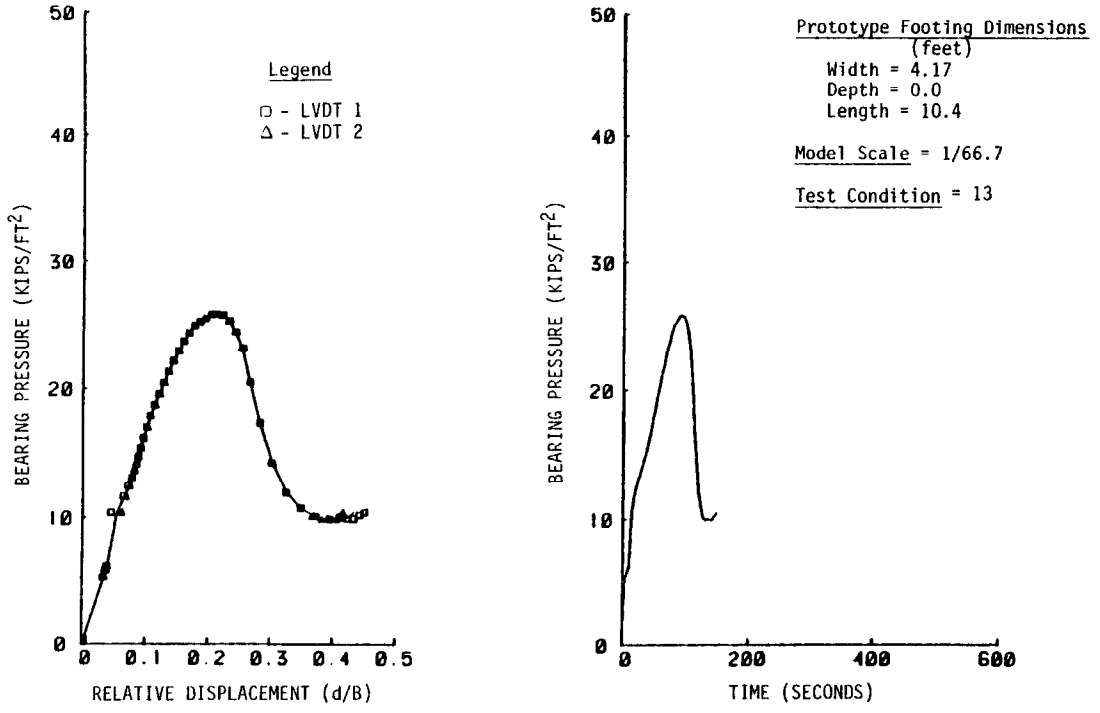

Figure A-55. – Results of test No. 55.

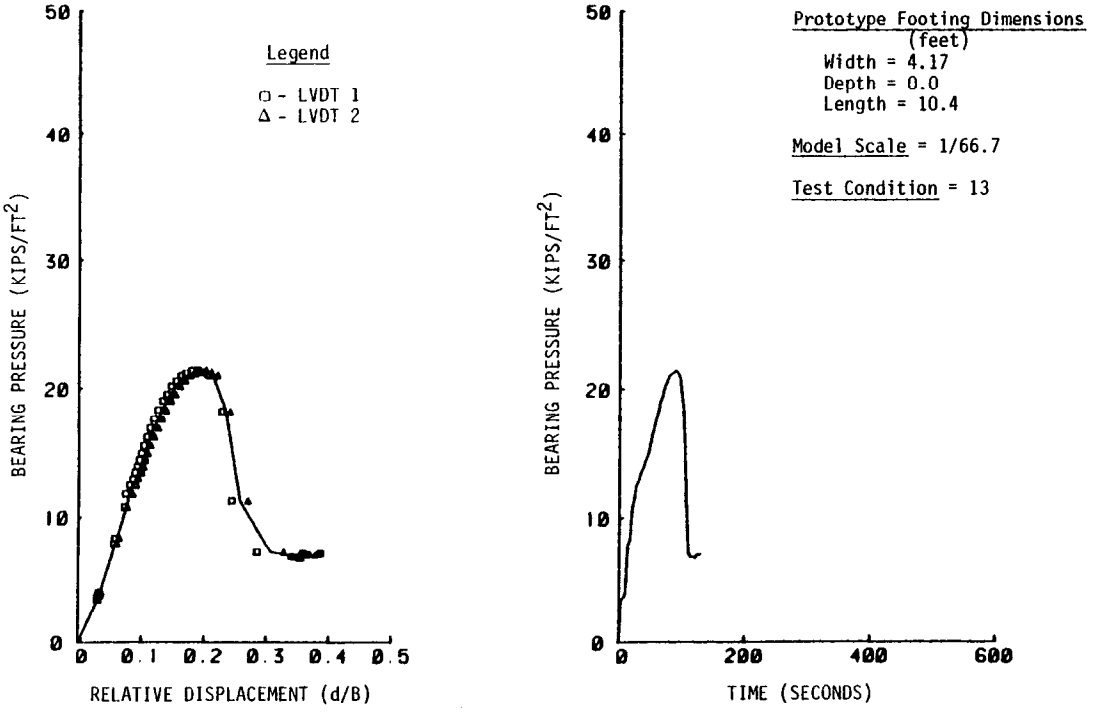

Figure A-56. – Results of test No. 56.

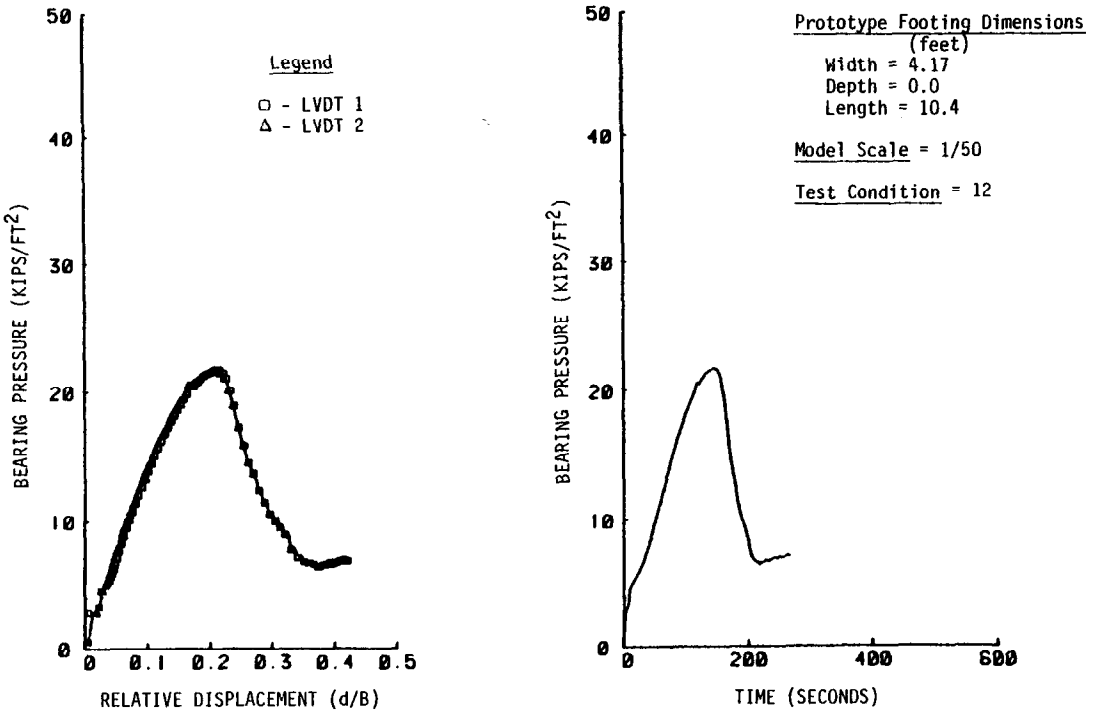

Figure A-57. – Results of test No. 57.

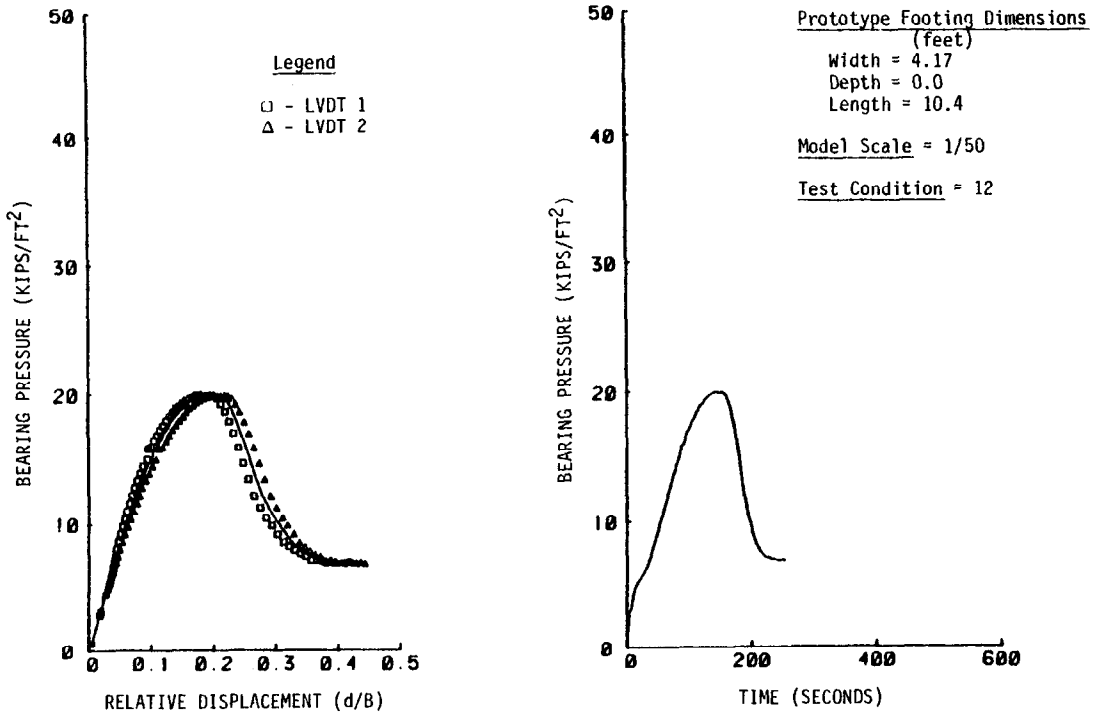

Figure A-58. – Results of test No. 58.

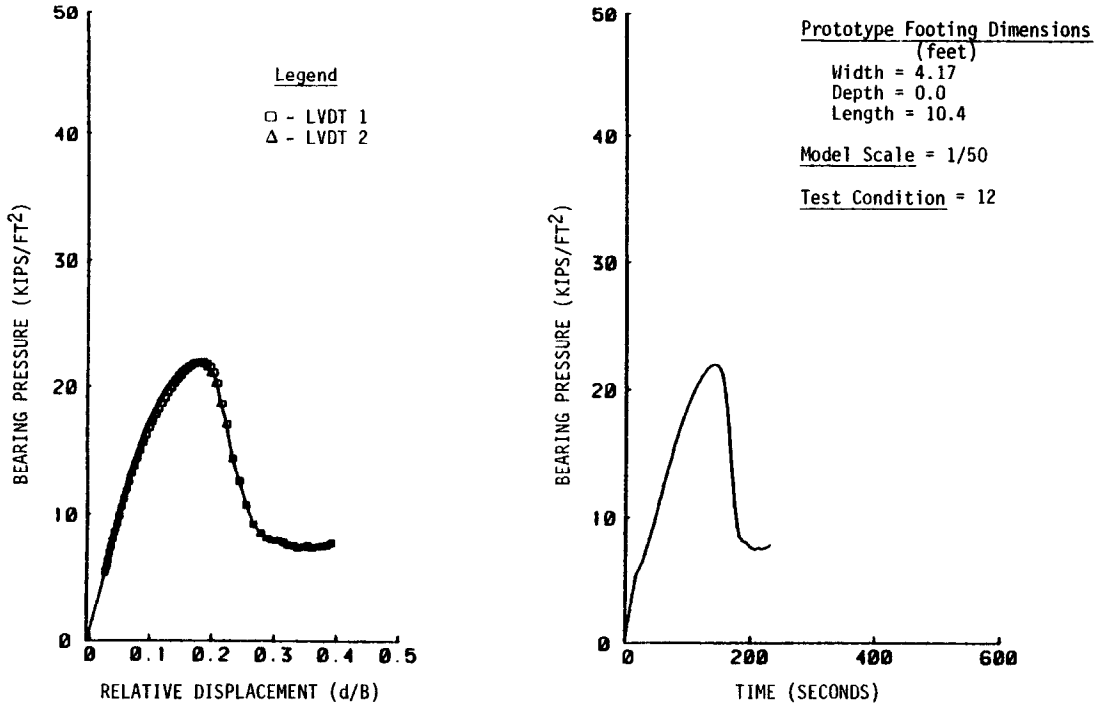

Figure A-59. – Results of test No. 59.

APPENDIX B

GROUPS OF BEARING PRESSURE VERSUS RELATIVE DISPLACEMENT PLOTS FOR TESTS REPRESENTING CONDITIONS 1 THROUGH 17

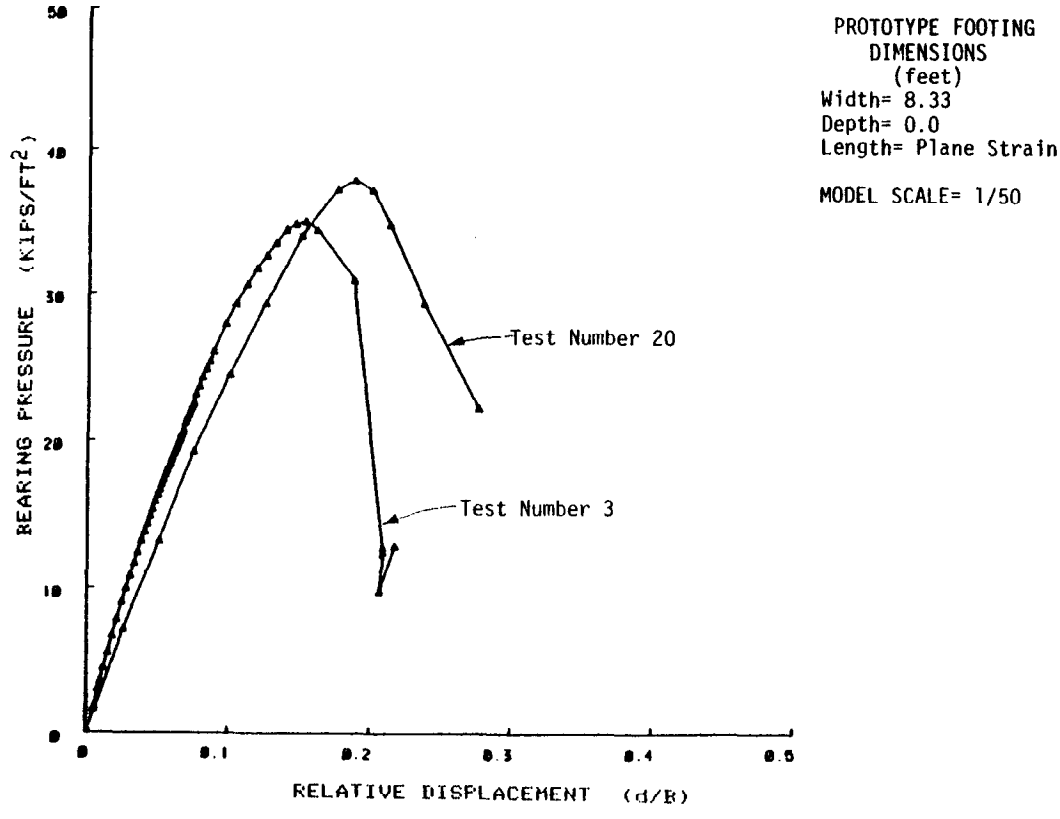

Figure B-1. – Bearing pressure vs. relative displacement for conditions 1 tests

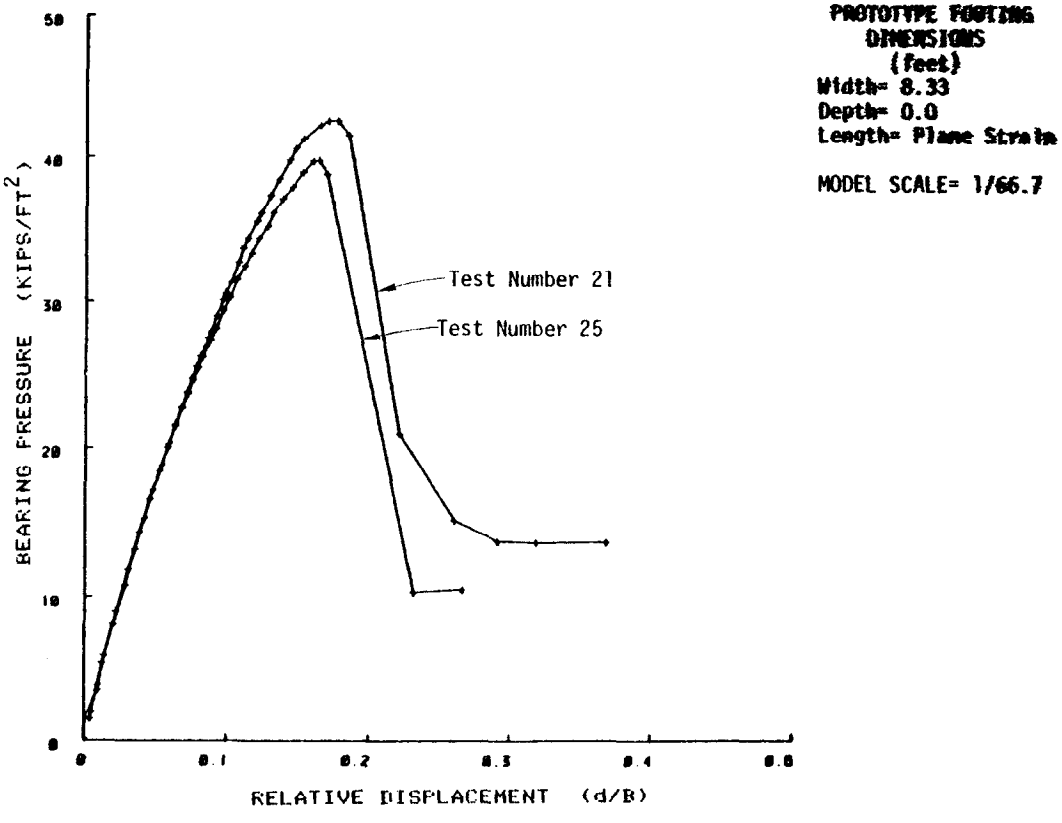

Figure B-2. – Bearing pressure vs. relative displacement for conditions 2 tests.

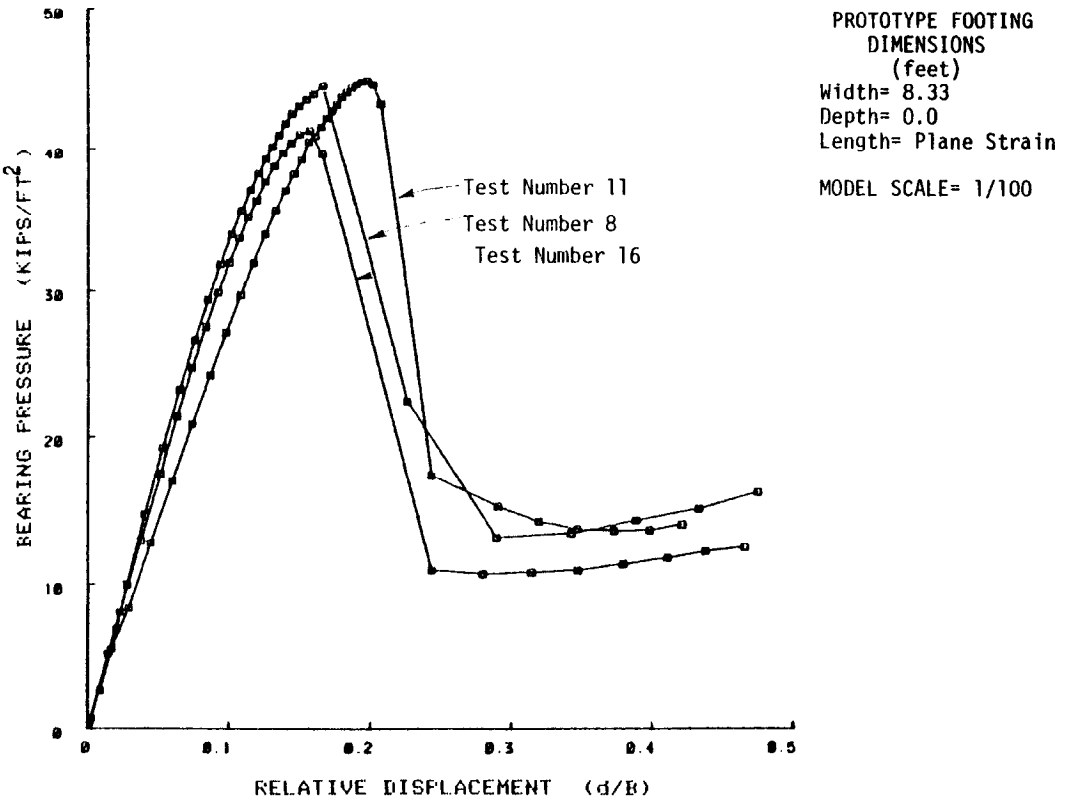

Figure B-3. – Bearing pressure vs. relative displacement for condition 3 tests.

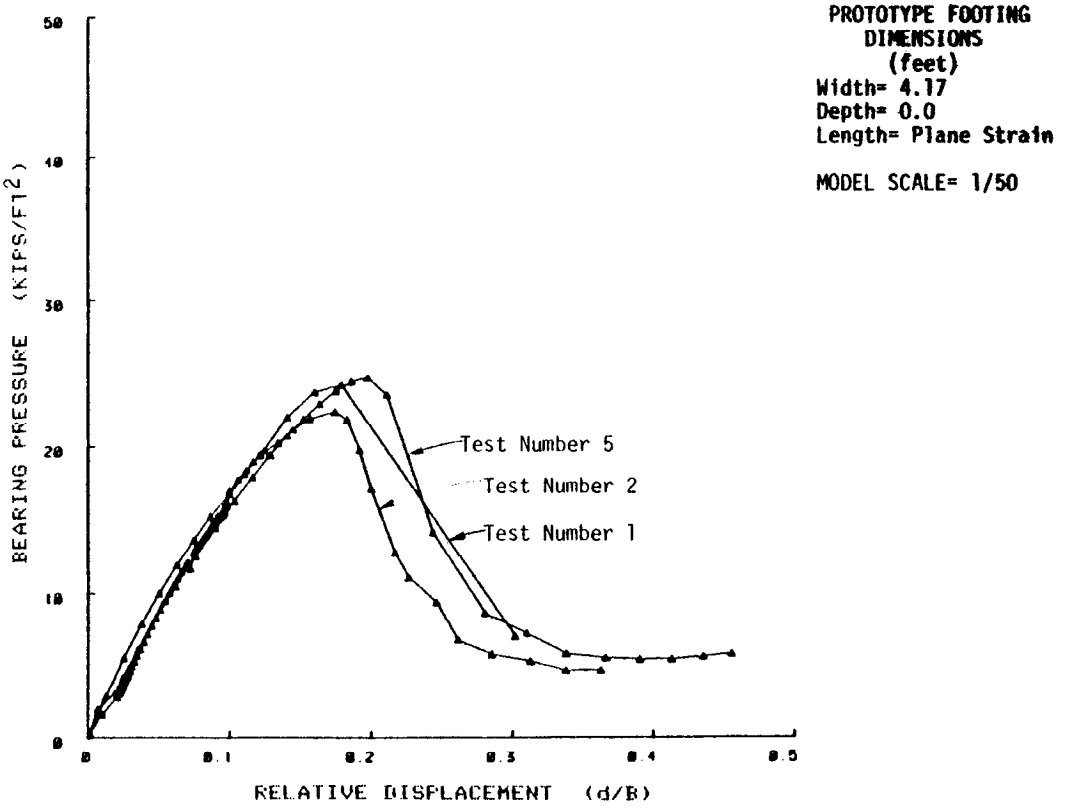

Figure B-4. – Bearing pressure vs. relative displacement for condition 4 tests.

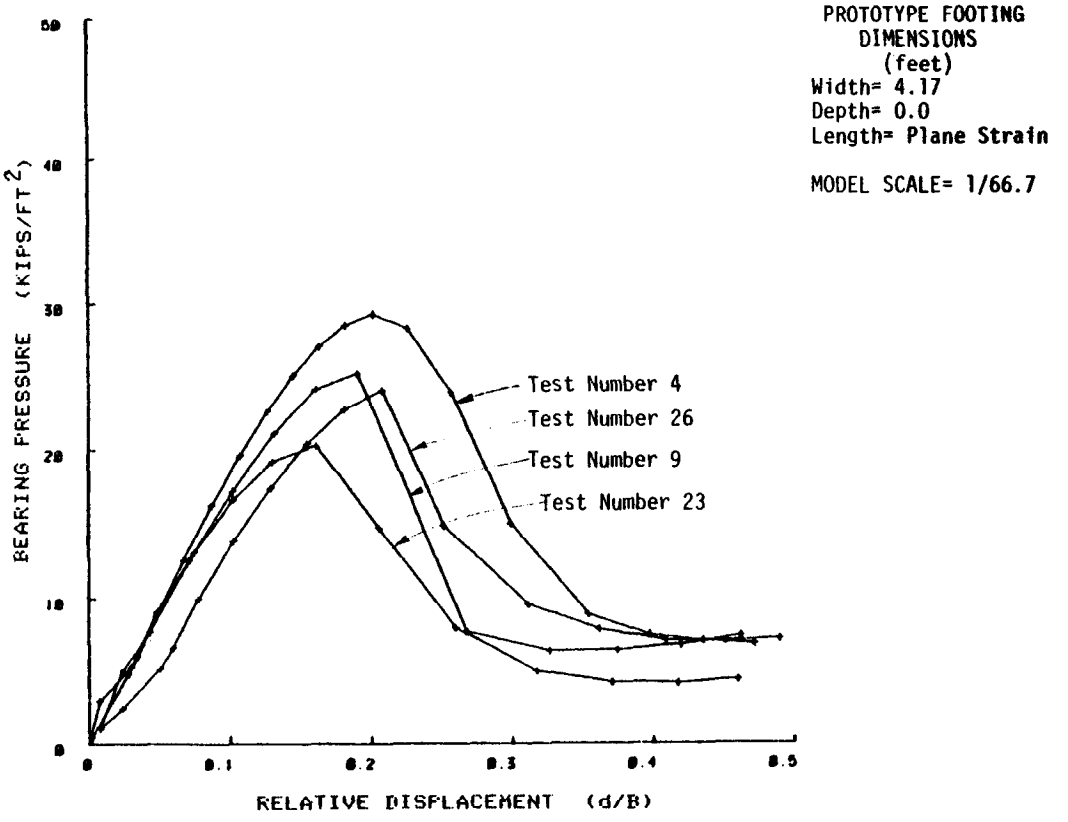

Figure B-5. – Bearing pressure vs. relative displacement for condition 5 tests.

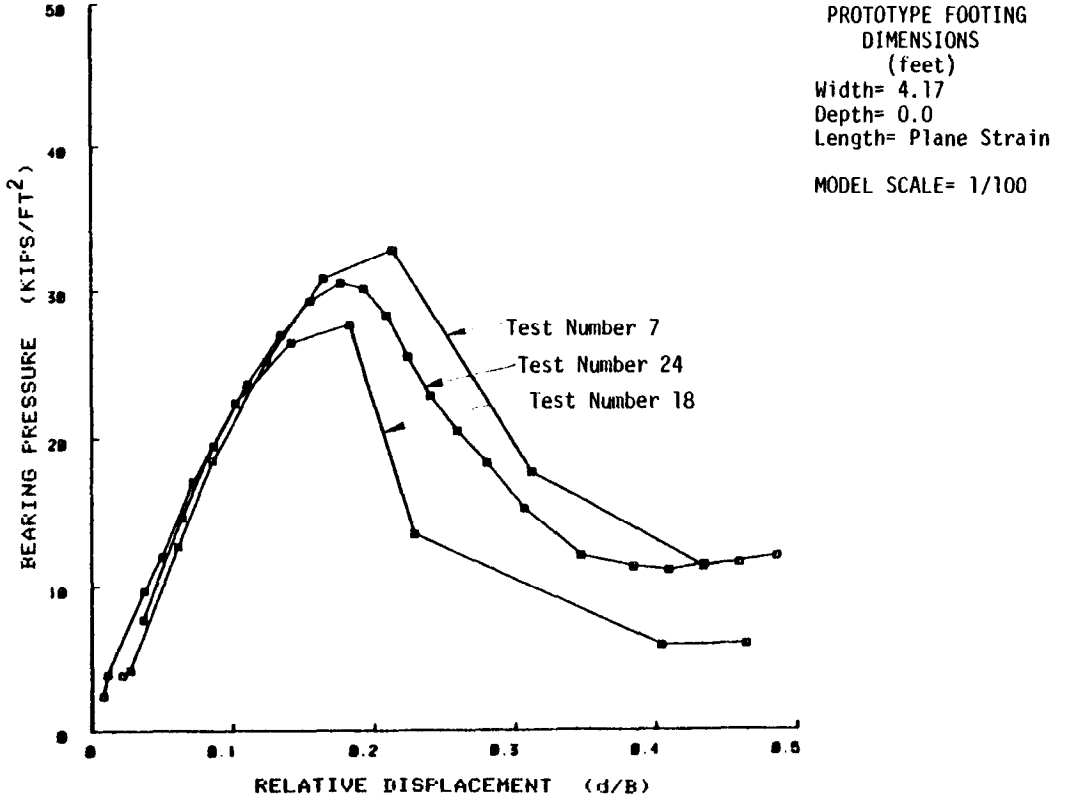

Figure B-6. – Bearing pressure vs. relative displacement for condition 6 tests.

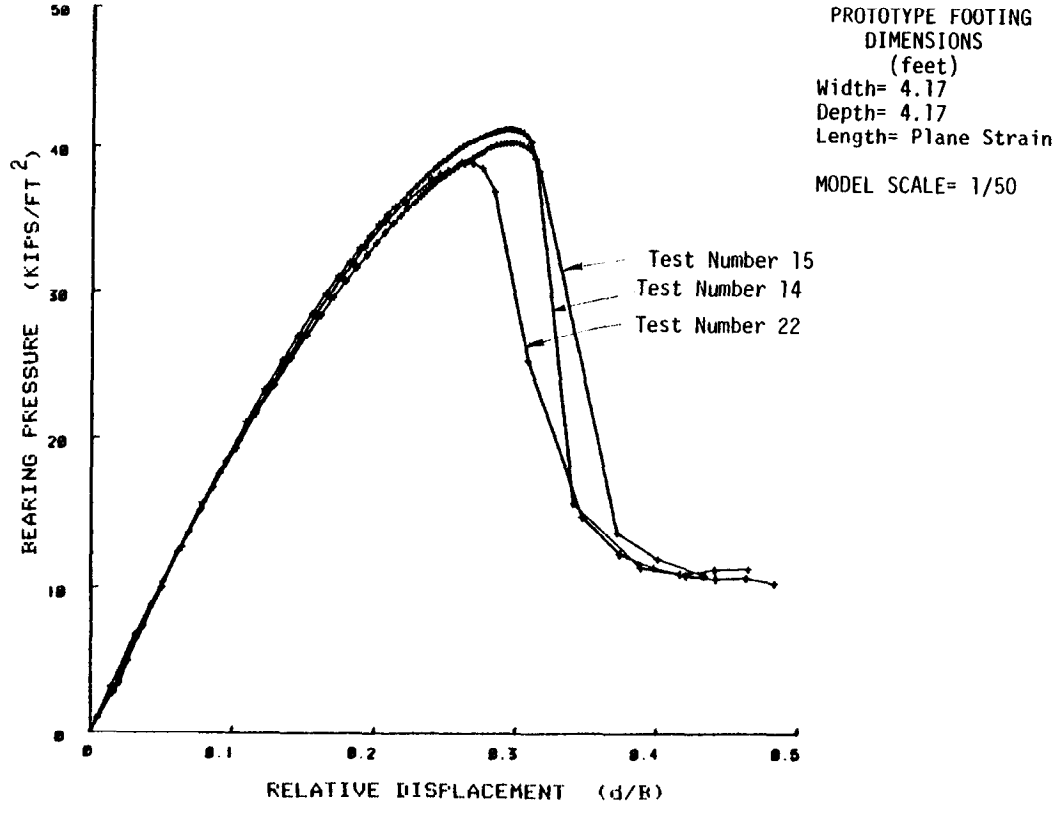

Figure B-7. – Bearing pressure vs. relative displacement for condition 7 tests.

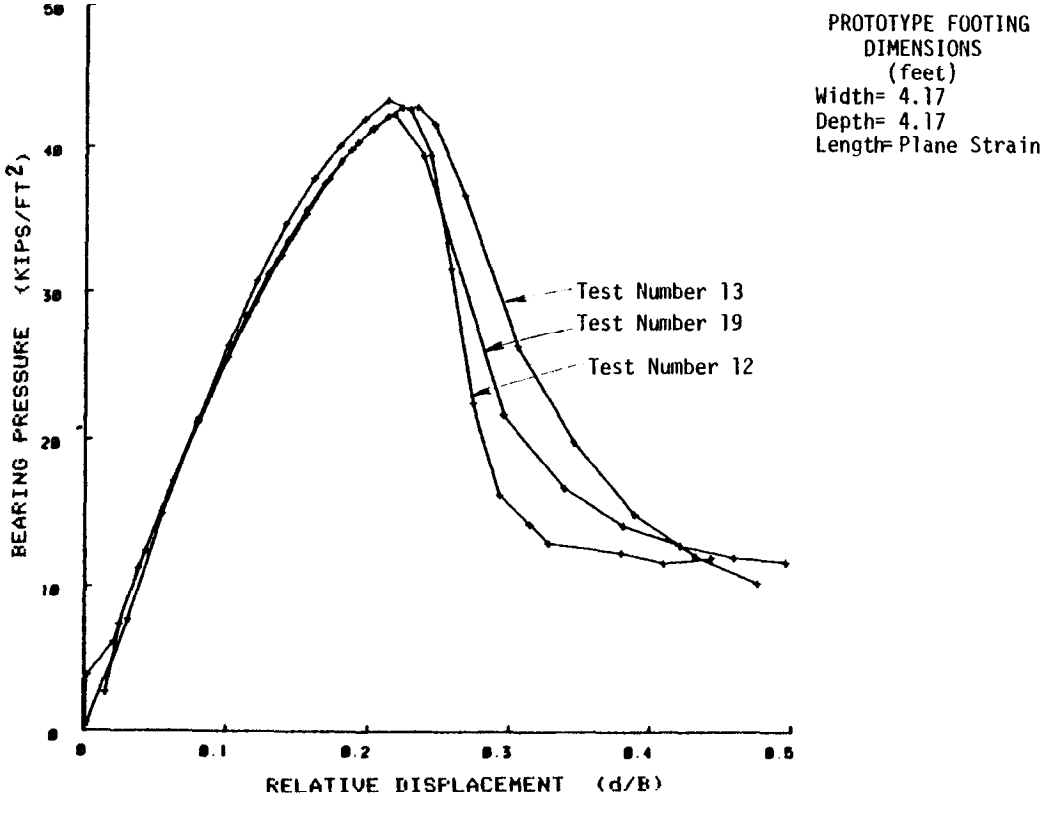

Figure B-8. – Bearing pressure vs. relative displacement for condition 8 tests.

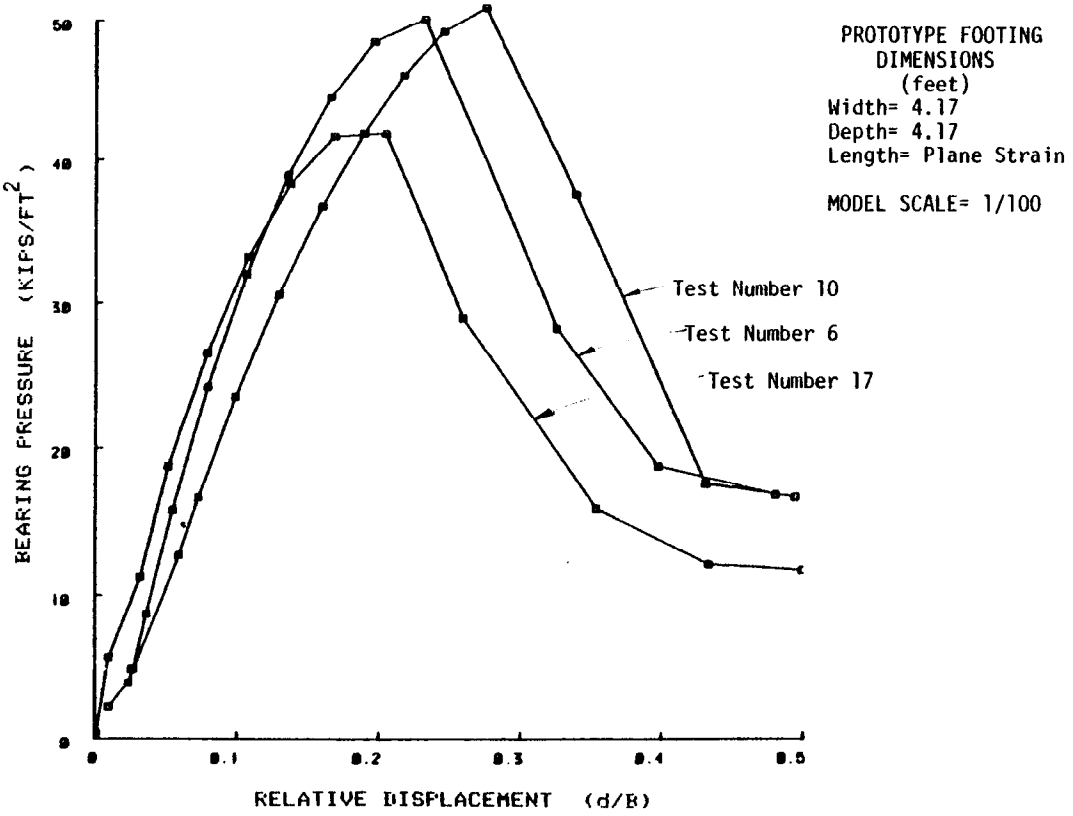

Figure B-9. – Bearing pressure vs. relative displacement for condition 9 tests.

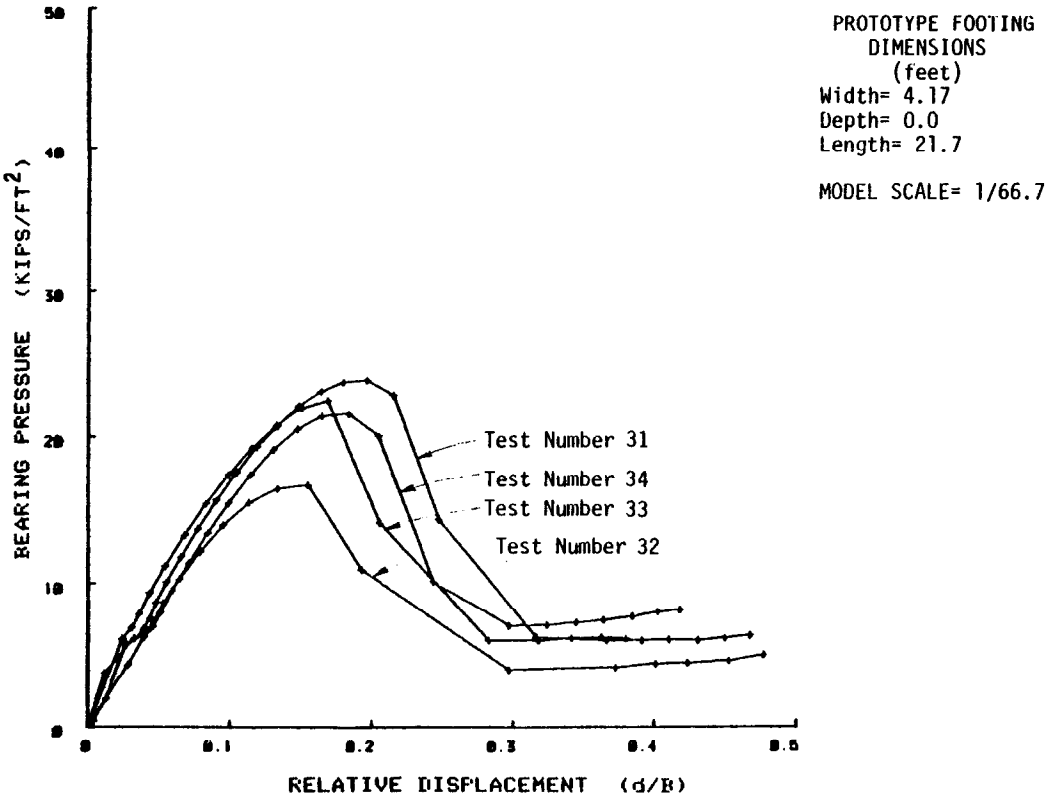

Figure B-10. – Bearing pressure vs. relative displacement for condition 10 tests.

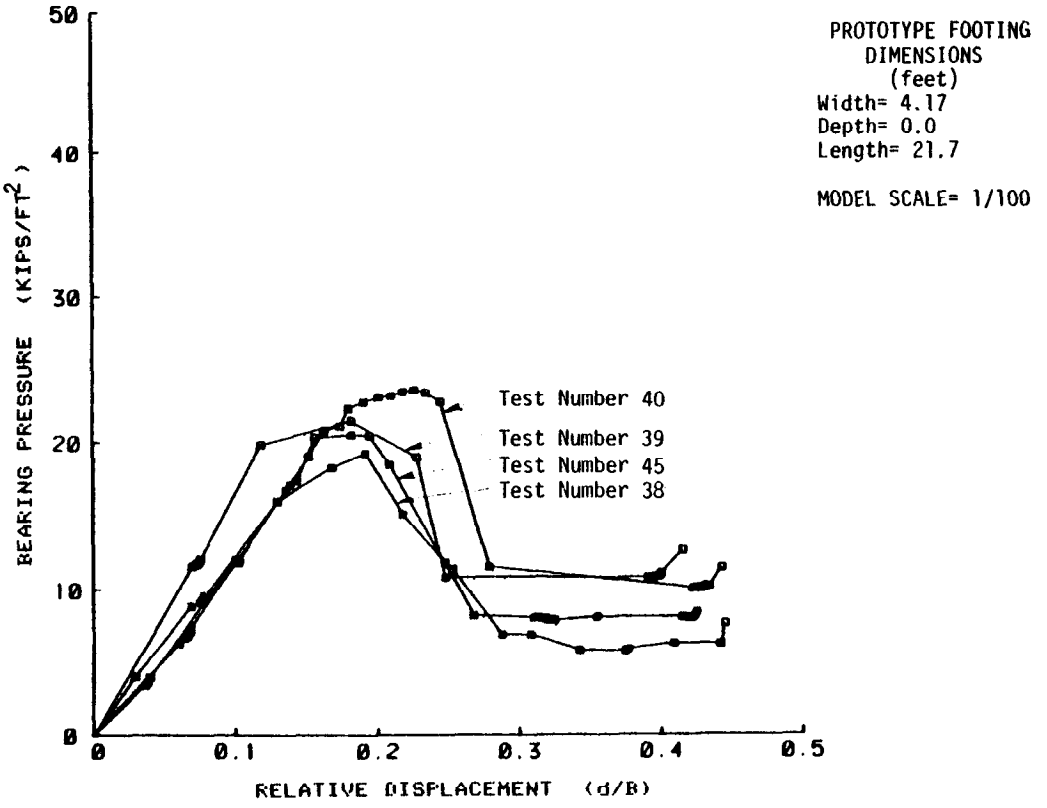

Figure B-11. – Bearing pressure vs. relative displacement for condition 11 tests.

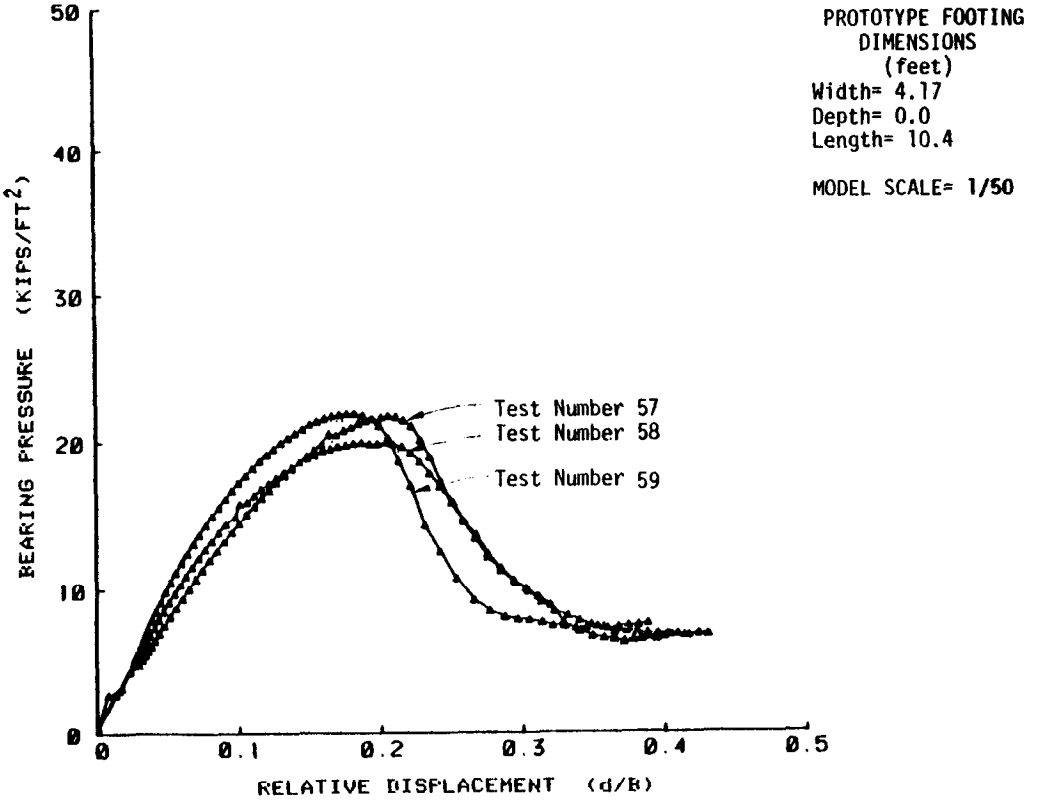

Figure B-12. – Bearing pressure vs. relative displacement for condition 12 tests.

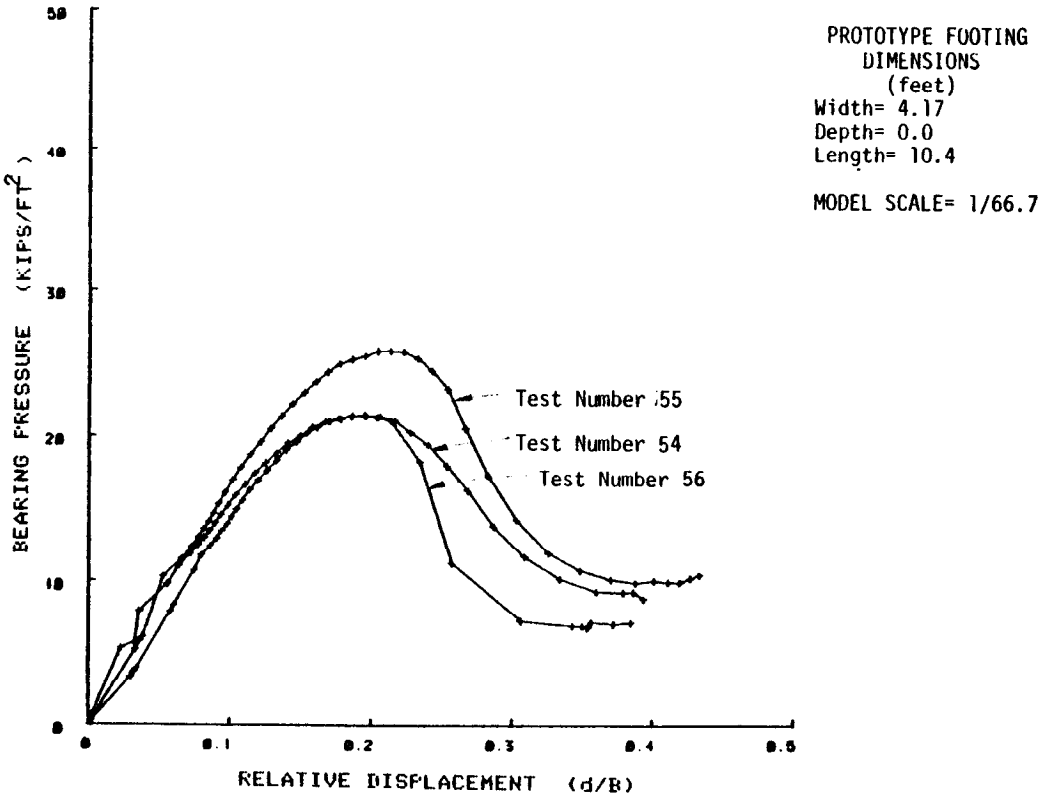

Figure B-13. – Bearing pressure vs. relative displacement for condition 13 tests.

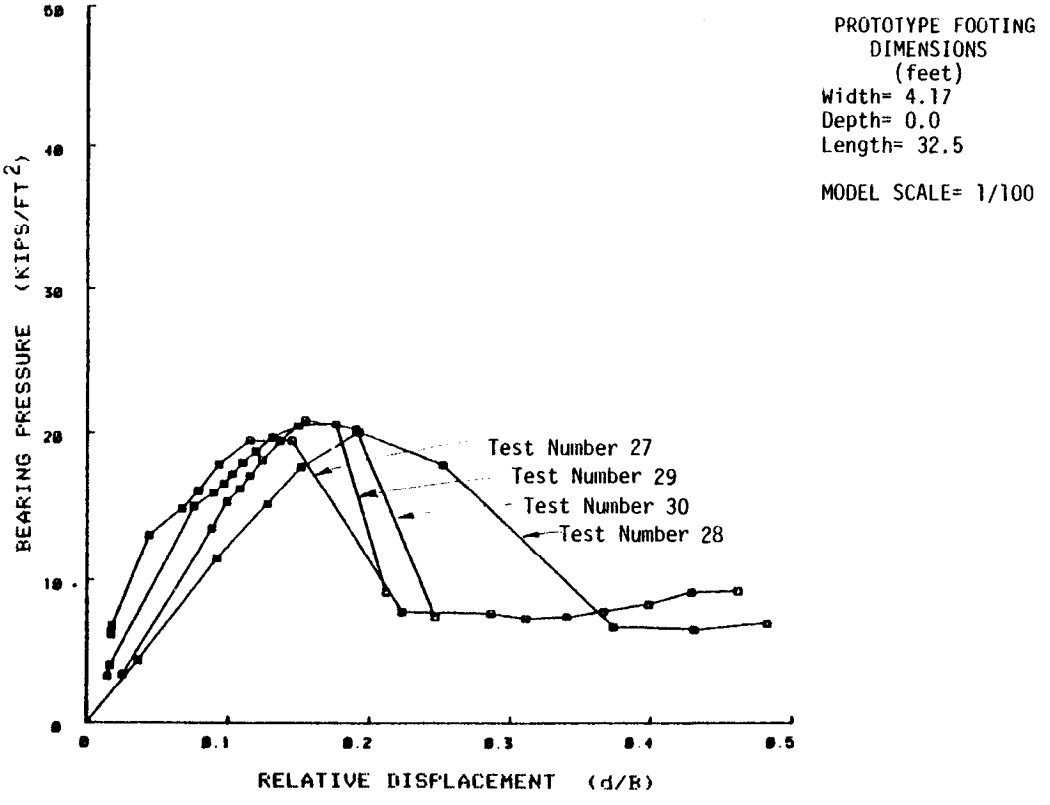

Figure B-14. – Bearing pressure vs. relative displacement for condition 14 tests.

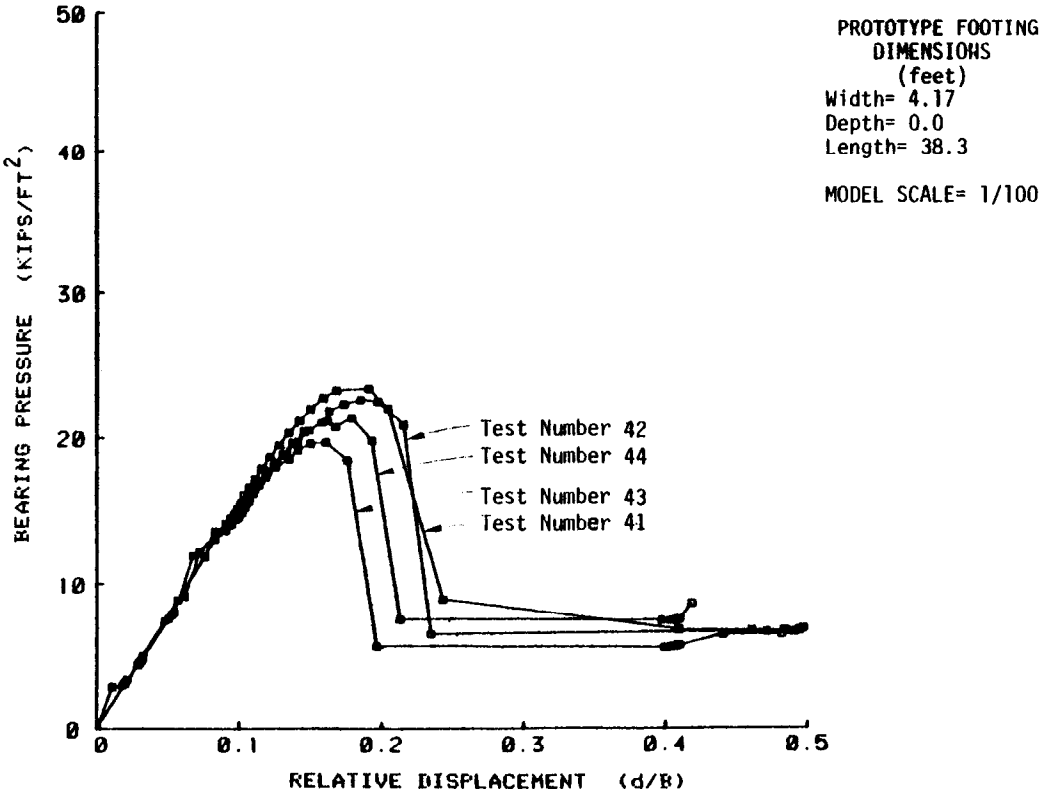

Figure B-15. – Bearing pressure vs. relative displacement for condition 15 tests.

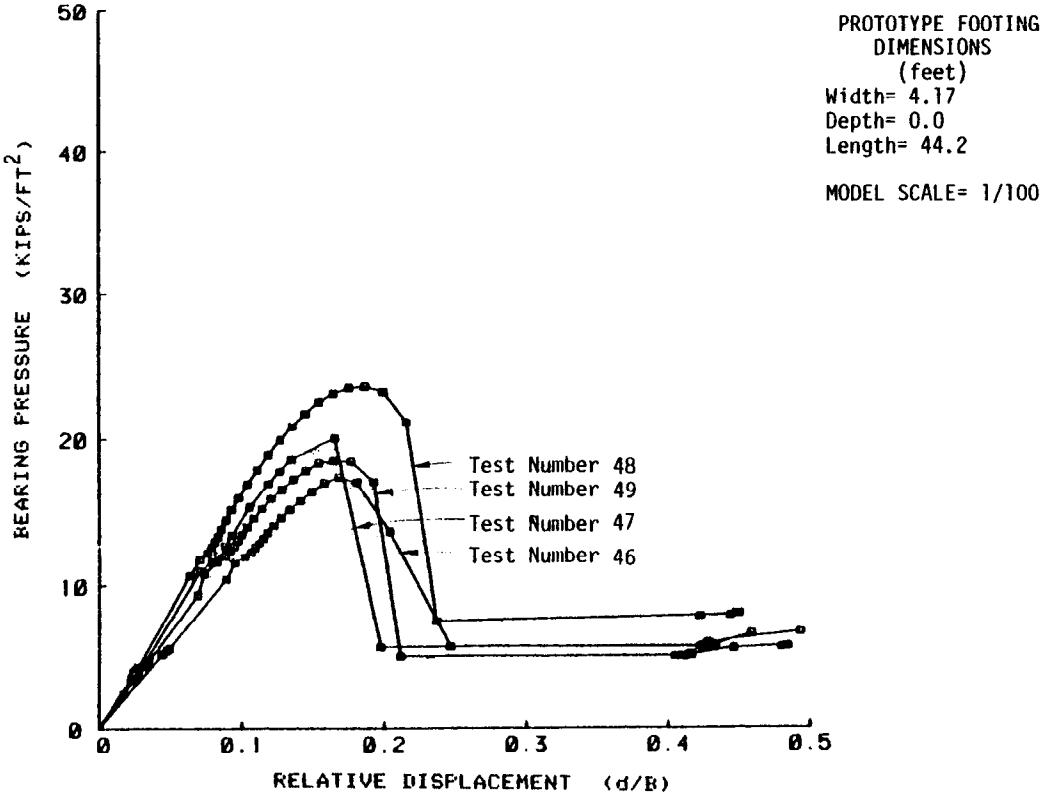

Figure B-16. – Bearing Pressure vs. relative displacement for condition 16 tests.

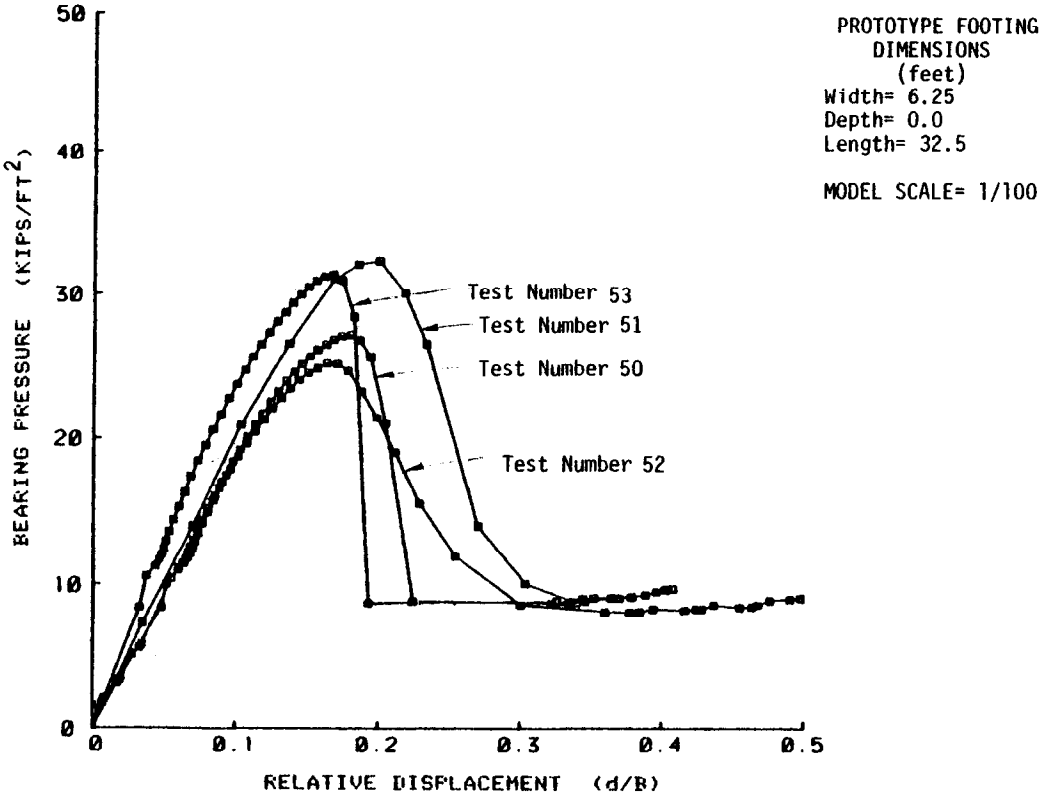

Figure B-17. – Bearing Pressure vs. relative displacement for condition 17 tests.

APPENDIX C

BEARING PRESSURE VERSUS RELATIVE DISPLACEMENT PLOTS FOR GROUPS OF TESTS REPRESENTING THE SAME PROTOTYPE FOOTING WIDTH, DEPTH, AND LENGTH

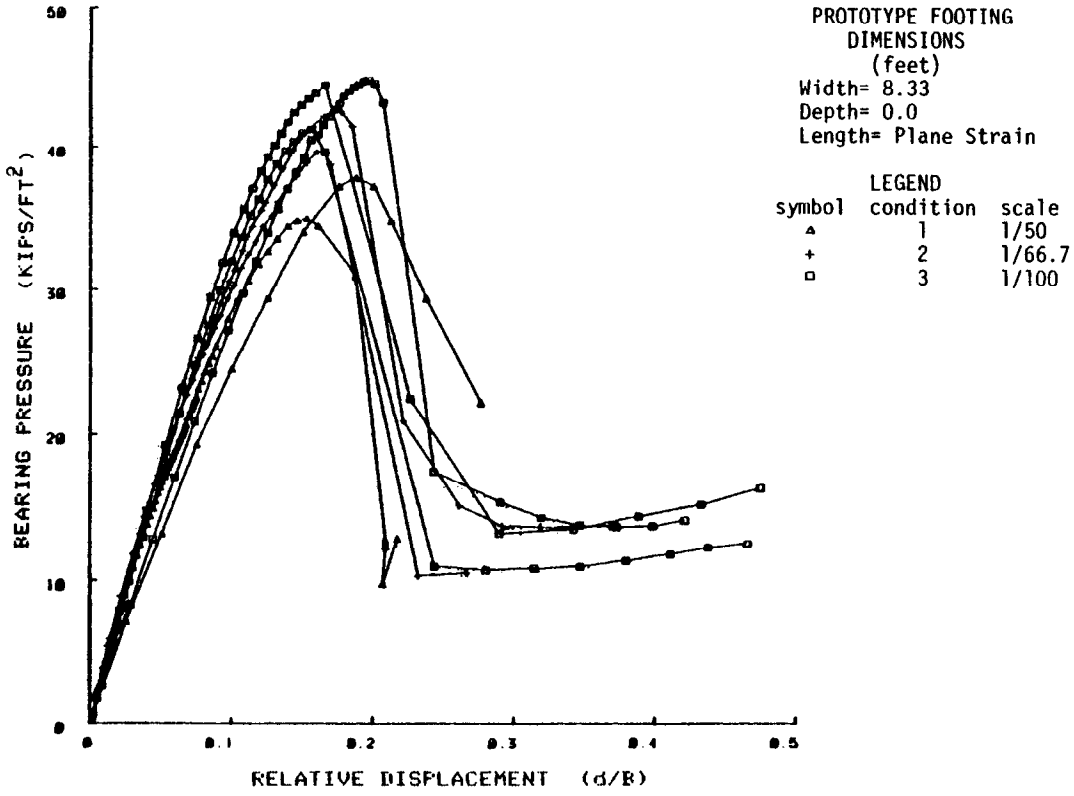

Figure C-1. – Bearing pressure vs. relative displacement for conditions 1, 2, and 3.

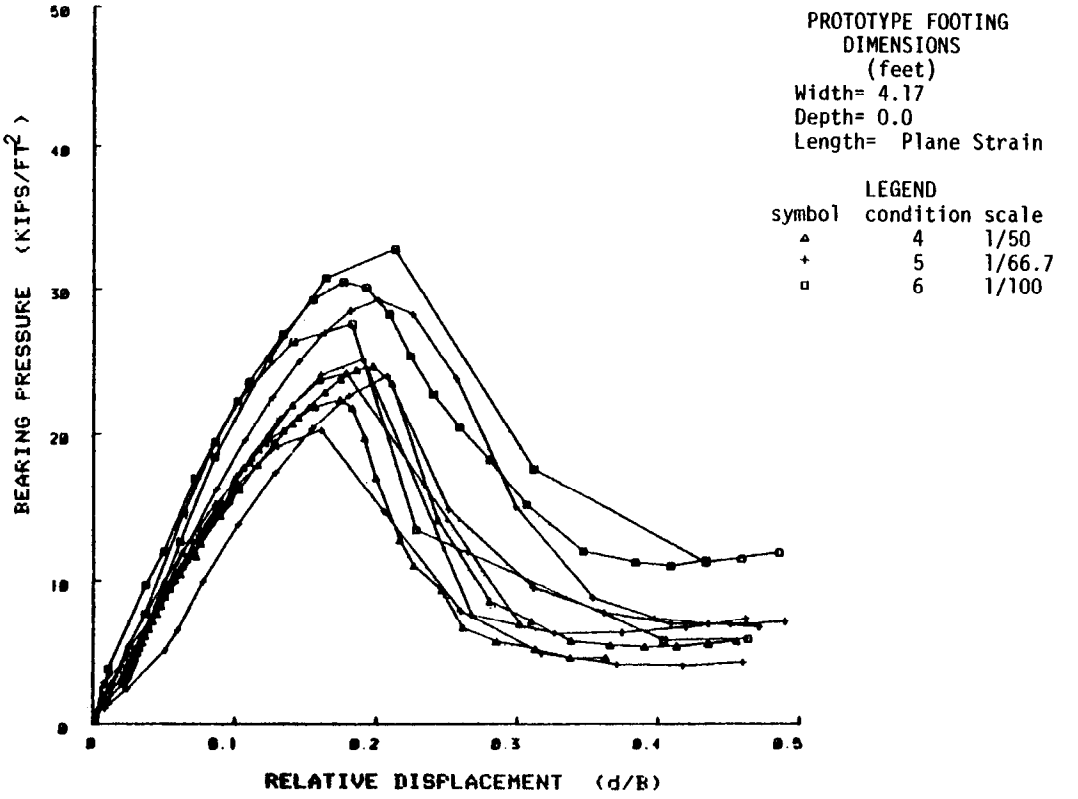

Figure C-2. – Bearing pressure vs. relative displacement for conditions 4, 5, and 6.

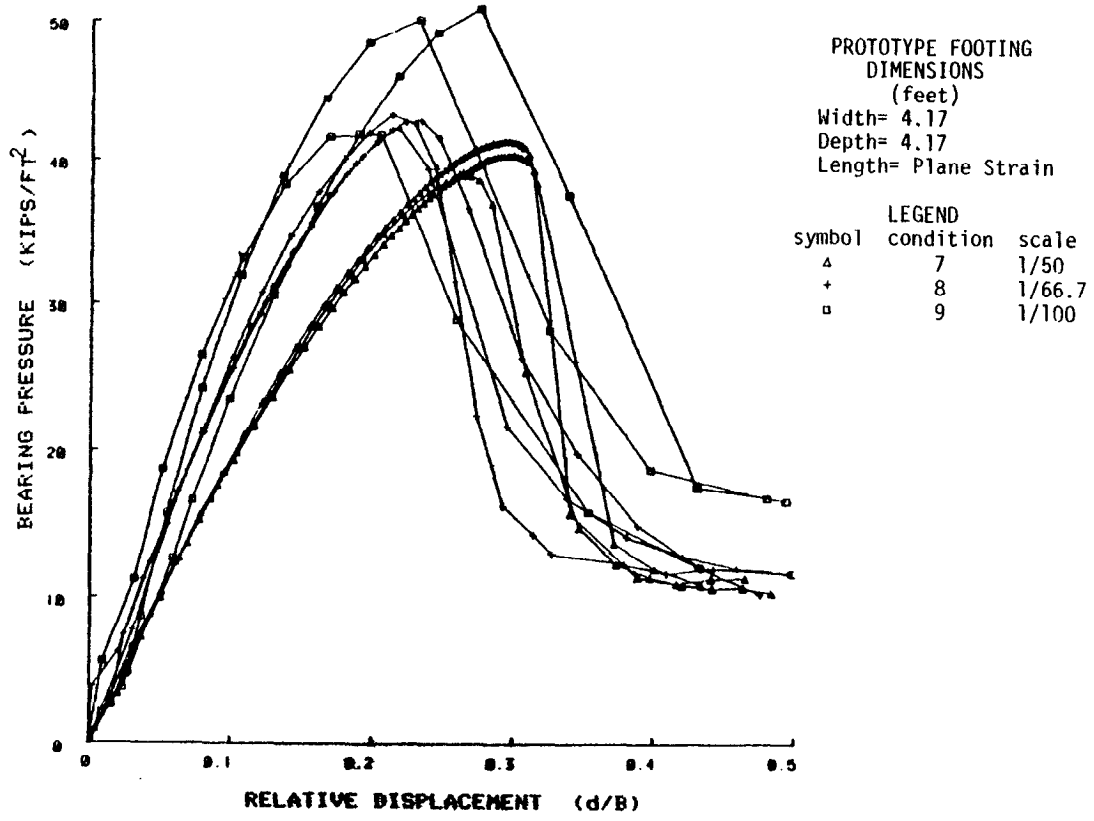

Figure C-3. – Bearing pressure vs. relative displacement for conditions 7, 8 and 9.

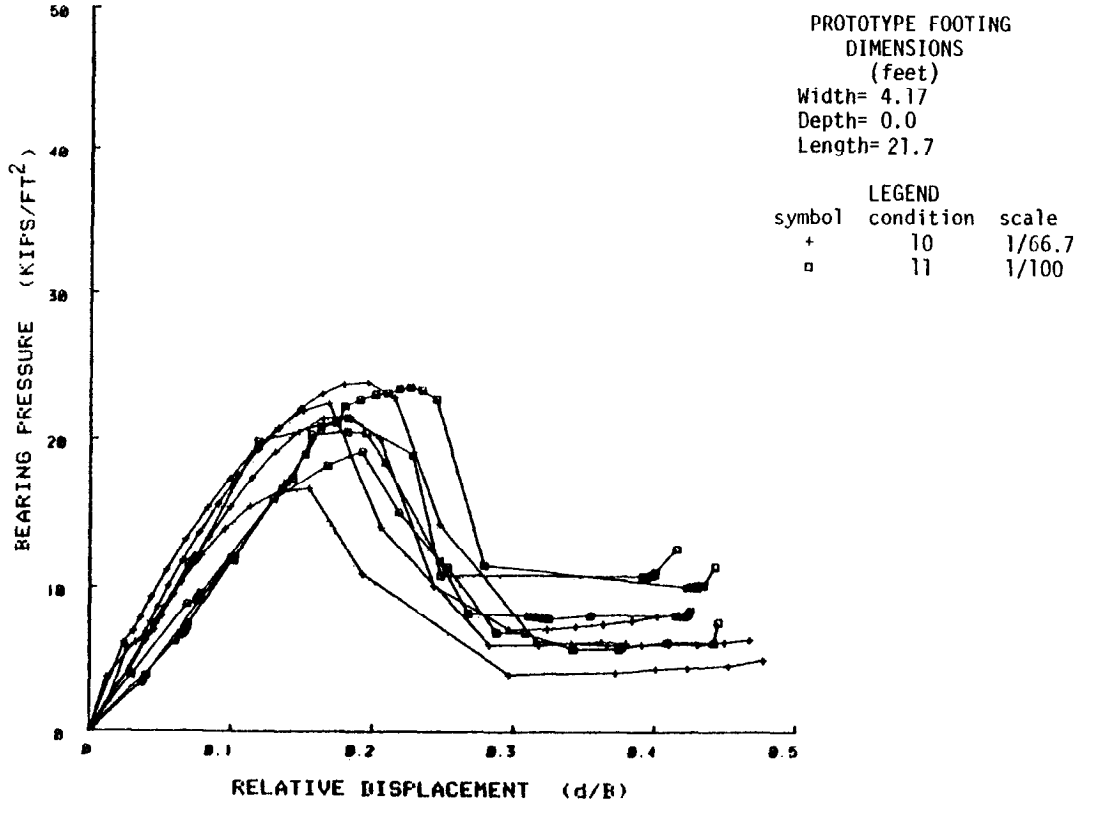

Figure C-4. – Bearing pressure vs. relative displacement for conditions 10 and 11.

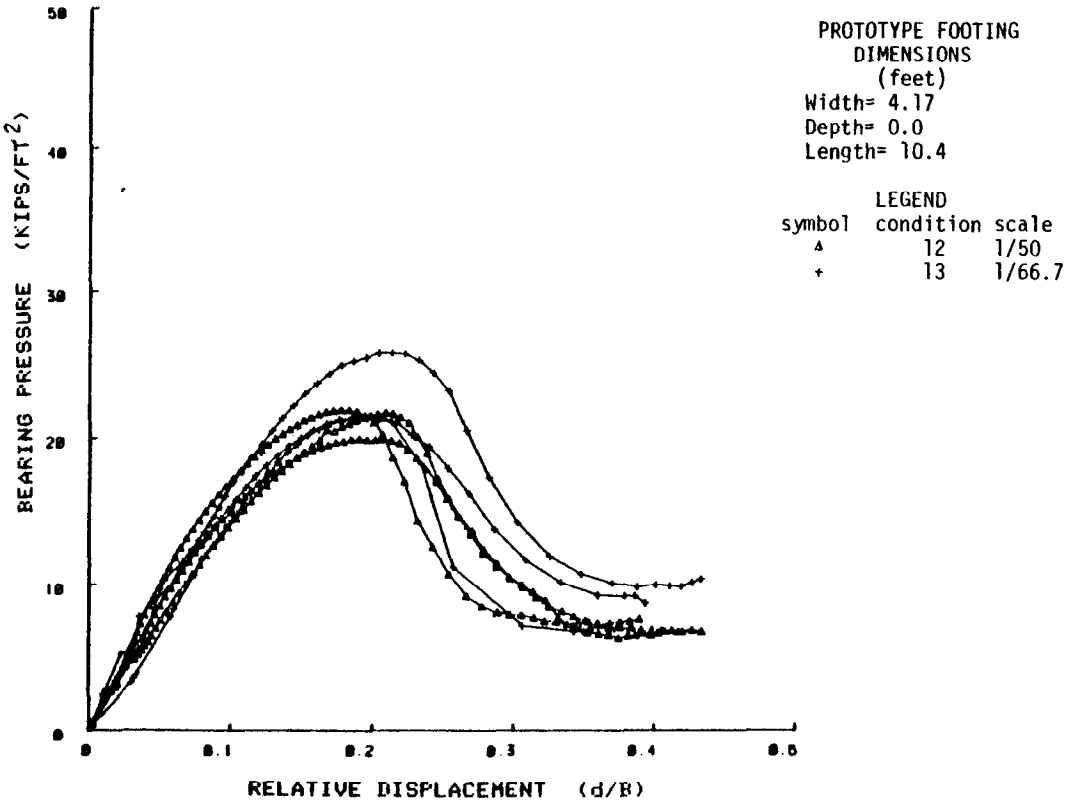

Figure C-5. – Bearing pressure vs. relative displacement for conditions 12 and 13.

APPENDIX D

PHOTOGRAPHS AND SKETCHES OF OBSERVED SHEAR SURFACES FOR SEVERAL TESTS

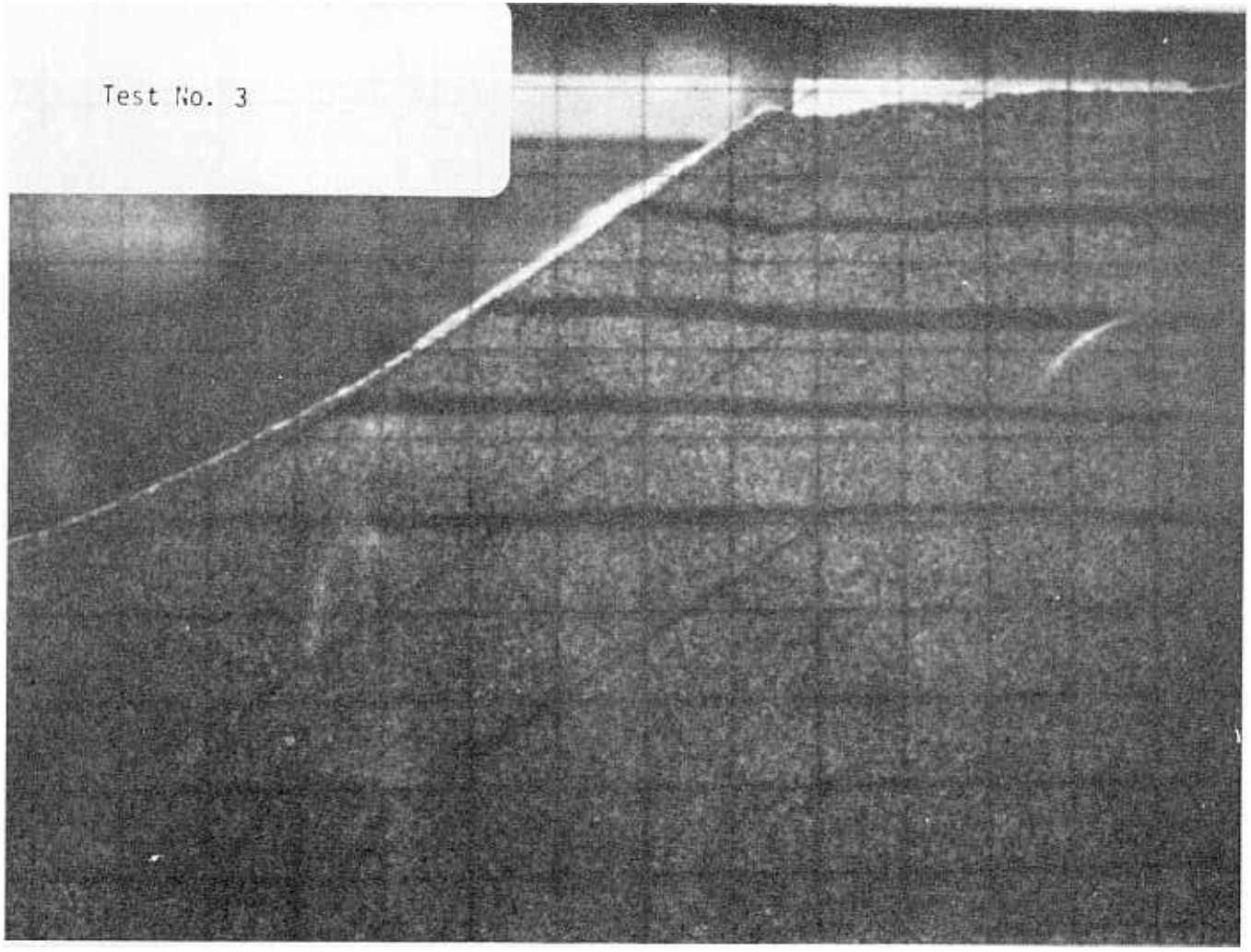
Test No. 3

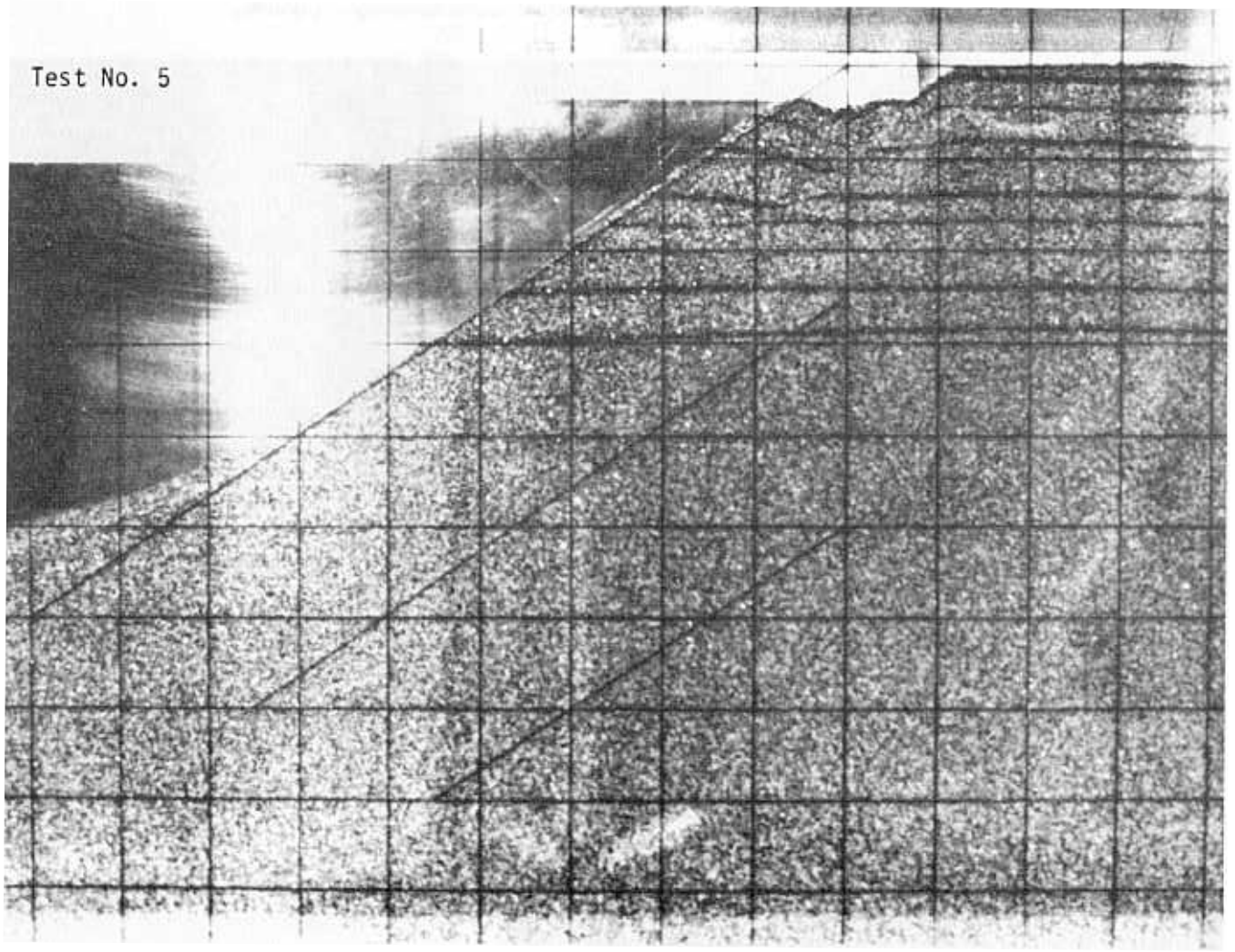

Figure D-2. – Photograph after completion of model test No. 5. Photo P801-D-80810

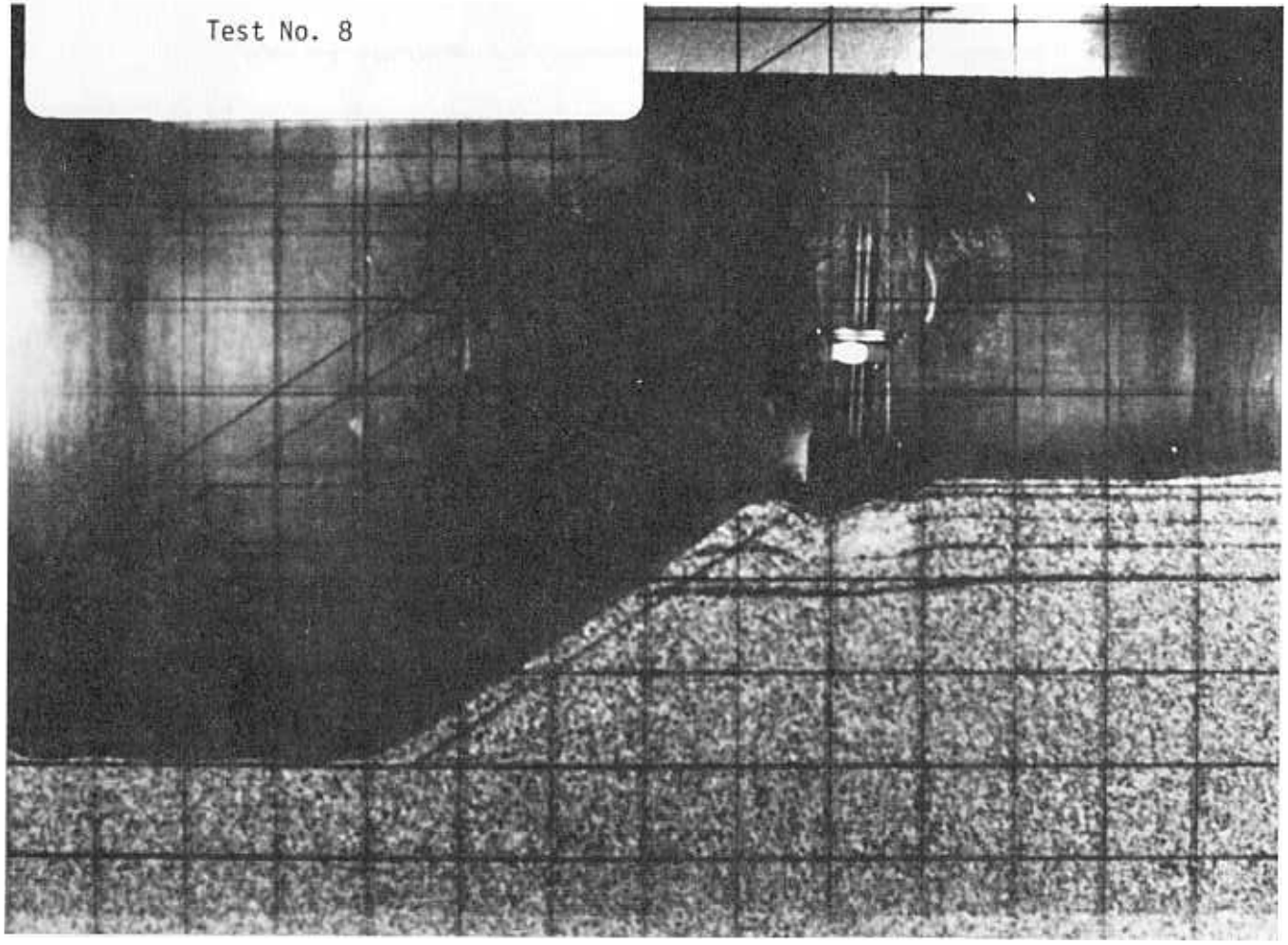
Test No. 8

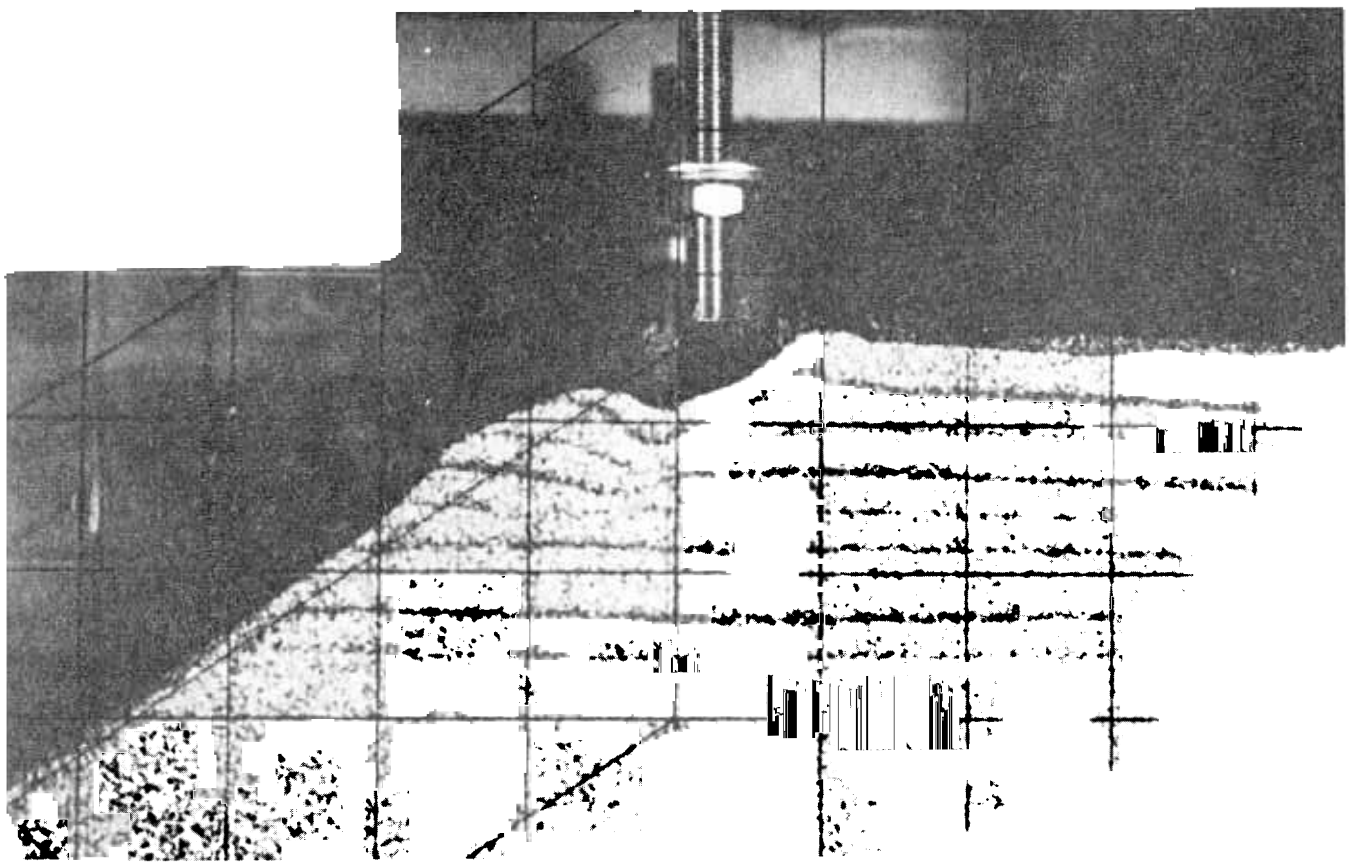

Figure D-4. – Photograph after mpletion of model test No. 9. Photo P80 808

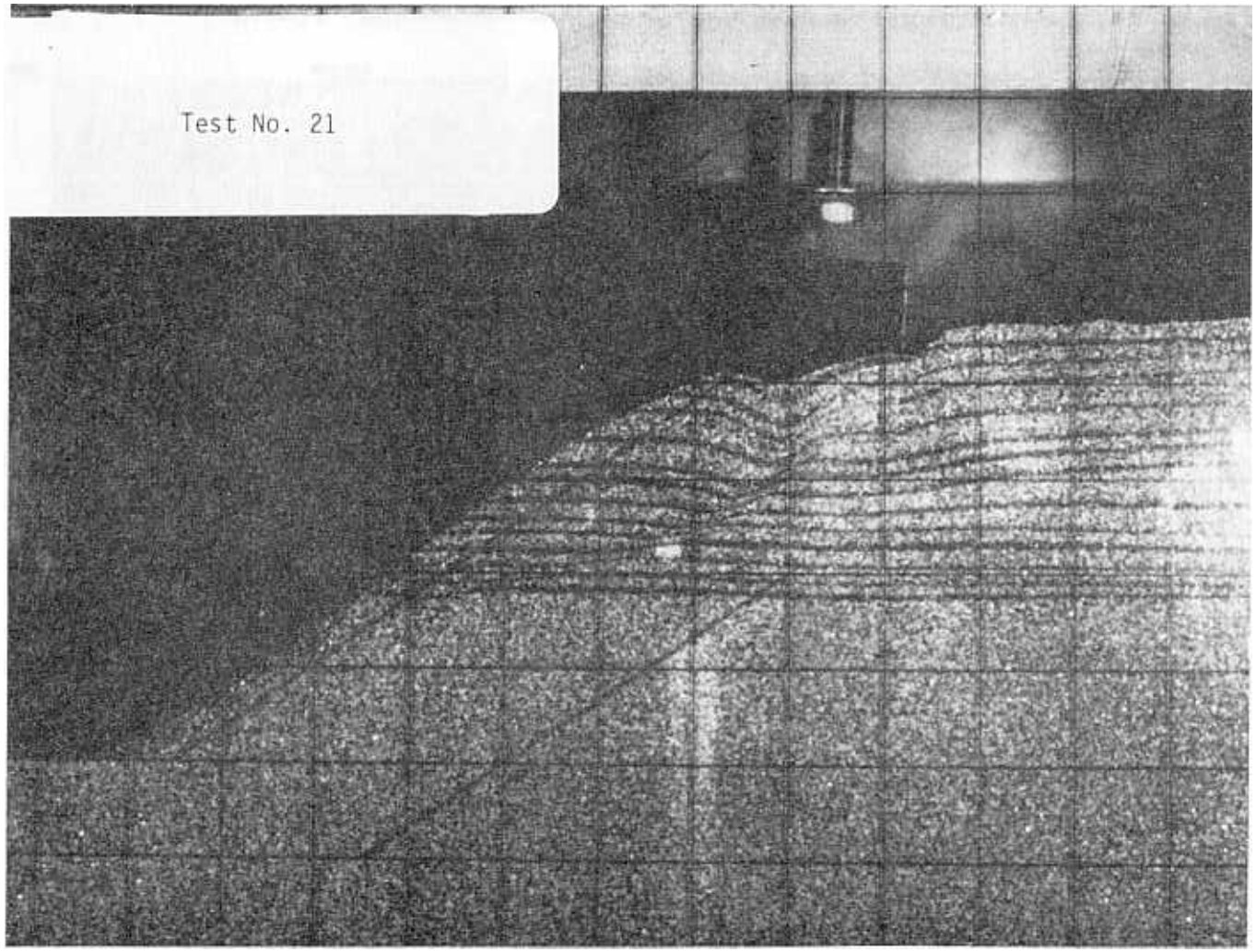
Test No. 21

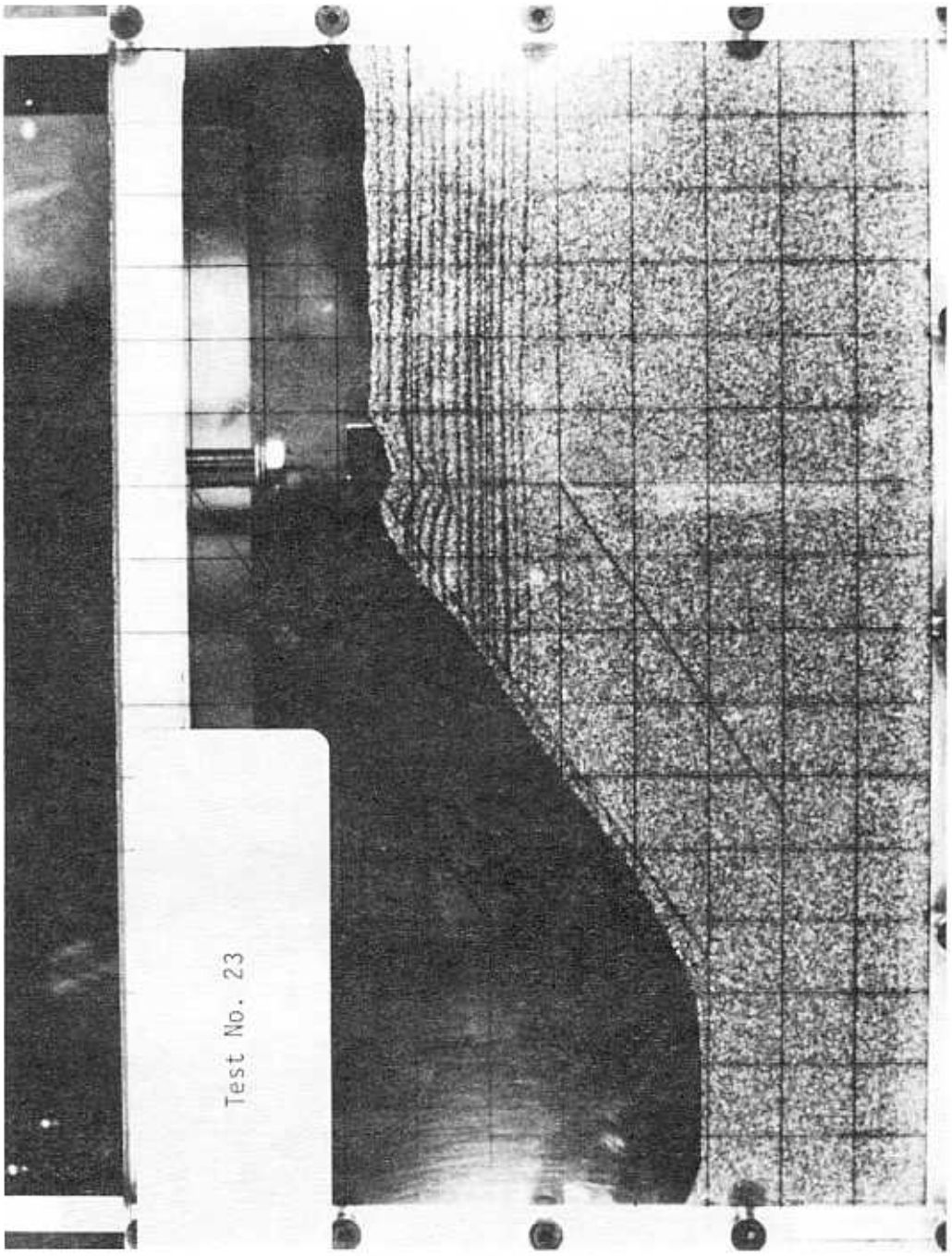
Test No. 23

Test No. 25

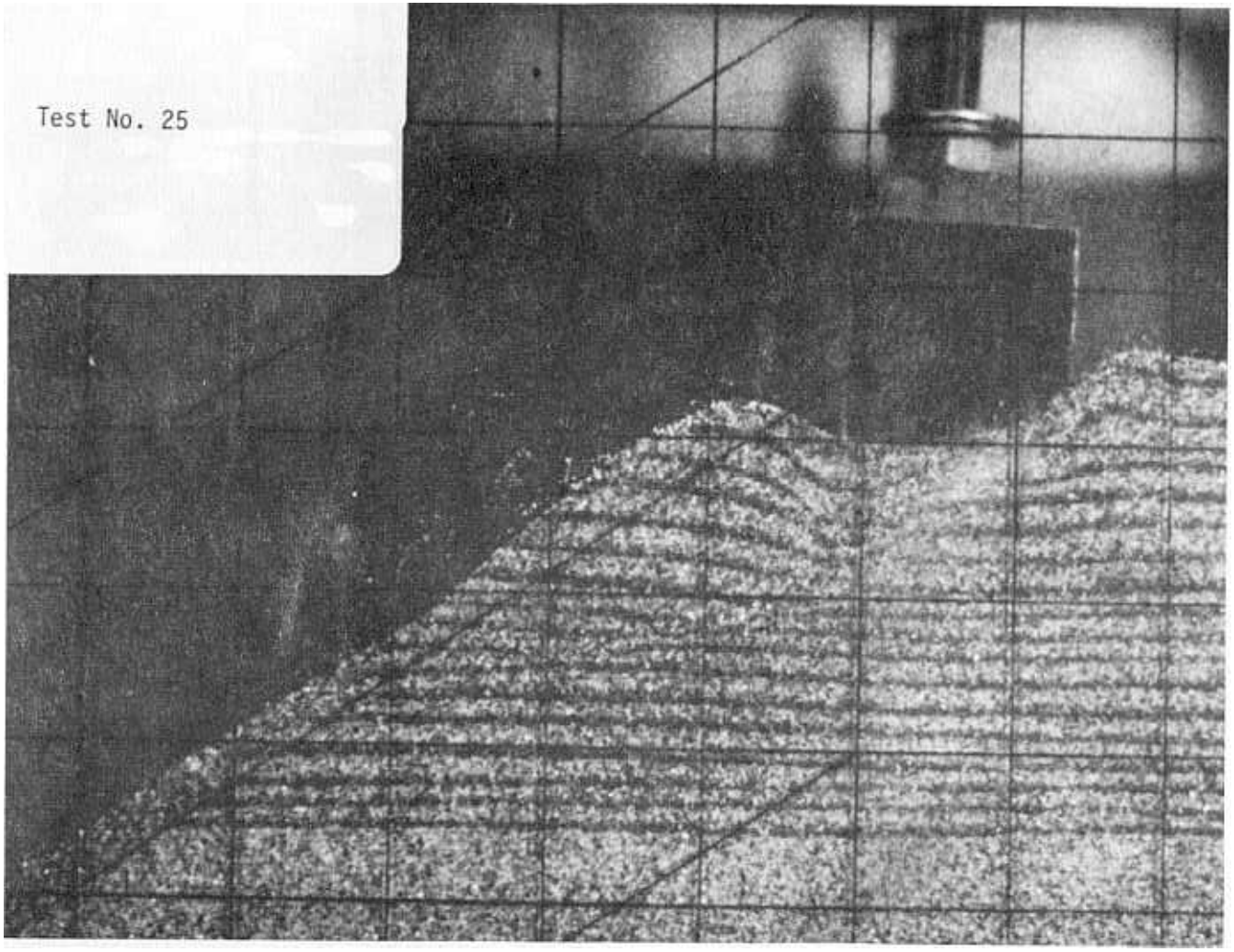

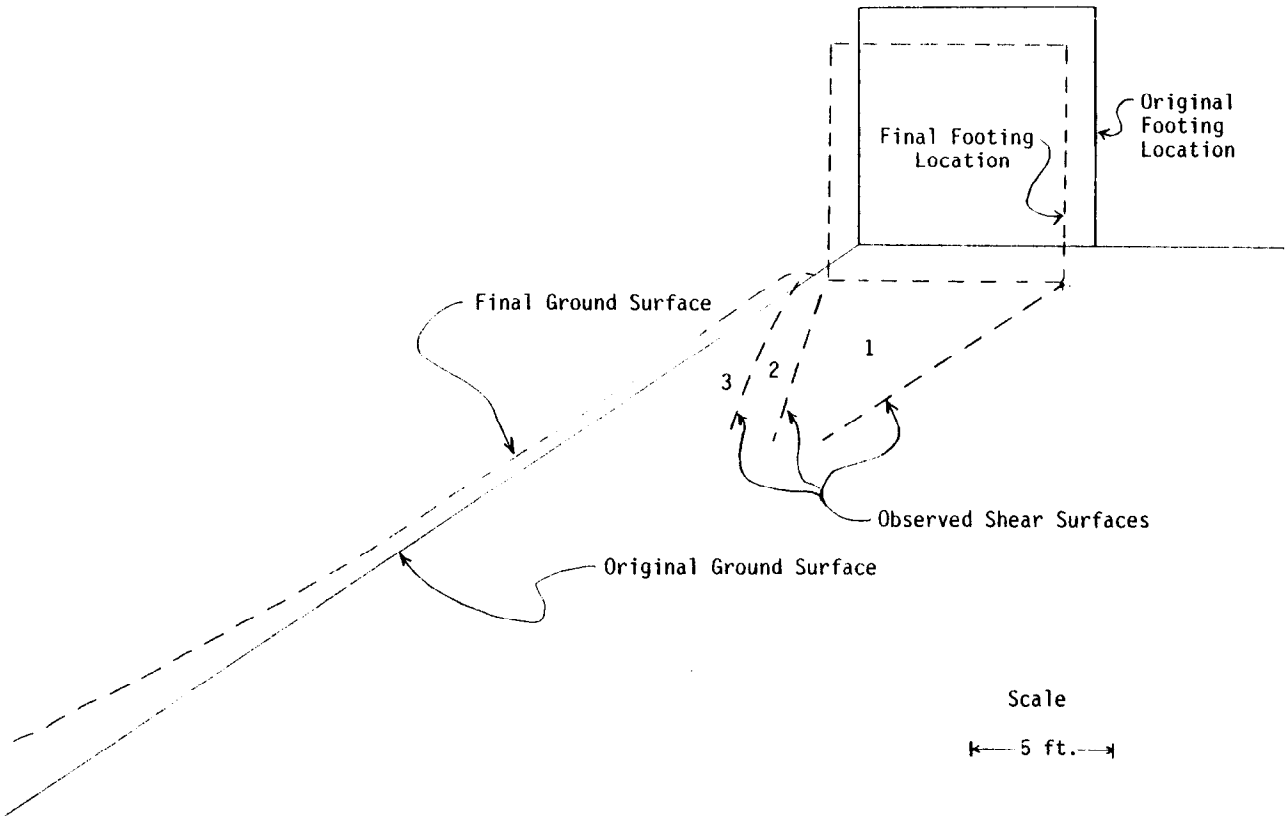

Figure D-8. – Failure mechanism interpreted from photograph of model test No. 3.

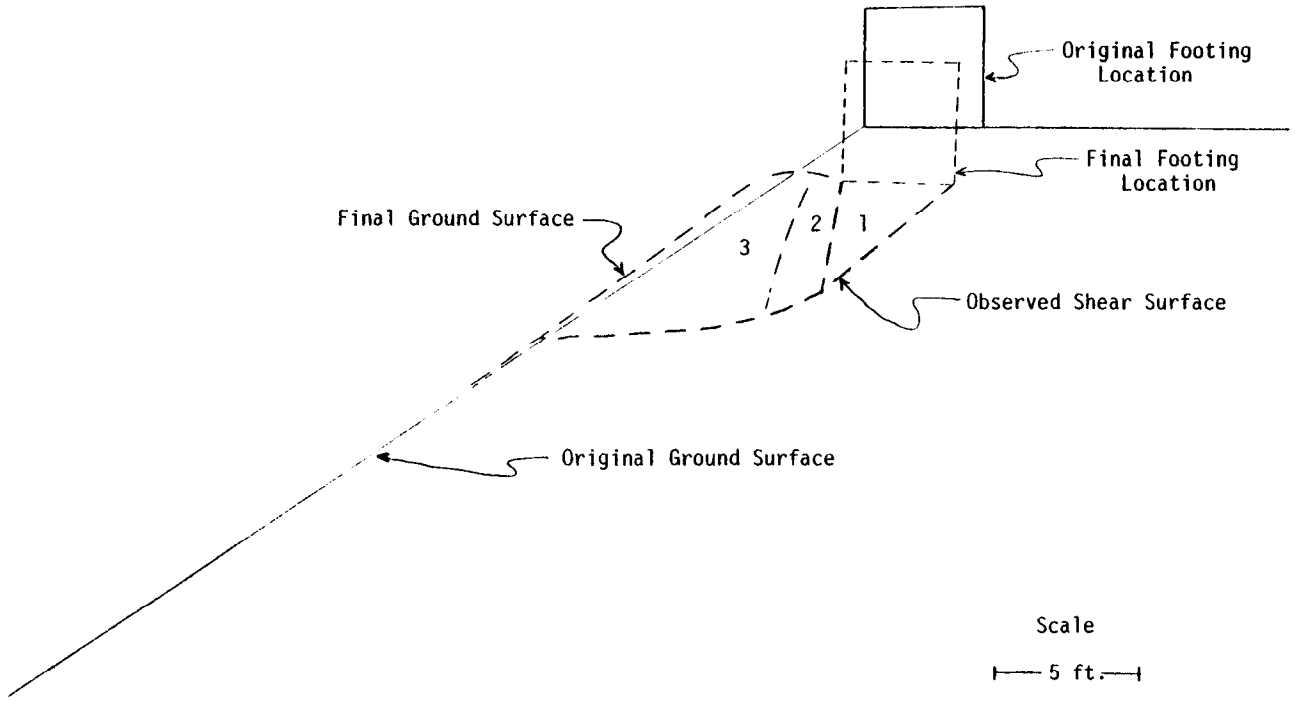

Figure D-9. – Failure mechanism interpreted from photograph of model test No. 5.

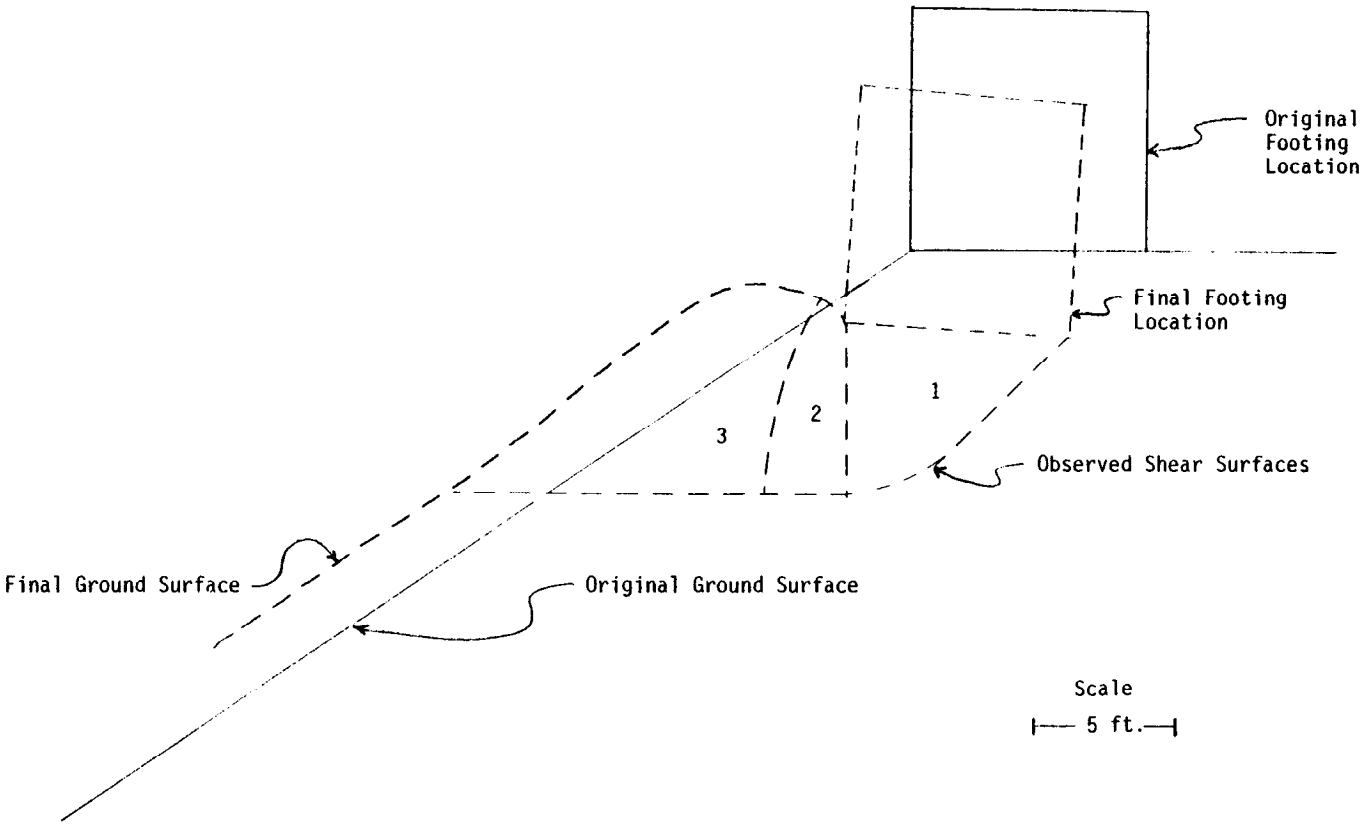

Figure D-10. – Failure mechanism interpreted from photograph of model test No. 8.

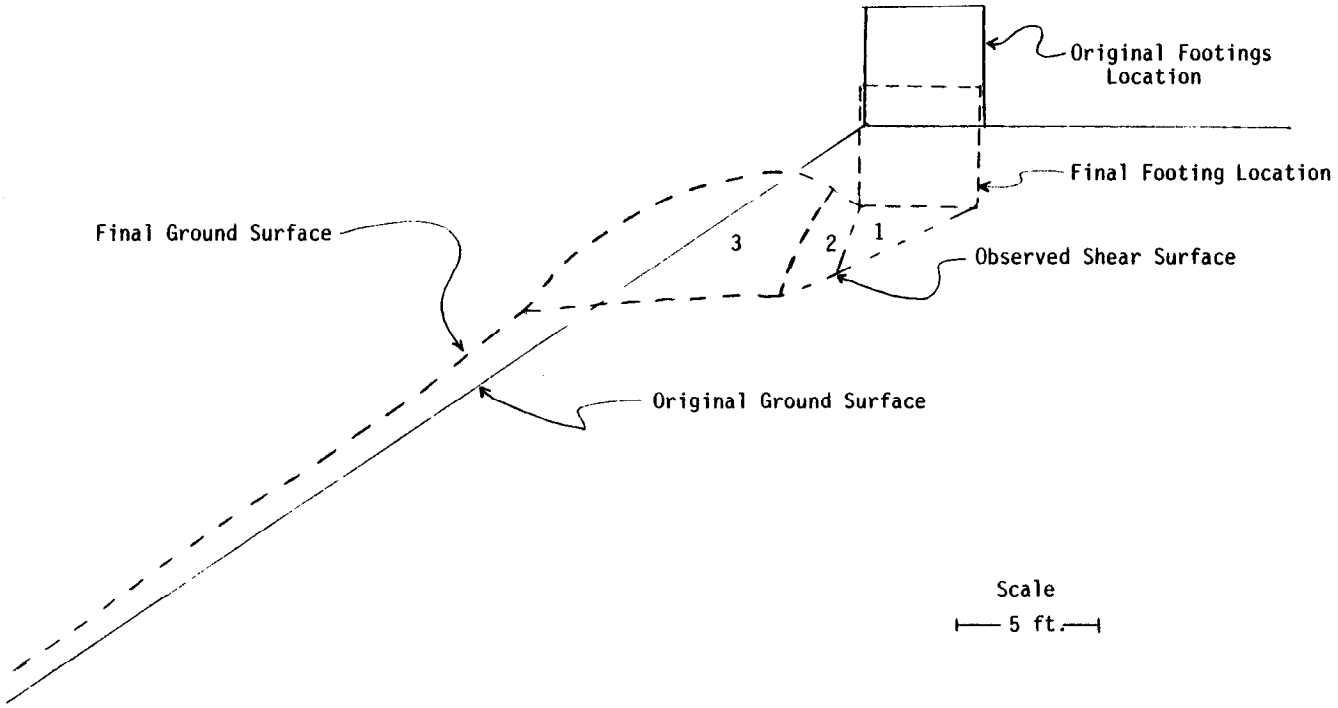

Figure D-11. – Failure mechanism interpreted from photograph of model test No. 9.

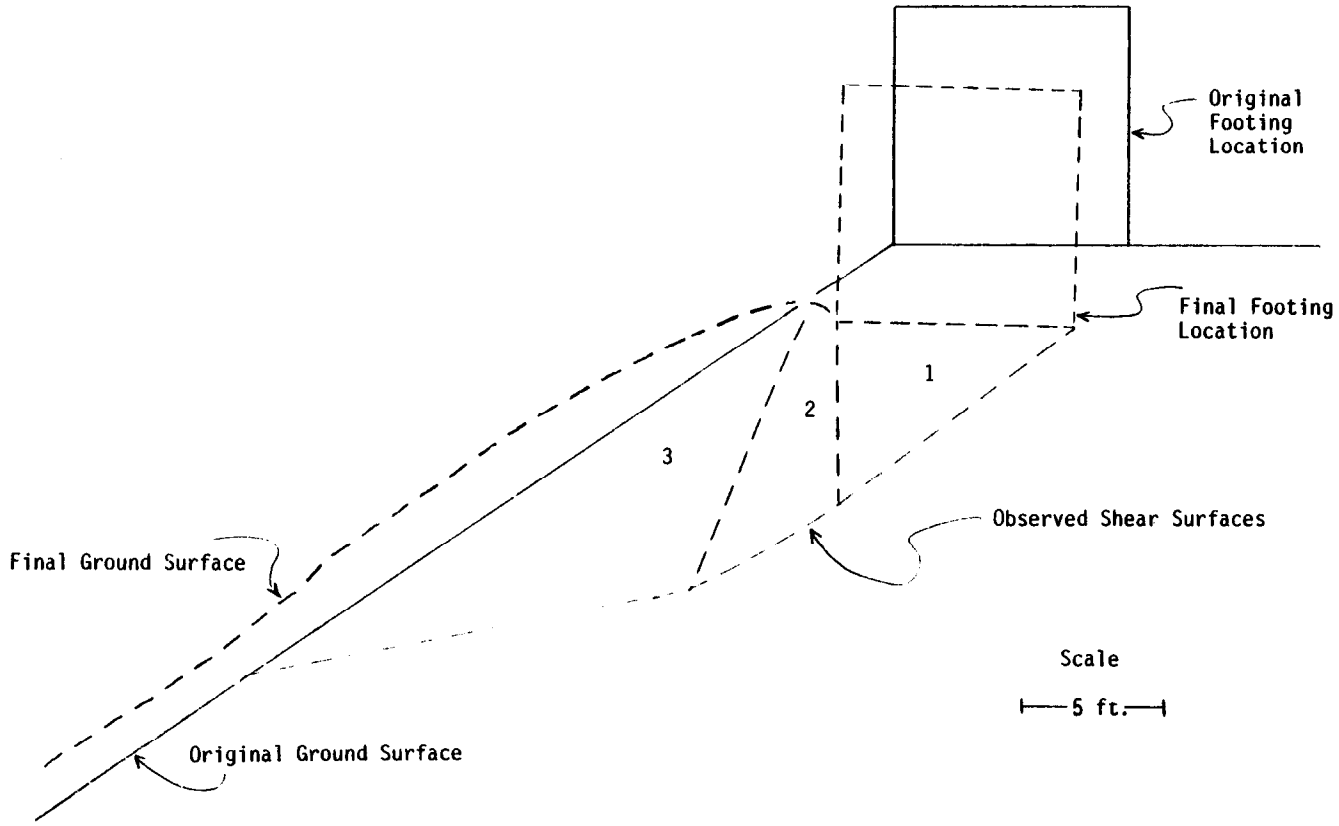

Figure D-12. – Failure mechanism interpreted from photograph of model test No. 21.

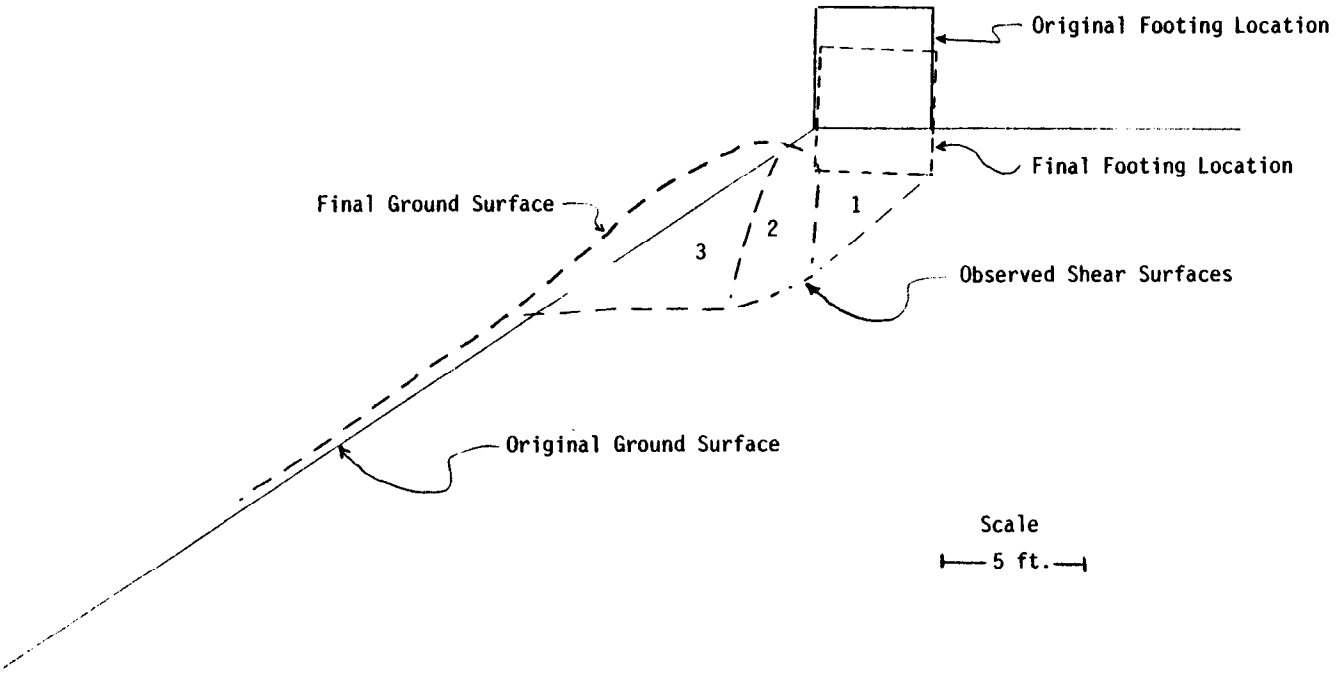

Figure D-13. – Failure mechanism interpreted from photograph of model test No. 23.

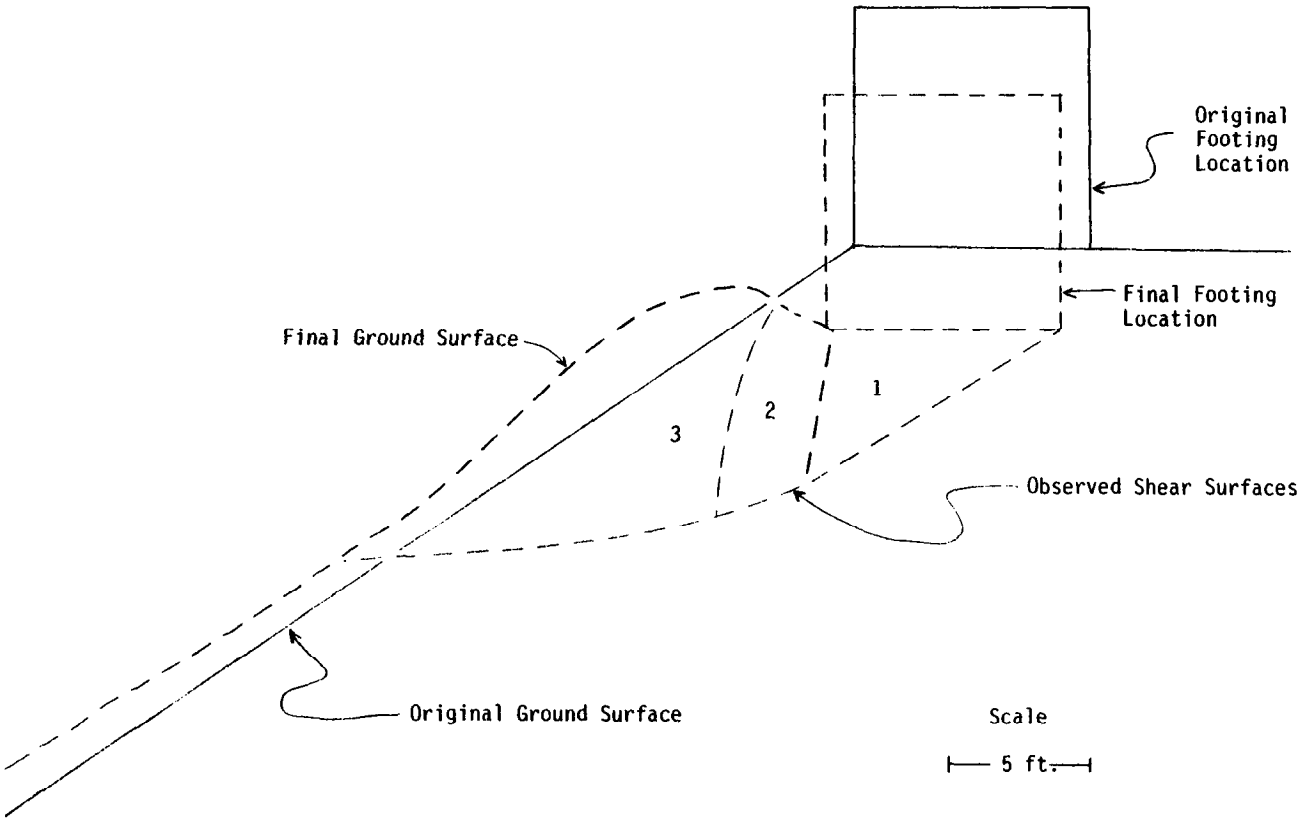

Figure D-14. – Failure mechanism interpreted from photograph of model test No. 25.

APPENDIX E

RESULTS OF LABORATORY TESTS ON SAND

Table E-1. – Summary of triaxial shear test results.

SAMPLE IDENTIFICATION			CLASSIFICATION SYMBOL	SPECIFIC GRAVITY	SPECIMEN NUMBER	PLACEMENT			VOID RATIO				TEST VALUES AT FAILURE						SHEAR VALUES CORRECTED FOR PORE PRESSURE	
SAMPLE NUMBER 44T-	HOLE NUMBER	DEPTH - feet (m)				DRY DENSITY - pcf (gm/cm³)	WATER CONTENT - %	DEGREE OF SATURATION - %	PLACEMENT	CONSOLIDATED	FAILURE		APPLD LATERAL PRESSURE - psi σ_3 (kg/cm²)	PORE PRESSURE - psi u_w (kg/cm²)	EFF LATERAL PRESSURE - psi (kg/cm²) $\sigma_3 - u = \emptyset_3$	VOLUME CHANGE - % OF INITIAL	AXIAL STRAIN - %	DEVIATOR STRESS - psi (kg/cm²) $\sigma_1 - \sigma_3$	ϕ Degrees	COHESION - psi (kg/cm²)
	(CD) Consolidated-Drained Triaxial Shear																			
4			SP	2.66	31	101	0.0	0.0	0.639	0.625	0.670		25.0	0.0	25.0	-1.9	5.19	121.5		
					32	101	0.0	0.0	0.635	0.639	0.670		50.0	0.0	25.0	-2.1	6.45	246.6		
					33	101	0.0	0.0	0.635	0.610	0.630		100.0	0.0	25.0	0.3	6.64	432.7		
					34	101	0.0	0.0	0.644	0.598			200.0							
											$\emptyset$, computed using specimens 31, 32, and 33								43.7	0
											$\emptyset_2$ computed using specimens 31 and 32								45.3	0

Table E-2. – Summary of direct shear test results.

SAMPLE IDENTIFICATION			CLASSIFICATION SYMBOL	SPECIFIC GRAVITY	RATE OF STRAIN - in./min (cm/min)	SPECIMEN NUMBER	TEST	DRY DENSITY - pcf (gm/cm³)		MOISTURE CONTENT - %		DEGREE OF SATURATION - %		TEST VALUE AT FAILURE			SHEAR VALUE	
SAMPLE NUMBER 44T-	HOLE NUMBER	DEPTH - feet (m)						INITIAL		INITIAL		INITIAL		NORMAL STRESS - psi (kg/cm²)	SHEAR STRESS - psi (kg/cm²)	STRAIN - %	Ø DEGREES	COHESION - psi (kg/cm²)
4			SP	2.66	0.028	1	A	101		0.0		0.0		20	23.8	3.62		
						2	A	101		0.0		0.0		40	40.4	2.95		
						3	A	101		0.0		0.0		80	80.5	3.19		
						4	A	101		0.0		0.0		160	149.7	4.45		
										Ø computed using specimens 1, 2, 3 and 4							43.7	0.0
						1	B	100		0.0		0.0		20	24.6	6.70		
						2	B	100		0.0		0.0		40	42.6	2.91		
						3	B	100		0.0		0.0		80	72.0	3.60		
						4	B	100		0.0		0.0		160	147.4	4.45		
										Ø computed using specimens 1, 2, 3, and 4							42.8	0.0

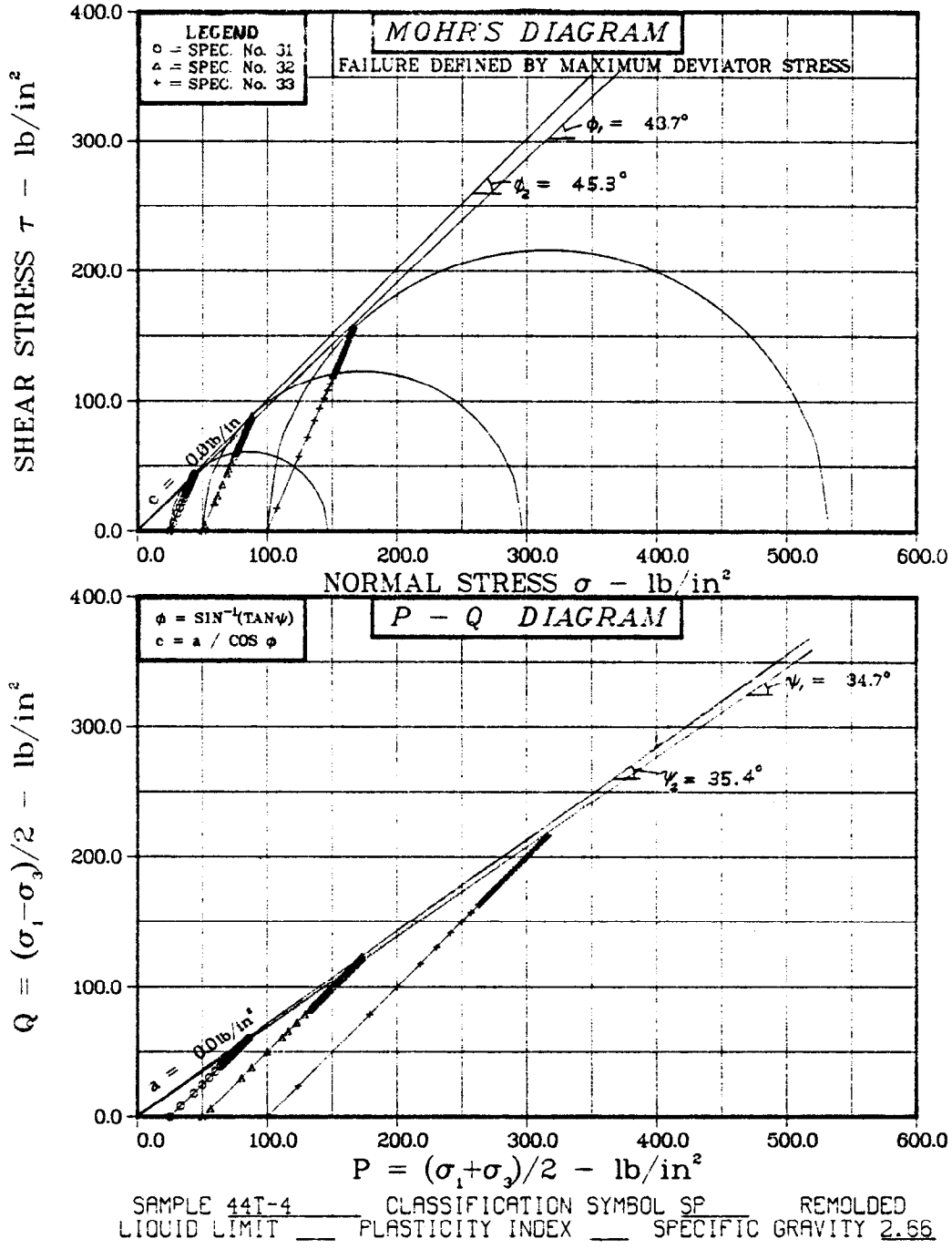

Figure E-1. – CD (consolidated-drained) triaxial shear test effective stress analysis.

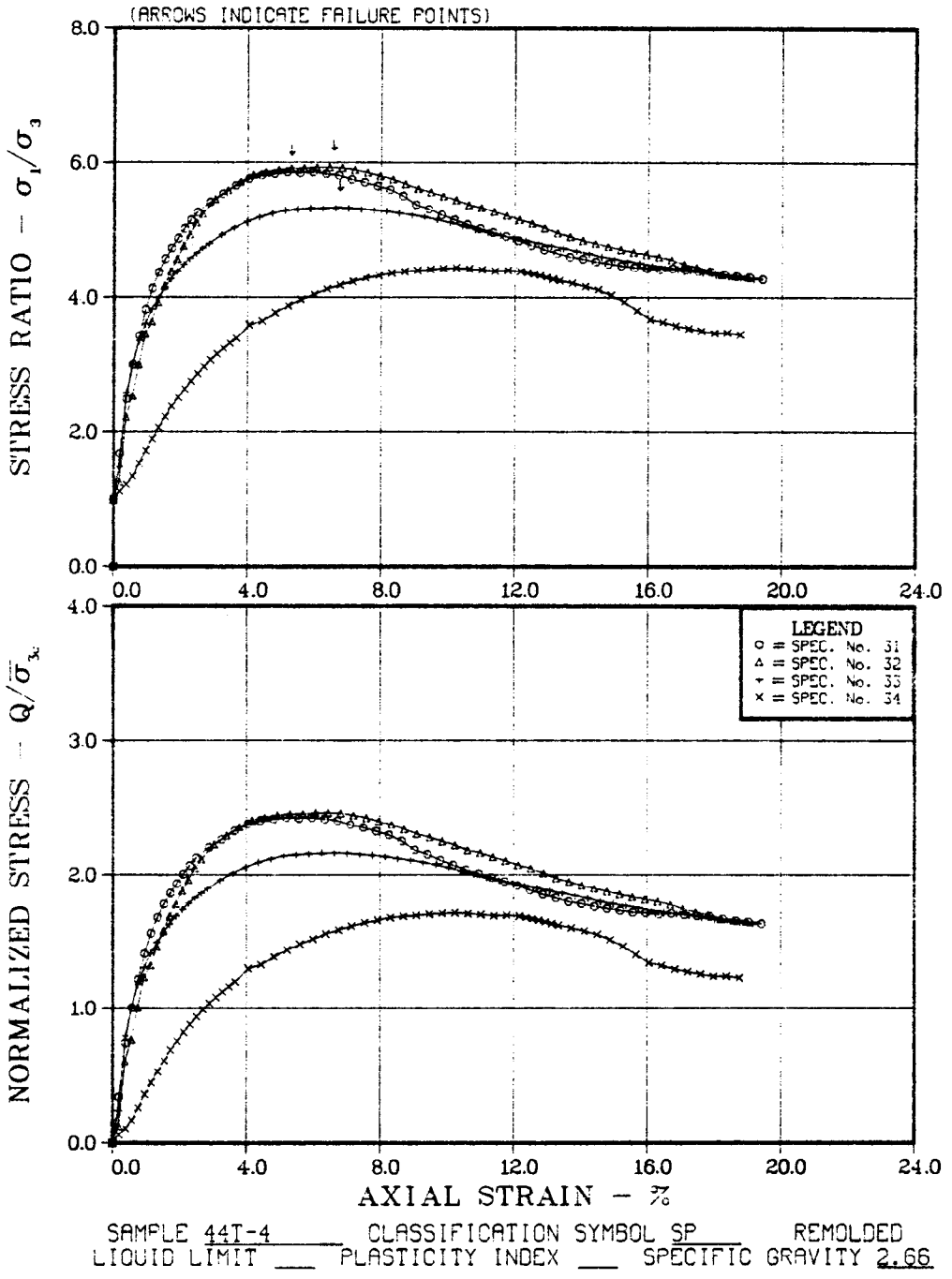

Figure E-2. – Triaxial shear test stress ratio and normalized stress versus axial strain plots.

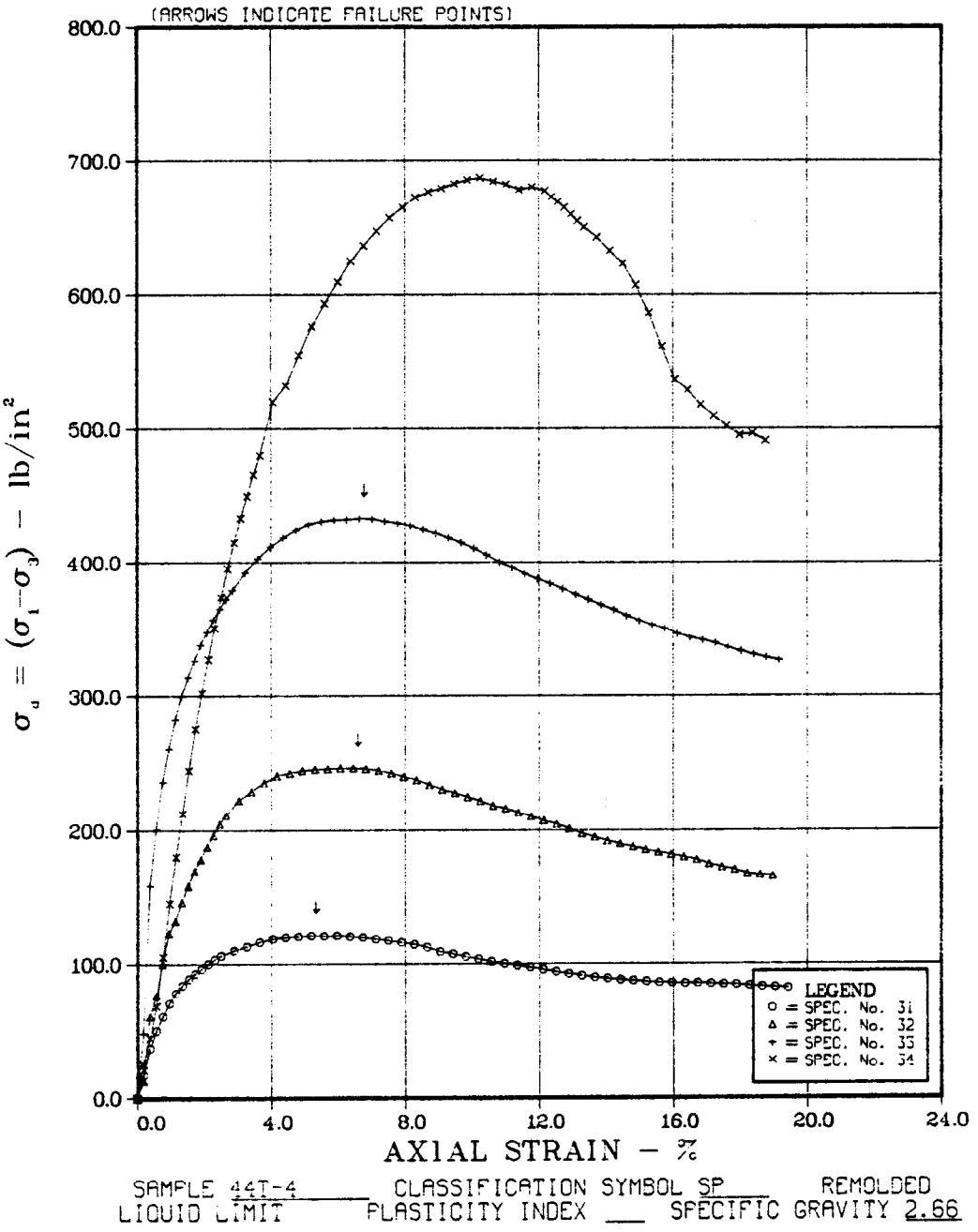

Figure E-3. – Triaxial shear test deviator stress versus axial strain plot.

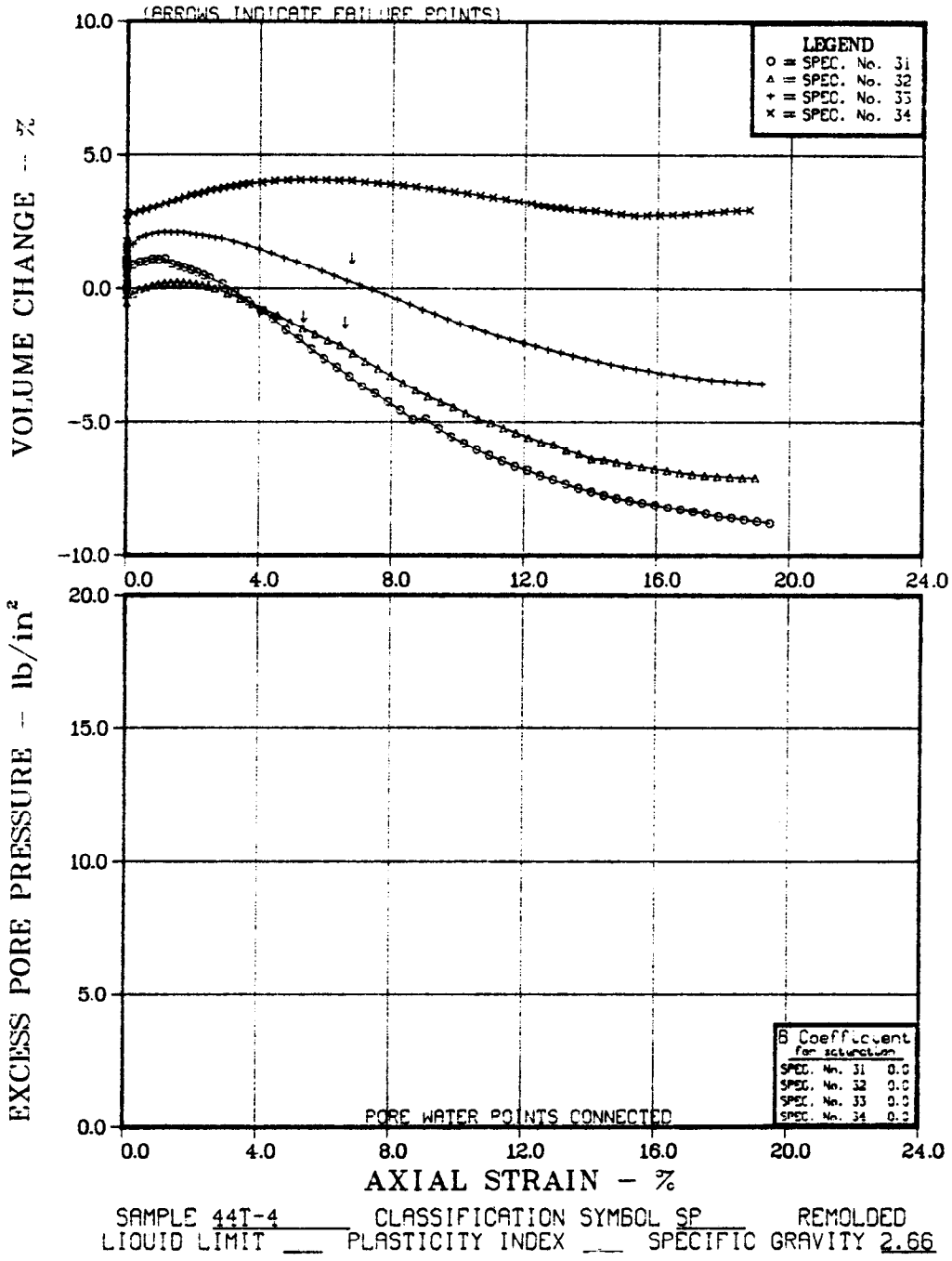

Figure E-4. – Triaxial shear test volume change versus axial strain plot.

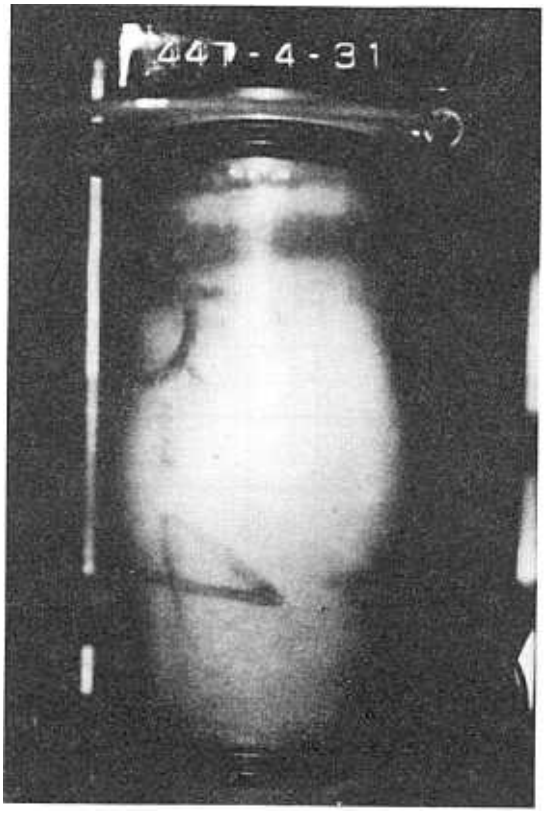

Photo P801-D-80816

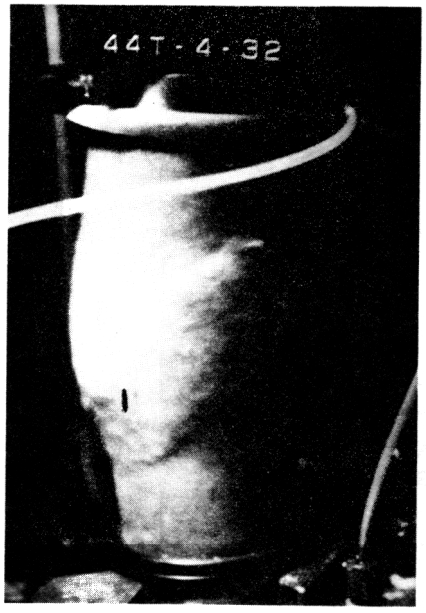

Photo P801-D-80817

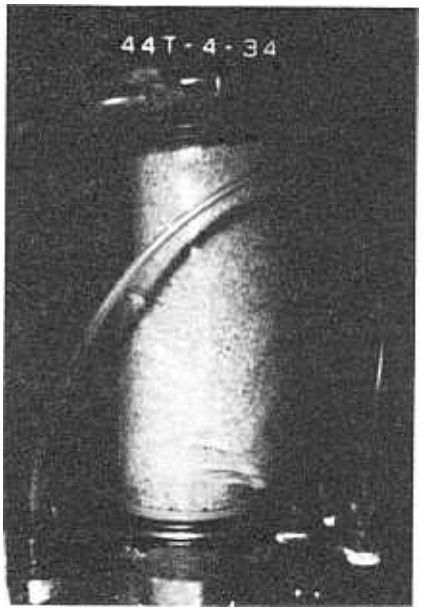

Photo P801-D-80818

Figure E-5. – Photographs of triaxial shear test specimens 31, 32, and 34.

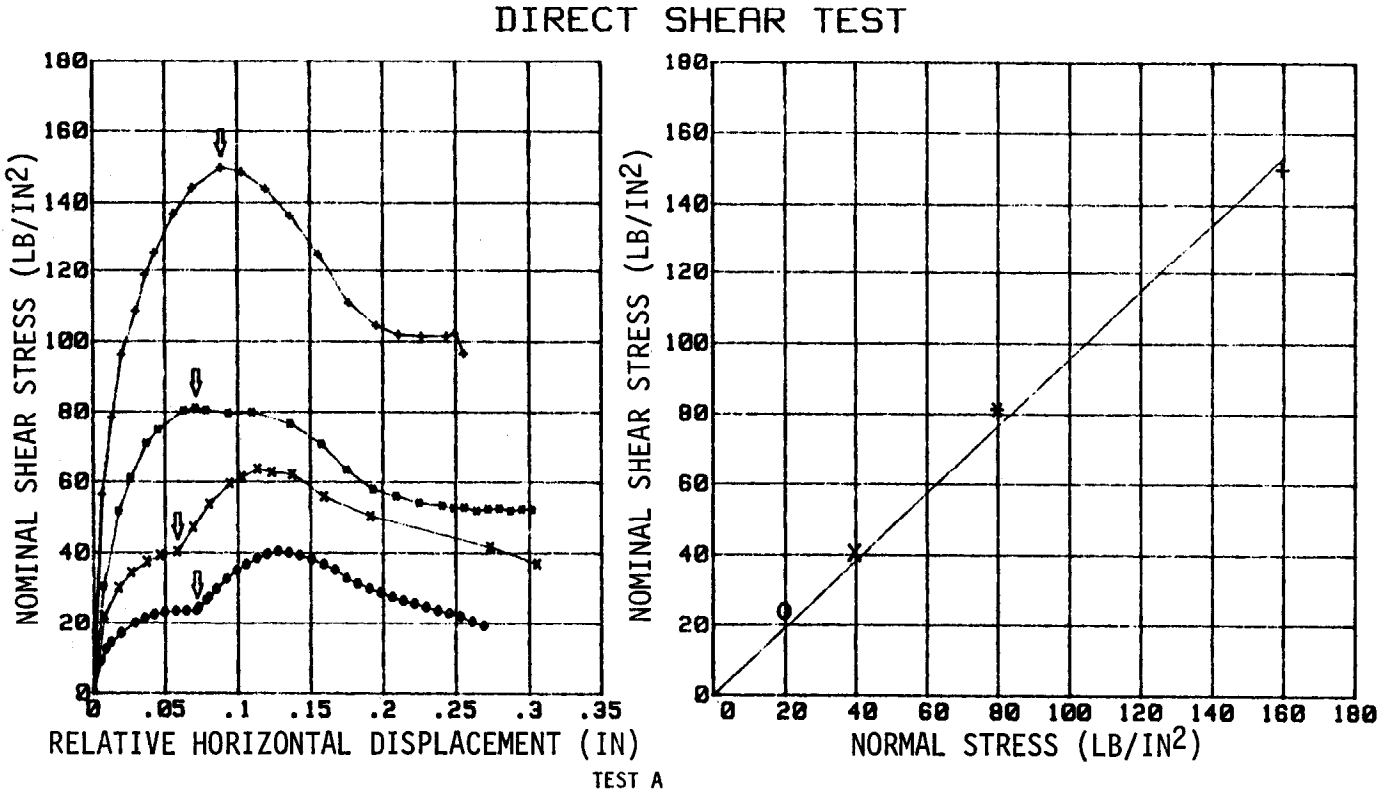

Figure E-6. – Results of direct shear test (test A).

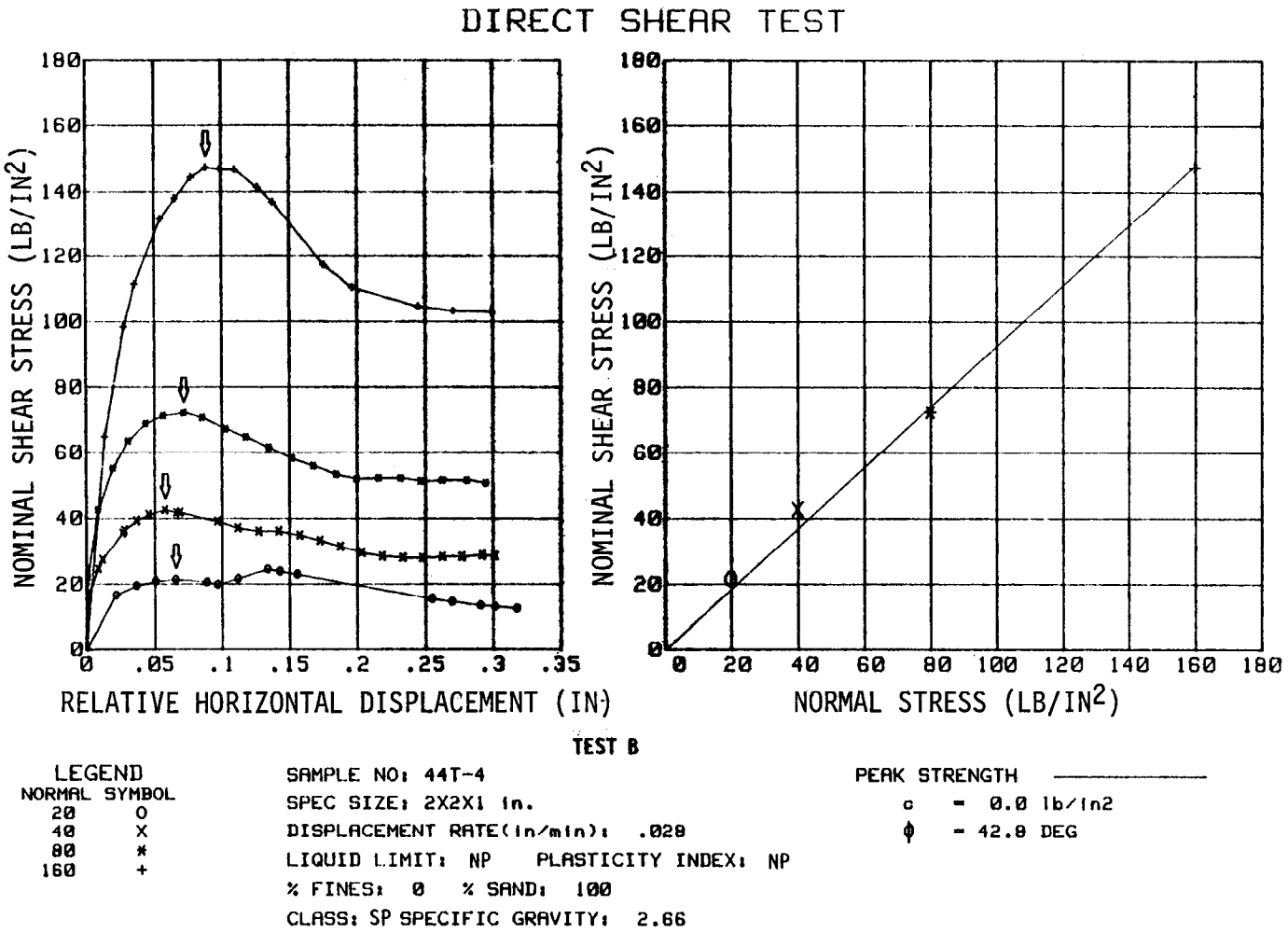

Figure E-7. – Results of direct shear test (test B).

GPO 846-465

Mission of the Bureau of Reclamation

The Bureau of Reclamation of the U.S. Department of the Interior is responsible for the development and conservation of the Nation's water resources in the Western United States.

The Bureau's original purpose "to provide for the reclamation of arid and semiarid lands in the West" today covers a wide range of interrelated functions. These include providing municipal and industrial water supplies; hydroelectric power generation; irrigation water for agriculture; water quality improvement; flood control; river navigation; river regulation and control; fish and wildlife enhancement; outdoor recreation; and research on water-related design, construction, materials, atmospheric management, and wind and solar power.

Bureau programs most frequently are the result of close cooperation with the U.S. Congress, other Federal agencies, States, local governments, academic institutions, water-user organizations, and other concerned groups.

A free pamphlet is available from the Bureau entitled "Publications for Sale." It describes some of the technical publications currently available, their cost, and how to order them. The pamphlet can be obtained upon request from the Bureau of Reclamation, Attn D-922, P O Box 25007, Denver Federal Center, Denver CO 80225-0007.